

PACIFIC EARTHQUAKE ENGINEERING
RESEARCH CENTER

**Self-Centering Precast Concrete Dual-Steel-Shell
Columns for Accelerated Bridge Construction:
Seismic Performance, Analysis, and Design**

Gabriele Guerrini

Civil Engineering and Architecture Department
University of Pavia, Italy

Jose I. Restrepo

Department of Structural Engineering
University of California, San Diego

Athanassios Vervelidis

Professional Engineer
Pescara, Italy

Milena Massari

Department of Civil, Chemical, Environmental,
and Materials Engineering
University of Bologna, Italy

PEER Report No. 2015/13

Pacific Earthquake Engineering Research Center
Headquarters at the University of California, Berkeley

December 2015

Disclaimer

The opinions, findings, and conclusions or recommendations expressed in this publication are those of the author(s) and do not necessarily reflect the views of the study sponsor(s) or the Pacific Earthquake Engineering Research Center.

Self-Centering Precast Concrete Dual-Steel-Shell Columns for Accelerated Bridge Construction: Seismic Performance, Analysis, and Design

Gabriele Guerrini

Civil Engineering and Architecture Department
University of Pavia, Italy

José I. Restrepo

Department of Structural Engineering
University of California, San Diego

Athanassios Vervelidis

Professional Civil Engineer
Pescara, Italy

Milena Massari

Department of Civil, Chemical, Environmental and Materials Engineering
University of Bologna, Italy

PEER Report 2015/13
Pacific Earthquake Engineering Research Center
Headquarters at the University of California, Berkeley

December 2015

ABSTRACT

This study presents an innovative bridge column technology for application in seismic regions. The proposed technology combines a precast, post-tensioned, composite steel–concrete, hollow-core column with supplemental energy dissipation, in such way to reduce on-site construction burdens and minimize earthquake-induced residual deformations, damage, and associated repair costs. The column consists of two steel cylindrical shells, with high-performance concrete cast in between. Both shells act as permanent formwork. The outer shell substitutes the longitudinal and transverse reinforcement, as it works in composite action with the concrete, whereas the inner shell removes unnecessary concrete volume from the column, prevents concrete implosion, and prevents buckling of energy dissipating dowels when embedded in the concrete. Large inelastic rotations can be accommodated at the end joints with minimal structural damage, since gaps are allowed to open at these locations and to close upon load reversal. Longitudinal post-tensioned high-strength steel threaded bars, designed to respond elastically, in combination with gravity forces ensure self-centering behavior. Internal or external steel devices provide energy dissipation by axial yielding. This report reviews the main principles and requirements for the design of such columns, presents experimental findings from two quasi-static reversed cyclic tests, and proposes numerical simulations of the observed behavior.

ACKNOWLEDGMENTS

This work was sponsored by the Pacific Earthquake Engineering Research Center (PEER) and funded by the California Transportation Systems Research Program. Material support was made by Salit Specialty Rebars and Hill Brothers Chemical Co. Any opinions, findings, and conclusions or recommendations expressed in this material are those of the authors and do not necessarily reflect those of the sponsoring agencies.

The participation of Dr. Giovanni De Francesco and Maura Torres, and the work of the technical staff of the Charles Lee Powell Structural Engineering Laboratories of the University of California, San Diego, are thankfully acknowledged. Discussions with Professor Stefano Pampanin and Dr. Alessandro Palermo from the University of Canterbury, New Zealand, were of valuable importance for the development of the buckling-restrained energy dissipators.

CONTENTS

| | |
|---|------------|
| ABSTRACT | iii |
| ACKNOWLEDGMENTS | v |
| TABLE OF CONTENTS | vii |
| LIST OF TABLES | xi |
| LIST OF FIGURES | xi |
| 1 INTRODUCTION | 1 |
| 1.1 Objectives | 1 |
| 1.2 Dual-Shell Column Technology | 2 |
| 1.3 Background on Self-Centering Hybrid Systems | 4 |
| 1.4 Background on Concrete-Filled Tube Columns | 5 |
| 2 DESIGN CRITERIA AND SIMPLIFIED ANALYSIS | 7 |
| 2.1 Design Criteria | 7 |
| 2.1.1 Criterion (i): Minimum Outer Shell Thickness..... | 7 |
| 2.1.2 Criterion (ii): Energy Dissipators Strength..... | 8 |
| 2.1.3 Criterion (iii): Composite Action..... | 8 |
| 2.1.4 Criterion (iv): Mortar Bed Integrity..... | 8 |
| 2.1.5 Criterion (v): Concrete Strain Control and Inner Shell Diameter..... | 9 |
| 2.1.6 Criterion (vi): Prevention of Early Dissipator Fracture..... | 9 |
| 2.1.7 Criterion (vii): Prevention of Early Loss of Post-Tensioning Force..... | 11 |
| 2.2 Design Procedure | 13 |
| 2.3 Simplified Analysis Procedure | 16 |
| 2.3.1 Material Stress–Strain Relationships..... | 16 |
| 2.3.1.1 <i>Outer-Shell Steel</i> | 16 |
| 2.3.1.2 <i>Post-Tensioning Steel</i> | 16 |
| 2.3.1.3 <i>Energy-Dissipator Steel</i> | 17 |
| 2.3.1.4 <i>Concrete</i> | 17 |
| 2.3.1.5 <i>Mortar</i> | 18 |
| 2.3.1.6 <i>Elastomeric Bearings</i> | 19 |
| 2.3.2 Simplified Interface Section Analysis..... | 20 |
| 2.3.2.1 <i>Decompression Limit State</i> | 20 |
| 2.3.2.2 <i>Rocking Joint Analysis</i> | 20 |
| 2.3.2.3 <i>First-Yield and Reference Yield Limit States</i> | 23 |
| 2.3.3 Simplified Pushover Analysis..... | 24 |

| | | |
|------------|--|-----------|
| 2.3.3.1 | <i>First-Order Base Shear</i> | 24 |
| 2.3.3.2 | <i>First-Order Displacement and Drift Ratio</i> | 24 |
| 2.3.3.3 | <i>Simplified Consideration of P-Delta Effects</i> | 25 |
| 2.3.3.4 | <i>Elastic Stiffness and Displacement Ductility</i> | 25 |
| 2.3.4 | Experimental Validation | 26 |
| 3 | EXPERIMENTAL PROGRAM | 29 |
| 3.1 | Test Overview | 29 |
| 3.1.1 | Target Performance Objectives..... | 29 |
| 3.1.2 | Specimens Configuration..... | 29 |
| 3.2 | Specimen Components | 31 |
| 3.2.1 | Composite Column | 31 |
| 3.2.2 | Footing | 33 |
| 3.2.3 | Load Stub | 33 |
| 3.2.4 | Mortar Bed..... | 36 |
| 3.2.5 | Energy Dissipators | 36 |
| 3.2.5.1 | <i>Unit 1A: External Buckling-Restrained Devices</i> | 36 |
| 3.2.5.2 | <i>Unit 1B: Internal Dowels</i> | 37 |
| 3.2.6 | Post-Tensioning Bars | 38 |
| 3.2.7 | Elastomeric Pads..... | 39 |
| 3.2.7.1 | <i>Unit 1A: Natural Rubber Pads</i> | 39 |
| 3.2.7.2 | <i>Unit 1B: Polyurethane Pads</i> | 40 |
| 3.3 | Material Properties | 41 |
| 3.3.1 | Concrete | 41 |
| 3.3.2 | Mortar | 41 |
| 3.3.3 | Grout | 42 |
| 3.3.4 | Energy Dissipator Steel..... | 43 |
| 3.3.5 | Rubber Pads | 43 |
| 3.3.6 | Polyurethane Pads..... | 44 |
| 3.4 | Instrumentation | 44 |
| 3.4.1 | Overall Displacement and Rotation Measurements..... | 44 |
| 3.4.2 | Column Deformation Measurements | 44 |
| 3.4.3 | Outer-Shell Strain Measurements | 45 |
| 3.4.4 | Post-Tensioning Bar Strain Measurements..... | 46 |
| 3.4.5 | External Energy Dissipator Response Measurements | 47 |
| 3.4.6 | Internal Energy Dissipator Strain Measurements | 47 |

| | | |
|------------|--|------------|
| 3.4.7 | Gravity-Equivalent Load Measurements | 47 |
| 3.4.8 | Miscellaneous | 47 |
| 3.5 | Loading Protocol and Test Outcomes | 48 |
| 3.5.1 | Normalization of Response Parameters | 48 |
| 3.5.2 | Loading Protocol..... | 48 |
| 3.5.3 | Outcomes for Unit 1A..... | 49 |
| | 3.5.3.1 <i>Response Summary</i> | 49 |
| | 3.5.3.2 <i>Mortar Bed</i> | 50 |
| | 3.5.3.3 <i>Energy Dissipators</i> | 50 |
| | 3.5.3.4 <i>Composite Column</i> | 52 |
| 3.5.4 | Outcomes for Unit 1B..... | 53 |
| | 3.5.4.1 <i>Response Summary</i> | 53 |
| | 3.5.4.2 <i>Mortar Bed</i> | 54 |
| | 3.5.4.3 <i>Energy Dissipators</i> | 54 |
| | 3.5.4.4 <i>Composite Column</i> | 55 |
| 3.5.5 | Comparison between Unit 1A and Unit 1B | 57 |
| 4 | NUMERICAL SIMULATIONS..... | 59 |
| 4.1 | Numerical Model..... | 59 |
| 4.1.1 | Composite Column | 60 |
| 4.1.2 | Mortar Bed..... | 60 |
| 4.1.3 | Post-Tensioning Bars | 61 |
| 4.1.4 | Energy Dissipators | 61 |
| | 4.1.4.1 <i>Unit 1A: External Buckling-Restrained Devices</i> | 61 |
| | 4.1.4.2 <i>Unit 1B: Internal Dowels</i> | 61 |
| 4.1.5 | Analysis Procedure | 62 |
| 4.2 | Numerical Analysis Results..... | 62 |
| 4.2.1 | Lateral Force-Displacement Response | 62 |
| 4.2.2 | Overall Energy Dissipation..... | 62 |
| 4.2.3 | Post-Tensioning Bar Strain History | 64 |
| 4.2.4 | Energy Dissipators Hysteretic Response | 65 |
| 5 | CONCLUSIONS | 67 |
| | REFERENCES..... | 69 |
| | APPENDIX A: CONSTRUCTION DRAWINGS | 73 |
| | APPENDIX B: OPENSEES SCRIPTS..... | 105 |

LIST OF TABLES

| | | |
|-----------|---|----|
| Table 3.1 | Measured compressive strength of cementitious materials. | 42 |
| Table 3.2 | Measured steel mechanical properties. | 43 |

LIST OF FIGURES

| | | |
|------------|--|----|
| Figure 1.1 | Schematics of the proposed system: (a) column typical cross-section; (b) bent components and rocking kinematics; and (c) joint rotation. | 3 |
| Figure 1.2 | Hysteretic response: (a) conventional ductile system; (b) purely rocking system; and (c) hybrid rocking system. | 4 |
| Figure 2.1 | Energy dissipator details: (a) unbonded yield segment of an internal dowel, wrapped with duct tape; (b) dog-bone milled bar of a buckling-restrained device; and (c) milled bar taper detail. | 10 |
| Figure 2.2 | Elastomeric bearings in series with post-tensioning bars: (a) conceptual elevation; and (b) design chart. | 11 |
| Figure 2.3 | Confined mortar equivalent stress-block parameters (adapted from Paulay and Priestley [1992]). | 22 |
| Figure 2.4 | Mortar compressive resultant parameters. | 22 |
| Figure 2.5 | Comparison between simplified pushover envelopes and experimental cyclic responses: (a) Unit 1A and (b) Unit 1B. | 27 |
| Figure 2.6 | Comparison between simplified prediction and experimental neutral-axis depth: (a) Unit 1A and (b) Unit 1B. Only positive cycles are shown. | 27 |
| Figure 3.1 | Test configuration and dimensions: (a) side elevation; (b) plan view; (c) overview of Unit 1A; and (d) overview of Unit 1B. | 30 |
| Figure 3.2 | Column details: (a) Unit 1A base cross-section; (b) Unit 1B base cross-section; (c) column longitudinal section; (d) outer shell with brackets for connection of external dissipators; (e) concentric shells and ducts for future grouting of internal dissipators; (f) weld beads on the outer-shell internal surface; and (g) roughened concrete surface. | 32 |
| Figure 3.3 | Footing details: (a) horizontal section; (b) longitudinal section; (c) reinforcement, ducts, and formwork; and (d) steel ducts and spiral reinforcement. | 34 |
| Figure 3.4 | Load-stub details: (a) horizontal section; (b) longitudinal section; and (c) reinforcement, ducts, and formwork. | 35 |
| Figure 3.5 | Mortar bed: (a) wood template and nylon-rod shims, during mortar placement; and (b) mortar scraped from underneath the outer shell. | 36 |

| | | |
|-------------|--|----|
| Figure 3.6 | External energy dissipators: (a) location around column perimeter; (b) milled-bar dimensions; (c) dog-bone milled steel bar; and (d) assembled buckling-restrained device. | 37 |
| Figure 3.7 | Internal energy dissipators: (a) dowels grouted in the footing; (b) ducts in the column; (c) dowel dimensions; and (d) detail of bar wrapping across the interface. | 38 |
| Figure 3.8 | Post-tensioning bars: (a) bars screwed into the footing anchorages; (b) sleeved bars inside the hollow core; (c) anchorage components; and dimensions; (d) assembled anchorage device. | 39 |
| Figure 3.9 | Rubber bearing of Unit 1A: (a) components; (b) single pad; and (c) assembled bearings. | 40 |
| Figure 3.10 | Polyurethane bearing of Unit 1B: (a) components; (b) single pad; and (c) assembled bearings. | 41 |
| Figure 3.11 | Monotonic tensile stress-strain relationships for the energy dissipator steel: (a) full response; and (b) zoom up to 1% strain. (1 ksi = 6.895 MPa)..... | 43 |
| Figure 3.12 | Instrumentation: (a) displacement transducers and (b) inclinometers. | 45 |
| Figure 3.13 | Outer-shell strain gages: (a) Unit 1A and (b) Unit 1B..... | 46 |
| Figure 3.14 | Post-tensioning bars strain gages..... | 46 |
| Figure 3.15 | Energy dissipators instrumentation: (a) external buckling-restrained devices of Unit 1A; and (b) internal dowels of Unit 1B..... | 47 |
| Figure 3.16 | Loading protocol: (a) force-controlled cycles; and (b) displacement-controlled cycles. | 48 |
| Figure 3.17 | Response of Unit 1A: (a) lateral hysteretic response up to 3% drift ratio; (b) lateral hysteretic response up to 10% drift ratio; (c) maximum and residual drift ratios for positive cycles; and (d) residual post-tensioning force at the end of each cycle on the north–east bar. | 49 |
| Figure 3.18 | Crushed mortar bed at the end of testing of Unit 1A..... | 50 |
| Figure 3.19 | Unit 1A buckling-restrained energy dissipators: (a) south–east energy dissipator hysteretic loops up to 5% drift ratio; (b) north–west energy dissipator hysteretic loops up to 5% drift ratio; and (c) distortion of external energy dissipators..... | 51 |
| Figure 3.20 | Unit 1A composite column: (a) outer-shell hoop strain profiles on the south side; (b) outer-shell hoop strain profiles on the north side; and (c) permanent concrete and shell deformations at the end of testing. | 52 |
| Figure 3.21 | Response of Unit 1B: (a) lateral hysteretic response up to 3% drift ratio; (b) lateral hysteretic response up to 10% drift ratio; (c) maximum and residual drift ratios for positive cycles; and (d) residual post-tensioning force at the end of each cycle on the south–west bar..... | 53 |
| Figure 3.22 | Crushed mortar bed at the end of testing of Unit 1B. | 54 |

| | | |
|-------------|--|----|
| Figure 3.23 | Unit 1B energy-dissipating dowels: (a) fractured dowel in the column; and (b) fractured dowel in the footing. | 55 |
| Figure 3.24 | Unit 1B composite column: (a) outer-shell longitudinal strain profiles in front of the south-west dowel; (b) outer-shell longitudinal strain profiles in front of the north-east dowel (c) outer-shell hoop strain profiles on the south side; (d) outer-shell hoop strain profiles on the north side; and (e) permanent concrete and shell deformations at the end of testing. | 56 |
| Figure 3.25 | Neutral axis depth at peak lateral displacements: (a) Unit 1A and (b) Unit 1B. | 57 |
| Figure 4.1 | Numerical model sketches: (a) Unit 1A and (b) Unit 1B. | 59 |
| Figure 4.2 | Numerical prediction of the lateral force-displacement response: (a) Unit 1A up to 1% drift ratio; (b) Unit 1A up to 5% drift ratio; (c) Unit 1B up to 1% drift ratio; and (d) Unit 1B up to 5% drift ratio. | 63 |
| Figure 4.3 | Comparison between numerical prediction and simplified analysis of the lateral force-displacement response: (a) Unit 1A and (b) Unit 1B. | 63 |
| Figure 4.4 | Numerical prediction of the cumulative hysteretic energy: (a) Unit 1A and (b) Unit 1B. | 64 |
| Figure 4.5 | Numerical prediction of the post-tensioning bar strain history: (a) Unit 1A, north-east bar; and (b) Unit 1B, south-west bar. | 64 |
| Figure 4.6 | Numerical prediction of the hysteretic response of the north-west energy dissipator in Unit 1A: (a) cycles up to 1% drift ratio; and (b) cycles up to 5% drift ratio. | 65 |

1 Introduction

1.1 OBJECTIVES

According to the U.S. Department of Transportation [FHWA 2014], as of 2014 approximately 10% of the 610,749 bridges in the U.S. were considered structurally deficient, while 14% were deemed functionally obsolete: this means that more than 145,000 bridges throughout the U.S. may need some kind of repair, ranging from minor retrofit to full replacement. Many of these structurally deficient or functionally obsolete bridges serve as key links in local and national transportation networks, with severe impacts associated with their closures. Many of these structures can be found in densely populated urban areas, where the impacts of construction work on traffic, environment, society, and economy are considerable; moreover, lengthy on-site bridge construction projects expose construction workers to increased risk. Therefore, minimizing construction time becomes essential to reduce the aforementioned consequences on the public, workers, and the environment.

Considering that a significant number of bridges are located in earthquake-prone regions, the impact and cost of earthquake-induced damage on these structures have raised serious questions on whether the current seismic design philosophy can satisfy the needs of modern society. Designing a structure to respond elastically under severe earthquakes has generally been considered impractical for economic reasons; as a result, current bridge seismic design provisions [Caltrans 2010; AASHTO 2012] allow columns to respond beyond the elastic limit and to be damaged under the design-basis earthquake (DBE), provided that collapse is prevented. Inelastic behavior is typically localized within flexural plastic-hinge regions at the bottom and/or top of the columns: these regions experience structural damage during the DBE.

However, the consequences of structural damage in a bridge system can be critical if associated with the temporary interruption of an important road path, obstruction of rescue, and recovery operations in the immediate disaster aftermath, and economical losses related to medium- and long-term business interruption and displacement of people and goods [Palermo and Pampanin 2008]. While the concept of structural damage is widely accepted in design practices, resilient communities expect strategic structures and bridges to survive moderately strong earthquakes with little or no disturbance to traffic and business.

The significant number of bridge structures requiring replacement, the continuous construction of new infrastructures throughout the country, and the extent of the nation's bridge stock vulnerable to seismic activity underline the need for innovative design approaches to reduce public and environmental impacts, improve jobsite safety and construction quality, and ultimately save money. As a consequence, research efforts have been directed to the development of bridge technologies that minimize structural damage, encompass self-centering

properties [Restrepo et al. 2011; Guerrini and Restrepo 2011], and reduce construction time and traffic impact [FHWA 2012; Culmo 2011].

This report summarizes the main features and seismic performance of a precast composite concrete-dual steel shell bridge column technology with self-centering behavior induced by unbonded post-tensioning [Guerrini et al. 2015]. The column is designed to display only minor incipient damage under the same earthquake demands that would cause extensive damage on conventional columns. Even under displacement demands 50% larger than the design one, damage is maintained at a minimum level. This results in a dramatic reduction of repair cost and downtime. The work presented here is an enhancement to earlier research, as described in Restrepo et al. [2011].

The remainder of this introductory chapter covers the main features of the proposed technology, and the background on self-centering systems and composite concrete-filled tube columns. Chapter 2 illustrates the design criteria and simplified analysis tools for bridge bents incorporating these columns. Findings from quasi-static cyclic experimental investigations are presented in Chapter 3. Numerical simulations of the experiments are summarized in Chapter 4.

1.2 DUAL-SHELL COLUMN TECHNOLOGY

The “dual-shell” precast composite steel-concrete column developed in this study consists of two concentric cylindrical steel shells running for its entire height, with high-performance concrete (i.e., high-strength, high-slump, and shrinkage-compensating concrete) sandwiched in between (Figure 1.1a). The outer shell acts as permanent formwork and works in composite action with the concrete, substituting longitudinal and transverse reinforcement. The inner shell provides permanent formwork as well, reducing unnecessary weight and making the technology suitable for prefabrication and rapid erection. It also prevents concrete implosion under large compressive strains that may arise upon rocking, and delays buckling of steel dowels embedded in the concrete at the column-footing and column-bent cap interfaces.

Large inelastic rotations can be sustained at the column-footing and column-cap beam joints with minimal structural damage. These rotations are accommodated within the connections themselves, through the formation of gaps at the member ends (Figures 1.1b and 1.1c): gaps are allowed to open in tension under severe lateral displacement demand, and to nearly close at the end of the excitation, generating a rocking kinematic. Self-centering capability is provided by gravity forces and unbonded threaded post-tensioning bars designed to remain elastic.

Yielding of post-tensioning bars should be avoided because it would result in post-tensioning losses; if the elongation demand due to gap opening exceeds the bar elastic limit, additional deformable elements need to be added in series with them, such as rubber pads or ring springs. Post-tensioning bars must be protected from corrosion, e.g., by epoxy coating or sleeving and grouting. The threaded bar anchorages at the bent cap and foundation allow for eventual bar replacement should corrosion or other sources of damage be a concern. *In situ* construction tolerances require a mortar bed to be cast at the joints between the column and the footing or the cap beam; large stresses and strains may develop on the mortar upon gap opening, and crushing should be avoided to prevent post-tensioning losses.

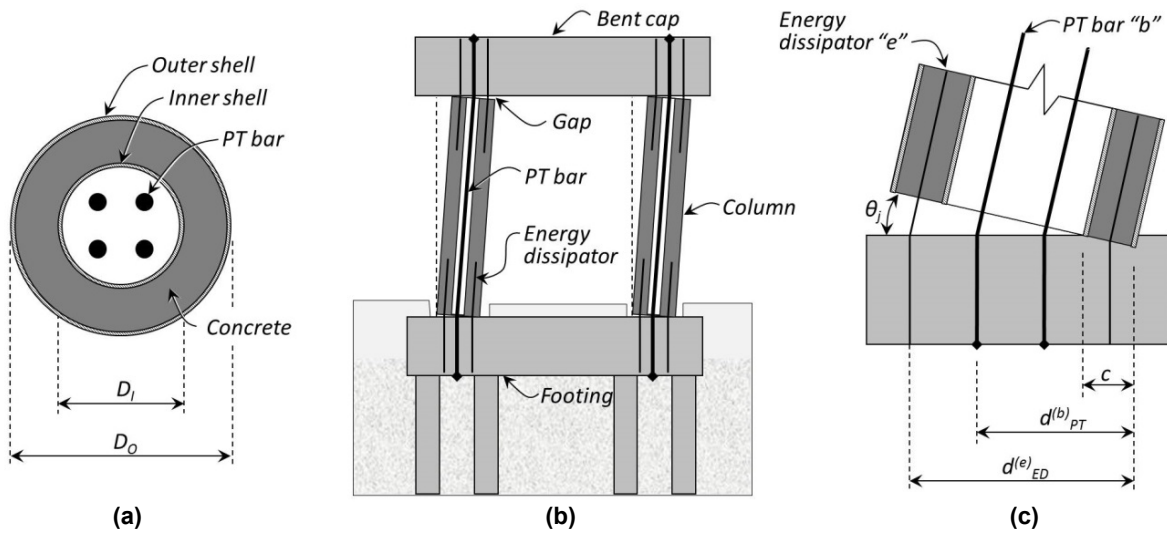


Figure 1.1 Schematics of the proposed system: (a) column typical cross-section; (b) bent components and rocking kinematics; and (c) joint rotation.

Energy dissipation takes place through axial yielding of internal steel dowels [Restrepo and Rahman 2007; Restrepo et al. 2011], or external devices [Cormack 1998; Marriott et al. 2009; and Toranzo et al. 2009], located across the column-footing or column-bent cap interfaces, as schematically shown in Figure 1.1. Under strong-intensity earthquake excitation only, these devices may undergo multiple cycles into the inelastic range, with possible need of replacement. Instead, the main structural members are prevented from experiencing significant inelastic deformations and damage, and the structure is expected to remain functional overall. Circumferential weld beads are provided on the internal surface of the outer shell near its ends [Gebman et al. 2006; Restrepo et al. 2011] that transfer tension between the internal dowels and the outer shell. External dissipators are simply connected to brackets preinstalled on the outer shell and on the footing or bent cap.

Structural systems that under the effect of lateral forces are able to rock and recenter back to their original configuration while dissipating energy within specific devices, are referred to as “hybrid systems.” Figure 1.2 compares the typical hysteretic response of these systems to conventional ductile structures and purely rocking structures. A conventional ductile system (Figure 1.2a) offers large energy dissipation, represented by “fat” hysteretic loops, at the expense of structural integrity and significant residual displacement. A purely rocking system (Figure 1.2b) is characterized by nonlinear elastic behavior with self-centering capability, but insufficient energy dissipation resulting in excessive peak displacement demand [Makris and Roussos 1998]. A hybrid system (Figure 1.2c) provides a trade-off between these two extremes: proper tuning of self-centering forces and energy dissipation produces a “flag-shaped” hysteretic response, with very small residual displacement but peak demand comparable to that of a conventional ductile system.

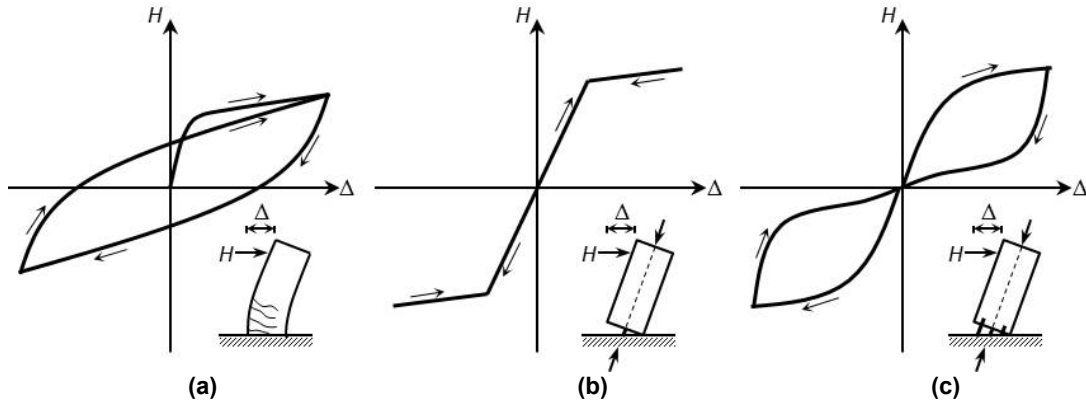


Figure 1.2 Hysteretic response: (a) conventional ductile system; (b) purely rocking system; and (c) hybrid rocking system.

1.3 BACKGROUND ON SELF-CENTERING HYBRID SYSTEMS

The concept of self-centering hybrid systems originated from the features of the “stepping” railway bridge over the South Rangitikei River, New Zealand, commissioned in 1981, where rocking is combined with torsional hysteretic energy dissipator devices [Cormack 1988]. Similar features were also provided a few years earlier to an industrial chimney of the Christchurch, New Zealand, airport [Sharpe and Skinner 1983], built in 1977.

Priestley and Tao [1993] expanded this idea and analytically investigated the behavior of moment frames incorporating partially unbonded post-tensioning tendons as lateral-force resisting systems for buildings: the lack of residual drifts following an earthquake was pointed out as the main advantage. Subsequently, MacRae and Priestley [1994] conducted experimental work on beam–column sub-assemblies featuring unbonded post-tensioning details. Stone et al. [1995] proposed a hybrid rocking system that incorporated mild reinforcement across the joint to provide hysteretic energy dissipation.

The promising results from these preliminary studies led to the “PREcast Seismic Structural Systems” (PRESSSS) program, in which an array of precast self-centering systems was investigated [El-Sheikh et al. 1999; Kurama et al. 1999]. This program culminated with the test of a 60%-scale, five-story building [Nakaki et al. 1999; Priestley et al. 1999]: the building incorporated a hybrid coupled wall designed to provide lateral force resistance in one direction of loading, and moment frames with and without unbonded tendons in the other direction.

Christopoulos et al. [2002] extended the concept of unbonded post-tensioning combined with energy dissipation to steel moment frames. Pérez et al. [2003] conducted experiments on vertically stacked wall segments prestressed with unbonded tendons. Holden et al. [2003] tested a precast hybrid wall incorporating mild steel energy dissipators, carbon fiber tendons, and steel-fiber-reinforced concrete. Restrepo and Rahman [2007] performed experiments on self-centering structural walls, by developing design strategies and details for energy dissipators. Toranzo et al. [2009] adapted the self-centering wall idea to confined masonry construction, and developed an innovative external hysteretic energy dissipator device.

Apart from the South Rangitikei River Bridge, the early development of self-centering hybrid systems focused mainly on implementation in buildings; however, interest in their

application to bridges has increased over the past twenty years. One of the pioneering experimental studies on the use of rocking bridge columns incorporating unbonded post-tensioning was carried out by Mander and Cheng [1997]. This project was followed by an experimental program conducted by Hewes and Priestley [2002], who investigated the response of segmental bridge piers incorporating unbonded post-tensioning.

A number of analytical studies were subsequently carried out that considered potential applications of self-centering solutions to bridge columns [Kwan and Billington 2003a, 2003b; Sakai and Mahin 2004; Palermo et al. 2005; Heiber et al. 2005; Ou et al. 2006; and Palermo and Pampanin 2008]. Shake table testing of cast-in-place hybrid concrete bridge columns was performed to investigate the dynamic response characteristics of these systems [Sakai et al. 2006]. Palermo et al. [2007] and Marriott et al. [2009; 2011] carried out analytical studies and quasi-static cyclic tests on monolithic, purely rocking, and hybrid concrete columns, and developed different solutions for energy dissipation. Solberg et al. [2009] conducted quasi-static and pseudo-dynamic bi-directional tests on hybrid post-tensioned bridge columns with armored rocking interfaces. Ou et al. [2010] performed large-scale experiments on precast segmental post-tensioned bridge columns.

1.4 BACKGROUND ON CONCRETE-FILLED TUBE COLUMNS

“Concrete-filled tubes” (CFTs), also termed “steel columns filled with concrete” or “in-filled composite columns,” are a type of composite steel-concrete columns which has gained interest for seismic applications in the past three decades [Shanmugam and Lakshmi 2001].

Tests conducted by Ghosh [1977] demonstrated the beneficial effect of concrete filling on the axial load and bending moment capacities. Suzuki and Kato [1981] observed that in relatively short CFTs, the confined concrete can act as a diagonal compression strut together with tension field action of the steel side walls. Experiments on circular CFT columns were performed by Prion and Boehme [1989] to study the effect of steel yield stress, tube thickness, concrete compressive strength, concrete confinement, aspect ratio (length to diameter), and load application on the whole section as opposed to load application on concrete alone. Shakir-Khalil and Zeghiche [1989] tested rectangular in-filled composite columns under pure compression and in combination with uniaxial and biaxial bending, and concluded that the failure mode of all columns was overall buckling, with no sign of local buckling of the steel section. Ge and Usami [1992] studied the buckling modes of stiffened and unstiffened in-filled columns and observed a beneficial interaction between stiffeners and concrete in delaying buckling.

Further tests on rectangular CFT columns by Shakir-Khalil and Mouli [1990] showed that the relative carrying capacity of composite-to-steel column increases when the size of the steel section is increased by using high-strength concrete. Rangan and Joyce [1992], O’Brien and Rangan [1993], and O’Shea and Bridge [1995] tested eccentrically loaded slender steel tubular columns filled with high-strength concrete: all specimens failed due to crushing of the compressed concrete, with the extreme tensile strains not reaching the yield strain of steel. Uy and Patil [1996] studied the behavior of concrete-filled high-strength steel fabricated box columns observing a similar failure mode. A number of analytical methods for the calculation of the ultimate strength of CFT columns have been proposed by Knowles and Park [1969], Neogi et al. [1969], Rangan and Joyce [1992], Ge and Usami [1994], Bradford [1996], Kato [1996], Wang and Moore [1997], and Leon et al. [2007].

Sakino and Ishibashi [1985] and Sakino and Tomii [1981] examined the behavior of short and intermediate length square CFT columns subjected to cyclic lateral forces with a constant axial load: the hysteretic loops indicated a stable response with a considerable amount of energy dissipation and some strength degradation due to local buckling in the steel shell, leading to crushing of the encased concrete. Park et al. [1983] performed an experimental and theoretical investigation into the seismic behavior of steel-encased circular reinforced-concrete (RC) bridge piles, with variable axial-load level, inclusion or exclusion of internal reinforcing cages, and continuous or discontinuous steel casing at the critical flexural sections.

Virdi and Dowling [1973] investigated the bond between concrete and the steel tube. Mechanical connectors are necessary for transferring shear between concrete and steel tube when bond capacity is likely to be exceeded such as in case of significant shear demand or under seismic loading [Gebman et al. 2006]. Boyd et al. [1995] found that the flexural ductility for columns with studded and non-studded steel shells is similar, and that the hysteretic energy dissipated by composite columns is higher than that for conventionally reinforced columns, with local steel shell buckling and concrete cracking causing some irregularities in the hysteretic response. A study was conducted by Itani [1996] to investigate the ductility of composite steel–concrete columns for use in seismic areas; full composite action between the steel jacket; the concrete was ensured by shear studs distributed throughout the length of the column.

Kitada [1998] investigated the difference in local buckling modes between cross sections of steel and composite columns in bridge columns and buildings; he observed that the ductility of the composite beam–column specimen with a rectangular cross section is smaller compared to that with a circular cross section in the case of large axial compression. As confirmed by Matsui et al. [1995], circular tubes provide a significant amount of confinement, while this effect is negligible in the case of rectangular tubes, as the hoop tension developed along the side walls is not constant.

2 Design Criteria and Simplified Analysis

2.1 DESIGN CRITERIA

Dual-shell hybrid columns can be easily designed for a single performance level that is tied to the DBE. Seven criteria should be met to ensure satisfactory performance of these columns under the corresponding target displacement: (i) minimum outer shell thickness; (ii) energy dissipators strength; (iii) composite action; (iv) mortar bed integrity; (v) concrete strain control and inner shell diameter; (vi) prevention of early dissipator fracture; and (vii) prevention of early loss of post-tensioning force [Guerrini 2014; Guerrini et al. 2015].

These criteria are implemented in a displacement-based design procedure. In compliance with Caltrans' provisions [2010], expected material properties should be used for the analysis of components undergoing significant inelastic deformations (hysteretic energy dissipators and mortar bed). Specified material properties should be referred to for components that are capacity-designed to remain elastic (post-tensioning system, column concrete, and steel shells).

2.1.1 Criterion (i): Minimum Outer Shell Thickness

As the outer shell provides confinement to the compressed concrete, tensile hoop strains rise in the shell itself. When the column is subjected to the target lateral displacement, these strains should be kept below the yield threshold to avoid permanent deformation and damage to the shell, and to preserve the composite action with the encased concrete. To meet this objective, based on previous experiments [Gebman et al. 2006; Restrepo et al. 2011] and those reported herein, the outer shell should satisfy the condition:

$$D_o/t_o \leq 100 \quad (2.1)$$

where D_o is the outer diameter and t_o the outer-shell thickness. This ratio results in a 4%-minimum volumetric confinement ratio for the concrete calculated over the solid volume of the column, which adequately confines the high-strength concrete recommended for this application.

In addition, the composite-section flexural strength needs to be equal or greater than that required by capacity design at the section where the interface dowel bars end or where the external energy dissipators are connected to the shell, assuming that flexural overstrength develops at the column rocking end(s). Similarly, adequate shear strength needs to be provided along the entire column by the outer shell and the enclosed concrete. However, these capacity-design requirements are not expected to control the design of the outer shell in typical applications.

2.1.2 Criterion (ii): Energy Dissipators Strength

Recentering forces—provided by gravity and post-tensioning—and energy dissipating forces need to be properly tuned to achieve the desired self-centering response and provide sufficient energy dissipation. Gravity and post-tensioning forces must be large enough to close the gap by overcoming the overstrength capacity of the energy dissipators, thus forcing them to yield in compression upon each load reversal [Restrepo and Rahman 2007]; that is:

$$\Lambda_C = \frac{F_{ED,O}}{P_u + F_{PT,e}} \leq 1.0 \quad (2.2)$$

where P_u is the design gravity force, $F_{PT,e}$ is the total effective post-tensioning force (after time-dependent losses), $F_{ED,O}$ is the total ultimate strength of all energy dissipators, and Λ_C is a recentering coefficient. The limitation on Λ_C could theoretically be taken as high as 1.0 (i.e., equality between dissipators overstrength force and recentering forces), but a limit of 0.6 is recommended to account for uncertainties on post-tensioning losses and for the formation of debris in the gaps.

In parallel, enough energy dissipation should be provided to the system, to avoid the large scatter on lateral displacement and acceleration demands observed on purely rocking systems [Makris and Roussos 1998]. Therefore, a second condition should be satisfied:

$$\Lambda_D = \frac{F_{ED,O}}{P_u + F_{PT,e} + F_{ED,O}} \geq 0.1 \quad (2.3)$$

where Λ_D is an energy dissipation coefficient. Combining together Equations (2.2) and (2.3) and setting the limitation $\Lambda_C \leq 0.6$ yields the following relationship:

$$0.1 \leq \Lambda_D \leq 0.4 \quad (2.4)$$

2.1.3 Criterion (iii): Composite Action

If internal dowels are used as energy dissipators, tensile stresses need to be transferred from the dowels to the outer shell through the concrete in order to develop composite steel–concrete action. As friction between steel and concrete cannot be relied on, mechanical connectors are needed: for this purpose, circumferential weld beads on the internal surface of the outer shell can be provided along the development length of the dowels [Gebman et al. 2006; Restrepo et al. 2011]. Weld beads of similar size to the outer shell thickness, spaced at about 10 times their size, have proved to be sufficient to develop the stress transfer and ensure composite action [Gebman et al. 2006].

2.1.4 Criterion (iv): Mortar Bed Integrity

In situ construction tolerances requires the casting of a mortar bed between the column ends and the adjoining footing and superstructure. Under the DBE, crushing of the mortar layer between column and footing or column and cap beam should be avoided, as it would lead to post-tensioning losses. The integrity of the mortar can be ensured by checking that, at the joint

rotation corresponding to the target lateral displacement, the neutral axis depth meets the condition:

$$c/D_o \leq 0.25 \quad (2.5)$$

where c is the neutral axis depth and D_o is the column outer diameter. This upper-bound value is suggested to limit the area of mortar subjected to large compressive strain demand and to retain enough stiffness.

The use of high-performance (i.e., high-strength, fatigue-resistant, shrinkage-compensating) cementitious materials is recommended; grout mixes incorporating metallic aggregate and polypropylene fibers are suitable for this application. Embedding headed bars in the column and in the adjoining members, with the heads matching at the interface, can help significantly in relieving the mortar bed from carrying high compressive stresses. Care needs to be taken at avoiding direct contact between the mortar bed and the stiffer steel outer shell, which may cause early crushing; it is recommended to remove any excess mortar from below (or above) the outer shell so that compression is transferred only between concrete and mortar, and between headed bars.

Bond breaker needs to be applied to the surface where gap opening is desired. The surfaces of both adjoining members should be roughened to improve shear-friction strength.

2.1.5 Criterion (v): Concrete Strain Control and Inner Shell Diameter

In order to prevent significant inner shell damage due to column concrete dilation, the neutral axis at the rocking interface should not cut the hollow core under the design-basis lateral displacement, even though a compressive strain of the order of 0.001 could be tolerated on the column concrete at the inner circle. Once the neutral-axis location is known from analysis, this limitation defines the maximum allowed inner shell diameter. Additionally, to limit column damage and inelastic deformations, the confined concrete compressive strength needs to be equal or larger than the mortar compressive strength.

In practical applications, a readily available lock-seam, helical corrugated steel pipe conforming to ASTM A760 [2010] can be used as inner shell. Strength and stiffness of the thinnest commercially-available corrugated drainage pipes are expected to be sufficient to prevent inward concrete dilation and buckling of embedded energy dissipating dowels.

2.1.6 Criterion (vi): Prevention of Early Dissipator Fracture

Particular care needs to be dedicated to the design, detailing, and fabrication of hysteretic energy dissipators, as they are expected to yield and sustain significant inelastic deformations before fracturing upon gap opening (Figure 1.1c). Two alternatives for hysteretic energy dissipators are explored herein: unbonded internal dowels with uniform cross section; and external buckling-restrained devices, consisting of a dog-bone milled steel bar encased and grouted within a steel pipe.

Both internal and external steel devices have to yield along a specific segment of length L_y (Figure 2.1) to accommodate the elongation demand, without fracturing under the design-basis lateral displacement. To prevent low-cycle fatigue fracture, the strain along the yield

segment should be limited to two-thirds the value $\varepsilon_{ED,O}$ corresponding to the peak tensile stress [Caltrans 2010]. For a design-basis joint rotation, θ_j , the required yield length L_y is given by:

$$L_y = \frac{1.5 \times \left[\theta_j \times (d_{ED}^{(e)} - c) - 12 \times \Lambda_s \times \varepsilon_{ED,y} \times d_{b,ED} \right]}{\varepsilon_{ED,O}} \quad (2.6)$$

where $d_{ED}^{(e)}$ is the distance of the extreme tensile dissipator e from the extreme compressive fiber, $\varepsilon_{ED,y}$ is the yield strain of the dissipator steel, $d_{b,ED}$ is the diameter of the energy dissipating bar (the reduced diameter for dog-bone milled bars), and c is the neutral axis depth at the design-basis lateral displacement demand.

The term $12 \times \Lambda_s \times \varepsilon_{ED,y} \times d_{b,ED}$ in Equation (2.6) accounts for yield strain penetration along the development length of non-milled energy dissipators embedded in concrete, which is assumed to be six times the bar diameter at each end [Park and Paulay 1990]. Λ_s is a strain-penetration coefficient: $\Lambda_s = 1$ for non-milled bars, in which strain penetration out of the yield segment occurs; and $\Lambda_s = 0$ for dog-bone milled bars, where strain penetration is prevented.

When using internal dowels (such as stainless-steel deformed bars) as hysteretic dissipators, it is sufficient to unbond the yield segment across the rocking interface by wrapping it with tape (Figure 2.1a). Stainless steel is recommended for this application because of its high ductility and low sensitivity to corrosion. In fact, because cracking concentrates at the rocking interface, thus exposing the dowels to corrosive environments, reducing the dowels sensitivity to corrosion is essential to guarantee a durable performance, as replacing them would be challenging. Beyond the yield segment, enough anchorage length should be provided within column and footing concrete to develop the full tensile strength of the dowel bar.

If externally connected buckling-restrained devices are chosen, highly ductile carbon steel can be used to fabricate the dog-bone milled bar: these devices can be easily inspected and replaced, bypassing the issue of corrosion sensitivity. Yielding is forced within a segment of reduced diameter d_{bR} (Figure 2.1b) by ensuring that when it reaches its maximum tensile strength $f_{ED,O}$, the stress on the virgin bar ends of diameter d_{bV} is below $f_{ED,y}$.

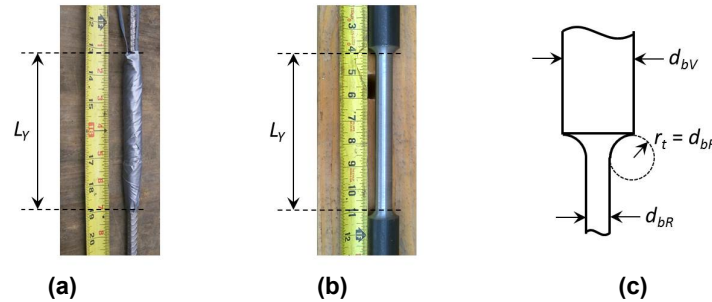


Figure 2.1 Energy dissipator details: (a) unbonded yield segment of an internal dowel, wrapped with duct tape; (b) dog-bone milled bar of a buckling-restrained device; and (c) milled bar taper detail.

In other words:

$$d_{bR} \leq d_{bV} \times \sqrt{\frac{f_{ED,y}}{f_{ED,O}}} \quad (2.7)$$

Holden et al. [2003] recommend a circular tapered transition from d_{bR} to d_{bV} , with a taper radius $r_t = d_{bR}$, as shown on Figure 2.1c, to prevent stress concentrations. A pocket should be created between the bar taper and the grout fill to avoid direct bearing and undesired overstrength when the device is in compression.

Welded connections between the virgin bar ends and brackets attached to the outer shell and the footing have been used for the experimental work described in the next sections. An undesired effect of welded connections consists of parasite moments being transferred to the bar ends, while buckling-restrained devices are intended to work in pure axial deformation. As a consequence, it is recommended to use true-pin connections at the dissipator ends.

2.1.7 Criterion (vii): Prevention of Early Loss of Post-Tensioning Force

When the gap opens at the column-footing and/or column-cap interface, the post-tensioning bars will elongate, as shown in Figure 1.1c. If a post-tensioning bar yields, that bar will display a permanent plastic elongation when the gap closes, causing a loss of post-tensioning force and compromising the system self-centering ability. To delay yielding of post-tensioning bars under the DBE and to maintain self-centering behavior, the effective post-tensioning force after time-dependent losses should range between 20% and 25% of the bar tensile strength.

When limiting the post-tensioning force is not sufficient, additional deformability can be added to each post-tensioning bar by placing elastic devices in series with the bars. Elastomeric bearing pads, inserted between the top anchor plate and the bent cap (see Figure 2.2a), have proved to be satisfactory for this application. With this configuration, the tensile deformation demand on the bars is partially transformed into compressive deformation of the bearing pads.

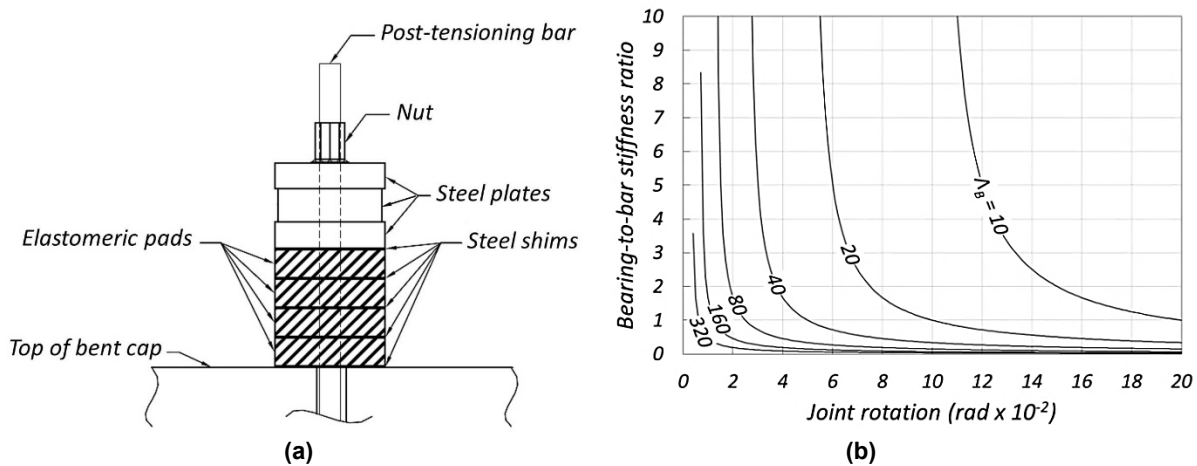


Figure 2.2 Elastomeric bearings in series with post-tensioning bars: (a) conceptual elevation; and (b) design chart.

If $F_{PT,e}^{(b)}$ and $F_{PT,y}^{(b)}$ are the effective (after time-dependent losses) and yield post-tensioning forces on the extreme tensile bar b , located at a distance $d_{PT}^{(b)}$ from the extreme compressive fiber, the yield condition under a joint rotation θ_j is expressed as:

$$F_{PT,y}^{(b)} = F_{PT,e}^{(b)} + \frac{\theta_j \times \left[(2 - n_j)(d_{PT}^{(b)} - c) + (n_j - 1)(D_O - 2 \times c) \right]}{\frac{1}{K_{PT}^{(b)}} + \frac{1}{K_B^{(b)}}} \quad (2.8)$$

where n_j is the number of column end joints subjected to gap opening ($n_j = 1$ for cantilever columns, $n_j = 2$ for fixed-fixed columns in double curvature); c is the neutral axis depth from the extreme compressive fiber; D_O is the column outer diameter; $K_{PT}^{(b)} = E_{PT} \times A_{PT}^{(b)} / L_U$ is the axial stiffness of post-tensioning bar b ; L_U , E_{PT} , and $A_{PT}^{(b)}$ are the unbonded length, elastic modulus, and cross-sectional area of post-tensioning bar b ; and $K_B^{(b)}$ is the stiffness of the bearing or other deformable device in series with bar b .

The term $\theta_j \times (2 - n_j)(d_{PT}^{(b)} - c)$ in Equation (2.8) is the elongation demand on the extreme tensile bar of a cantilever column ($n_j = 1$). Instead, the term $\theta_j \times (n_j - 1)(D_O - 2 \times c)$ gives the elongation demand for a fixed-fixed column subjected to double curvature ($n_j = 2$), which is constant for all post-tensioning bars independently of their location.

For a design-basis joint rotation θ_j , the required bearing-to-bar stiffness ratio can be found by solving Equation (2.8):

$$\frac{K_B^{(b)}}{K_{PT}^{(b)}} = \frac{1}{\theta_j \times \frac{(2 - n_j)(d_{PT}^{(b)} - c) + (n_j - 1)(D_O - 2 \times c)}{(\varepsilon_{PT,y}^{(b)} - \varepsilon_{PT,e}^{(b)}) \times L_U} - 1} = \frac{1}{\theta_j \times \Lambda_B - 1} \quad (2.9)$$

where $\varepsilon_{PT,e}^{(b)}$ and $\varepsilon_{PT,y}^{(b)}$ are the strains on bar b corresponding to effective post-tensioning and yield conditions, and:

$$\Lambda_B = \frac{(2 - n_j)(d_{PT}^{(b)} - c) + (n_j - 1)(D_O - 2 \times c)}{(\varepsilon_{PT,y}^{(b)} - \varepsilon_{PT,e}^{(b)}) \times L_U} \quad (2.10)$$

is a non-dimensional coefficient. Smaller values of Λ_B denote systems less sensitive to post-tensioning bar yielding.

If Equation (2.9) gives a negative value, bearings are not required. Furthermore, a positive value larger than 10 calculated from Equation (2.9) indicates that the required bearing pad would be very stiff compared to the bar and would accommodate very small deformations, thus providing negligible additional flexibility.

A design chart derived from Equation (2.9) is plotted in Figure 2.2b. Note that for large joint rotations θ_j , very flexible bearings are required (i.e., the required stiffness ratio is low), and their stiffness is quite insensitive to the rotation demand. However, because of the inverse proportionality relationship between the stiffness ratio and the joint rotation, when θ_j decreases, the need for bearings becomes suddenly negligible (i.e., the required stiffness ratios is high), as the curves become very steep. The transition between these two regions depends on the coefficient Λ_B . Note that the bearings become completely ineffective (i.e., the required stiffness ratio goes to infinity) when $\theta_j = 1/\Lambda_B$: this is the case when the elastic elongation capacity of the bar equals the elongation demand due to joint rotation.

The force-deformation characteristics of some elastomers—those belonging to the Voigt materials family—are sensitive to loading rate and temperature. The bearing stiffness $K_B^{(b)}$ should then be based on material properties evaluated at temperature and loading rate comparable to the expected values. The loading rate under seismic excitation can be estimated by dividing the difference $F_{PT,y}^{(b)} - F_{PT,e}^{(b)}$ by one quarter of the structure's fundamental period: in fact, due to the shallow neutral-axis depth, each bar is expected to undergo significant elongation demands under both positive and negative excursions within a full cycle.

Creep properties of the elastomeric material should be accurately known and accounted for as time-dependent deformations of the bearings may affect significantly the long-term magnitude of the post-tensioning force. Time-dependent post-tensioning losses on the order of 20%–40% of the initial force (after lock-off losses) may be anticipated, depending on the applied force, the area and thickness of the bearing, and the length of the post-tensioning bar. Incremental post-tensioning can help reduce the amount of losses due to bearing creep: most of the creep deformation happens during the first few hours after loading and can be partially compensated by staged post-tensioning.

Implementing deformable devices made of other materials such as steel ring springs may reduce the influence of loading rate and creep. However, space constraints could make these alternative options not viable in some applications.

2.2 DESIGN PROCEDURE

A step-by-step procedure for the proportioning of a dual-shell post-tensioned column is proposed herein based on the seven criteria illustrated in the previous paragraphs and on a number of design assumptions. Expected material properties shall be used for energy dissipators and mortar as they experience inelastic deformations. Specified properties shall be considered for post-tensioning bars, rubber bearings (or other similar devices), column concrete, and the outer shell, which are capacity-protected components.

Step 1: Determine the outer and inner shell diameters

Several approaches can be adopted to select the outer-shell diameter. One considers sizing an equivalent solid conventional RC column with the same diameter as the dual-shell column. Assuming a concrete strength $f'_{c,eq} = 35$ MPa (5 ksi) for the equivalent column, the outer

diameter can be determined by limiting the axial-force ratio to 10% of the capacity of the equivalent column:

$$A_{g,eq} \geq \frac{P_u}{0.1 \times f'_{c,eq}} \quad \Rightarrow \quad D_o \geq 3.6 \times \sqrt{\frac{P_u}{f'_{c,eq}}} \quad (2.11)$$

Alternatively, the designer may choose the outer-shell diameter from geometric considerations—such as limiting the shear span-to-diameter ratio—or following other proportioning criteria.

The inner-shell diameter can be sized based on initial guesses on Criteria (iv) and (v): assuming a neutral axis depth equal to $(0.20 \text{ to } 0.25) \times D_o$ and preventing it from cutting through the hollow core, the inner diameter can be taken as:

$$D_i = (0.5 \text{ to } 0.6) \times D_o \quad (2.12)$$

Step 2: Determine the outer-shell thickness

The required outer-shell thickness can be determined based on the considerations summarized in Criterion (i) and Equation (2.1), that is: $D_o/t_o \leq 100$. The chosen thickness must be confirmed for capacity-design principles at the end of the design process.

Step 3: Calculate the post-tensioning force and dissipators' strength

Several approaches can be adopted to determine the required flexural strength of the rocking interface. For this purpose, an equivalent RC column as defined in Step 1, with a longitudinal reinforcement ratio of 2% can be considered. The ultimate tensile strength of the equivalent longitudinal reinforcement is:

$$T_{O,eq} = 0.02 \times A_{g,eq} \times f_{u,eq} \quad (2.13)$$

where the ultimate (peak) steel strength for conventional Grade 60 reinforcing steel, $f_{u,eq}$, can be taken equal to 655 MPa (95 ksi) in accordance with Caltrans' provisions [2010].

The force $T_{O,eq}$ needs to be allocated among the effective post-tensioning force, $F_{PT,e}$, and the energy dissipators strength, $F_{ED,O}$, in a proportion that satisfies Criterion (ii) requirements. Assuming $F_{PT,e} = 0.25 \times F_{PT,u} \cong 0.3 \times F_{PT,y}$ in accordance with Criterion (vii), the effective post-tensioning force and energy-dissipator strength need to satisfy Equation (2.4) and:

$$T_{O,eq} = F_{PT,y} + F_{ED,O} \cong 3 \times F_{PT,e} + F_{ED,O} \quad (2.14)$$

Equation (2.14) is just a proportioning equation and need not be strictly verified. In fact, other strategies could be followed to determine $F_{PT,e}$ and $F_{ED,O}$; however, Equation (2.4) needs to be enforced whatever method is adopted, as it ensures a proper response of the hybrid system.

Step 4: Size the post-tensioning bars and elastomeric bearings

Post-tensioning bars layout shall account for the space required by anchorage devices and jacking operations. The ideal location of post-tensioning bars is close to the section centroid to

reduce the elongation demand upon gap opening; however, this may not always be possible due to space constraints. Criterion (vii) must be checked to determine if elastomeric bearings (or other deformable devices) are needed; if this is the case, then it requires determining their stiffness. At this stage of the design, the neutral axis depth c can be conservatively taken as $c \cong 0.1 \times D_o$. The target joint rotation θ_j can be approximated with an initial guess of $\theta_j = 0.03$ to 0.04 rad., but it may be desirable to associate post-tensioning bar yielding to a larger joint rotation.

Step 5: Size the energy-dissipator devices

Typically, energy dissipators are placed close to the perimeter of the column; they are embedded in the concrete or externally connected to the outer shell. The authors recommend providing at least six devices that are evenly distributed around the perimeter. Criterion (vi) can be used to determine the required yield length L_y of these components. For design purposes, it is conservative to determine L_y by assuming $\Lambda_s = 0$ in Equation (2.6). The neutral-axis depth c can be conservatively taken as $c \cong 0.1 \times D_o$. The target joint rotation θ_j can be approximated with an initial guess of $\theta_j = 0.03$ to 0.04 rad., but it may be desirable to associate energy dissipator fracture to a larger joint rotation.

Step 6: Perform interface section analysis and pushover analysis

After the main components of the column have been sized, a moment-rotation analysis of the interface section and a lateral force-displacement (pushover) analysis of the bent must be performed. A simplified analysis procedure as outlined in the following paragraphs can be used for this purpose, or a more refined approach can be adopted. Based on the secant stiffness through the reference yield point (defined below), the target lateral displacement and joint rotation demands can be determined from elastic design spectra; the equal displacement assumption between nonlinear and linear systems is typically valid for structural periods equal to or longer than 0.5 sec. It is then necessary to check that all seven criteria are met at the target joint rotation.

If Criterion (iv) is not satisfied and the neutral-axis depth is deemed excessive, then possible mitigations strategies consisting of increasing the outer diameter or the mortar compressive strength are necessary. If Criterion (v) is not met and the neutral axis cuts the hollow core, thus causing excessive strain on the concrete at the inner circle, possible solutions include reducing the inner diameter or increasing the mortar compressive strength. The confined concrete compressive strength needs to be at least equal or larger than the mortar compressive strength to limit column damage and inelastic deformations.

If Criterion (vi) is not satisfied, a longer yielding segment may be provided to the hysteretic dissipators across the interface to accommodate the target elongation. If Criterion (vii) is violated, softer bearings can be placed in series with the post-tensioning bars to prevent them from yielding, or a lower post-tensioning stress level can be adopted.

Step 7: Capacity design and detailing

The composite-section flexural strength needs to be equal or greater than that required by capacity design at the section where the interface dowel bars end or where the external energy dissipators are connected to the shell, assuming that flexural overstrength develops at the column rocking end(s). Similarly, adequate shear strength needs to be provided along the entire column by the outer shell and the enclosed concrete. Shear-friction strength across the rocking interfaces should also be checked. Conventional methods can be used to determine the above capacities.

If internal dowels are used as energy dissipators, Criterion (iii) provides guidelines to size the weld beads on the internal surface of the outer shell. If dog-bone milled steel bars are used to form external buckling-restrained dissipators, diameter ratio and taper geometry should conform to the requirements of Criterion (vi) and Equation (2.7).

2.3 SIMPLIFIED ANALYSIS PROCEDURE

Once the column cross sections and its components have been sized, it is possible to derive a pushover relationship for the bent from the moment-rotation response of the column end sections at a few loading stages [Guerrini 2014]. The pushover curve provides information on the reference yield displacement and the elastic stiffness of the system, from which its elastic period and the corresponding lateral displacement demand can be evaluated for comparison with the capacity of the system. The proposed simplified analysis method can be easily implemented in a spreadsheet.

2.3.1 Material Stress–Strain Relationships

2.3.1.1 Outer-Shell Steel

The composite steel–concrete section shall be capacity designed to remain elastic when rocking kinematics develops. In addition, the outer shell must provide adequate confinement to the column concrete before yielding. Since the outer shell is a capacity-protected component, it is necessary to know the following material properties:

- elastic modulus: E_{OS}
- specified yield stress: $f_{OS,y}$

The relationship between outer-shell steel stress f_{OS} and strain ε_{OS} is taken as elastic-perfectly plastic:

$$f_{OS} = E_{OS} \times \varepsilon_{OS} \leq f_{OS,y} \quad (2.15)$$

2.3.1.2 Post-Tensioning Steel

Linear-elastic response of the post-tensioning bars, at least up to the target drift ratio, should be ensured. Elastomeric bearings or other deformable devices may be required in series with the bars to meet this objective. Since post-tensioning bars are capacity-protected elements, it is necessary to know the following material properties:

- elastic modulus: E_{PT}
- specified yield stress: $f_{PT,y}$

The relationship between post-tensioning steel stress f_{PT} and strain ε_{PT} is taken as elastic-perfectly plastic:

$$f_{PT} = E_{PT} \times \varepsilon_{PT} \leq f_{PT,y} \quad (2.16)$$

2.3.1.3 Energy-Dissipator Steel

Energy dissipators constitute the fuse and are designed to yield under lateral displacement of the column. Consequently, the following material properties need to be assigned:

- elastic modulus: E_{ED}
- expected yield stress: $f_{ED,y}$
- expected peak stress: $f_{ED,O}$
- expected peak strain: $\varepsilon_{ED,O}$

The relationship between energy-dissipator steel stress f_{ED} and strain ε_{ED} , for both tensile and compressive deformations, is taken as elastic-perfectly plastic. Since energy dissipators will elongate far beyond their yielding limit at the target joint rotation, the elastic response is capped at the expected ultimate (peak) stress in lieu of the yield stress:

$$f_{ED} = E_{ED} \times \varepsilon_{ED} \leq f_{ED,O} \quad (2.17)$$

This is a rough approximation of the steel stress–strain relationship; however, it has proved to give satisfactorily accurate results. Knowledge of the expected yield stress and strain is required to define the first-yield and reference-yield limit states.

2.3.1.4 Concrete

The column concrete is very effectively confined by the outer steel shell. Its specified confined compressive strength needs to be greater than expected compressive strength of the mortar in order to minimize damage within the column itself. Since the column is a capacity-protected element designed to remain nearly elastic, the following concrete property needs to be defined:

- specified unconfined compressive strength: $f'_{C,c}$

The concrete behavior is mainly defined by its elastic modulus E_C . Its confined compressive strength can be calculated according to model by Mander et al. [1988]. The confinement efficiency coefficient is set to 1.0 because arching does not affect confinement provided by a continuous shell. The following set of parameters can be calculated:

$$\bullet \text{ unconfined elastic modulus: } E_C = \begin{cases} 1800 \times \sqrt{f'_{C,c}} & \text{(ksi)} \\ 4,700 \times \sqrt{f'_{C,c}} & \text{(MPa)} \end{cases} \quad (2.18)$$

- volumetric confinement ratio: $\rho_s = \frac{4 \times t_o}{D_o}$ (2.19)

- confinement efficiency coefficient: $K_{C,e} = 1.0$ (2.20)

- effective lateral confining pressure: $f'_{C,\ell} = K_{C,e} \times f_{OS,y} \times \frac{\rho_s}{2}$ (2.21)

- confined-to-unconfined strength ratio:

$$K_C = -1.254 + 2.254 \times \sqrt{1 + 7.94 \times \frac{f'_{C,\ell}}{f'_{C,c}}} - 2 \times \frac{f'_{C,\ell}}{f'_{C,c}} \quad (2.22)$$

- confined compressive strength: $f'_{C,cc} = K_C \times f'_{C,c}$ (2.23)

2.3.1.5 Mortar

The mortar bed is partially confined by the outer steel shell and the footing or bent cap thanks to the friction developed with the concrete. Since the mortar is most likely undergoing significant inelastic deformations acting as a secondary fuse, the following material property must be considered:

- expected unconfined compressive strength: $f'_{M,c}$

The mortar behavior can be represented by the model by Mander et al. [1988] and by Paulay and Priestley's [1992] equivalent stress-block. Analytical equations for the confined stress-block parameters have been formulated by Karthik and Mander [2011]. The confinement efficiency coefficient is set to 0.1 because of the low confining effect transferred through friction. The following set of parameters can be calculated:

- unconfined elastic modulus: $E_M = \begin{cases} 1800 \times \sqrt{f'_{M,c}} & \text{(ksi)} \\ 4,700 \times \sqrt{f'_{M,c}} & \text{(MPa)} \end{cases}$ (2.24)

- unconfined peak strain: $\varepsilon_{M,c0} = \begin{cases} 0.0017 + \frac{f'_{M,c}}{8700} & \text{(ksi)} \\ 0.0017 + \frac{f'_{M,c}}{60,000} & \text{(MPa)} \end{cases}$ (2.25)

- volumetric confinement ratio: $\rho_s = \frac{4 \times t_o}{D_o}$ (2.26)

- confinement efficiency coefficient: $K_{M,e} = 0.1$ (2.27)

- effective lateral confining pressure: $f'_{M,\ell} = K_{M,e} \times f_{OS,y} \times \frac{\rho_s}{2}$ (2.28)

- confined-to-unconfined strength ratio:

$$K_M = -1.254 + 2.254 \times \sqrt{1 + 7.94 \times \frac{f'_{M,\ell}}{f'_{M,c}} - 2 \times \frac{f'_{M,\ell}}{f'_{M,c}}} \quad (2.29)$$

- confined compressive strength: $f'_{M,cc} = K_M \times f'_{M,c}$ (2.30)

- confined peak strain: $\varepsilon_{M,cc0} = \varepsilon_{M,c0} \times [1 + 5 \times (K_M - 1)]$ (2.31)

- secant modulus at peak confined strength, and ratios:

$$E_{M,sec} = \frac{f'_{M,cc}}{\varepsilon_{M,cc0}} \quad (2.32)$$

$$r_M = \frac{E_M}{E_M - E_{M,sec}} \quad (2.33)$$

$$n_M = \frac{E_M}{E_{M,sec}} \quad (2.34)$$

- confined crushing strain and ratio:

$$\varepsilon_{M,ccu} = 0.004 + 2.5 \times \rho_s \quad (2.35)$$

$$x_{M,u} = \frac{\varepsilon_{M,ccu}}{\varepsilon_{M,cc0}} \quad (2.36)$$

- confined crushing strength: $f_{M,ccu} = \frac{f'_{M,cc} \times x_{M,u} \times r_M}{r_M - 1 + x_{M,u}^M}$ (2.37)

2.3.1.6 Elastomeric Bearings

Since bearings (or other devices) are intended to remain elastic together with the post-tensioning bars mounted in series, it is necessary to know the following material property:

- specified elastic stiffness: $K_B^{(b)}$

As mentioned in Criterion (vii), the force-deformation characteristics of some elastomers are sensitive to loading rate and temperature. The bearing stiffness $K_B^{(b)}$ should then be evaluated at temperature and loading rate comparable to the expected values. The loading rate under seismic excitation can be estimated by dividing the difference $F_{PT,y}^{(b)} - F_{PT,e}^{(b)}$ by one quarter of the structure's fundamental period.

Creep properties of the elastomeric material should be known and accurately accounted for, as time-dependent deformations of the bearings may significantly affect the long-term magnitude of the post-tensioning force.

2.3.2 Simplified Interface Section Analysis

For the section analysis of the rocking interface, concrete material properties are based on the expected mortar compressive strength. As discussed below, the propagation of inelastic strain within the column concrete near the interface is approximately accounted for.

2.3.2.1 Decompression Limit State

At this loading stage, the gap(s) at the column end(s) are still closed and all materials respond elastically. Since bond breaker is applied at the interface, concrete and mortar tensile strengths are taken equal to zero. Thus, from basic elastic section analysis methods, the decompression moment can be calculated as:

$$M_{j,dec} = (P_u + F_{PT,e}) \times \frac{S_C}{A_C} \quad (2.38)$$

where P_u is the design gravity force, $F_{PT,e}$ is the total effective post-tensioning force (after time-dependent losses), and the cross-section properties are based on the concrete ring alone, while the thickness of the shells can be ignored:

$$A_C = \frac{\pi}{4} \times (D_o^2 - D_i^2) \quad (2.39)$$

$$I_C = \frac{\pi}{64} \times (D_o^4 - D_i^4) \quad (2.40)$$

$$S_C = \frac{2 \times I_C}{D_o} \quad (2.41)$$

2.3.2.2 Rocking Joint Analysis

Once the decompression moment is exceeded at a joint, a gap starts opening and the rocking mechanism is activated. At any joint rotation θ_j , a trial-and-error approach is needed to determine the neutral-axis depth c , so that translation equilibrium is satisfied:

$$P_u + F_{PT} + F_{ED} - C_M = 0 \quad (2.42)$$

where P_u is the design gravity force (compression positive), F_{PT} is the total post-tensioning force at joint rotation θ_j (tension positive), F_{ED} is the total energy-dissipator force at joint rotation θ_j (tension positive), and C_M is the compressive resultant force on the mortar (compression positive).

For a given joint rotation θ_j and a trial neutral-axis depth c , the elongation on any single post-tensioning bar b located at a distance $d_{PT}^{(b)}$ from the extreme compressive fiber is:

$$\Delta L_{PT}^{(b)} = \theta_j \times \left[(2 - n_j)(d_{PT}^{(b)} - c) + (n_j - 1)(D_o - 2 \times c) \right] \quad (2.43)$$

and the corresponding resultant force on that bar is:

$$F_{PT}^{(b)} = F_{PT,e}^{(b)} + \frac{\Delta L_{PT}^{(b)}}{\frac{1}{K_{PT}^{(b)}} + \frac{1}{K_B^{(b)}}} \leq F_{PT,y}^{(b)} \quad (2.44)$$

where the symbols have the same meaning defined earlier in this chapter. The total post-tensioning force due to n_{PT} bars becomes:

$$F_{PT} = \sum_{b=1}^{n_{PT}} F_{PT}^{(b)} \quad (2.45)$$

Similarly, for a given joint rotation θ_j and a trial neutral-axis depth c , the strain increment on any single energy dissipator e located at a distance $d_{ED}^{(e)}$ from the extreme compressive fiber is:

$$\varepsilon_{ED}^{(e)} = \frac{\theta_j \times (d_{ED}^{(e)} - c)}{L_y} \quad (2.46)$$

from which the corresponding stress can be calculated based on Equation (2.17). The resultant force on that dissipator is then:

$$F_{ED}^{(e)} = E_{ED} \times \varepsilon_{ED}^{(e)} \times A_{ED}^{(e)} \leq f_{ED,O} \times A_{ED}^{(e)} \quad (2.47)$$

where $A_{ED}^{(e)}$ is the area of energy dissipator e , and all other symbols have the same meaning defined earlier in this chapter. The total energy-dissipator force due to n_{ED} devices becomes:

$$F_{ED} = \sum_{e=1}^{n_{ED}} F_{ED}^{(e)} \quad (2.48)$$

The mortar extreme compressive strain is taken equal to the joint rotation θ_j . In fact, it is reasonably accurate to assume that upon gap opening, the extreme compressive fiber shortens by $\theta_j \times c$, with inelastic deformations spreading over a length equal to c into the well-confined column concrete [Restrepo and Rahman 2007]. This leads to the equality:

$$\varepsilon_{M,cm} = \frac{\theta_j \times c}{c} = \theta_j \quad (2.49)$$

For a given joint rotation, knowing $\varepsilon_{M,cm} = \theta_j$ and the ratio $x_{M,m} = \varepsilon_{M,cm} / \varepsilon_{M,cc0}$, one can use the charts of Figure 2.3 or the equations by Karthik and Mander [2011] to determine the equivalent stress-block parameters α_{cc} and β_{cc} . For a trial neutral-axis depth c , the compressive resultant C_M and its location y_M from the section centroid can be calculated as follows (see Figure 2.4 for the geometric meaning of γ_M):

$$\gamma_M = \arccos\left(\frac{D_o - 2 \times \beta_{cc} \times c}{D_o}\right) \quad (2.50)$$

If the equivalent compression stress-block extends within the hollow core, or in other words $(\beta_{cc} \times c) > (D_o - D_i)$, the mortar compressive resultant shall be modified to account for the removed material. In this case, one can consider a fictitious compressive resultant C_H over the hollow-core area, which needs to be subtracted from the mortar compressive resultant, and its location y_H from the section centroid (which is positive if towards the compression side):

$$\gamma_H = \arccos\left(\frac{D_o - 2 \times \beta_{cc} \times c}{D_i}\right) \quad (2.54)$$

$$C_H = \alpha_{cc} \times f'_{M,cc} \times D_i^2 \times \frac{\gamma_H - \sin \gamma_H \times \cos \gamma_H}{4} \quad (2.55)$$

$$y_H = \frac{D_i \times \sin^3 \gamma_H}{3 \times (\gamma_H - \sin \gamma_H \times \cos \gamma_H)} \quad (2.56)$$

The translation equilibrium and the moment capacity become, respectively:

$$P_u + F_{PT} + F_{ED} - C_M + C_H = 0 \quad (2.57)$$

$$M_j = \sum_{b=1}^{n_{PT}} (F_{PT}^{(b)} \times y_{PT}^{(b)}) + \sum_{e=1}^{n_{ED}} (F_{ED}^{(e)} \times y_{ED}^{(e)}) + C_M \times y_M - C_H \times y_H \quad (2.58)$$

2.3.2.3 First-Yield and Reference-Yield Limit States

The first-yield limit state is defined as the stage when the extreme tensile energy dissipator reaches its yield strain. This corresponds to a joint rotation:

$$\theta'_{j,y} = \frac{\varepsilon_{ED,y} \times L_Y}{d_{ED}^{(e)} - c} \quad (2.59)$$

where $d_{ED}^{(e)}$ is the distance of the extreme tensile dissipator e from the most compressive fiber. This value can be input in the above rocking joint analysis to determine by trial-and-error the neutral-axis depth and the corresponding first-yield moment $M'_{j,y}$.

Stiffness reduction on the moment-rotation response becomes significant after yielding propagates to the location of the tensile resultant. It can be assumed that the strain on the extreme tensile dissipator is twice the yield strain at this stage:

$$\theta_{j,y} = \frac{2 \times \varepsilon_{ED,y} \times L_Y}{d_{ED}^{(e)} - c} \quad (2.60)$$

where $d_{ED}^{(e)}$ is the distance of the extreme tensile dissipator e from the most compressive fiber. This value can be input in the above rocking joint analysis to determine by trial-and-error the neutral-axis depth and the corresponding reference-yield moment $M_{j,y}$. This loading stage can be taken as a reference point to establish yielding at the cross-section level, even though other definitions could be used as well.

2.3.3 Simplified Pushover Analysis

By knowing the moment-rotation relationship for the end joints at a few significant points (e.g., decompression, first-yield moment, reference-yield moment, and target drift), a simplified relationship between base-shear and drift-ratio can be derived. For columns in fixed-fixed conditions, it is assumed that equal moments are resisted at the two ends.

2.3.3.1 First-Order Base Shear

The first-order base shear V corresponding to a given end moment M_j , resisted by a column of length H , is:

$$V = \frac{n_j \times M_j}{H} \quad (2.61)$$

where $n_j = 1$ for a cantilever column, and $n_j = 2$ for a fixed-fixed column in double curvature. For cantilever columns, H shall be taken as the height of the center of mass above the rocking interface at the column base. For fixed-fixed columns, H shall be taken as the longitudinal distance between the top and bottom rocking interfaces.

Note that due to shear in the bent cap, the column axial load in multiple-column bents varies as the superstructure displaces laterally. This variation, which has an effect on the interface section response, can be captured by a more refined analysis; however, in the context of this simplified approach, one can assume that the effects of increasing and decreasing axial load in opposite columns cancel out, and that the average lateral response is not significantly affected. Another approximation is assuming the location of the inflection point at column mid-height, while bent-cap flexibility may cause it to shift at a higher location.

2.3.3.2 First-Order Displacement and Drift Ratio

End joint rotation, elastic flexural deformation, and elastic shear deformation contribute to the total lateral displacement [Restrepo and Rahman 2007; Tobolski 2010]:

$$\Delta = \Delta_j + \Delta_f + \Delta_v \quad (2.62)$$

The joint-rotation contribution is activated only after reaching the decompression limit state, and is given by a rigid-body rotation of the column:

$$\Delta_j = \theta_j \times H \quad (2.63)$$

The elastic contributions due to flexural and shear deformations are, respectively:

$$\Delta_f = \frac{V \times H^3}{3 \times n_j^2 \times E_C \times I_T} \quad (2.64)$$

$$\Delta_v = \frac{V \times H}{G_C \times A_{T,s}} \quad (2.65)$$

Reasonable approximations for the concrete shear modulus and shear area are $G_C \cong 0.4 \times E_C$ and $A_{T,s} \cong 0.9 \times A_T$, respectively; under these assumptions, the elastic displacement due to column deformation becomes:

$$\Delta_f + \Delta_v \cong \frac{V \times H}{E_C} \times \left(\frac{H^2}{3 \times n_j^2 \times I_T} + \frac{2.8}{A_T} \right) \quad (2.66)$$

where the transformed area and moment of inertia are, respectively:

$$A_T = \pi \times \left[\frac{D_o^2 - D_I^2}{4} + \left(\frac{E_{OS}}{E_C} - 1 \right) \times D_o \times t_o \right] \quad (2.67)$$

$$I_T = \pi \times \left[\frac{D_o^4 - D_I^4}{64} + \left(\frac{E_{OS}}{E_C} - 1 \right) \times \frac{D_o^3 \times t_o}{8} \right] \quad (2.68)$$

Summing the above components and dividing by the column length, the total drift ratio becomes:

$$\theta = \frac{\Delta}{H} \cong \theta_j + \frac{V}{E_C} \times \left(\frac{H^2}{3 \times n_j^2 \times I_T} + \frac{2.8}{A_T} \right) \quad (2.69)$$

Before reaching the decompression limit state, the term θ_j is equal to zero as there is no rigid-body rotation at the column end(s).

2.3.3.3 Simplified Consideration of P-Delta Effects

Given the moment M_j at the column end(s), one can think that a fraction of M_j balances the overturning effect induced by the lateral force (second-order base shear V_{II}), while another part resists the overturning effect caused by lateral displacement of the gravity force (the P - Δ effect):

$$n_j \times M_j = V_{II} \times H + P_u \times \Delta \quad (2.70)$$

An approximate correction for P - Δ effects consists of calculating the lateral displacement based on first-order principles—as illustrated earlier—then subtracting from the first-order base shear the amount of overturning resistance taken by the displaced gravity force:

$$V_{II} \cong \frac{n_j \times M_j}{H} - \frac{P_u \times \Delta}{H} = V - P_u \times \theta \quad (2.71)$$

The exact formulation would require determining the elastic component of the drift under the second-order base shear in combination with the uniform bending moment due to the displaced vertical force, thus leading to an iterative approach. However, this simplified method provides a good estimate of P - Δ effects incidence on the lateral response.

2.3.3.4 Elastic Stiffness and Displacement Ductility

Following the procedure exposed above, the lateral displacement Δ_y and the first-order base shear V_y corresponding to the reference yield moment $M_{j,y}$ can be calculated. The elastic stiffness can be taken as the secant stiffness through the reference yield point:

$$K = \frac{V_y}{\Delta_y} \quad (2.72)$$

This stiffness can be used to determine the elastic period of the bent and the associated displacement demand. The reference yield point can be used to establish the displacement ductility μ_{Δ} at any stage of loading:

$$\mu_{\Delta} = \frac{\Delta}{\Delta_y} \quad (2.73)$$

2.3.4 Experimental Validation

The proposed simplified analysis procedure has been applied to the two test units described in Chapter 3. Both units were designed for a target drift ratio equal to 3%. Due to the test configuration, gravity-like forces were always parallel to the column longitudinal axis and did not cause P - Δ interaction; consistently, the pushover curves have not been corrected for P - Δ effects.

The measured mechanical properties have been assigned to the energy dissipator steel (elastic modulus, yield stress and strain, peak stress and strain), to the mortar bed and column concrete (compressive strength on the day of testing), and to the elastomeric bearings (elastic stiffness). Specified properties have been used for the post-tensioning bars and outer-shell steel.

Five points have been determined to build the monotonic moment-rotation and pushover relationships for Unit 1A with external buckling-restrained energy dissipators, and for Unit 1B with internal stainless-steel dowels:

- decompression at the column base
- first-yielding of the extreme energy dissipator in tension
- base joint rotation of 0.003 rad
- base joint rotation of 0.015 rad
- base joint rotation of 0.03 rad
- fracture of the most-tensile dissipator when reaching two-thirds of its peak strain.

The backbone curves obtained from the simplified pushover analysis are compared with the recorded cyclic experimental responses plotted in Figure 2.5. Lateral displacements have been normalized by the height of the lateral force application point above the column base and thus expressed as drift ratios; lateral forces have been normalized by the applied vertical load (equivalent to the seismic weight) and thus transformed into base shear coefficients.

Good agreement can be observed throughout the force-displacement response, with approximations of the order of 10% or less on the base-shear coefficient. Also the drift ratios at onset of energy dissipator fracture (sudden jumps on the experimental curves at drift ratios of about $\pm 7\%$) are anticipated with satisfactory accuracy. Different post-yield slopes can be observed in the two predicted relationships: this is mainly caused by the different stiffness of the rubber pads in series with the post-tensioning bars, since Unit 1A was equipped with pads about three times stiffer than Unit 1B.

The same method has been used to anticipate the neutral-axis depth at every displacement increment of the test protocol. The simplified procedure shows less accuracy when predicting this parameter, as shown in Figure 2.6 where the neutral-axis depth is normalized by the column

outer diameter. Only the general trend has been captured by the analysis. This may be due to (1) the approximation in the material stress–strain relationships, and (2) the lack of consideration for damage accumulation in the monotonic constitutive laws.

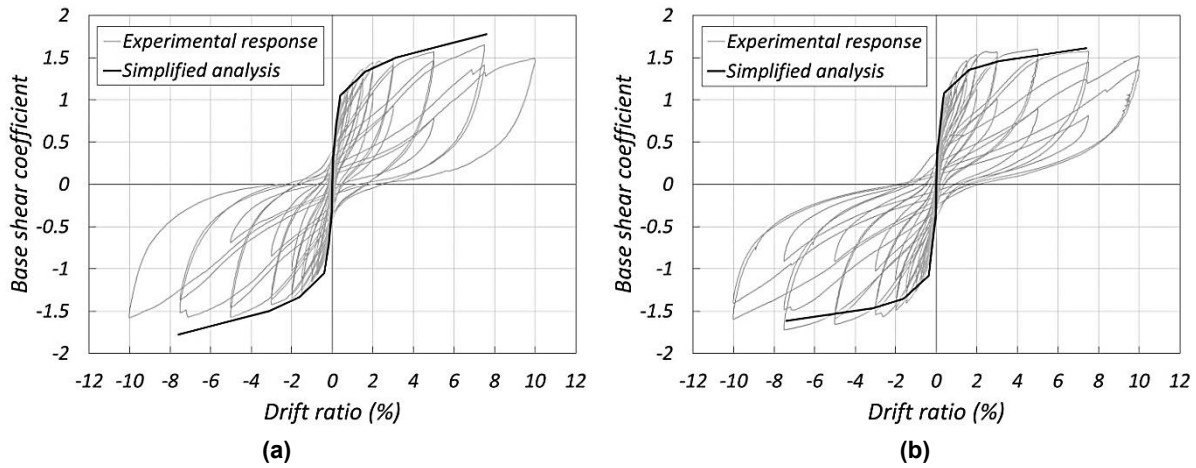


Figure 2.5 Comparison between simplified pushover envelopes and experimental cyclic responses: (a) Unit 1A and (b) Unit 1B.

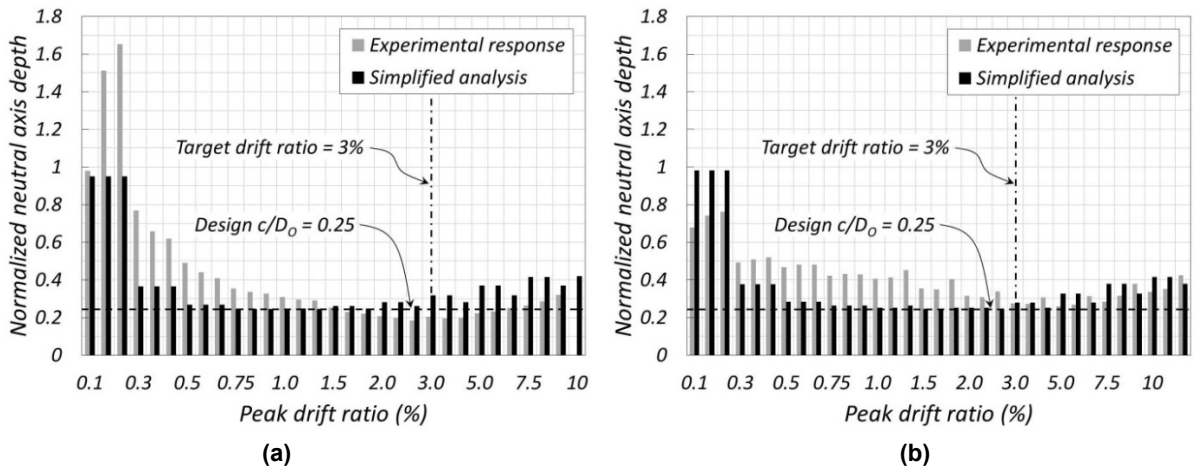


Figure 2.6 Comparison between simplified prediction and experimental neutral-axis depth: (a) Unit 1A and (b) Unit 1B. Only positive cycles are shown.

3 Experimental Program

3.1 TEST OVERVIEW

Two dual-shell column test units, named Unit 1A and Unit 1B, were subjected to quasi-static cyclic tests at the U.C. San Diego Powell Structural Engineering Laboratories. The specimens were built at 1-to-2.4 length scale. Detailed construction drawings are provided in Appendix A.

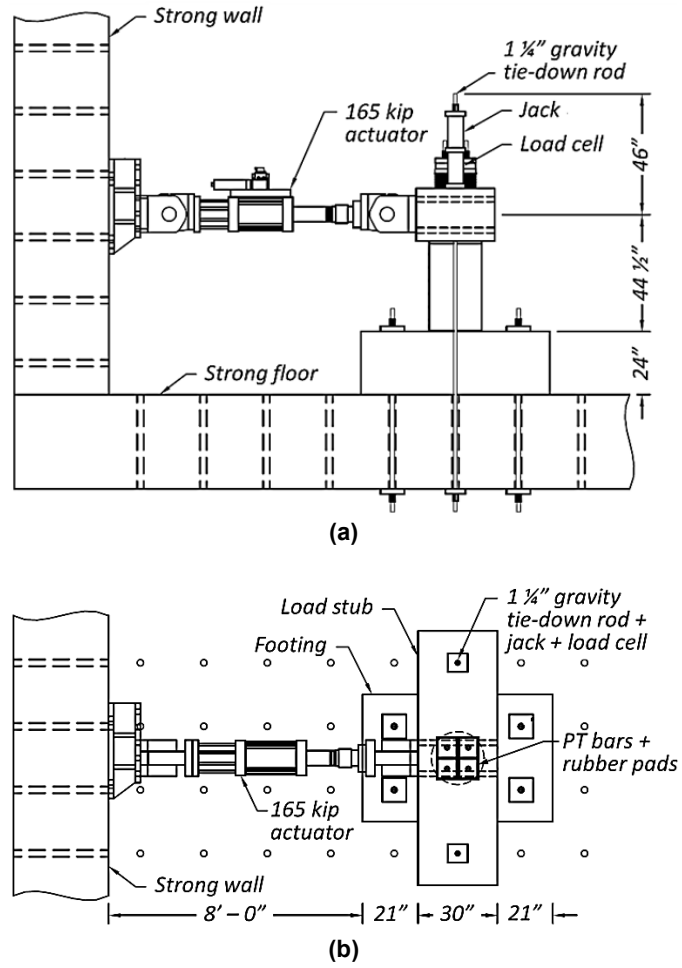
3.1.1 Target Performance Objectives

The test specimens were designed for a target drift ratio of 3% without structural damage. At this drift ratio, post-tensioning bars were expected to remain elastic, and the stiffness of the elastomeric bearings was determined accordingly. Also, the energy dissipators were designed to not fracture at the target drift ratio: the milled length of the external buckling-restrained devices and the unbonded length of the internal dowels were calculated on this basis. In order to preserve the system's self-centering behavior at the target drift ratio, the mortar bed was designed to crush under larger lateral displacements. Energy dissipation coefficients $\Lambda_D = 0.30$ and $\Lambda_D = 0.37$ were provided to Unit 1A and Unit 1B, respectively.

3.1.2 Specimens Configuration

Figure 3.1 shows the two dual-shell cantilever column units in cantilever configuration, with fixed base and lateral forces/displacements applied to the top. Both test units included:

- composite column
- footing
- load stub
- mortar bed
- energy dissipators
- post-tensioning bars
- elastomeric pads



(c)



(d)

Figure 3.1 Test configuration and dimensions: (a) side elevation; (b) plan view; (c) overview of Unit 1A; and (d) overview of Unit 1B.

Unit 1A was equipped with external buckling-restrained energy dissipators, while Unit 1B incorporated internal dowel bars. Given their precast nature, the footing, column, and load stub were cast separately; after the concrete had hardened, they were initially assembled as Unit 1A. When testing of Unit 1A was completed, the three components were taken apart, the column was flipped upside-down, and they were reassembled as Unit 1B. Only the bottom region of the column was subjected to large strains and experienced minor damage during the first test; the other end was still free of any damage. By doing this, it was possible to take advantage of both ends of the element [Massari 2012; Vervelidis 2012; Guerrini 2014; and Guerrini et al. 2015].

The overall column diameter was $D_o = 0.51$ m (20 in.), its clear height was $H_c = 0.84$ m (33 in.), and the total cantilever span from the base to the point of lateral load application was $H = 1.13$ m (44.5 in.). A low aspect ratio of $H/D_o = 2.2$ was chosen to impose more critical conditions for shear sliding at the base. Moreover, a short element can accommodate short post-tensioning bars, which are more susceptible to yielding due to their lower axial deformability.

3.2 SPECIMEN COMPONENTS

3.2.1 Composite Column

The column outer shell had a diameter $D_o = 0.51$ m (20 in.) and a thickness $t_o = 6.4$ mm (0.25 in.): that is $D_o/t_o = 80$. The inner shell had a diameter $D_i = 0.36$ m (14 in.) and a thickness $t_i = 3.2$ mm (0.125 in.): that is $D_i/t_i = 112$. Details are shown in Figure 3.2. The shells were obtained by folding and welding plates made of Grade 50 A572 steel, with yield stress of 345 MPa (50 ksi). In practice, the inner shell would be a corrugated drainage pipe [Restrepo et al. 2011]. Figures 3.2a and 3.2b show the two end sections, which served as base cross sections for Unit 1A and Unit 1B, respectively. A longitudinal section with the column oriented as in Unit 1A is depicted in Figure 3.2c.

The outer shell was equipped with six radially distributed 12.7-mm- (0.5-in.-) thick steel brackets welded to the external surface (Figure 3.2d) for the connection of the buckling-restrained dissipators of Unit 1A. Six 50.8-mm- (2-in.-) diameter, 0.46-m- (18-in.-) long corrugated metal ducts were embedded in the concrete for the installation of the internal dowels of Unit 1B; see Figure 3.2e. Three circumferential 9.5-mm- (3/8-in.-) weld beads on the internal surface of the outer shell provided tensile stress transfer between the dowels and the shell; see Figure 3.2f.

High-performance, normal-weight concrete was used to cast the column, with a specified compressive strength of 62 MPa (9.0 ksi) at 56 days. The compressive strengths measured at 28 days, 49 days (day of testing of Unit 1A) and 96 days (day of testing of Unit 1B) were 66 MPa (9.5 ksi), 70 MPa (10.2 ksi), and 72 MPa (10.4 ksi), respectively. After hardening, the concrete surfaces were roughened to improve shear-friction between column and mortar bed, as shown on Figure 3.2g. A bond-breaker film was applied to the bottom surface of the column to facilitate separation from the mortar bed and opening of the gap.

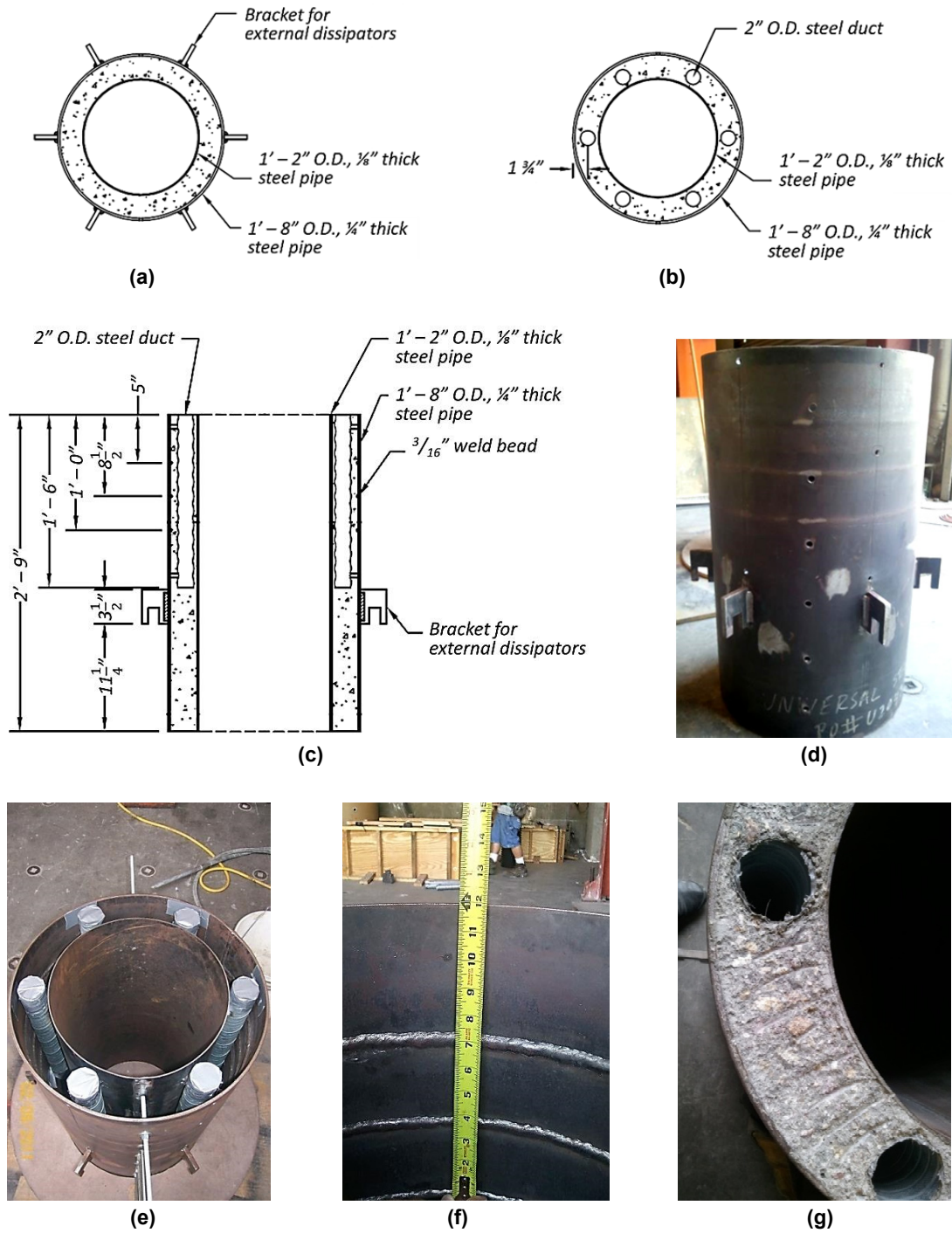


Figure 3.2 Column details: (a) Unit 1A base cross-section; (b) Unit 1B base cross-section; (c) column longitudinal section; (d) outer shell with brackets for connection of external dissipators; (e) concentric shells and ducts for future grouting of internal dissipators; (f) weld beads on the outer-shell internal surface; and (g) roughened concrete surface.

3.2.2 Footing

The footing consisted of a 1.83-m- (6-ft-) long, 1.22-m- (4-ft-) wide, 0.61-m- (2-ft-) deep RC block (Figure 3.3), which was cast with the same concrete used for the column.

Ten #6 (19-mm-diameter) top and bottom “U” bent bars provided longitudinal reinforcement, while ten #3 (9.5-mm-diameter) four-leg stirrups constituted the transverse reinforcement. Two #3 bars were placed along each side face of the foundation as skin reinforcement. All the reinforcement consisted of Grade 60 A615 steel bars, with a specified yield strength of 420 MPa (60 ksi).

Two series of six 50.8-mm- (2-in.-) diameter corrugated steel ducts were placed in the footing for future installation of the energy dissipators. Four PT-bar anchorages were also preassembled and embedded in the footing. A #3 (9.5-mm-diameter) spiral at 76.2-mm- (3-in.-) pitch, with a diameter of 660 mm (26 in.), was placed around the corrugated steel ducts and PT-bar anchorages to confine the concrete (Figure 3.3d). After the concrete had hardened, the footing surface below the column base was roughened to improve shear-friction between footing and mortar bed.

The footing was connected to the strong floor by means of four 44.5-mm- (1.75-in.-) diameter tie-down rods tensioned at 979 kN (220 kips) each. Four 63.5-mm- (2.5-in.-) diameter PVC pipes were provided in the footing to accommodate these rods.

3.2.3 Load Stub

The load stub on the top of the column consisted of a 2.44-m- (8-ft-) long, 0.76-m- (30-in.-) wide, 0.51-m- (20-in.-) deep RC beam (Figure 3.4), cast with the same concrete used for the column.

Four #6 (19-mm diameter) top and bottom “U” bent bars provided longitudinal reinforcement, while sixteen #3 (9.5-mm-diameter) two-leg stirrups at 150-mm (6-in) on-center constituted the transverse reinforcement. All the reinforcement consisted of Grade 60 A615 steel bars, with a specified yield strength of 420 MPa (60 ksi).

Four horizontal 63.5-mm- (2.5-in.-) diameter PVC pipes were provided in the load stub for connecting the actuator. Four vertical 50.8-mm- (2-in.-) diameter PVC ducts allowed the post-tensioning bars to run through the load stub. After the concrete had hardened, the load-stub surface right above the column top was roughened to improve shear-friction between load stub and hydrostone.

Two vertical 63.5-mm- (2.5-in.-) diameter PVC pipes were placed close to the beam ends; tie-down rods ran through these pipes to apply vertical forces simulating gravity.

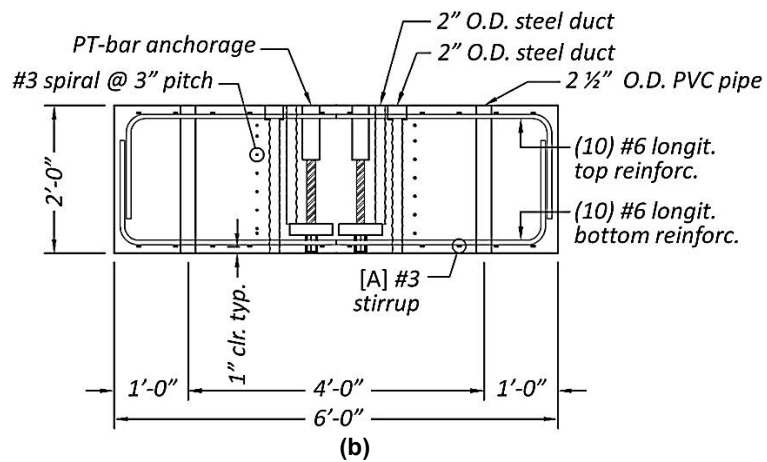
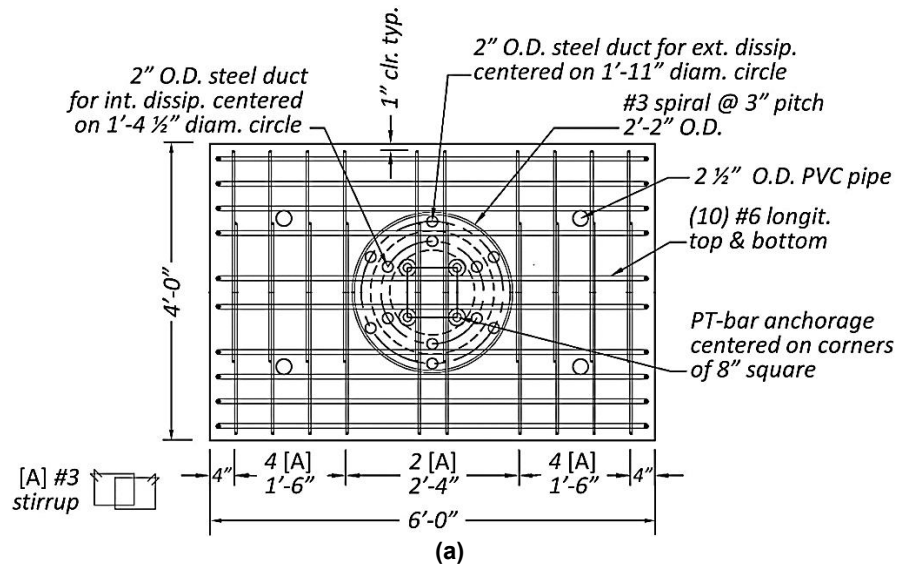


Figure 3.3 Footing details: (a) horizontal section; (b) longitudinal section; (c) reinforcement, ducts, and formwork; and (d) steel ducts and spiral reinforcement.

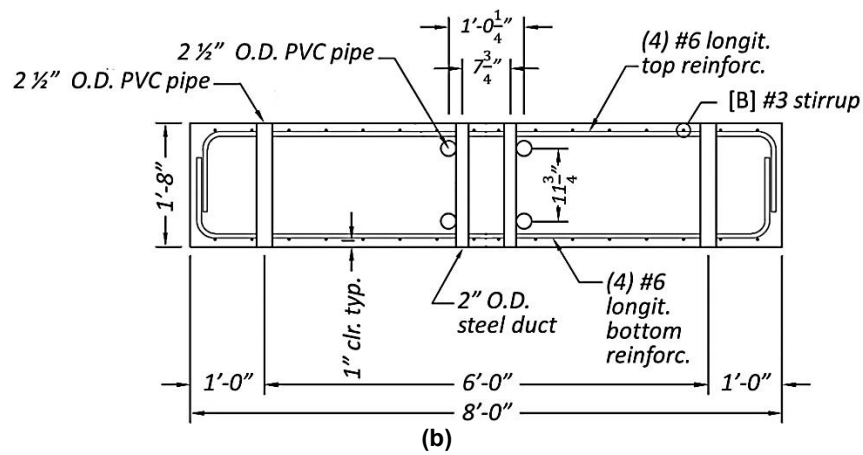
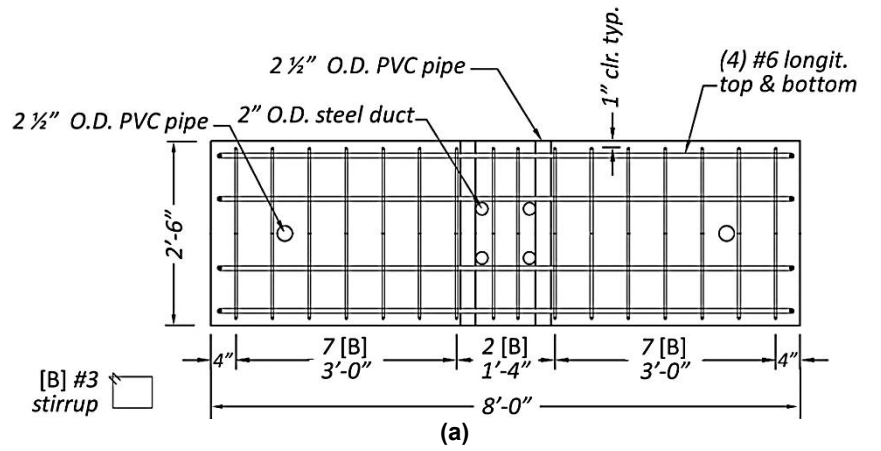


Figure 3.4 Load-stub details: (a) horizontal section; (b) longitudinal section; and (c) reinforcement, ducts, and formwork.

3.2.4 Mortar Bed

A 12.7-mm- (0.5-in.-) thick mortar bed was cast at the column-to-footing connection to compensate for expected *in situ* construction tolerances. A high-performance metallic grout mix, formulated to a plastic consistency in the form of a mortar bed, was used in Unit 1A. The mortar compressive strengths were 45.8 MPa (6.6 ksi) and 50.4 MPa (7.3 ksi) at 21 and 23 days (day of testing of Unit 1A), respectively. For the column-footing joint of Unit 1B, the same product was used, but to increase the mortar toughness polypropylene fibers were added in the proportion of 0.035% by weight; strengths of 53.4 MPa (7.8 ksi) and 52.9 MPa (7.7 ksi) were obtained at 28 and 35 days (day of testing of Unit 1B).

A wood template was employed to guide the column, and 12.7-mm- (0.5-in.-) diameter nylon rods were used as shims to hold the column in place while the mortar was wet; see Figure 3.5a). The mortar was scraped from underneath the outer shell (Figure 3.5b) to prevent the shell from causing premature crushing under direct compression transfer, a problem noted in earlier experiments [Restrepo et al. 2011]. All interface surfaces had been previously roughened to improve shear-friction transfer. Since the upper joint between column and load stub was not critical because of the low bending moment at this location, hydrostone was placed to match the two pieces there.

3.2.5 Energy Dissipators

3.2.5.1 Unit 1A: External Buckling-Restrained Devices

Six external, buckling-restrained energy dissipators were incorporated in test Unit 1A and radially distributed around the column perimeter (Figure 3.6). These devices consisted of dog-bone milled steel bars, which provided dissipation by material hysteresis over a specific reduced-diameter segment. Each 343-mm- (13.5-in.-) long steel bar had an original diameter of 25.4 mm (1 in.), which was reduced to 14.3 mm (9/16 in.) in the 165-mm- (6.5-in.-) long milled portion. Hot-rolled A576 steel was used, with a measured yield strength of 331 MPa (48 ksi), ultimate (peak) tensile strength of 490 MPa (71 ksi), and strain of 20% at the peak.



Figure 3.5 Mortar bed: (a) wood template and nylon-rod shims, during mortar placement; and (b) mortar scraped from underneath the outer shell.

In order to prevent buckling, the milled part was encased and grouted within a steel pipe; grease was used to reduce friction between bar and grout. Mastic tape, about 3 mm (0.125 in.) thick, was applied along the tapered segments, to create pockets and reduce bearing of the non-milled ends on the grout.

The external dissipators were welded to brackets connected to the footing and to the column outer shell. All brackets were obtained from 12.7-mm- (0.5-in.-) thick A572 Grade 50 steel plates, with a specified yield stress of 345 MPa (50 ksi), and were proportioned to resist the ultimate strength of the devices. The footing brackets were welded to #6 Grade 60 A706 steel reinforcing bars that were grouted within prepositioned ducts. The grout was mixed to a fluid consistency and had compressive strength equal to 47.1 MPa (6.8 ksi) on the day of testing.

All welds were performed with an E70 electrode (strength at least equal to 480 MPa or 70 ksi) and were designed to withstand the ultimate strength of the dissipators.

3.2.5.2 Unit 1B: Internal Dowels

Unit 1B was equipped with six internal dowels at the column-footing joint, which acted as internal energy dissipators; see Figure 3.7. Grade 75 316LN stainless steel #4 deformed bars were used for this purpose. To inhibit the bond along the length of the dowel, they were wrapped with duct-tape for a length of 178 mm (7 in.) across the column-footing interface. Material testing showed a yield stress of 745 MPa (108 ksi), an ultimate (peak) tensile strength of 889 MPa (129 ksi), and a strain of 15% at the peak.

The dowels were first grouted within corrugated steel ducts predisposed in the footing, then, after column placement on the footing, they were grouted within the column ducts. The footing grout, mixed at fluid consistency, had compressive strength of 52.7 MPa (7.6 ksi) on the day of testing, while the column grout attained a compressive strength of 59.2 MPa (8.6 ksi).

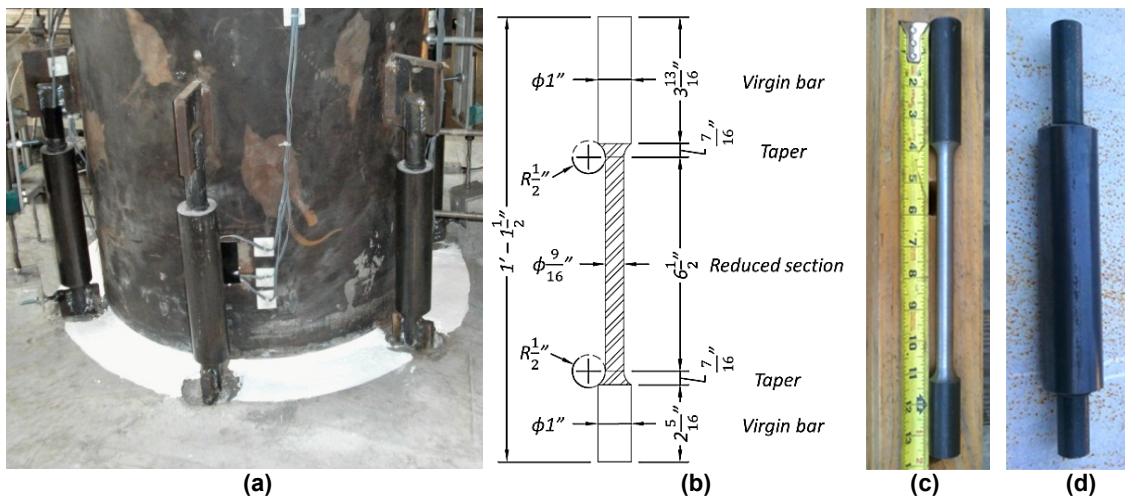


Figure 3.6 External energy dissipators: (a) location around column perimeter; (b) milled-bar dimensions; (c) dog-bone milled steel bar; and (d) assembled buckling-restrained device.

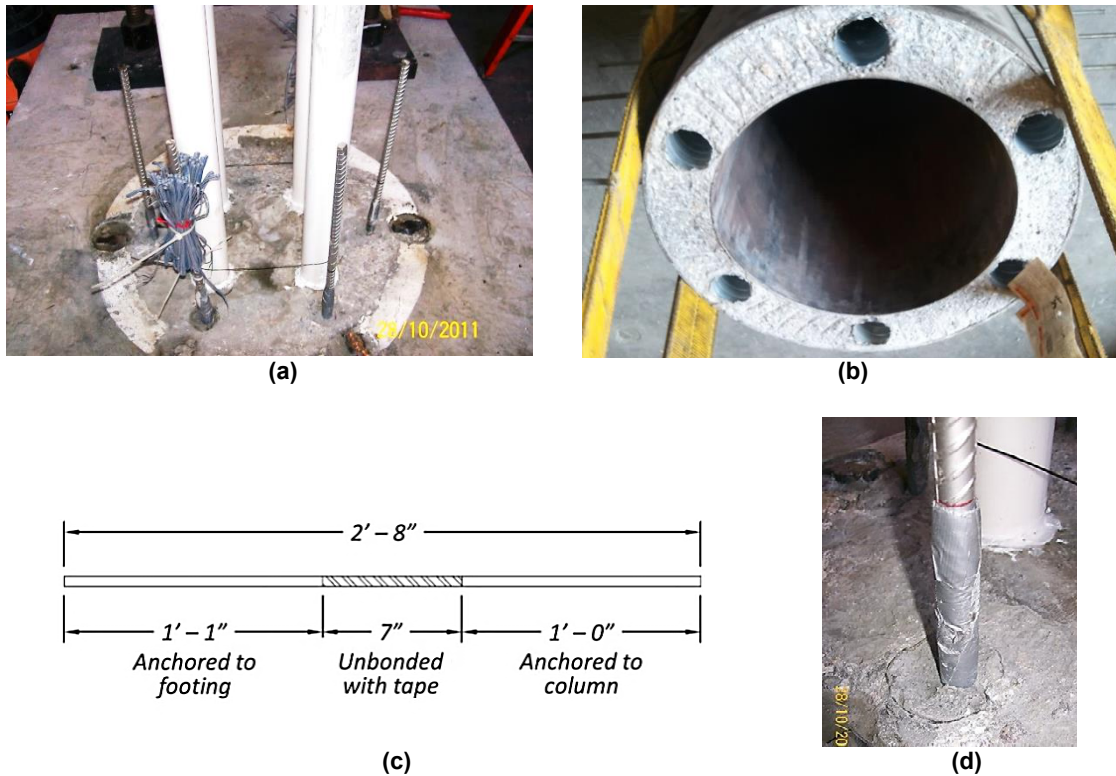


Figure 3.7 Internal energy dissipators: (a) dowels grouted in the footing; (b) ducts in the column; (c) dowel dimensions; and (d) detail of bar wrapping across the interface.

3.2.6 Post-Tensioning Bars

Four 34.9-mm- (1-3/8-in.-) diameter, A722-Grade-150 threaded bars provided the post-tensioning force to both units (Figure 3.8). After all losses, the total effective post-tensioning force was 845 kN (190 kips) in Unit 1A and 890 kN (200 kips) in Unit 1B. Jacking forces of 311 kN (70 kips) were applied to each bar to compensate for lock-off and bearing creep losses. The post-tensioning bars were screwed into anchorage devices prearranged in the footing, allowing for bar replacement; see Figure 3.8a. They were placed inside the column hollow core and sleeved in ducts filled with fluid grout to protect them from corrosion; see Figure 3.8b. Additional bar deformability was provided by rubber (Unit 1A) or polyurethane (Unit 1B) bearings that were placed in series with the post-tensioning bars between the top anchorage plates and the load stub.

Each bar anchorage in the footing was made of a bar segment, with the same 34.9 mm (1 3/8 in). diameter dimensions as the anchoring bar, and a length of 0.5 m (19.5 in). A plate and a nut were provided at the lower end, while a coupler was provided at the upper end to connect the bar; see Figures 3.8c and 3.8d). In order to rely exclusively on bearing of the bottom plate against the concrete, the bar segment was unbonded by duct-tape wrapping: this detail was intended to prevent post-tensioning losses due to bar slippage following bond failure along the threads. Combining the main bar and the anchorage segment, the total unbonded bar length was 2.16 m (85 in.).

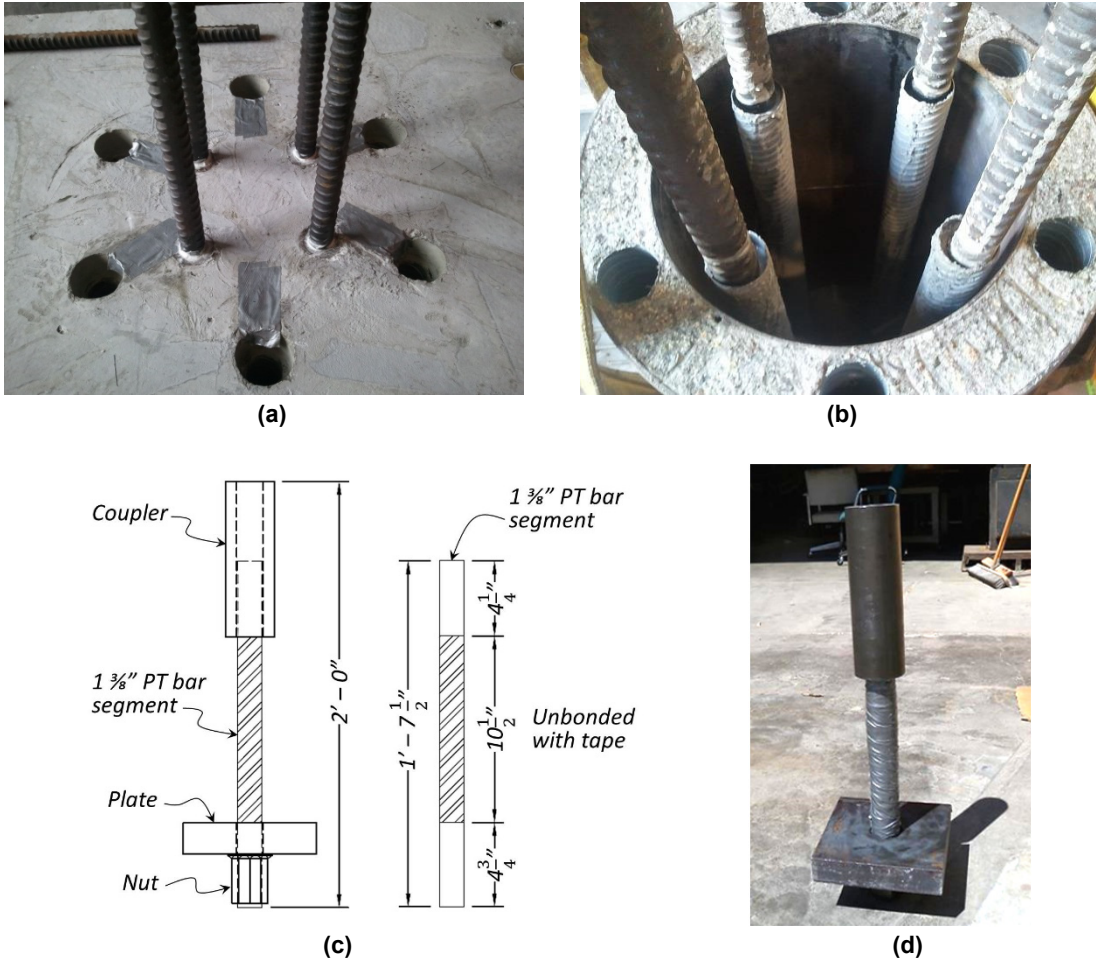
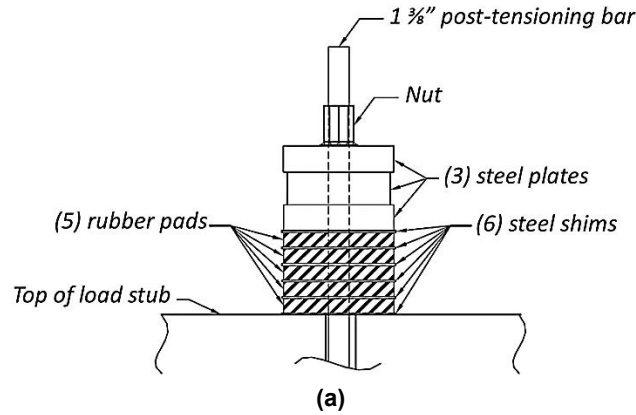


Figure 3.8 Post-tensioning bars: (a) bars screwed into the footing anchorages; (b) sleeved bars inside the hollow core; (c) anchorage components; and dimensions; (d) assembled anchorage device.

3.2.7 Elastomeric Pads

3.2.7.1 Unit 1A: Natural Rubber Pads

A bearing consisting of five square 80-Shore-A hardness rubber pads was provided to each post-tensioning bar in test Unit 1A (Figure 3.9). The pads were 190.5 mm (7.5 in.) square \times 25.4 mm (1 in.) thick, with a 41.3-mm- (1-5/8-in.-) diameter central hole to accommodate the post-tensioning bars. The pads were stacked and alternated with 3.2-mm- (1/8-in.-) thick square steel shims of the same plan dimensions. The shims were bonded to the pads by an epoxy adhesive, with the scope of limiting lateral dilation of the rubber pads under compression; however, this practice proved to be ineffective as bond failure occurred between the connected parts. Each bearing stack had stiffness equal to 1.46×10^5 kN/m (836 kip/in.) when tested at ambient temperature and at a rate varying between 40 and 120 kips/sec.



(b)

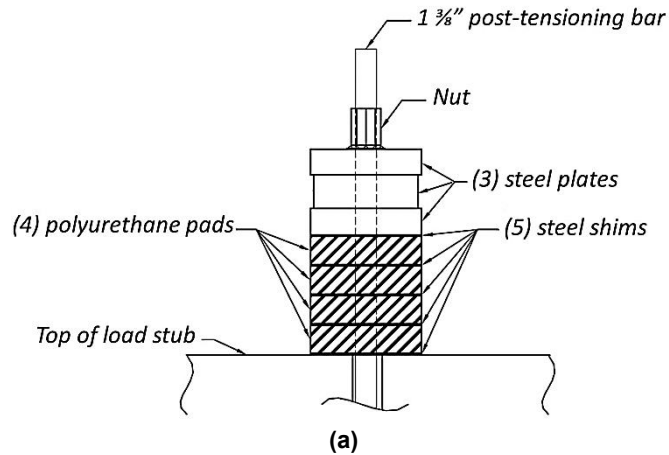


(c)

Figure 3.9 Rubber bearing of Unit 1A: (a) components; (b) single pad; and (c) assembled bearings.

3.2.7.2 Unit 1B: Polyurethane Pads

A bearing consisting of four 90 Shore-A hardness polyurethane pads was provided to each post-tensioning bar in test Unit 1B (Figure 3.10). The pads were 190.5 mm (7.5 in.) in diameter and 47.6 mm (1-7/8 in.) thick, with a 47.6-mm- (1-7/8-in.-) diameter central hole to accommodate the post-tensioning bars. The pads were stacked and alternated with 190.5-mm- (7.5-in.-) diameter \times 3.2-mm- (1/8-in.-) thick circular steel shims. The shims were bonded to the pads by an epoxy adhesive, with the scope of limiting lateral dilation of the polyurethane pads under compression; however this practice proved to be ineffective, as bond failure occurred between the connected parts. Each bearing stack had stiffness equal to 4.38×10^4 kN/m (250 kip/in.) when tested at ambient temperature and at a rate of 0.5 kips/sec.



(b)



(c)

Figure 3.10 Polyurethane bearing of Unit 1B: (a) components; (b) single pad; and (c) assembled bearings.

3.3 MATERIAL PROPERTIES

3.3.1 Concrete

High-performance concrete was used to cast column, load stub, and footing. The compressive strength was measured on 152-mm- (6-in.-) diameter, and 305-mm- (12-in.-) high standard cylinders. Tests were performed at 28 days after casting, at 49 days (day of test of unit 1A) and at 96 days (day of test of unit 1B). Results are listed in Table 3.1. Each value is the average from three specimens. The measured values were larger than the specified strength of 62 MPa (9 ksi) at 28 days.

Consistency and workability of the concrete were assessed through the standard slump (Abram's cone) test. The resulting slump was equal to 216 mm (8.5 in.), indicating high workability of the concrete. A value larger than 200 mm (8 in.) was required to ensure adequate consolidation.

3.3.2 Mortar

The mortar layer between column and footing for both test units was obtained from BASF Embecco 885 cementitious grout with plastic consistency. This material is a prepackaged

hydraulic cement-based, metallic-aggregate, high-strength, non-shrink grout, with an extended working time. This grout meets the requirements of ASTM C 1107. For the specific application it was mixed with a low percentage of water (20% of prepackaged mix volume).

The mortar bed in Unit 1B was reinforced with Durafiber polypropylene fibers that meet ASTM C 1116 standards. Fibers were added in the proportion of 0.037% of hardened grout weight. Fibers inhibit the growth of cracks once they form, thus maintaining the integrity of the mortar and delaying crushing under large compressive strains.

Compressive strengths were measured on 51-mm-diameter, 102-mm- (4-in.-) high standard cylinders. Values are reported in Table 3.1. Each value is the average from three specimens. For comparison, the manufacturer-specified strengths for the grout with plastic consistency at 7 and 28 days were 62 MPa (9 ksi) and 76 MPa (11 ksi), respectively.

3.3.3 Grout

BASF Embeco 885, mixed at fluid consistency with a larger percentage of water (17% of prepackaged mix weight) was employed for grouting:

- external buckling-restrained energy dissipators
- post-tensioning bar ducts for corrosion protection
- external dissipator anchorages into footing ducts (Unit 1A/F)
- internal dissipator into footing ducts (Unit 1B/F) and into column ducts (Unit 1B/C).

Compressive strengths were measured on 51-mm-diameter, 102-mm- (4-in.-) high standard cylinders. Values are reported in Table 3.1. Each value is the average from three specimens. For comparison, the manufacturer-specified strengths for the grout with fluid consistency at 7 and 28 days were 48 MPa (7 ksi) and 62 MPa (9 ksi), respectively.

Table 3.1 Measured compressive strength of cementitious materials.

| Material | Age (days) | Compressive strength | |
|-----------------|------------------|----------------------|-------|
| | | (MPa) | (ksi) |
| Concrete | 28 | 65.5 | 9.5 |
| | 49 (DoT Unit 1A) | 70.2 | 10.2 |
| | 96 (DoT Unit 1B) | 71.8 | 10.4 |
| Mortar Unit 1A | 23 (DoT Unit 1A) | 50.4 | 7.3 |
| | 29 | 46.4 | 6.7 |
| Mortar Unit 1B | 28 | 53.4 | 7.8 |
| | 35 (DoT Unit 1B) | 52.9 | 7.7 |
| Grout Unit 1A/F | 18 (DoT Unit 1A) | 47.1 | 6.8 |
| Grout Unit 1B/F | 41 (DoT Unit 1B) | 52.7 | 7.6 |
| Grout Unit 1B/C | 27 (DoT Unit 1B) | 59.2 | 8.6 |

3.3.4 Energy Dissipator Steel

Hot rolled, ASTM A576 Grade 1018 carbon steel bars were used for the external dissipators; a 25.4-mm- (1-in.-) diameter bar was tested in monotonic tension to characterize the material. The internal dissipators consisted of 316LN, Grade 75 stainless-steel reinforcing bars; a 12.7-mm- (0.5-in.-) diameter bar was tested in monotonic tension to characterize the material. Since 316LN steel does not exhibit a yield plateau, the yield point has been determined with the 0.2% offset method.

Yield stresses and strains, elastic moduli, and ultimate stresses and strains (at peak) are reported in Table 3.2 for the two materials. The corresponding full stress–strain curves are shown on Figure 3.11.

3.3.5 Rubber Pads

The rubber bearings provided to the post-tensioning bars of Unit 1A consisted of SA-47 rubber pads produced by Fabreeka International. These pads are made of recycled rubber compounds and synthetic fiber reinforcement. Randomly oriented fibers enhance compressive strength, stiffness, and tensile strength when compared to unreinforced or virgin rubber.

Table 3.2 Measured steel mechanical properties.

| Material | Elastic modulus | | Yield stress | | Yield strain | Peak stress | | Peak strain |
|----------|-----------------|--------|--------------|-------|--------------|-------------|-------|-------------|
| | (MPa) | (ksi) | (MPa) | (ksi) | (%) | (MPa) | (ksi) | (%) |
| A576 | 221,000 | 32,000 | 331 | 48 | 0.15 | 490 | 71 | 20.0 |
| 316LN | 200,000 | 29,000 | 745 | 108 | 0.37 | 889 | 129 | 15.0 |

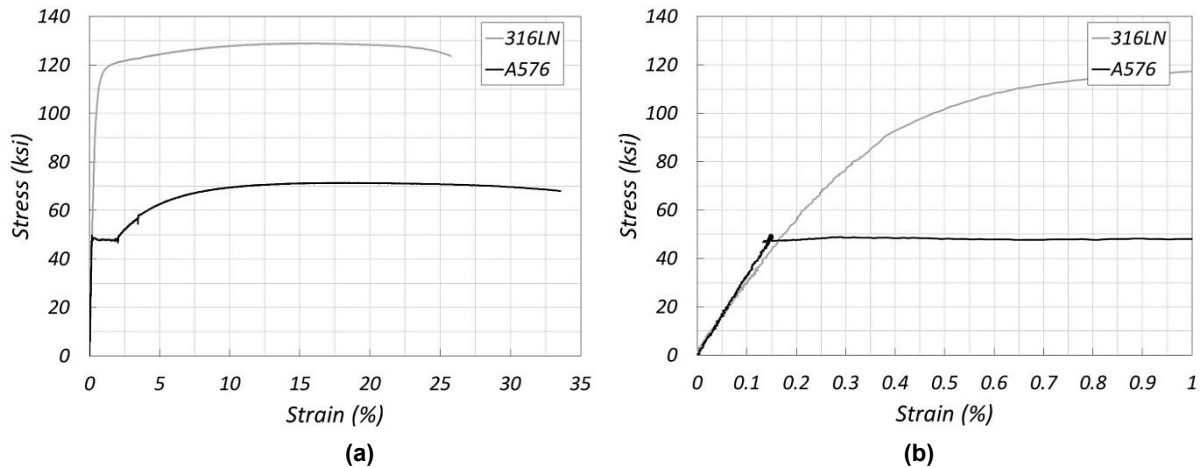


Figure 3.11 Monotonic tensile stress-strain relationships for the energy dissipator steel: (a) full response; and (b) zoom up to 1% strain. (1 ksi = 6.895 MPa).

The design of the bearings was initially based on the stiffness provided by manufacturer's specifications; then it was refined on the basis of cyclic compressive tests performed on two rubber pads. The resulting elastic modulus under cyclic loading was 524 MPa (76 ksi). During testing the material underwent significant creep deformations, even under cyclic loading. Moreover, the behavior appeared to depend on the loading rate, with larger stiffness at higher rates.

3.3.6 Polyurethane Pads

The polyurethane bearings provided to the post-tensioning bars of Unit 1B consisted of adiprene pads. This material, a thermosetting elastomer characterized by elevated toughness, combines resilience and high load-bearing capacity with resistance to impact, abrasion, compression set and degradation by oxygen, ozone, and oil. In addition to the properties distinguishing it from conventional elastomers, adiprene also differs in its physical form: it is a liquid polymer that is mixed with a curing agent and can be fabricated by casting.

The design of the bearings was initially based on the stiffness provided by manufacturer's specifications; then it was refined on the basis of a cyclic compressive test performed on one polyurethane pad. The resulting elastic modulus under cyclic loading was 331 MPa (48 ksi). During testing the material underwent significant creep deformations, even under cyclic loading. Moreover, the behavior appeared to depend on the loading rate, with larger stiffness at higher rates.

3.4 INSTRUMENTATION

The test specimens were instrumented to measure deformations, displacements, and forces during testing. Strain gages, potentiometers, and load cells were used, respectively. More details about sensor locations can be found in Appendix A.

3.4.1 Overall Displacement and Rotation Measurements

A cable-extension displacement transducer, referred to as a horizontal string potentiometer, was connected to the load stub at the lateral loading point to record the lateral displacement of the column and control the actuator (Figure 3.12a). Two horizontal spring-loaded displacement transducers were added at the column base in Unit 1B to monitor eventual shear sliding. One inclinometer was mounted on the foundation and one on top of the load stub to measure their rotations, as shown on Figure 3.12b.

3.4.2 Column Deformation Measurements

To evaluate the average column curvature, four vertical spring-loaded displacement transducers were installed between mounting rods on both north and south faces of the column (Figure 3.12a). The rods were located at 102 mm, 229 mm, 483 mm, and 737 mm (4 in., 9 in., 19 in., and 29 in.) from the bottom of the column.

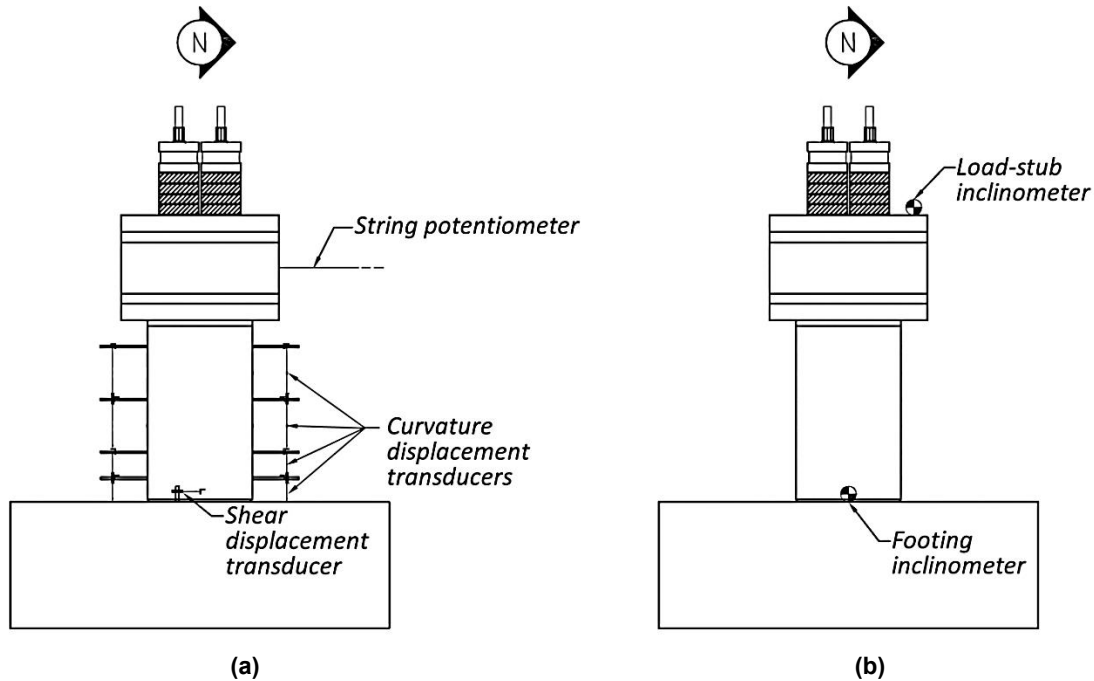


Figure 3.12 Instrumentation: (a) displacement transducers and (b) inclinometers.

Average relative rotations between two mounting rods were obtained by measuring the relative displacements on two opposite sides of the column, taking their difference, and dividing this difference by the horizontal distance between the transducer centerlines. Average curvatures were calculated dividing relative rotations by the displacement transducer gage lengths, equal to the longitudinal distances between mounting rods. The bottom pair of sensors was used to measure the joint rotation.

3.4.3 Outer-Shell Strain Measurements

Figures 3.13a and 3.13b show the strain gage locations on the outer shell for Units 1A and 1B, respectively. Five 5-mm horizontal strain gages attached to the north and south faces of the outer shell were used to record hoop stresses induced on the shell by dilation of compressed concrete. Five 5-mm vertical strain gages were applied to the north face of the column to measure longitudinal stresses on the shell. Horizontal and vertical gages were located at 13 mm, 44 mm, 76 mm, 127 mm, and 165 mm (0.5 in., 1.75 in., 3 in., 5 in., and 6.5 in.) from the bottom of the shell in both units. Three 5-mm strain gages, arranged in a delta-rosette configuration, were attached to the east and west sides of the column to determine the shear strains in both specimens.

Eight additional 5-mm vertical strain gages were applied to the north–east and south–west faces of the outer shell only in Unit 1B, corresponding to the internal energy-dissipating dowels. These sensors were intended to record the shell longitudinal strains induced by the stresses transferred from the dowels. They were located at 51 mm, 102 mm, 152 mm, 203 mm, 254 mm, 305 mm, 356 mm, and 406 mm (2 in., 4 in., 6 in., 8 in., 10 in., 12 in., 14 in., and 16 in.) from the bottom of the shell.

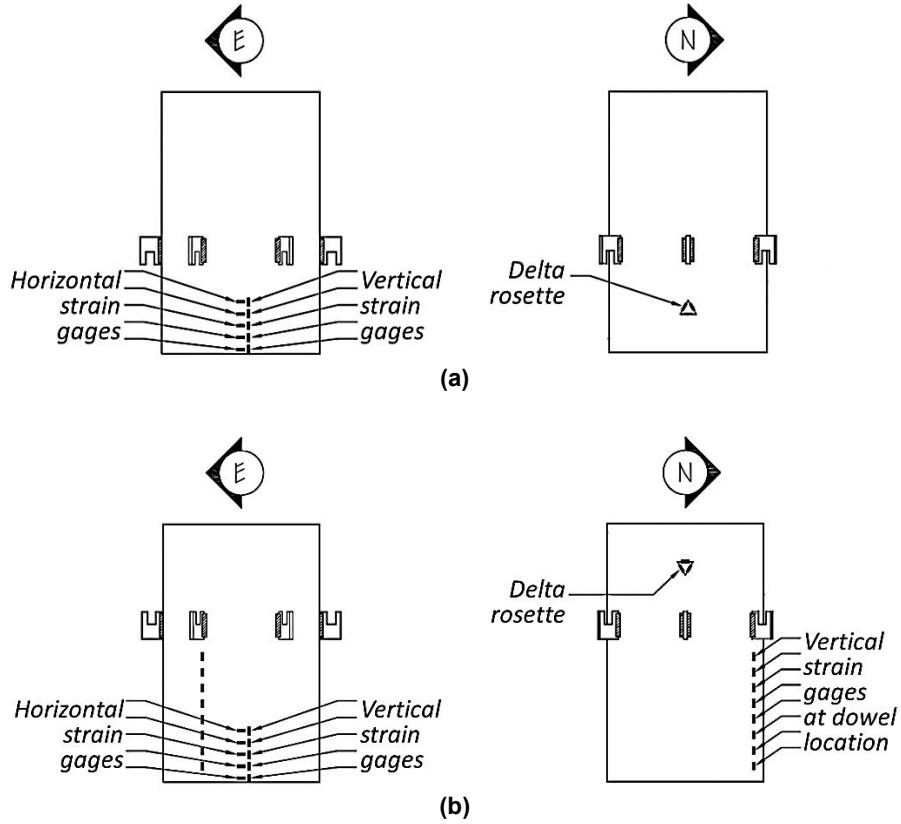


Figure 3.13 Outer-shell strain gages: (a) Unit 1A and (b) Unit 1B.

3.4.4 Post-Tensioning Bar Strain Measurements

Strain gages were used to measure the elongation of two diametrically opposite post-tensioning bars (north–east and south–west) in both Units 1A and 1B (Figure 3.14), right below the load stub. A pair of sensors was applied to each bar, in order to capture axial and flexural deformations.

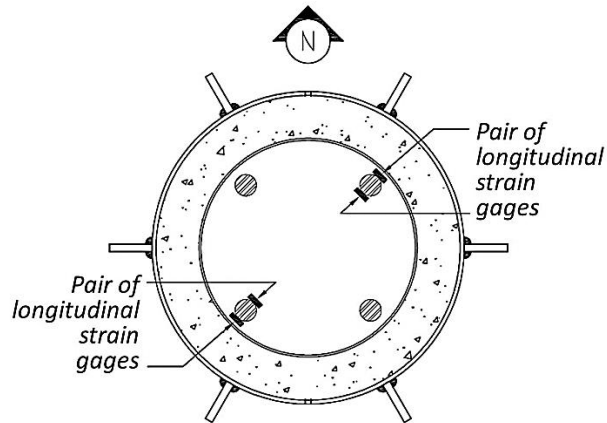


Figure 3.14 Post-tensioning bars strain gages.

3.4.5 External Energy Dissipator Response Measurements

Two diametrically opposite external dissipators (north–west and south–east) were instrumented in Unit 1A, as illustrated on Figure 3.15a. Each device was provided with two strain gages and a spring-loaded displacement transducer. The pair of strain gages was attached to the virgin portion of the bar, which was expected to remain elastic; it was used to obtain the dissipator forces through elasticity relationships.

The displacement transducer, which was connected to the dissipator bar ends right outside the casing, recorded the axial deformation and captured the hysteretic response of the device. An equivalent gage length of 178 mm (7 in.) was used to calculate smeared strains over the non-prismatic bar, as short segments of virgin bar were included in the actual gage length of 216 mm (8.5 in.) between the connections.

3.4.6 Internal Energy Dissipator Strain Measurements

Strain gages were applied to two diametrically opposite internal dissipators (north–east and south–west) in Unit 1B, as shown on Figure 3.15b. Four sensors were mounted in pairs on each bar to measure axial and flexural deformations at two locations of the unbonded segment.

3.4.7 Gravity-Equivalent Load Measurements

Load cells were used to monitor the axial force on two tie-down rods, which were tensioned by vertical hollow plunger jacks and intended to apply a gravity-equivalent load to the specimen. They were mounted between the load stub and the jacks, as shown on Figure 3.1.

3.4.8 Miscellaneous

In addition to active measurement provided by the instrumentation described above, three video cameras were mounted on site: one zoomed on the column-footing joint from north; one recorded the whole column from the east side; and the last one recorded the whole test unit from the laboratory reaction wall. In addition, the specimen response was documented through digital photos and notes.

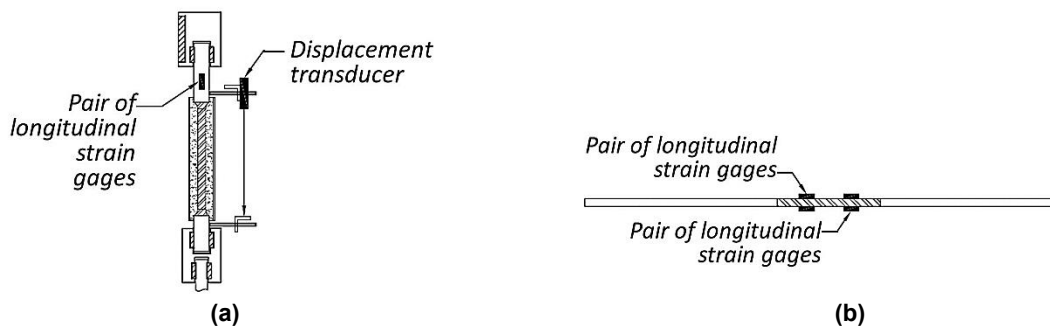


Figure 3.15 Energy dissipators instrumentation: (a) external buckling-restrained devices of Unit 1A; and (b) internal dowels of Unit 1B.

3.5 LOADING PROTOCOL AND TEST OUTCOMES

3.5.1 Normalization of Response Parameters

Lateral displacements have been normalized by the height of the lateral force application point above the column base and thus are expressed as drift ratios. Lateral forces have been normalized by the applied vertical load (equivalent to the weight), and thus are transformed into base shear coefficients. Residual post-tensioning forces have been normalized by their initial value after losses and application of gravity loads. Energy-dissipator stresses have been normalized by the steel yield stress. Neutral axis depths have been normalized by the column outer diameter.

3.5.2 Loading Protocol

A vertical force simulating gravity loads was applied to the test units by two vertical hollow hydraulic plunger jacks, which were positioned above the load stub and connected to the strong floor by one 31.8-mm- (1-1/4 in.-) diameter tie-down rod each (Figure 3.1). Actual axial forces of 293 kN (63 kips) and 268 kN (60 kips) were applied to Unit 1A and Unit 1B, respectively.

Keeping the gravity force constant, the test unit was subjected to quasi-static reversed cyclic loading by a horizontal actuator in the north–south direction, with positive values to the north. After three lateral force-controlled cycles to a base shear coefficient of ± 0.4 and three to ± 0.8 (Figure 3.16a), the test proceeded in lateral displacement control (Figure 3.16b). Three cycles to $\pm 0.5\%$ drift ratio and three to $\pm 0.75\%$ were completed. Subsequent loading consisted of two cycles at a new peak drift ratio, followed by a smaller cycle at the largest drift ratio reached before: drift ratios of $\pm 1\%$, $\pm 1.5\%$, $\pm 2\%$, $\pm 3\%$, $\pm 5\%$, $\pm 7.5\%$, and $\pm 10\%$ were targeted.

For drift ratios larger than 0.3%, the base joint rotation contributed to more than 90% of the lateral displacement: as a consequence, drift ratios and joint rotations practically coincide and only drift ratios have been considered in the results analysis.

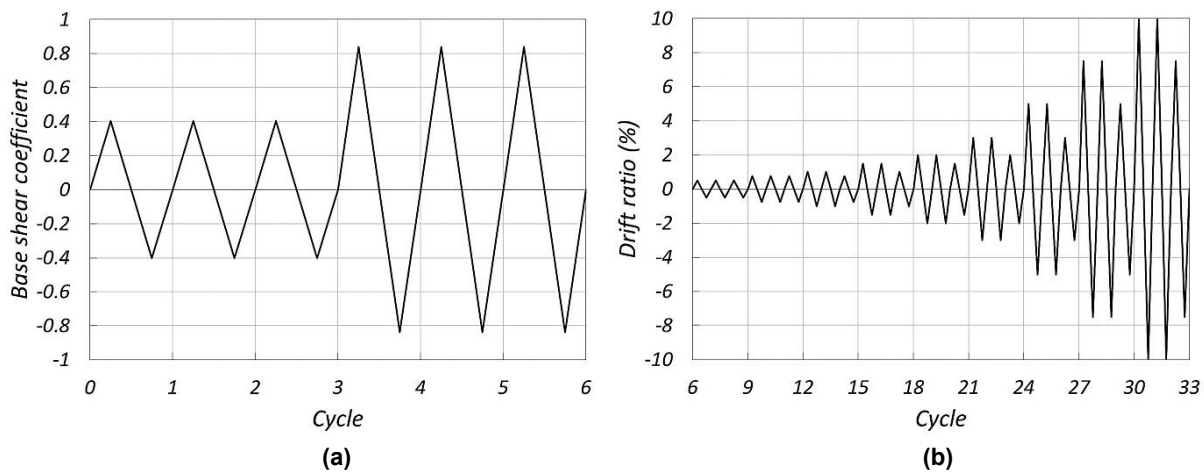


Figure 3.16 Loading protocol: (a) force-controlled cycles; and (b) displacement-controlled cycles.

3.5.3 Outcomes for Unit 1A

3.5.3.1 Response Summary

The hysteretic response of Unit 1A was stable up to the end of testing; see Figures 3.17a and 3.17b. Stiffness degradation was initially observed during cycles at $\pm 3\%$ drift ratio and became more pronounced at larger cycles due to progressive damage of the mortar bed. Additional stiffness degradation was caused by three (out of six) energy dissipators fracturing during cycles at $\pm 7.5\%$ and $\pm 10\%$ drift ratio, but the specimen retained its strength even under larger amplitude cycles.

Recentring behavior was maintained up to the design drift ratio of $\pm 3\%$; see Figure 3.17c. Starting during $\pm 5\%$ drift ratio cycles, significant post-tensioning losses caused by mortar crushing impaired the self-centering capability of the column: Figure 3.17d illustrates the residual post-tensioning force at the end of each cycle as a ratio of the initial effective force.

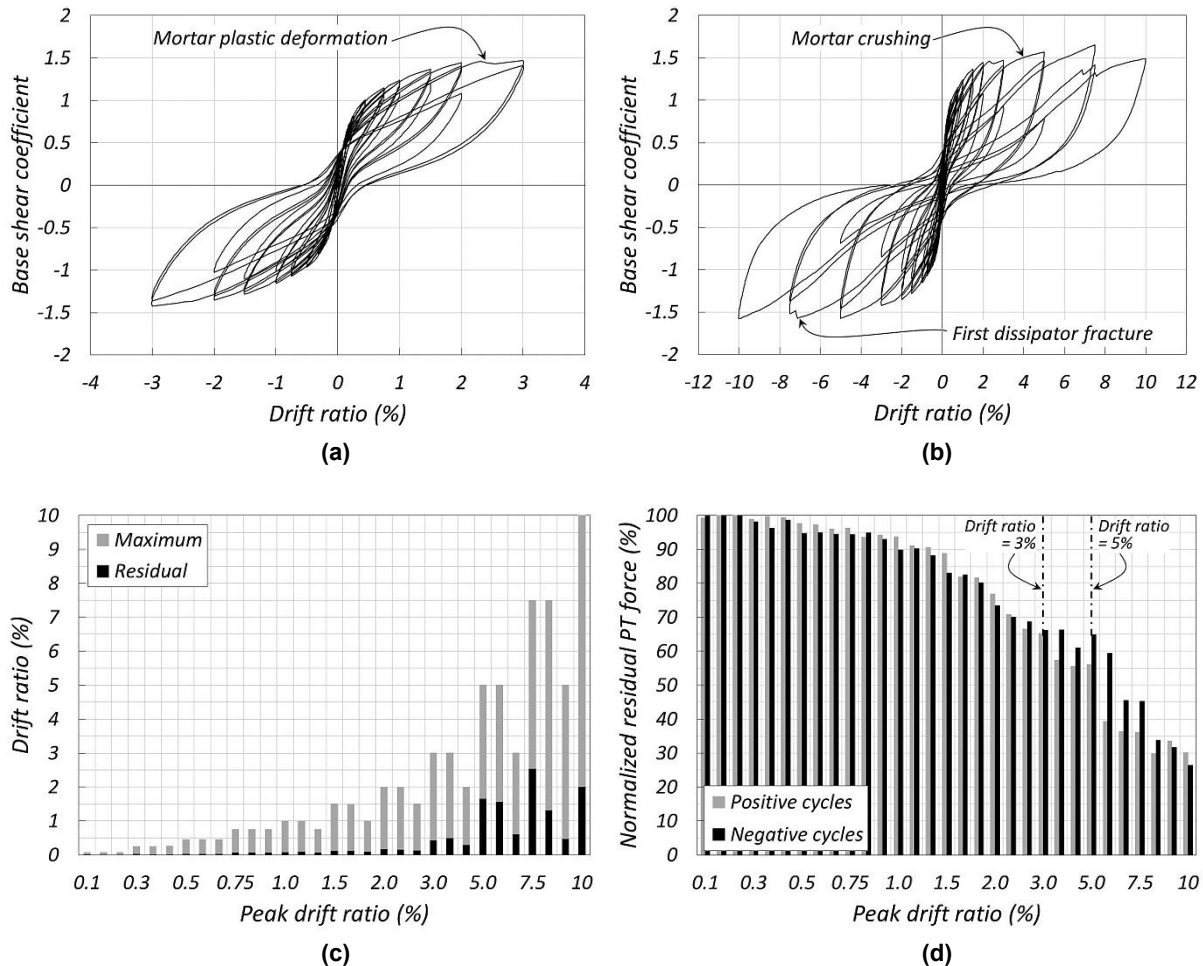


Figure 3.17 Response of Unit 1A: (a) lateral hysteretic response up to 3% drift ratio; (b) lateral hysteretic response up to 10% drift ratio; (c) maximum and residual drift ratios for positive cycles; and (d) residual post-tensioning force at the end of each cycle on the north-east bar.

3.5.3.2 Mortar Bed

Testing of Unit 1A resulted in joint opening at the column–mortar bed interface during cycles to a base shear coefficient of ± 0.8 , corresponding to a lateral stiffness reduction on the hysteretic response. The mortar bed started to flake off during $\pm 1.5\%$ drift ratio cycles. Extensive flaking-off and permanent compressive deformation without crushing were observed on the north and south sides (extreme fibers) during $\pm 3\%$ drift ratio cycles; this resulted in visible stiffness degradation on the hysteretic loops.

The mortar bed started crushing during $\pm 5\%$ drift ratio cycles, causing significant reduction of both stiffness and self-centering capacity, as shown on Figure 3.17c: residual drift ratios of the order of 1.5% were noted. A significant loss of post-tensioning force was recorded upon mortar crushing during these cycles (Figure 3.17d); analysis of the post-tensioning bar strain history confirmed they remained below two-thirds of the yielding strain throughout the test. Extensive crushing of the mortar bed was visible at the end of the test, as shown on Figure 3.18.

3.5.3.3 Energy Dissipators

The north-west dissipator fractured during the first negative cycle to -7.5% drift ratio nearly at peak displacement. Two other dissipators fractured on the south side during subsequent cycles. Each fracture is evident by a sudden jump on the graph of Figure 3.17b. Due to failure of three out of six dissipators, the test was interrupted after the first cycle to $\pm 10\%$ drift ratio.

The hysteretic stress–strain responses of the south–east and north–west external dissipators are shown on Figures 3.19a and 3.19b, respectively, up to the first cycle to $\pm 5\%$ drift ratio. Average strains were determined with a linear potentiometer connected to the dissipator bar right above and below the casing. Stresses were calculated from the elastic strains measured with paired strain gages along the non-disturbed ends of the steel bar. Note that the compressive stresses on the device are larger than the tensile ones; this is due to partial composite behavior between the milled bar and the grout, induced by friction along the milled segment and by bearing of the bar non-milled ends on the grout.



Figure 3.18 Crushed mortar bed at the end of testing of Unit 1A.

An odd shape of the unloading branches of the hysteretic loops is also visible, which may be attributed to two sources of inaccuracy. First, the dissipator axial force was calculated from the axial strains measured by strain gages applied to the elastic non-milled end segments; however, these segments were subjected to bending during the test, which may have affected the determination of the axial force. Second, the average axial strain on the yielding segment was calculated from the relative displacement between two sections right outside the casing; bending of the end segments, between the buckling-restrained body and the connections, started during $\pm 3\%$ drift ratio cycles due to rotation imposed by the rocking body motion (Figure 3.19c. This in turn affected the measurement of the relative displacement. The same effect caused the displacement transducers to slip off the mounting brackets after reaching $\pm 5\%$ drift ratio.

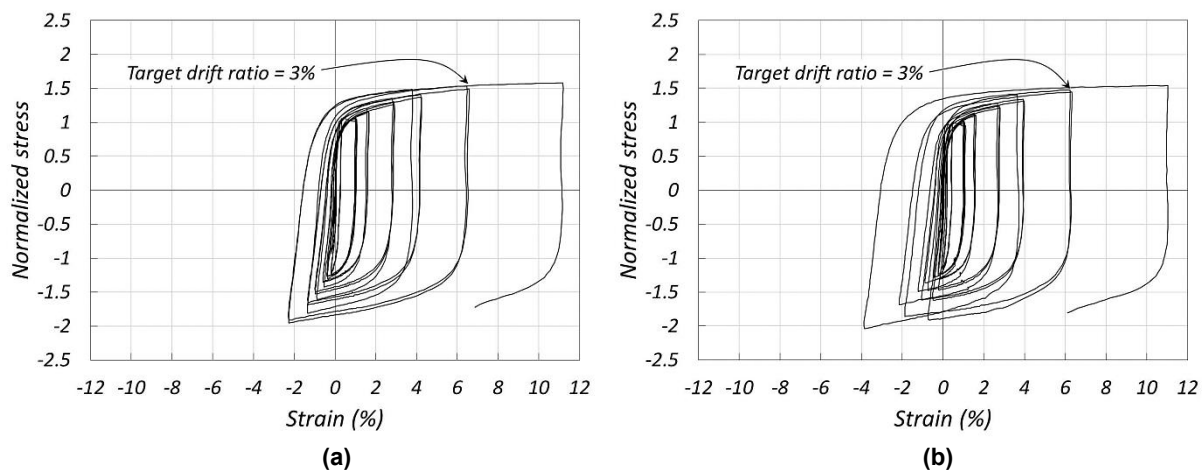


Figure 3.19 Unit 1A buckling-restrained energy dissipators: (a) south-east energy dissipator hysteretic loops up to 5% drift ratio; (b) north-west energy dissipator hysteretic loops up to 5% drift ratio; and (c) distortion of external energy dissipators.

3.5.3.4 Composite Column

Hoop strain profiles, measured on the south and north sides of the outer shell within 165 mm (6.5 in.) from the column base, are plotted on Figures 3.20a and 3.20b, respectively. The second cycles at drift ratios of $\pm 1\%$, $\pm 2\%$, $\pm 3\%$, and $\pm 5\%$ were considered. Positive loading induced longitudinal compression and associated tensile hoop strains on the north side. Significant hoop strains were observed within 0.2 times the column outer diameter from the base, where the concrete dilated due to concentrated compression demand.

In particular, the outer shell yielded on the north side within 0.12 times the outer diameter from the base during cycles to $+3\%$ drift ratio and beyond; however, the outer shell remained elastic on the south side. Figure 3.20 shows that even before yielding of the shell, tensile hoop strains on one side did not disappear when that side underwent longitudinal tension under opposite peaks: in fact, permanent compressive deformation of the column concrete built up, causing permanent dilation.

A 13-mm- (0.5-in.-) deep permanent compressive deformation of the column concrete, and permanent deformation of the shells due to concrete dilation were observed at the column base on the north and south sides at the end of the test; see Figure 3.20c. Plastic compression of the column concrete was an additional cause of the measured stiffness degradation and loss of post-tensioning force.

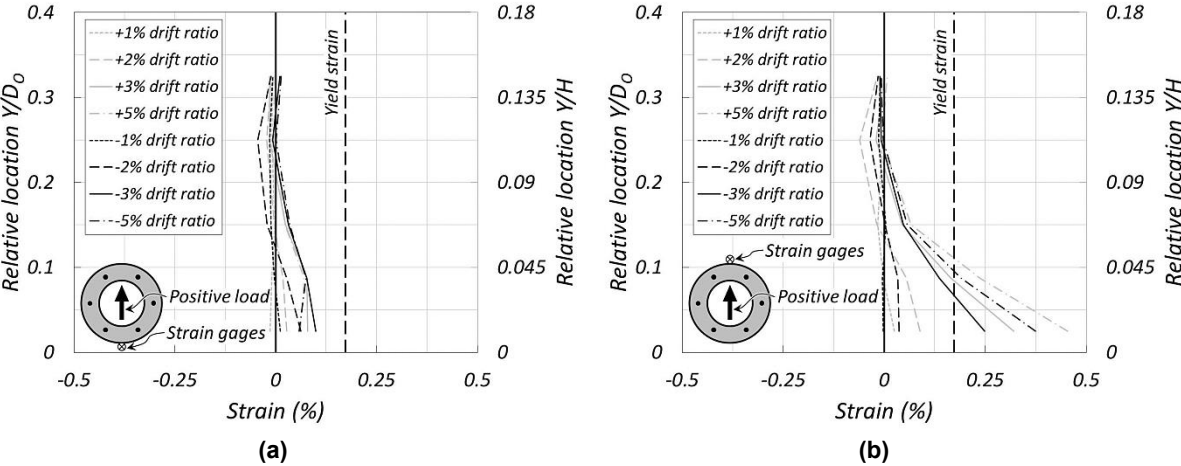


Figure 3.20 Unit 1A composite column: (a) outer-shell hoop strain profiles on the south side; (b) outer-shell hoop strain profiles on the north side; and (c) permanent concrete and shell deformations at the end of testing.

3.5.4 Outcomes for Unit 1B

3.5.4.1 Response Summary

The hysteretic response of Unit 1B, plotted on was stable up to the conclusion of testing; see Figures 3.21a and 3.21b. Stiffness degradation was initially observed during cycles at $\pm 3\%$ drift ratio and became more pronounced at larger cycles due to progressive damage of the mortar bed. Additional stiffness degradation was caused by four (out of six) energy dissipators fracturing during cycles at $\pm 7.5\%$ and $\pm 10\%$ drift ratio, but the specimen retained its strength even under larger amplitude cycles.

Recentering behavior was maintained beyond the design drift ratio, up to $\pm 5\%$; see Figure 3.21c. Starting during $\pm 7.5\%$ drift ratio cycles, significant post-tensioning losses caused by mortar crushing impaired the self-centering capability of the column: Figure 3.21d illustrates the residual post-tensioning force at the end of each cycle as a ratio of the initial effective force.

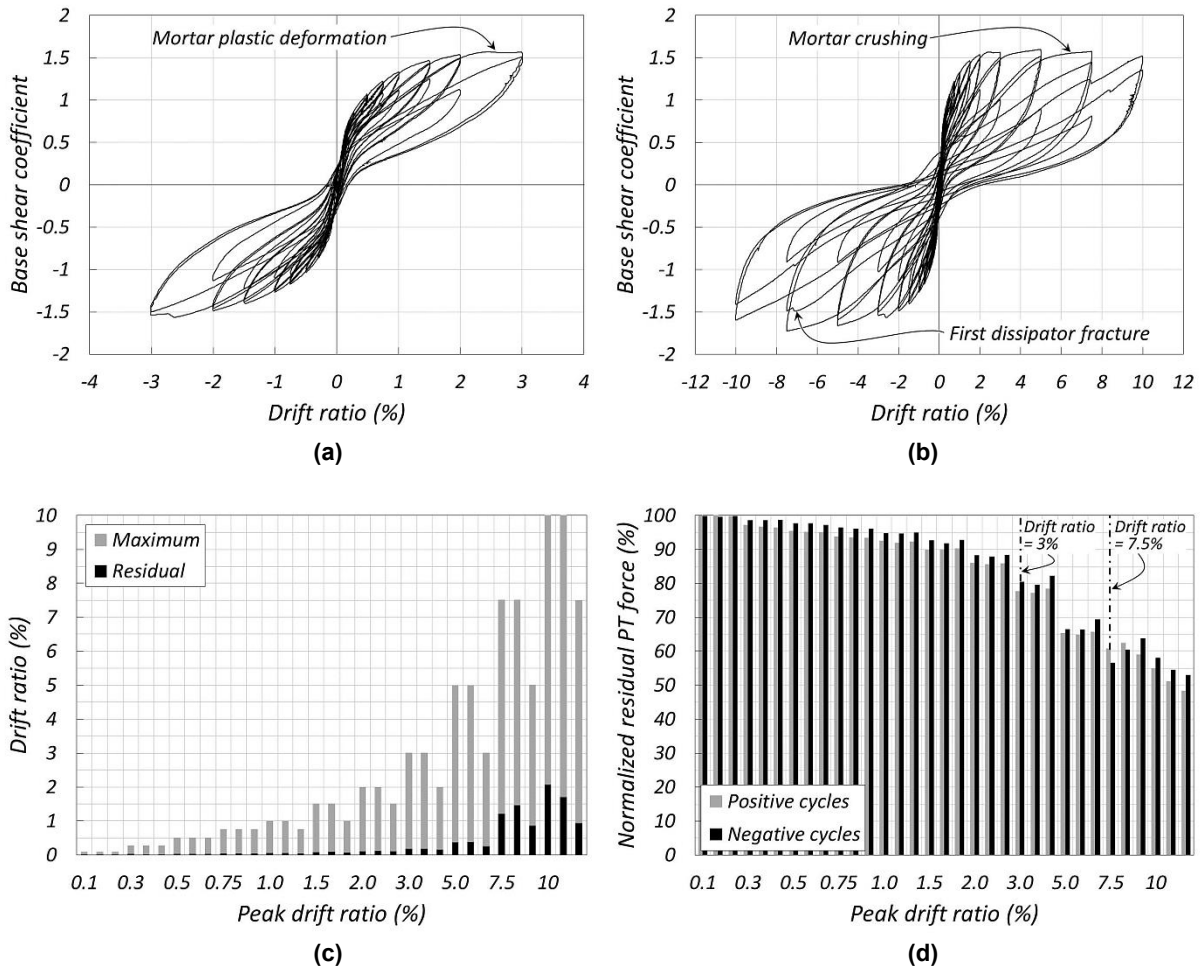


Figure 3.21 Response of Unit 1B: (a) lateral hysteretic response up to 3% drift ratio; (b) lateral hysteretic response up to 10% drift ratio; (c) maximum and residual drift ratios for positive cycles; and (d) residual post-tensioning force at the end of each cycle on the south-west bar.

3.5.4.2 Mortar Bed

Testing of Unit 1B resulted in joint opening at the column-mortar bed interface during cycles to a base shear coefficient of ± 0.8 , corresponding to a lateral stiffness reduction on the hysteretic response. The mortar bed started to flake off during $\pm 2\%$ drift ratio cycles. Extensive flaking-off and permanent compressive deformation without crushing were observed on the north and south sides (extreme fibers) during the $\pm 3\%$ drift ratio cycles; this resulted in visible stiffness degradation on the hysteretic loops.

The mortar bed started crushing during $\pm 5\%$ drift ratio cycles but not abruptly. Crushing progressed through $\pm 7.5\%$ drift ratio cycles, when both stiffness and self-centering capacity were significantly reduced, as shown on Figure 3.21c: residual drift ratios of the order of 1.5% were noted. A significant loss of post-tensioning force was recorded upon mortar crushing during these cycles (Figure 3.21d); analysis of the post-tensioning bar strain history confirmed they remained below two-thirds of the yielding strain throughout the test. Extensive crushing of the mortar bed was visible at the end of the test, as shown on Figure 3.22.

3.5.4.3 Energy Dissipators

The first dissipator fractured on the north side during the second negative cycle to -7.5% drift ratio nearly at peak displacement. A second dissipator fractured on the north side and two on the south side during subsequent cycles. Each fracture is evident by a sudden jump on the graph of Figure 3.21b.

Due to large strain demands and friction against the surrounding concrete, strain gages on the dowels were lost early in the test. At the end of the test, four dowels were found to have visibly buckled and fractured: two on the north side and two on the south side. Figure 3.23 shows the two pieces of a fractured dowel, in the column (Figure 3.23a) and in the footing (Figure 3.23b).



Figure 3.22 Crushed mortar bed at the end of testing of Unit 1B.

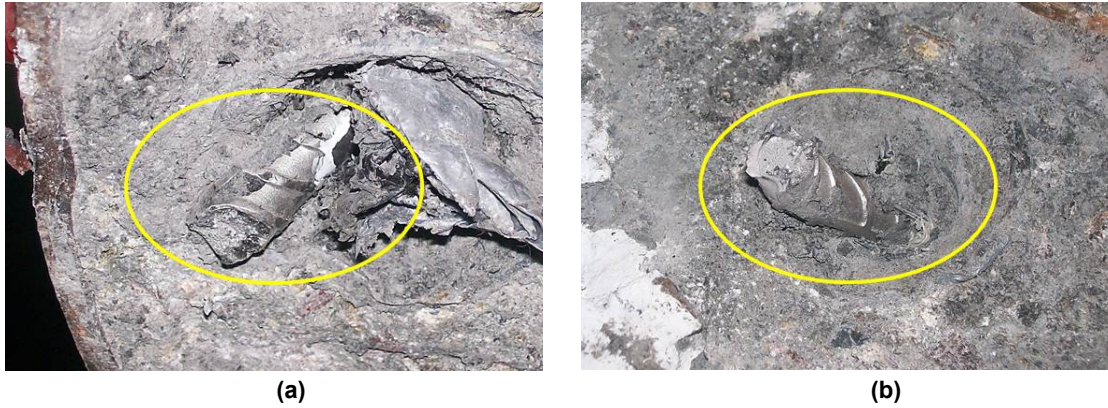


Figure 3.23 Unit 1B energy-dissipating dowels: (a) fractured dowel in the column; and (b) fractured dowel in the footing.

3.5.4.4 Composite Column

Longitudinal strains were measured on the outer shell in correspondence of two diametrically opposite dissipating dowels. The longitudinal strain profiles are plotted in Figures 3.24a and 3.24b for the second cycles at drift ratios of $\pm 1\%$, $\pm 2\%$, $\pm 3\%$, and $\pm 5\%$. Note that during cycles up to $\pm 2\%$ drift ratio transfer of tension from the dowel to the shell is distributed within 0.4 times the outer diameter from the base. At larger amplitude cycles, it concentrates within 0.2 to 0.3 diameters; above this length, strains remain about constant.

A compressive strain increment is visible at 0.6 times the column diameter from the base, particularly in front of the north–east dowel (Figure 3.24b): the top weld bead was located there, and concentrated stress transfer may be the cause of this local effect. Large compressive strains tend to develop close to the base, but no yielding was observed up to $\pm 5\%$ drift ratio cycles.

Hoop strain profiles, measured on the south and north sides of the outer shell within 165 mm (6.5 in.) from the column base, are plotted on Figures 3.24c and 3.24d, respectively. The second cycles at drift ratios of $\pm 1\%$, $\pm 2\%$, $\pm 3\%$, and $\pm 5\%$ were considered. Positive loading induced longitudinal compression and associated tensile hoop strains on the north side. Significant hoop strains were observed within 0.2 times the column outer diameter from the base, where the concrete dilated due to concentrated compression demand.

In particular, the outer shell yielded on both sides within 0.12 times the outer diameter from the base during cycles to $+3\%$ drift ratio and beyond. Figure 3.24 shows that even before yielding of the shell, tensile hoop strains on one side did not disappear when that side underwent longitudinal tension under opposite peaks: in fact, permanent compressive deformation of the column concrete built up, causing permanent dilation.

A 15-mm- (0.6-in.-) deep permanent compressive deformation of the column concrete, and permanent deformation of the shells due to concrete dilation were observed at the column base on the north and south sides at the end of the test Figure 3.24e. Plastic compression of the column concrete was an additional cause of the measured stiffness degradation and loss of post-tensioning force.

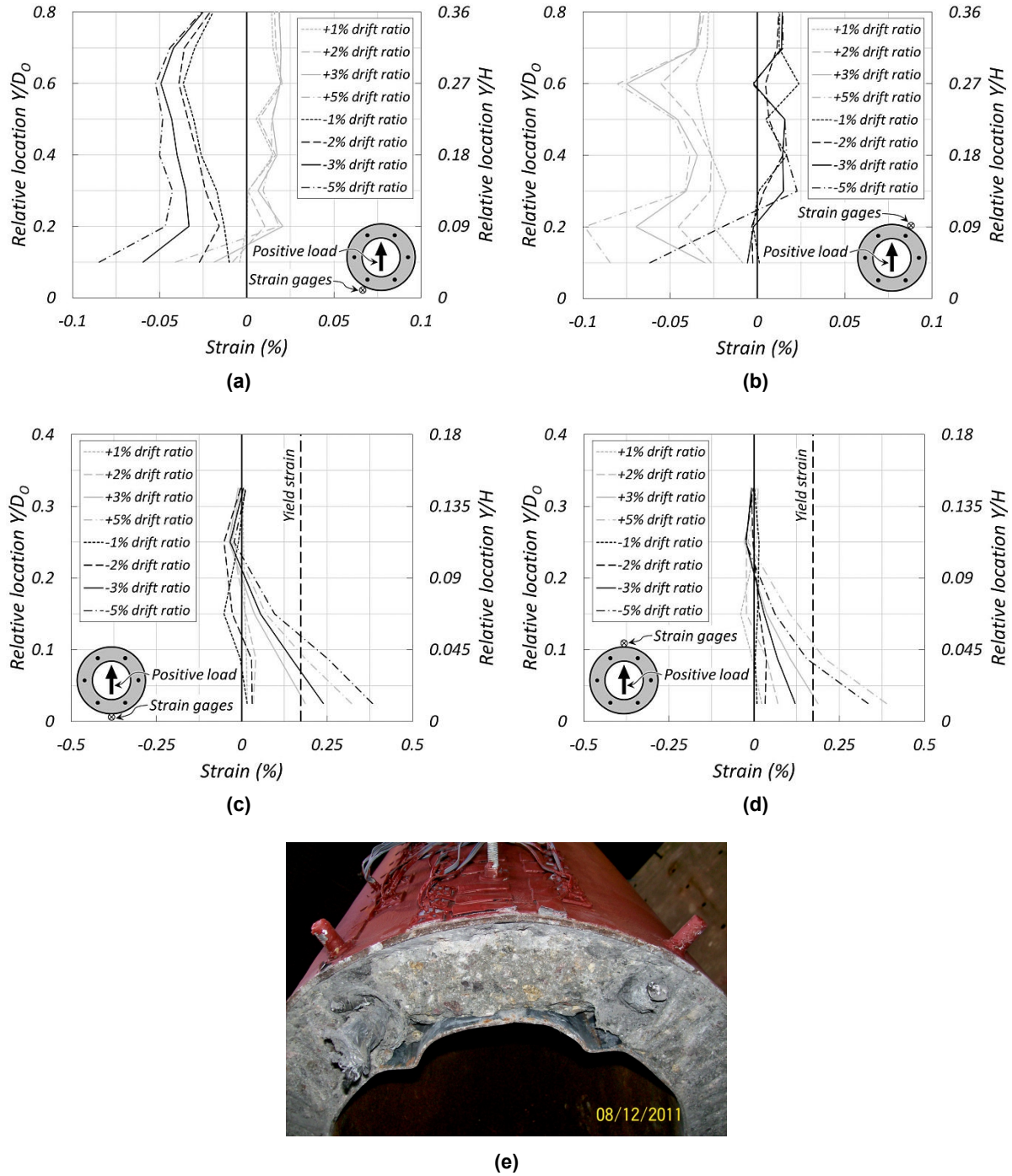


Figure 3.24 Unit 1B composite column: (a) outer-shell longitudinal strain profiles in front of the south-west dowel; (b) outer-shell longitudinal strain profiles in front of the north-east dowel (c) outer-shell hoop strain profiles on the south side; (d) outer-shell hoop strain profiles on the north side; and (e) permanent concrete and shell deformations at the end of testing.

3.5.5 Comparison between Unit 1A and Unit 1B

The overall responses of the two test units were very similar in terms of strength, hysteresis loop shape, energy dissipation, damage, and failure modes. The main difference in the lateral force-displacement responses shows the importance of preventing mortar bed crushing in order to maintain self-centering behavior: adding polypropylene fibers to the mortar in Unit 1B extended the self-centering response to $\pm 5\%$ drift ratio cycles in Unit 1B, whereas Unit 1A was already displaying residual drift ratios of 1.5% at that stage. A comparison between Figures 3.17d and 3.21d shows that increased mortar toughness delayed its crushing, leading to less pronounced post-tensioning losses in Unit 1B than in Unit 1A.

The neutral axis depth at the rocking interface, normalized by the column outer diameter, is plotted on Figure 3.25 at the peak drift of all cycles. Larger neutral-axis depths were measured at the base of Unit 1B compared to Unit 1A at and beyond 0.75% drift ratios: this implies that the mortar of Unit 1B was able to sustain larger compressive strains under the same joint rotations, before crushing.

In both cases, the neutral axis cut the hollow core ($c/D_o > 0.15$) with high compressive stresses arising on the concrete around the inner circle. The inner shell did not have sufficient strength to restrain the inward dilation associated to this stress state, resulting in permanent plastic compression of the concrete and damage to the inner shell, as is visible in Figures 3.20 and 3.24. This observation supports the need of enforcing Criterion (v) in the design of such columns. The use of a corrugated drainage pipe instead of a cylindrical pipe should provide more strength against inward pressure and minimize this type of damage.

The hoop strain profiles of Figures 3.20 and 3.24 show that concrete dilation was significant, within 0.2 times the column outer diameter from the column base, a length very close to the measured neutral axis depth. The assumption that concrete inelastic compressive strains would extend a length equal to the neutral-axis depth from the rocking interface, which was made in the context of the simplified interface section analysis, is justified by this observation. The same assumption will be used also in the more refined numerical model presented in the next chapter.

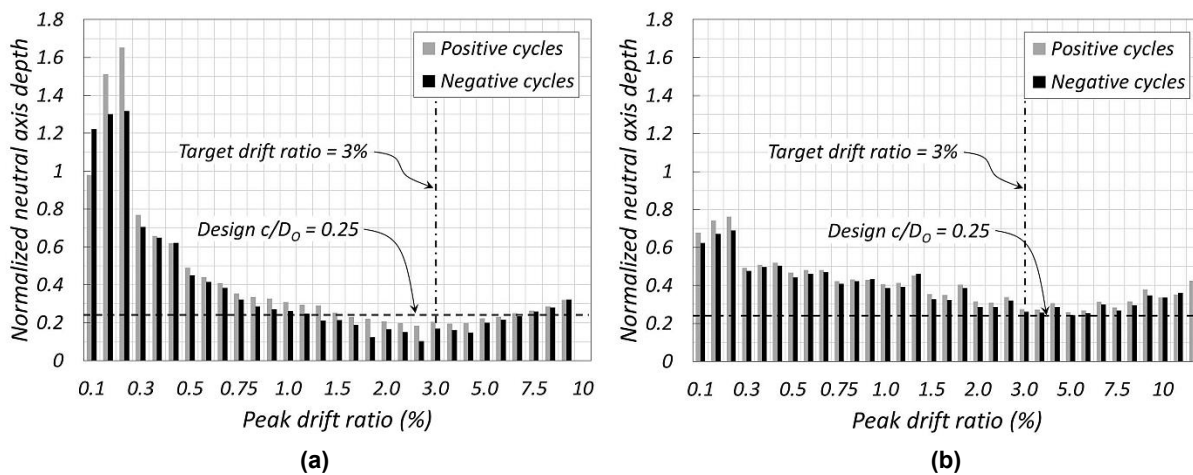


Figure 3.25 Neutral axis depth at peak lateral displacements: (a) Unit 1A and (b) Unit 1B.

4 Numerical Simulations

4.1 NUMERICAL MODEL

A three-dimensional numerical model of the test units was built and validated by experimental results. For this purpose, the software OpenSees [Mazzoni et al. 2007; McKenna et al. 2010] developed by the Pacific Earthquake Engineering Research Center (PEER) was used. The input *.tcl* files for the program can be found in Appendix B.

A sketch illustrating the main model components is shown on Figure 4.1 [Vervelidis, 2012; Guerrini et al. 2012; and Guerrini 2014]. The composite steel–concrete column was modeled with elastic frame elements connected to the mortar bed at the base and to the point of application of the load at the top. Multiple nonlinear truss elements represented the mortar at the column-footing joint; they were fixed at the base and connected to the bottom node of the column by rigid links.

Post-tensioning bars were modeled as nonlinear truss elements, with an initial stress equal to the effectively applied prestress; they were fixed at the base and connected to the top node of the column by rigid links. Energy-dissipating devices were represented by nonlinear frame elements, with the lower ends fixed to the footing and the upper ends connected to a column intermediate node by rigid links.

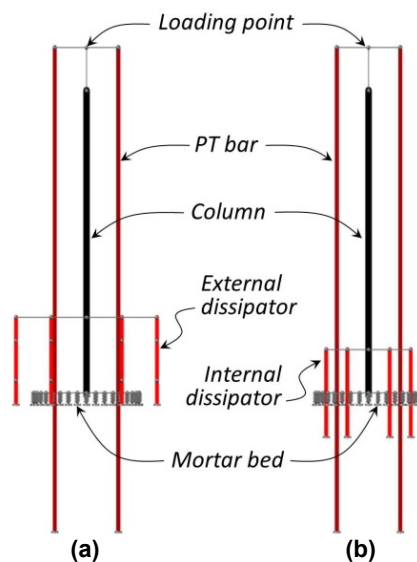


Figure 4.1 Numerical model sketches: (a) Unit 1A and (b) Unit 1B.

Since the deformations within the load stub are negligible, the loading point was connected to the column top with a rigid link. All rigid links mentioned in this chapter were modeled as elastic elements with very high stiffness compared to the adjoining elements.

4.1.1 Composite Column

The column was modeled with two elastic beam–column elements in series, connected to the mortar bed at the base and to the loading point at the top; the intermediate node was used to connect the energy-dissipator elements. The stiffness of the lower segment was based on the concrete hollow section only, as the outer shell does not transfer directly compression at the interface (contact with the mortar is avoided), and tension is resisted by the energy dissipators at that location. Instead, the transformed-section stiffness was assigned to the upper segment, where the outer steel is effective in composite action with the concrete.

The concrete elastic modulus was taken as $E_c = 4700 \times \sqrt{f'_c}$ (MPa) or $E_c = 1800 \times \sqrt{f'_c}$ (ksi), where f'_c is the concrete compressive strength on the day of testing, while for the steel shell $E_s = 200$ GPA (29,000 ksi) was used. At a distance equal to half the load-stub height, a node was defined just above the column for the application of the vertical load and lateral displacement histories; since the deformations of the loading stub are expected to be negligible, this node was linked to the top of the column with a rigid element.

4.1.2 Mortar Bed

Multiple non-linear truss elements [Taylor 1977; Vulcano and Bertero 1987; and Carr 2008] represented the mortar at the interface between column and footing; the mortar bed was discretized into 36 wedges along the circumference, and 3 rings along the radius. The length of the truss elements was set equal to the actual mortar thickness, i.e., 12.7 mm (0.5 in.).

The *Concrete01* nonlinear material model was applied to these elements; this concrete-specific rule includes no tensile strength, which is appropriate for capturing gap openings. Peak compressive stress and strain, and ultimate stress and strain need to be input. A parabola connects the origin to the peak point, and a straight line goes from the peak to the ultimate point; for strains larger than the ultimate one, stresses drop to zero. The initial tangent elastic modulus is automatically derived by fitting a parabola through the origin, with its vertex being the peak point.

Peak stresses of 56 MPa (8.1 ksi, Unit 1A) and 59 MPa (8.5 ksi, Unit 1B), and peak strains of 0.4% (Units 1A and 1B) were obtained from Mander's model for confined concrete [Mander et al. 1988], assuming a confinement efficiency coefficient equal to 0.1; such a low value is consistent with confinement being provided only by friction with column and footing surfaces; see Chapter 2. The ultimate strain was set to 15%, with a residual stress of 6.9 MPa (1 ksi).

Strains in the stress–strain relationship were amplified by the ratio of the theoretical neutral-axis depth [i.e. 127 mm (5 in.)] to the actual thickness of the mortar bed. With this transformation, the spread of inelastic behavior within the column, assumed to extend uniformly for a length equal to the neutral-axis depth [Restrepo and Rahman 2007] was approximately taken into account.

4.1.3 Post-Tensioning Bars

Post-tensioning bars were modeled as nonlinear truss elements that were fixed at the base and connected to the top node of the column by rigid elements. An intermediate node was defined at the column-footing interface, to constrain lateral translation at that location. An equivalent initial tangent elastic modulus and an equivalent bilinear factor were calculated to account for the stiffness of elastic rubber or urethane bearings in series with the bars.

The *Steel02* material hysteretic rule [Filippou et al. 1983], based on Giuffré-Menegotto-Pinto model, was assigned to these elements. Initial stresses of 207 MPa (30 ksi) for Unit 1A and 216 MPa (31 ksi) for Unit 1B were set to simulate the effective prestress after losses. The yield stress was set equal to 827 MPa (120 ksi). Curvature parameters $R_0 = 18$, $c_{R1} = 0.925$, and $c_{R2} = 0.15$ were chosen, while no isotropic hardening was introduced.

4.1.4 Energy Dissipators

Energy dissipators were modeled as nonlinear displacement-based beam-column elements. The lower ends were fixed to the footing, while the upper ends were connected to the column intermediate node by rigid links.

The element nonlinear properties were assigned in terms of internal forces rather than using fiber discretization, which is computationally burdensome; thus axial, flexural, and torsional behaviors were assigned to these elements at the cross-section level. The *Steel02* nonlinear material model [Filippou et al. 1983] was assigned to the dissipator axial and flexural relationships, while the torsional response was considered elastic. Decoupling axial and flexural behavior was particularly justified for external buckling-restrained devices, where the yielding segment was mainly subjected to axial deformations, while the non-milled ends were mainly interested by bending.

Three integration points were defined along each element, two at the ends and one in the middle. Even though an element is mainly subject to axial force, providing a minimum number of integration points would avoid numerical issues under bending.

4.1.4.1 Unit 1A: External Buckling-Restrained Devices

External energy dissipating devices for test Unit 1A were represented by three beam-column elements in series, to include the section variation between non-yielding ends and milled segment. The material parameters were selected to match the experimental hysteretic behavior of the device and considering the different behavior shown by the dissipators in tension and compression, due to partial composite action with the grout. A fictitious yield stress equal to 469 MPa (68 ksi) and peak strain equal to 0.06 were assigned for this scope, in combination with curvature parameters $R_0 = 18$, $c_{R1} = 0.925$, and $c_{R2} = 0.15$, and isotropic-hardening parameters $a_1 = 0.07$, $a_2 = 3$, $a_3 = 0$, and $a_4 = 1$.

4.1.4.2 Unit 1B: Internal Dowels

Internal dowel bars for Unit 1B were instead modeled with single beam-column elements, with length equal to the yielding debonded segment. In this case the material parameters were

calibrated with the results of a cyclic test conducted on a stainless-steel reinforcing bar with a length-to-diameter aspect ratio of 3. A fictitious yield stress equal to 827 MPa (120 ksi) was assigned for this scope, in combination with curvature parameters $R_0 = 18$, $c_{R1} = 0.925$, and $c_{R2} = 0.15$, and isotropic-hardening parameters $a_1 = 0$, $a_2 = 1$, $a_3 = 0$, and $a_4 = 1$.

4.1.5 Analysis Procedure

The analysis was performed in two stages: first, the vertical load was applied and held constant; then the cyclic quasi-static lateral displacement history was assigned to the load stub centroid. The Newton-Raphson algorithm was chosen to solve the nonlinear residual equation.

The analysis was performed under the hypothesis of small displacements, or “linear geometric transformation” in OpenSees language. This choice was justified by the vertical load being applied through tie-down rods, which were rotating together with the column under lateral displacement; as a consequence, the applied gravity-equivalent force was always acting (nearly) parallel to the column axis with no significant $P-\Delta$ interaction.

The numerical analysis was run up to 5% drift ratio. Modeling the near-failure material behavior requires implementation of more elaborated routines and the knowledge of a number of parameters that were not available from these experimental tests. Moreover, larger drift ratios would be extremely demanding for other components of a bridge, such as the superstructure or abutments, and typically the design would target drift ratios within this range. Thus, efforts were directed at capturing accurately the response up to this extent.

4.2 NUMERICAL ANALYSIS RESULTS

4.2.1 Lateral Force-Displacement Response

Figure 4.2 compares the experimental and numerical force-displacement relationships up to 1% and 5% drift ratios. The model captures accurately strength, stiffness, and self-centering characteristics of the system, as well as progressive stiffness degradation and loss of self-centering capacity. In the case of Unit 1A, the numerical model slightly underestimates the stiffness degradation, predicting higher lateral forces in particular after 2% drift ratio cycles (Figure 4.2b). In the case of Unit 1B the model overestimates the stiffness degradation for drift ratios between 1% and 3% (Figure 4.2d).

Similar discrepancies are observed between the backbone curve of the proposed simplified analysis and the experimental response. Figure 4.3 compares the refined numerical force-displacement cycles with the simplified backbone curve, showing consistency between the predictions of the two analysis methods.

4.2.2 Overall Energy Dissipation

Figure 4.4 confirms the good agreement between numerical and experimental response in terms of cumulative dissipated energy. In these plots, the energy has been normalized by the product of the maximum lateral displacement times the maximum lateral force measured during the test.

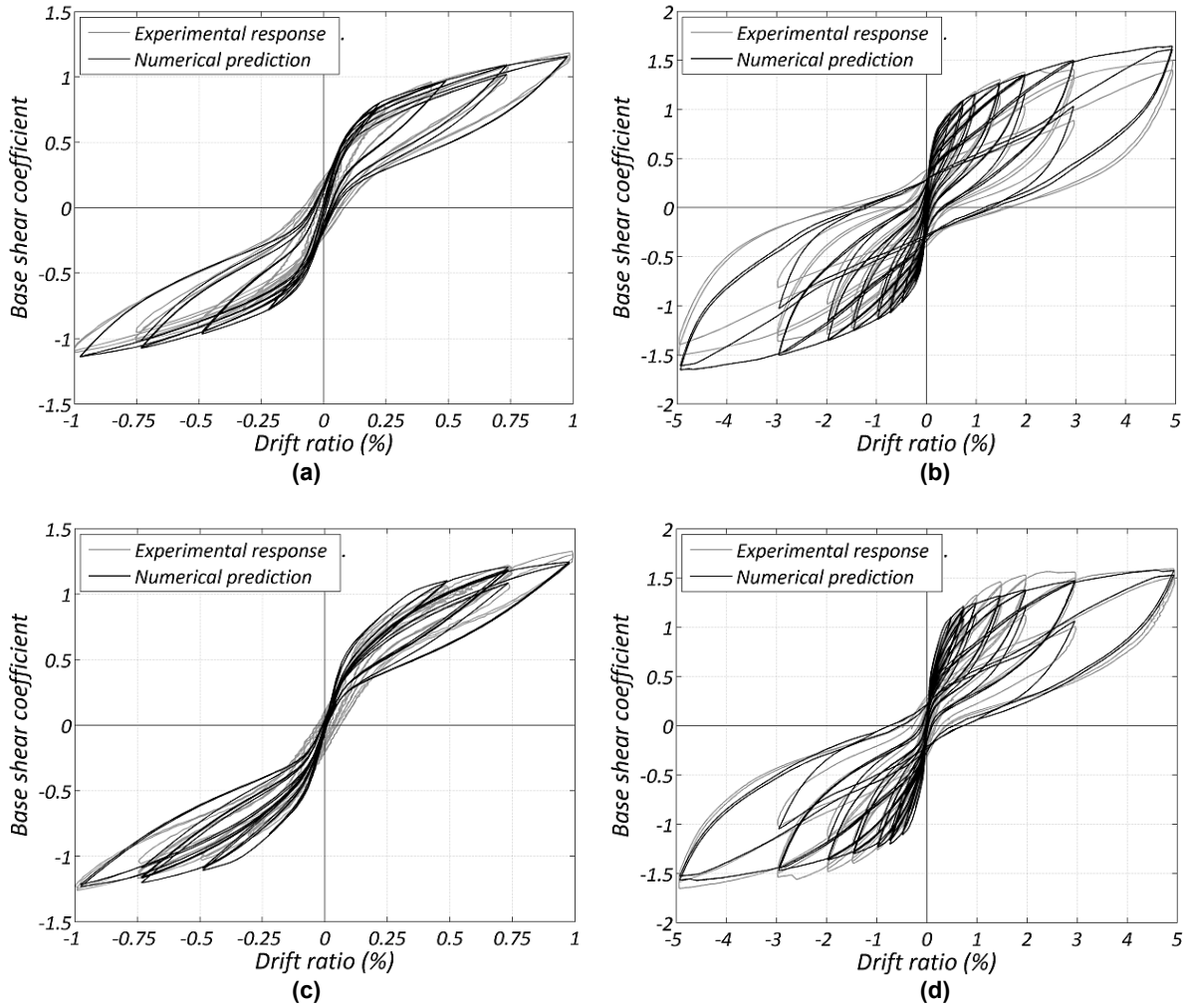


Figure 4.2 Numerical prediction of the lateral force-displacement response: (a) Unit 1A up to 1% drift ratio; (b) Unit 1A up to 5% drift ratio; (c) Unit 1B up to 1% drift ratio; and (d) Unit 1B up to 5% drift ratio.

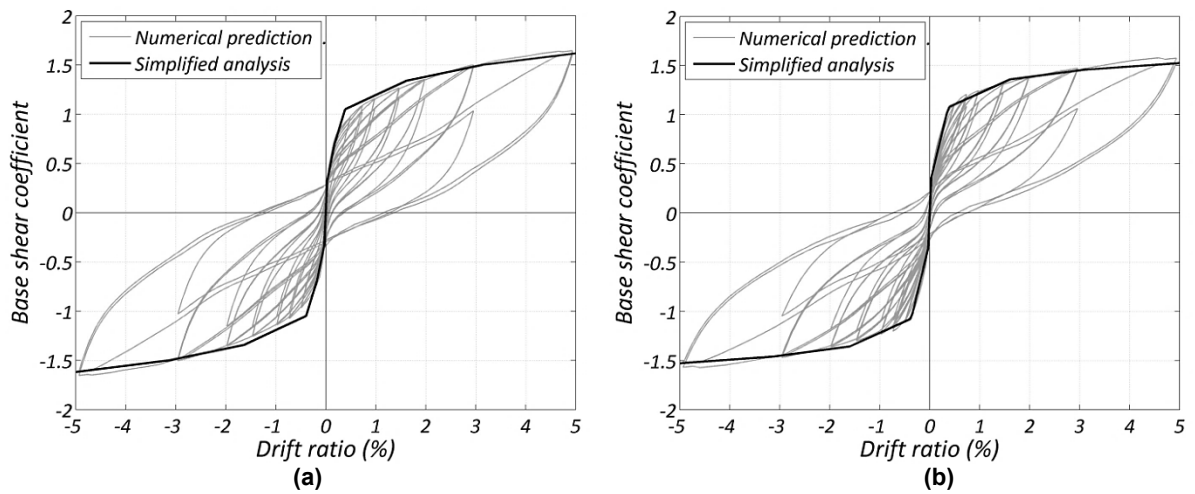


Figure 4.3 Comparison between numerical prediction and simplified analysis of the lateral force-displacement response: (a) Unit 1A and (b) Unit 1B.

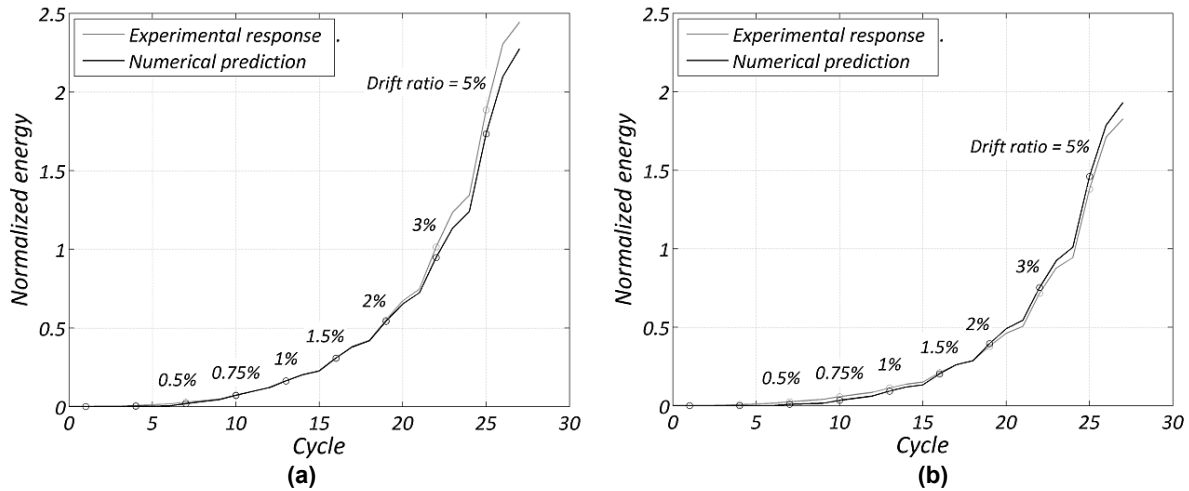


Figure 4.4 Numerical prediction of the cumulative hysteretic energy: (a) Unit 1A and (b) Unit 1B.

4.2.3 Post-Tensioning Bar Strain History

Figure 4.5 compares the numerical and experimental strain histories of the north-east post-tensioning bar of Unit 1A and of the south-west post-tensioning bar of Unit 1B up to 5% drift ratio. Generally good agreement with the experimental results is observed. A slight overestimation of the peak tensile strains is evident at higher drift ratios, especially for Unit 1A; this may have contributed to the under-prediction of the lateral stiffness degradation.

The different amount of prestress loss measured for the two test units at 5% drift ratio, due to more extensive crushing of the mortar bed in Unit 1A, is well captured by the model, contributing to a good prediction of the overall behavior of the system.

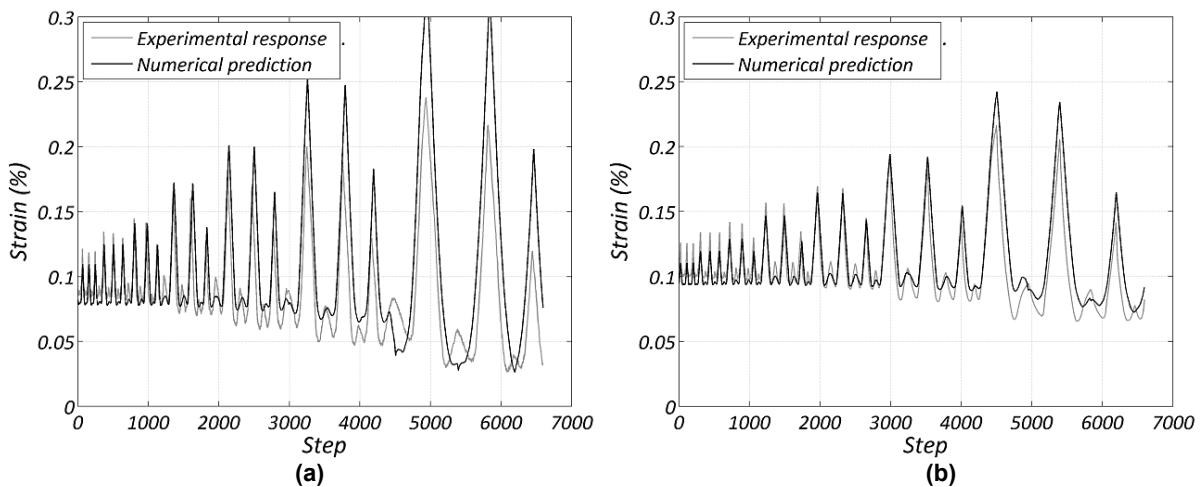


Figure 4.5 Numerical prediction of the post-tensioning bar strain history: (a) Unit 1A, north-east bar; and (b) Unit 1B, south-west bar.

4.2.4 Energy Dissipators Hysteretic Response

Figure 4.6 compares the numerical hysteretic axial strain–stress response of the north–west external dissipator of Unit 1A to the experimental one. A lower degree of accuracy was observed in the predicted hysteretic response of the energy dissipators compared to the global system response. Overestimation of the dissipator strength, both in tension and compression, is visible at low strains. Some numerical issues were observed and associated to a bug in the material model isotropic hardening: unexpected jumps can be observed on the plots at low deformation levels. However, the higher compressive strength compared to the tensile one, due to partial composite action with grout in the buckling-restrained segment, was correctly reproduced with the selected isotropic hardening parameters.

Note that in addition, the experimental measurement of the dissipators response was affected by two sources of inaccuracy; see Chapter 3. First, the dissipator axial force was calculated from the axial strains measured by strain gages applied to the elastic non-milled end segments; however, these segments were subjected to bending during the test, which may have affected the determination of the axial force. Second, the average axial strain of the yielding segment was calculated from the relative displacement between two sections right outside the casing; bending of the end segments caused relative rotations between these two sections, which in turn affected the measurement of the relative displacement. For these reasons, considering the overall satisfactory prediction of the test unit’s behavior, the energy dissipator model was considered acceptable.

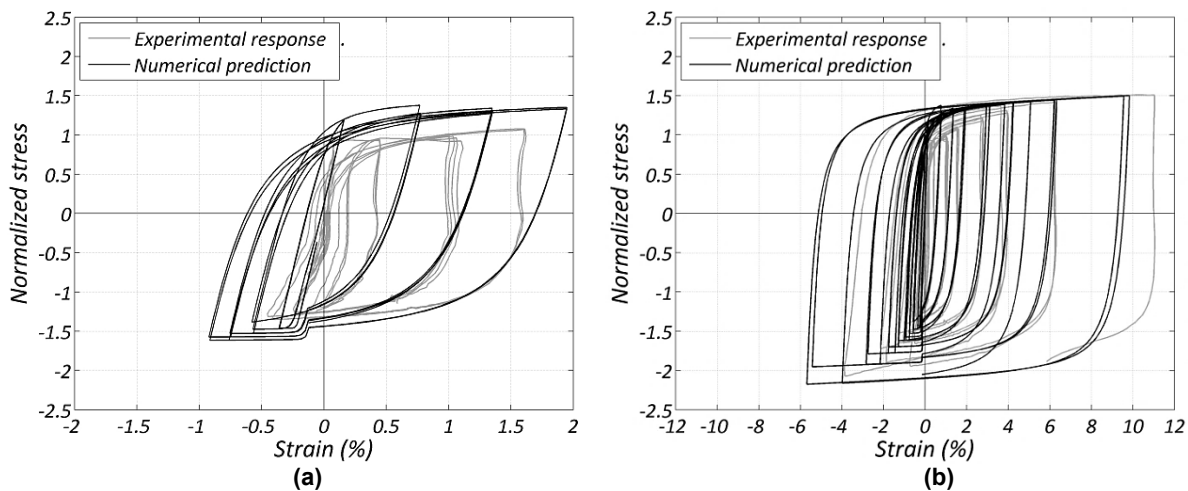


Figure 4.6 Numerical prediction of the hysteretic response of the north–west energy dissipator in Unit 1A: (a) cycles up to 1% drift ratio; and (b) cycles up to 5% drift ratio.

5 Conclusions

This report has discussed the design criteria, experimental performance, and numerical simulations of the composite-concrete dual-steel-shell bridge column technology. This type of column can be specifically designed to minimize damage at the design earthquake, and to exhibit rocking/self-centering response even after large inelastic displacements. Only minor incipient damage was experienced under the same earthquake demands that would cause extensive damage on conventional columns. Damage was maintained at a minimum level even under demands 50% larger than the design earthquake. This results in a dramatic reduction of repair costs and downtime.

The proposed technology also simplifies and accelerates bridge construction. The use of an external shell makes the conventional reinforcing cage obsolete, whereas the inner shell allows for removing unnecessary concrete volume and weight, making this technology ideal for prefabrication and quick erection.

Attention has been focused on details that make this technology effective and prevent undesired loss of self-centering ability under earthquake loading. The mortar bed at the base of the column, required for accommodating construction tolerances between precast elements, needs to be strong and tough enough to sustain the large compressive strain demands induced by rocking. The neutral axis should preferably not cut through the hollow core at the rocking interfaces under the target drift ratio. Post-tensioning bars need to be protected against premature yielding, especially in short-aspect-ratio columns.

Two units were built and tested with a quasi-static reversed cyclic protocol. The main variables between the two units were as follows: (i) the type of energy-dissipation devices, either external buckling-restrained braces or internal stainless steel dowels grouted into the concrete; (ii) the mortar bed, either a plain high-performance metallic-aggregate mix or a fiber-modified high-performance metallic-aggregate mix; and (iii) the type of elastomeric bearing placed in series with the post-tensioning bars, either rubber or polyurethane. The specimens were designed to display no damage at 3% drift ratio, which was assumed to be the drift ratio corresponding to the design earthquake.

Unit 1A, which had a plain metallic-aggregate mortar bed, exhibited mortar crushing and compromised self-centering ability during cycles to 5% drift ratio. Unit 1B incorporated polypropylene fibers in the metallic-aggregate mortar bed, which improved the mortar toughness and delayed its crushing, allowing this unit to display excellent performance beyond 5% drift ratio.

Fracture of the energy-dissipation devices occurred at a drift ratio of 7.5% in both specimens. Damage to the inner shell, which was due to inward concrete dilation, was observed

in both cases and was associated to the neutral axis cutting through the hollow core, causing high compressive strains in the concrete around the inner shell. Post-tensioning bars were effectively protected against yielding by the elastomeric pads mounted in series at their anchorages.

The tests were simulated with OpenSees up to a drift ratio of 5%. An accurate representation of the behavior of the two units was obtained in terms of both global response (lateral force-displacement relationship, cumulative hysteretic energy) and local response (post-tensioning bars strain history, energy dissipators stress-strain relationship). The simplified pushover analysis proposed for the design process also enveloped satisfactorily the experimental lateral force-displacement response. Consistency was observed between the predictions of the refined OpenSees model and those of the simplified analysis procedure.

REFERENCES

- AASHTO (2012). *AASHTO LRFD Bridge Design Specifications*, 6th Ed., American Association of State Highway and Transportation Officials, Washington, D.C.
- ASTM (2010). Standard specification for corrugated steel pipe, metallic-coated for sewers and drains, *ASTM Designation A760/A760M-10*, American Society for Testing and Materials, Philadelphia, PA.
- Boyd P.F., Cofer W.F., McLean D.I. (1995). Seismic performance of steel-encased composite columns under flexural loading, *American Concrete Institute, ACI Struct. J.*, 92(3): 335–364.
- Bradford M.A. (1996). Design strength of slender concrete-filled rectangular steel Tubes, *ACI Struct. J.*, 93(2): 229–235.
- Caltrans (2010). *Seismic Design Criteria*, California Dept. of Transportation, Sacramento, CA.
- Carr A.J. (2008). *Ruaumoko Manual*, Department of Civil Engineering, University of Canterbury, Christchurch, New Zealand.
- Christopoulos C., Filiatrault A., Uang C.-M., Folz B. (2002). Post-tensioned energy dissipating connections for moment resisting steel frames, *ASCE, J. Struct. Eng.*, 128(9): 1111–1120.
- Cormack L.G. (1998). The design and construction of the major bridges on the Mangaweka Rail Deviation, *Trans., Inst. Professional Engineers N.Z.*, 15: 6–23.
- Culmo M.P. (2011). Accelerated bridge construction - experience in design, fabrication and erection of prefabricated bridge elements and systems, *FHWA Report HIF-12.013*, Federal Highway Administration Washington, D.C.
- El-Sheikh M.T., Sause R., Pessiki S., Lu L.-W. (1999). Seismic behaviour and design of unbonded post-tensioned precast concrete frames, *Precast/Prestressed Concrete Institute, PCI J.*, 44(3): 54–71.
- FHWA (2012). <http://www.fhwa.dot.gov/bridge/abc/index.cfm>.
- FHWA (2014). <http://www.fhwa.dot.gov/bridge/nbi/no10/defbr14.cfm>.
- Filippou F.C., Popov E.P., Bertero V.V. (1983). Effects of bond deterioration on hysteretic behavior of reinforced concrete joints, *Report No. UCB/EERC-83/19*, Earthquake Engineering Research Center, University of California, Berkeley, CA.
- Ge H., Usami T. (1992). Strength of concrete-filled thin walled steel box columns: Experiment, *ASCE, J. Struct. Eng.*, 118(11): 3036–3054.
- Ge H., Usami T. (1994). Strength analysis of concrete filled thin walled steel box columns, *J. Construct. Steel Res.*, 37: 607–612.
- Gebman M., Ashford S., Restrepo J.I. (2006). Axial force transfer mechanisms within cast-in-steel-shell piles, *Report No. SSRP-94/10*, Department of Structural Engineering, University of California at San Diego, La Jolla, CA.
- Ghosh R.S. (1977). Strengthening of slender hollow steel columns by filling with concrete, *Canadian J. Civil Eng.*, 4(2): 127–133.
- Guerrini G. (2014). *Seismic Performance of Precast Concrete Dual-Shell Steel Columns for Accelerated Bridge Construction*, Ph.D. Thesis, Department of Structural Engineering, University of California at San Diego, La Jolla, CA.
- Guerrini G., Restrepo J.I. (2011). Advanced precast concrete dual-shell steel columns, *Proceedings, 8th International Conference on Urban Earthquake Engineering*, 1: 1125–1129, Tokyo, Japan.
- Guerrini G., Restrepo J.I., Massari M., Vervelidis A. (2012). Self-centering precast concrete dual-shell steel columns, *Proceedings, 15th World Conference on Earthquake Engineering*, Paper No. 2552, Lisbon, Portugal.
- Guerrini G., Restrepo J.I., Massari M., Vervelidis A. (2015). Seismic behavior of posttensioned self-centering precast concrete dual-shell steel columns, *ASCE, J. Struct. Eng.*, 141(4): 04014115.
- Heiber D.G., Wacker J.M., Eberhard M.O., Stanton J.F. (2005). Precast concrete pier systems for rapid construction of bridges in seismic regions, *Report No. WA-RD 611.1*, Washington Department of Transportation, Olympia, WA.

- Hewes J.T., Priestley M.J.N. (2002). Seismic design and performance of precast concrete segmental bridge columns, *Report No. SSRO-2001/25*, Department of Structural Engineering, University of California at San Diego, La Jolla, CA.
- Holden T., Restrepo J.I., Mander J.B. (2003). Seismic performance of precast reinforced and prestressed concrete walls, *ASCE, J. Struct. Eng.*, 129(3): 286–296.
- Itani A.M. (1996). Future use of composite steel-concrete columns in highway bridges, *American Institute of Steel Construction, AISC Eng.*, 33(3): 110–115.
- Karthik M.M., Mander J.B. (2011). Stress-block parameters for unconfined and confined concrete based on a unified stress-strain model, *ASCE, J. Struct. Eng.*, 137(2): 270–273.
- Kato B. (1996). Column curves of steel-concrete composite members, *J. Constructional Steel Res.*, 39(2): 121–135.
- Kitada T. (1998). Ultimate strength and ductility of state-of-the-art concrete-filled steel bridges piers in Japan, *Eng. Struct.*, 20(4-6): 347–354.
- Knowles R.B., Park R. (1969). Strength of concrete filled steel tubular columns, *ASCE, J. Struct. Div.*, 95(12): 2565–2587.
- Kurama Y., Sause R., Pessiki S., Lu L.-W. (1999). Lateral load behavior and seismic design of unbonded post-tensioned precast concrete walls, *American Concrete Institute, ACI Struct. J.*, 96(4): 622–632.
- Kwan W.P., Billington S. (2003a). Unbonded posttensioned concrete bridge piers. i: monotonic and cyclic analyses, *ASCE, J. Bridge Eng.*, 8(2): 92–101.
- Kwan W.P., Billington S. (2003b). Unbonded posttensioned concrete bridge piers. II: Seismic analyses, *ASCE, J. Bridge Eng.*, 8(2): 102–111.
- Leon R.T., Kim D.K., Hajjar J.F. (2007). Limit state response of composite columns and beam-columns: formulation of design provisions for the 2005 AISC specification, *American Institute of Steel Construction, AISC Eng., J.*, 44(4): 341–358.
- MacRae G.A., Priestley M.J.N. (1994). Precast post-tensioned ungrouted concrete beam-column subassemblage tests, *Report No. SSRP-94/10*, Department of Applied Mechanics and Engineering Sciences, University of California at San Diego, La Jolla, CA.
- Makris N., Roussos Y. (1998). Rocking response and overturning of equipment under horizontal-type pulses, *Report No PEER 1998/05*, Pacific Earthquake Engineering Research Center, University of California, Berkeley, CA.
- Mander J.B., Cheng C.-T. (1997). Seismic resistance of bridge piers based on damage avoidance Design, *Technical Report NCEER-97-0014*, NCEER, Department of Civil and Environmental Engineering, State University of New York at Buffalo, Buffalo, NY.
- Mander J.B., Priestley M.J.N., Park R. (1988). Theoretical stress-strain model for confined concrete, *ASCE, J. Struct. Eng.*, 114(8): 1804–1826.
- Marriott D., Pampanin S., Palermo A. (2009). Quasi-static and pseudo-dynamic testing of unbonded post-tensioned rocking bridge piers with external replaceable dissipators, *Earthq. Eng. Struct. Dyn.*, 38: 331–354.
- Marriott D., Pampanin S., Palermo A. (2011). Biaxial testing of unbonded post-tensioned rocking bridge piers with external replaceable dissipators, *Earthq. Eng. Struct. Dyn.*, 40: 1723–1741.
- Massari M. (2012). *Hybrid Precast Concrete Dual-Shell Steel Bridge Columns Under Lateral Loading*, Laurea Specialistica Thesis, Department of Civil, Environmental and Materials Engineering, University of Bologna, Bologna, Italy.
- Matsui C., Tsuda K., Ishibashi, Y. (1995). Slender concrete filled steel tubular columns under combined compression and bending, *Proceedings, 4th Pacific Structural Steel Conference*, Steel-Concrete Composite Structures, 3: 29–36, Singapore.
- Mazzoni S., McKenna F., Scott M.H., Fenves G.L. et al. (2007). *OpenSees Command Language Manual*, Pacific Earthquake Engineering Research Center, University of California, Berkeley, CA.
- McKenna F., Scott M.H., Fenves G.L. (2010). Nonlinear finite element analysis software architecture using object composition, *ASCE, J. Computing Civil Eng.*, 24(1): 95–107.

- Nakaki S.D., Stanton J.F., Sritharan S. (1999). An overview of the PRESSS five-story precast test building, Precast/Prestressed Concrete Institute, *PCI J.*, 44(2): 26–39.
- Neogi P.K., Sen H.K., Chapman J.C. (1969). Concrete-filled tubular steel columns under eccentric loading, *Struct. Engineer.* 47(5): 187–195.
- O'Brien A.D., Rangan B.V. (1993). Tests on slender tubular steel columns filled with high-strength concrete, *Australian Civil Eng. Trans.*, 35(4): 287–292.
- O'Shea M.D., Bridge R.Q. (1995). Circular thin walled concrete filled steel tubes, ASCE, *J. Struct. Eng.*, 126(11): 1295–1303.
- Ou Y.-C., Chiewanichakorn M., Ahn I.-S., Aref A.J., Chen S.S., Filiatrault A., Lee G.C. (2006). Cyclic performance of precast concrete segmental bridge columns: simplified analytical and finite element studies, *Transport. Res. Record: J. Transport. Res. Board.* 1976: 66–74.
- Ou Y.-C., Wang P.-H., Tsai M.-S., Chang K.-C., Lee G.C. (2010). Large-scale experimental study of precast segmental unbonded posttensioned concrete bridge columns for seismic regions, ASCE, *J. Struct. Eng.*, 136(3): 255–264.
- Palermo A., Pampanin S. (2008). Enhanced seismic performance of hybrid bridge systems: comparison with traditional monolithic solutions, *J. Earthq. Eng.*, 12(8): 1267–1295.
- Palermo A., Pampanin S., Calvi G.M. (2005). Concept and development of hybrid solutions for seismic resistant bridge systems, *J. Earthq. Eng.*, 9(6): 899–921.
- Palermo A., Pampanin S., Marriott D. (2007). Design, modeling, and experimental response of seismic resistant bridge piers with posttensioned dissipating connections, ASCE, *J. Struct. Eng.*, 133(11): 1648–1661.
- Park R.J.T., Paulay T. (1990). Strength and ductility of concrete substructures of bridges, *Transit N.Z. - Road Res. Unit Bull.*, 84(1): 14–29.
- Park R.J.T., Priestley M.J.N., Walpole W.R. (1983). The seismic performance of steel encased reinforced concrete bridge piles, *Bull. N.Z. Nat. Soc. Earthq. Eng.*, 16(2): 123–140.
- Paulay T., Priestley M.J.N. (1992). *Seismic Design of Reinforced Concrete and Masonry Buildings*. John Wiley and Sons, New York, NY.
- Pérez F.J., Pessiki S., Sause R., Lu L.-W. (2003). Lateral load tests of unbonded post-tensioned precast concrete walls, *Special Publication of Large-Scale Structural Testing, Paper No. SP 211-8*, American Concrete Institute, pp. 161–182, Detroit, MI.
- Priestley M.J.N., Sritharan S., Conley J.R., Pampanin S. (1999). Preliminary results and conclusions from the PRESSS five-story precast concrete test building, Precast/Prestressed Concrete Institute, *PCI J.*, 44(6): 42–67.
- Priestley M.J.N., Tao J.R.T. (1993). Seismic response of precast prestressed concrete frames with partially debonded tendons, Precast/Prestressed Concrete Institute, *PCI J.*, 38(1): 58–69.
- Prion H.G.L., Boehme J. (1989). Beam-column behaviour of steel tubes filled with high-strength concrete, *Proceedings, Fourth International Colloquium, SSRC*, pp. 439–449, New York.
- Rangan B.V., Joyce M. (1992). Strength of eccentrically loaded slender steel tubular columns filled with high strength concrete, American Concrete Institute, *ACI Struct. J.*, 89(6): 676–681.
- Restrepo J.I., Rahman A. (2007). Seismic performance of self-centering structural walls incorporating energy dissipators, ASCE, *J. Struct. Eng.*, 133(11): 1560–1570.
- Restrepo J.I., Tobolski M.J., Matsumoto E.E. (2011). Development of a precast bent cap system for seismic regions, *NCHRP Report 681*, Transportation Research Board, Washington, D.C.
- Sakai J., Jeong H., Mahin S.A. (2006). Reinforced concrete bridge columns that recenter following earthquakes, *Proceedings, 8th U.S. National Conference on Earthquake Engineering*, Paper No. 1421, San Francisco, CA.
- Sakai J., Mahin S.A. (2004). Analytical investigations of new methods for reducing residual displacements of reinforced concrete bridge column, *Report No. PEER 2004/02*, Pacific Earthquake Engineering Research Center, University of California, Berkeley, CA.

- Sakino K., Ishibashi H. (1985). Experimental studies on concrete filled square steel tubular short columns subjected to cyclic shearing force and constant axial force, *Trans., Arch. Inst. Japan*, Tokyo, Japan, 353: 81–89.
- Sakino K., Tomii M. (1981). Hysteretic behaviour of concrete filled square shell tubular beam-columns failed in flexure, *Trans., Japan Conc. Inst.*, Tokyo, Japan, 3: 439–446.
- Shakir-Khalil H., Mouli M. (1990). Further tests on concrete-filled rectangular hollow section columns, *Struct. Engineer*. 68(20): 405–413.
- Shakir-Khalil H., Zeghiche J. (1989). Experimental behaviour of concrete-filled rolled rectangular hollow section columns, *Struct. Engineer*, 67(19): 346–353.
- Shanmugam N.E., Lakshmi B. (2001). State of the art report on steel-concrete composite columns, *J. Construct. Steel Res*, 57: 1041–1080.
- Sharpe R.D., Skinner R.I. (1983). The seismic design of an industrial chimney with rocking base, *Bull. N.Z. Nat. Soc. Earthq. Eng.*, 16(2): 98–106.
- Solberg K., Mashiko N., Mander J.B., Dhakal R.P. (2009). Performance of a damage-protected highway bridge pier subjected to bidirectional earthquake attack, ASCE, *J. Struct. Eng.*, 135(5): 469–478.
- Stone W.C., Cheok G.S., Stanton J.F. (1995). Performance of hybrid moment-resisting precast beam-column concrete connections subjected to cyclic loading, American Concrete Institute, *ACI Struct. J.*, 91(2): 229–249.
- Suzuki H., Kato B. (1981). Shear strength of concrete filled box elements, *Proceedings, Conference on Joints in Structural Steelwork*, Middlesborough, England.
- Taylor R.G. (1977). *The Nonlinear Seismic Response of Tall Shear Wall Structures*, Ph.D. Thesis, Department of Civil Engineering, University of Canterbury, Christchurch, New Zealand.
- Tobolski M.J. (2010). *Improving the Design and Performance of Concrete Bridges in Seismic Regions*, Ph.D. Thesis, Department of Structural Engineering, University of California at San Diego, La Jolla, CA.
- Toranzo L.A., Restrepo J.I., Mander J.B., Carr A.J. (2009). Shake-table tests of confined-masonry rocking walls with supplementary hysteretic damping, *J. Earthq. Eng.*, 13(6): 882–898.
- Uy B., Patil S.B. (1996). Concrete-filled high strength steel box columns for tall buildings: behaviour and design, *Struct. Design Tall Bldgs.*, 5: 75–93.
- Vervelidis A. (2012). *Seismic Response of Self-Centering Precast Concrete Dual-Shell Steel Columns*, Laurea Specialistica Thesis, Department of Civil, Environmental and Materials Engineering, University of Bologna, Bologna, Italy.
- Virdi K.S., Dowling P.J. (1973). The ultimate strength of composite columns in biaxial bending, *Proceedings, Institution of Civil Engineers, Part 2*. 55: 251–272.
- Vulcano A., Bertero V.V. (1987). Analytical models for predicting the lateral response of RC shear walls: evaluation of their reliability, *Report No. UCB/EERC-87/19*, Earthquake Engineering Research Center, University of California, Berkeley, CA.
- Wang Y.C., Moore D.B. (1997). A design method for concrete-filled hollow section composite columns, *Struct. Engineer*, 75(21): 368–372.

Appendix A: Construction Drawings

The construction drawings for Unit 1A and Unit 1B, inclusive of structural details and instrumentation plans, are shown on the next pages. Due to formatting constraints, the drawings are not exactly to scale.

GENERAL NOTES:
 1. THE CLEAR COVER FOR ALL SECTIONS SHALL BE 1" UNLESS OTHERWISE NOTED

CONCRETE MATERIAL NOTES:

1. ALL CONCRETE SHALL HAVE 28 DAY COMPRESSIVE STRENGTH OF 9,000 PSI
2. ALL CONCRETE SHALL HAVE MINIMUM SLUMP OF 6"

GRAOUT AND MORTAR MATERIAL NOTES:

1. BASF EMBECCO 8895 GROUT SHALL BE USED
2. DURAFIBER POLYPROPYLENE FIBERS SHALL BE ADDED TO THE MORTAR AT THE COLUMN-FOOTING INTERFACE, WITH FIBER-TO-MORTAR WEIGHT RATIO OF 0.037%

MILD REINFORCEMENT MATERIAL NOTES:

1. MILD REINFORCEMENT INSIDE FOOTING AND LOAD-SLAB SHALL BE A615, GRADE 60 STEEL

POST-TENSIONING MATERIAL NOTES:

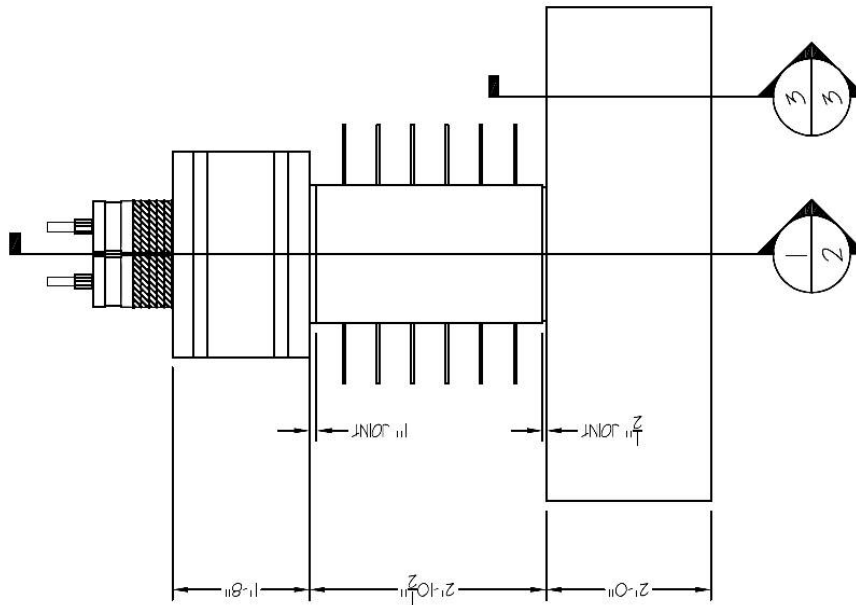
1. ALL POST-TENSIONING SHALL BE A722, GRADE 150, LOW-RELAXATION STEEL
2. POST-TENSIONING FORCE AFTER LOSSES SHALL BE 59 KIPS (25% GUP) PER POST-TENSIONING BAR

STEEL SHELL MATERIAL NOTES:

1. OTHER STEEL SHELL SHALL BE A572, GRADE 50

ENERGY DISSIPATOR MATERIAL NOTES:

1. EXTERNAL BUCKLING-RESTRAINED ENERGY DISSIPATORS SHALL BE A576, GRADE 1018, HOT ROLLED STEEL
2. ANCHOR BARS FOR EXTERNAL DISSIPATORS SHALL BE A706, GRADE 60 REINFORCING BARS
3. INTERNAL ENERGY DISSIPATORS SHALL BE #16LN, GRADE 60 STAINLESS STEEL REBARS



1 SPECIMEN ELEVATION
 1/2" = 1'-0"

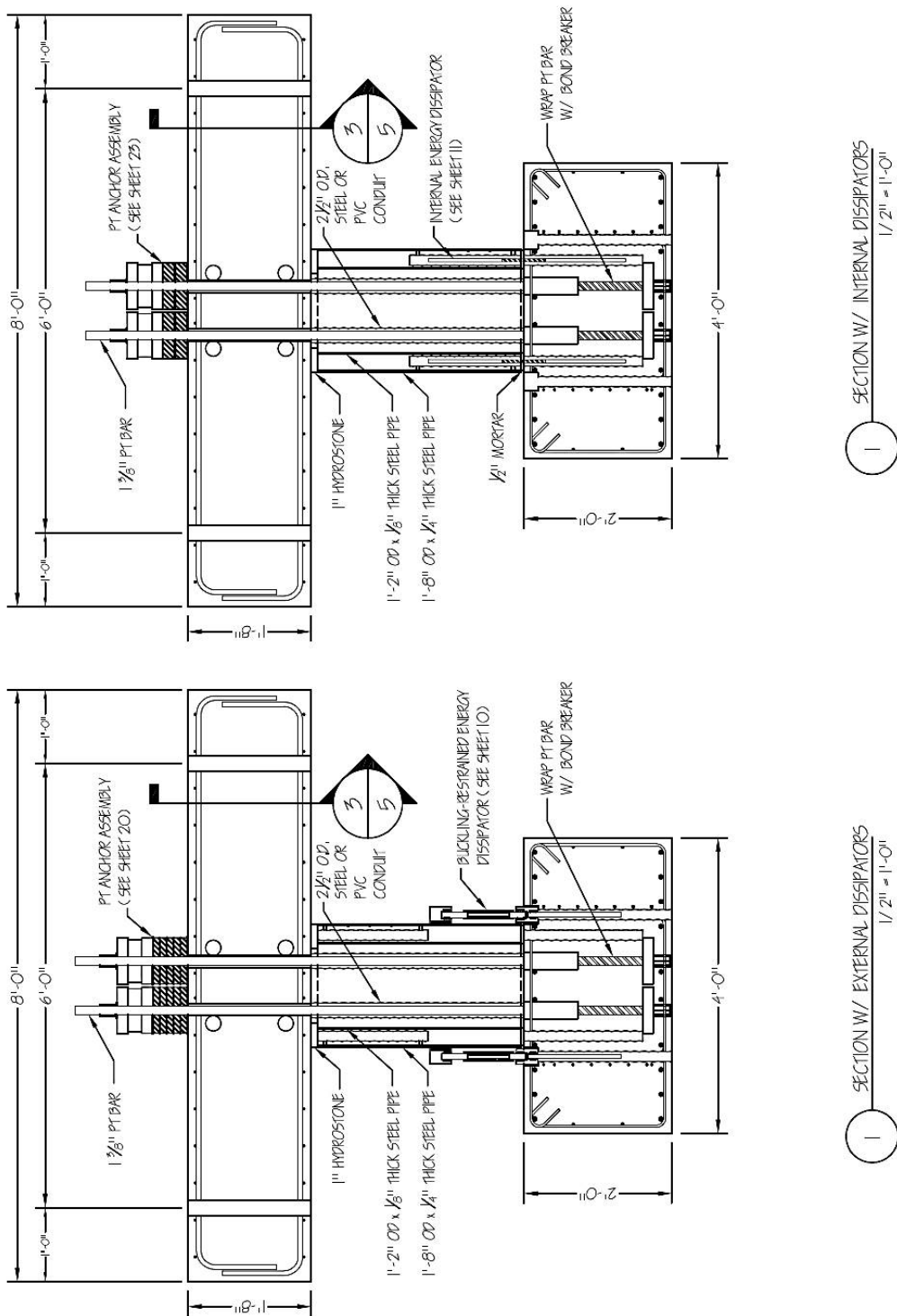
APPROVED FOR PRODUCTION



ADV. PRECAST CONCR. DUAL-SHELL STEEL COLUMNS

SPECIMEN ELEVATION

| | | | |
|-----------|-------|-------|--------------------|
| SPECIMEN: | UNIT: | TEST: | CONNECTION DETAIL: |
| 34: | GG | CHK: | DATE: |
| | | | 11/08/11 |
| | | | SCALE: |
| | | | 1/2" = 1'-0" |
| | | | SHEET: |
| | | | 01 |



SECTION W/ INTERNAL DISSIPATORS
1/2" = 1'-0"

SECTION W/ EXTERNAL DISSIPATORS
1/2" = 1'-0"

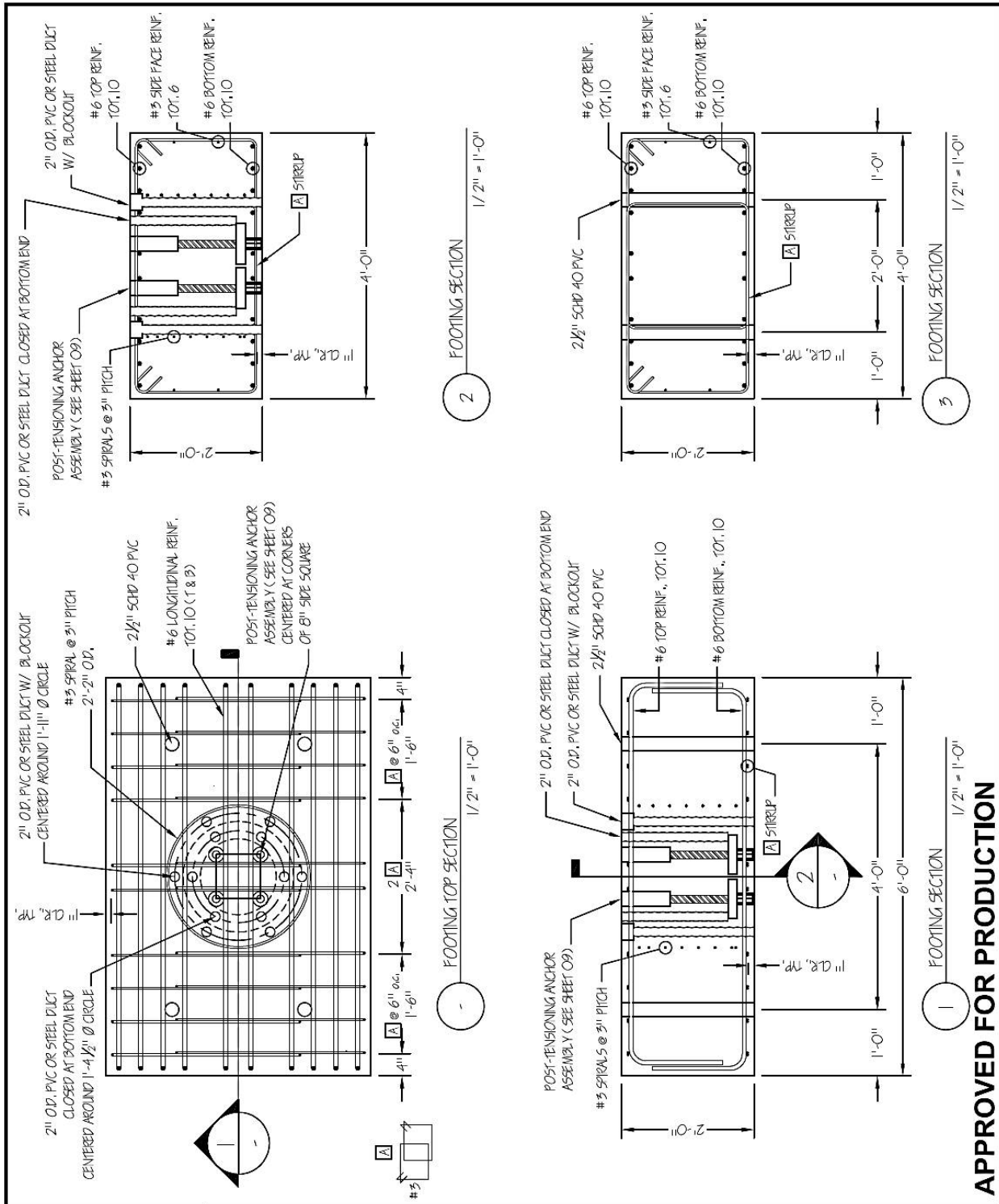
APPROVED FOR PRODUCTION



ADV. PRECAST CONCR. DUAL-SHELL STEEL COLUMNS

GENERAL SECTION

| | | | | | |
|-----------|------|---------------------|---------------------|--------------------------|--|
| SPECIMEN: | | TEST: | | CONNECTION DETAIL: | |
| UNIT I | | QUASI STATIC - UCSD | | HYBRID DUAL-SHELL COLUMN | |
| BY: GG | CHK: | DATE: 11/08/11 | SCALE: 1/2" = 1'-0" | SHEET: 02 | |



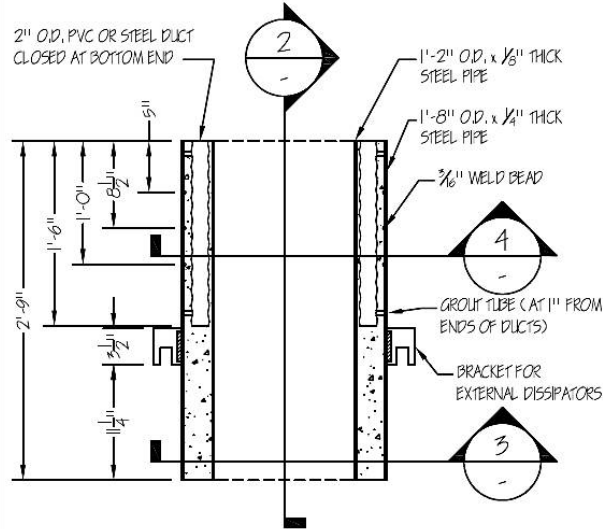
APPROVED FOR PRODUCTION



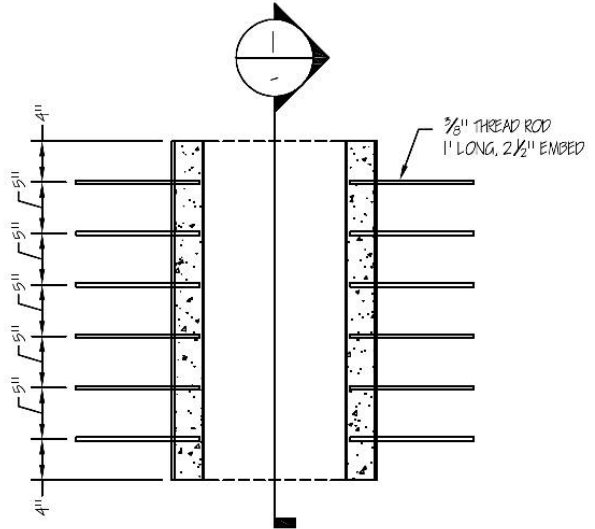
ADV. PRECAST CONCR. DUAL-SHELL STEEL COLUMNS

FOOTING DETAILS

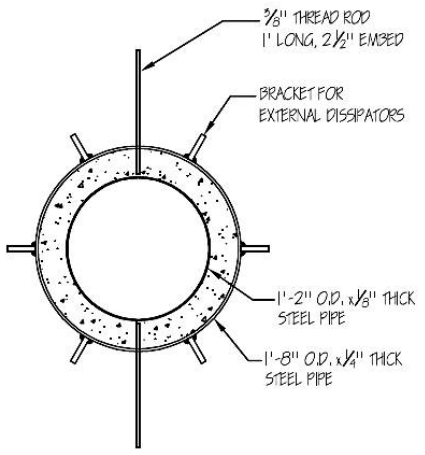
| | | | | | | | | |
|-----------|--------|-------|---------------------|------------------|--------------------------|--------------|--------|----|
| SPECIMEN: | UNIT I | TEST: | QUASI STATIC - UCSD | CONNECTION TYPE: | HYBRID DUAL-SHELL COLUMN | | | |
| BY: | GG | CHK: | DATE: | 10/25/11 | SCALE: | 1/2" = 1'-0" | SHEET: | 03 |



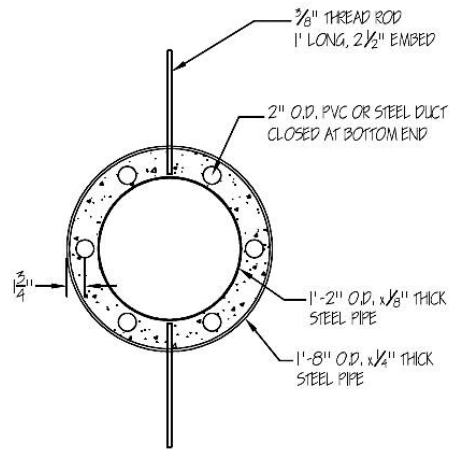
1 COLUMN SECTION
3/4" = 1'-0"



2 COLUMN SECTION
3/4" = 1'-0"



3 COLUMN SECTION - LOWER END
3/4" = 1'-0"



4 COLUMN SECTION - UPPER END
3/4" = 1'-0"

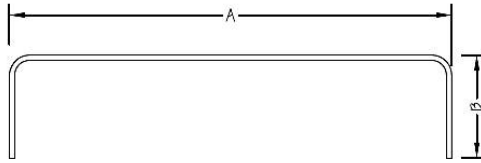
APPROVED FOR PRODUCTION



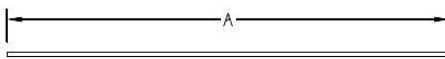
ADV. PRECAST CONCR. DUAL-SHELL STEEL COLUMNS

COLUMN SECTIONS

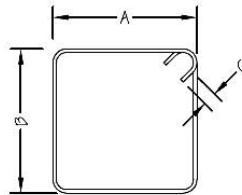
| | | | |
|-----------|--------|---------------------|--------------------------|
| SPECIMEN: | UNIT: | TEST: | CONNECTION DETAIL: |
| | UNIT I | QUASI STATIC - UCSD | HYBRID DUAL-SHELL COLUMN |
| BY: | GG | CHK: | DATE: 10/10/11 |
| | | | SCALE: 3/4" = 1'-0" |
| | | | SHEET: 04 |



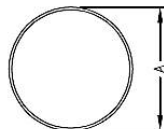
| ASTM | GRADE | BAR SIZE | A | B | C | QTY |
|------|-------|----------|-------|-------|---|-----|
| A615 | 60 | #6 | 5'-9" | 1'-5" | - | 20 |
| A615 | 60 | #6 | 7'-9" | 1'-1" | - | 8 |



| ASTM | GRADE | BAR SIZE | A | B | C | QTY |
|------|-------|----------|--------|---|---|-----|
| A615 | 60 | #3 | 5'-10" | - | - | 4 |
| A706 | 60 | #6 | 1'-3" | - | - | 6 |



| ASTM | GRADE | BAR SIZE | A | B | C | QTY |
|------|-------|----------|--------|--------|--------|-----|
| A615 | 60 | #3 | 2'-10" | 1'-10" | 2 1/4" | 20 |
| A615 | 60 | #3 | 2'-4" | 1'-6" | 2 1/4" | 16 |



*** SPIRAL REINFORCEMENT ***

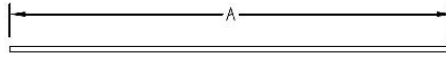
| ASTM | GRADE | BAR SIZE | A | TURNS | PITCH | QTY |
|------|-------|----------|-------|-------|-------|-----|
| A615 | 60 | #3 | 2'-2" | 7 | 3" | 1 |

APPROVED FOR PRODUCTION



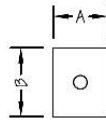
**ADV. PRECAST CONCR. DUAL-SHELL STEEL COLUMNS
REINFORCEMENT SCHEDULE**

| | | | | | | |
|-----------|--------|-------|---------------------|--------------------|--------------------------|-----|
| SPECIMEN: | UNIT I | TEST: | QUASI STATIC - UCSD | CONNECTION DETAIL: | HYBRID DUAL-SHELL COLUMN | |
| BY: | GG | CHK: | DATE: | 07/21/11 | SCALE: | NTS |
| | | | | | SHEET: | 06 |



*** DSI THREADBAR ***

| ASTM | GRADE | BAR SIZE | A | B | C | QTY |
|------|-------|----------|-----------|---|---|-----|
| A722 | 150 | 1 3/8" | 9'-5" | - | - | 8 |
| A722 | 150 | 1 3/8" | 1'-7 1/2" | - | - | 4 |



*** DSI ANCHOR PLATE ***

| BAR SIZE | A | B | THICKNESS | QTY |
|----------|----|--------|-----------|-----|
| 1 3/8" | 7" | 7 1/2" | 1 3/4" | 4 |

*** DSI COUPLER ***

| BAR SIZE | LENGTH | DIAMETER | QTY |
|----------|--------|----------|-----|
| 1 3/8" | 8 3/4" | 2 3/4" | 4 |

*** DSI NUT ***

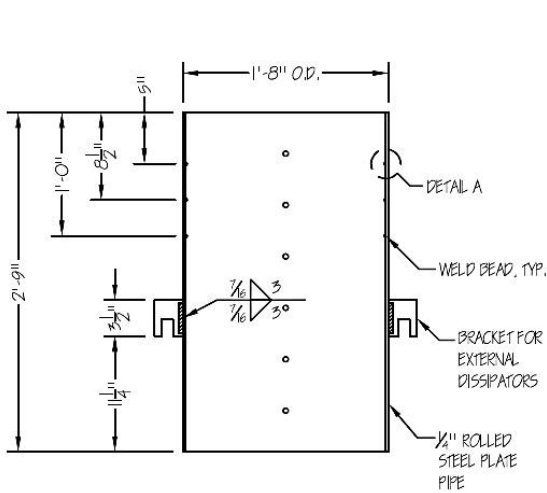
| BAR SIZE | QTY |
|----------|-----|
| 1 3/8" | 4 |

APPROVED FOR PRODUCTION

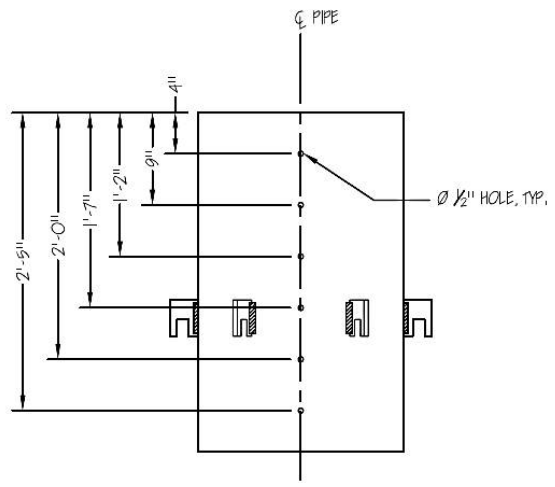


**ADV. PRECAST CONCR. DUAL-SHELL STEEL COLUMNS
PT BARS AND ACCESSORIES SCHEDULE**

| | | | | | | | | |
|-----------|--------|-------|---------------------|--------------------|--------------------------|-----|--------|----|
| SPECIMEN: | UNIT I | TEST: | QUASI STATIC - UCSD | CONNECTION DETAIL: | HYBRID DUAL-SHELL COLUMN | | | |
| BY: | GG | CHK: | DATE: | 07/21/11 | SCALE: | NTS | SHEET: | 07 |



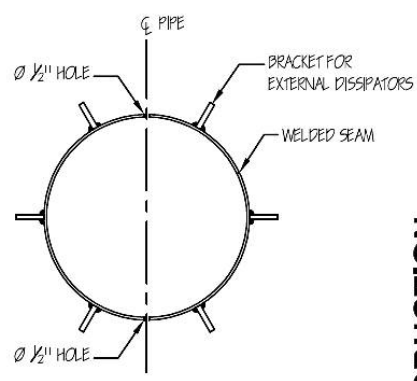
1 STEEL PIPE LONG SECTION
3/4" = 1'-0"



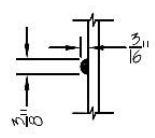
2 STEEL PIPE HOLE LOCATIONS
3/4" = 1'-0"

NOTES:

1. ROLLED STEEL PLATE PIPE SHALL BE A572 GRADE 50 AND WELDING SHALL BE COMPLETE JOINT PENETRATION.
2. ALL WELDING SHALL BE USING E70 ELECTRODE.
3. LOCATIONS OF WELD BEAD GIVEN TO CENTER OF BEAD.
4. WELD BEAD SHALL BE PLACED AROUND ENTIRE INNER CIRCUMFERENCE.



3 STEEL PIPE SECTION
3/4" = 1'-0"



A WELD BEAD DETAIL
1/4" = 1"

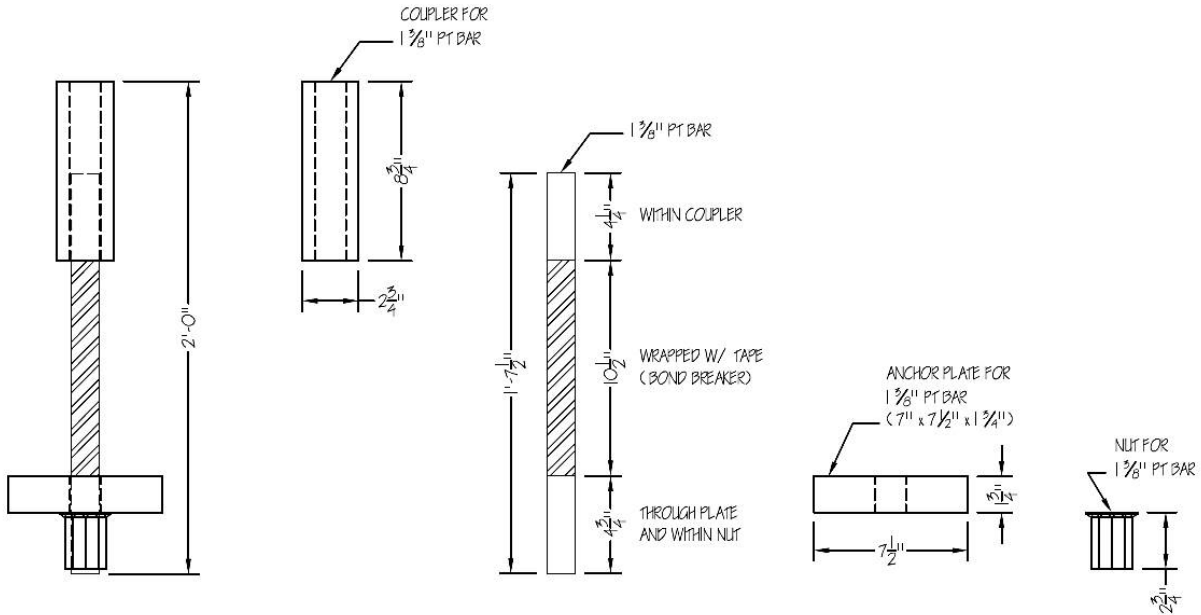
APPROVED FOR PRODUCTION



ADV. PRECAST CONCR. DUAL-SHELL STEEL COLUMNS

COLUMN OUTER SHELL DETAIL

| | | | | | | | | |
|-----------|--------|-------|---------------------|--------------------|--------------------------|----------|--------|----|
| SPECIMEN: | UNIT I | TEST: | QUASI STATIC - UCSD | CONNECTION DETAIL: | HYBRID DUAL-SHELL COLUMN | | | |
| BY: | GG | CHK: | DATE: | 10/10/11 | SCALE: | AS SHOWN | SHEET: | 08 |



1 FOOTING PT ANCHOR ASSEMBLY
1/8" = 1"

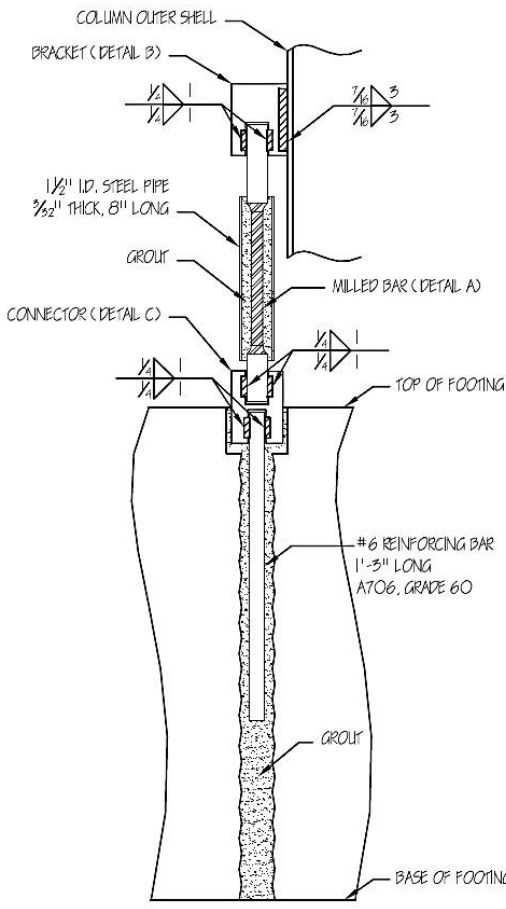
- NOTES:
1. FOUR FOOTING ANCHOR ASSEMBLIES NEED TO BE FABRICATED (ONE PER PT BAR)
 2. ASSEMBLIES ARE CENTERED AT THE CORNERS OF AN 8" SIDE SQUARE AS SHOWN ON SHEET 03

APPROVED FOR PRODUCTION

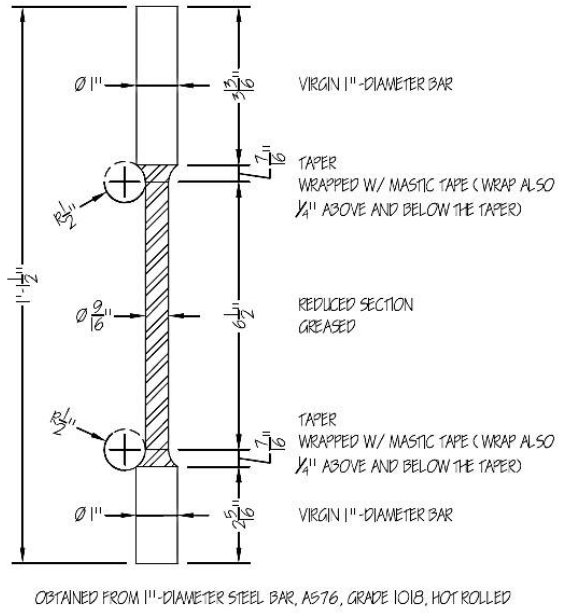


ADV. PRECAST CONCR. DUAL-SHELL STEEL COLUMNS
PT-FOOTING ANCHOR SYSTEM DETAIL

| | | | | | | | | |
|-----------|--------|-------|---------------------|--------------------|--------------------------|-----------|--------|----|
| SPECIMEN: | UNIT I | TEST: | QUASI STATIC - UCSD | CONNECTION DETAIL: | HYBRID DUAL-SHELL COLUMN | | | |
| BY: | GG | CHK: | DATE: | 10/25/11 | SCALE: | 1/8" = 1" | SHEET: | 09 |

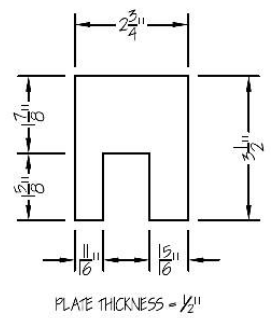


- NOTES:**
- SIX BUCKLING-RESTRAINED DISSIPATOR ASSEMBLIES NEED TO BE FABRICATED FOR THE COLUMN SPECIMEN + TWO FOR SEPARATE TESTING
 - SIX BRACKETS SHALL BE WELDED TO THE COLUMN OUTER SHELL PRIOR TO CONCRETE POURING, BRACKET LOCATION IS SHOWN ON SHEETS O4 AND O7
 - SIX #6 REINFORCING BARS SHALL BE WELDED TO CORRESPONDING SIX CONNECTORS PRIOR TO THEIR INSTALLATION IN THE FOOTING
 - MILLED BARS SHALL BE GROUTED INSIDE PIPES PRIOR TO THEIR INSTALLATION ON THE COLUMN SPECIMEN
 - THE ENDS OF THE MILLED BARS SHALL BE WELDED TO BRACKET AND CONNECTOR AFTER THE SPECIMEN HAS BEEN ASSEMBLED, BUT PRIOR TO POST-TENSIONING
 - ALL FILLET WELDS SHALL BE PERFORMED WITH E70 ELECTRODE

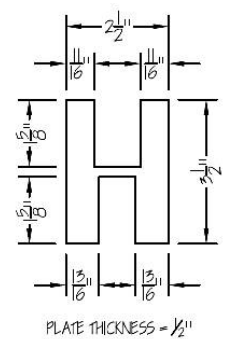


1 BUCKLING-RESTRAINED DISSIPATOR ASSEMBLY
1/8" = 1"

A MILLED BAR DETAIL
1/4" = 1"



B BRACKET DETAIL
1/4" = 1"



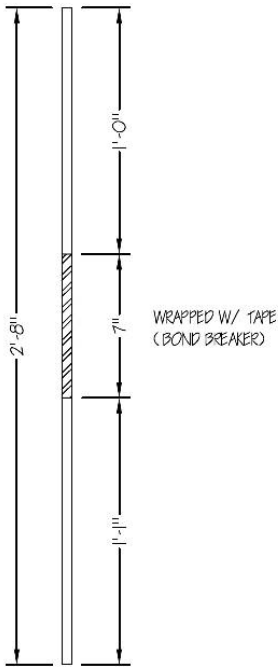
C CONNECTOR DETAIL
1/4" = 1"

APPROVED FOR PRODUCTION



ADV. PRECAST CONCR. DUAL-SHELL STEEL COLUMNS
BUCKLING-RESTRAINED ENERGY DISSIPATOR DETAIL

| | | | | | | | | |
|-----------|--------|-------|---------------------|--------------------|--------------------------|----------|--------|----|
| SPECIMEN: | UNIT I | TEST: | QUASI STATIC - UCSD | CONNECTION DETAIL: | HYBRID DUAL-SHELL COLUMN | | | |
| BY: | GG | CHK: | DATE: | 10/12/11 | SCALE: | AS SHOWN | SHEET: | 10 |



#4 REBAR, 316LN STAINLESS STEEL

INTERNAL DISSIPATOR ASSEMBLY
1/8" = 1"

NOTES:

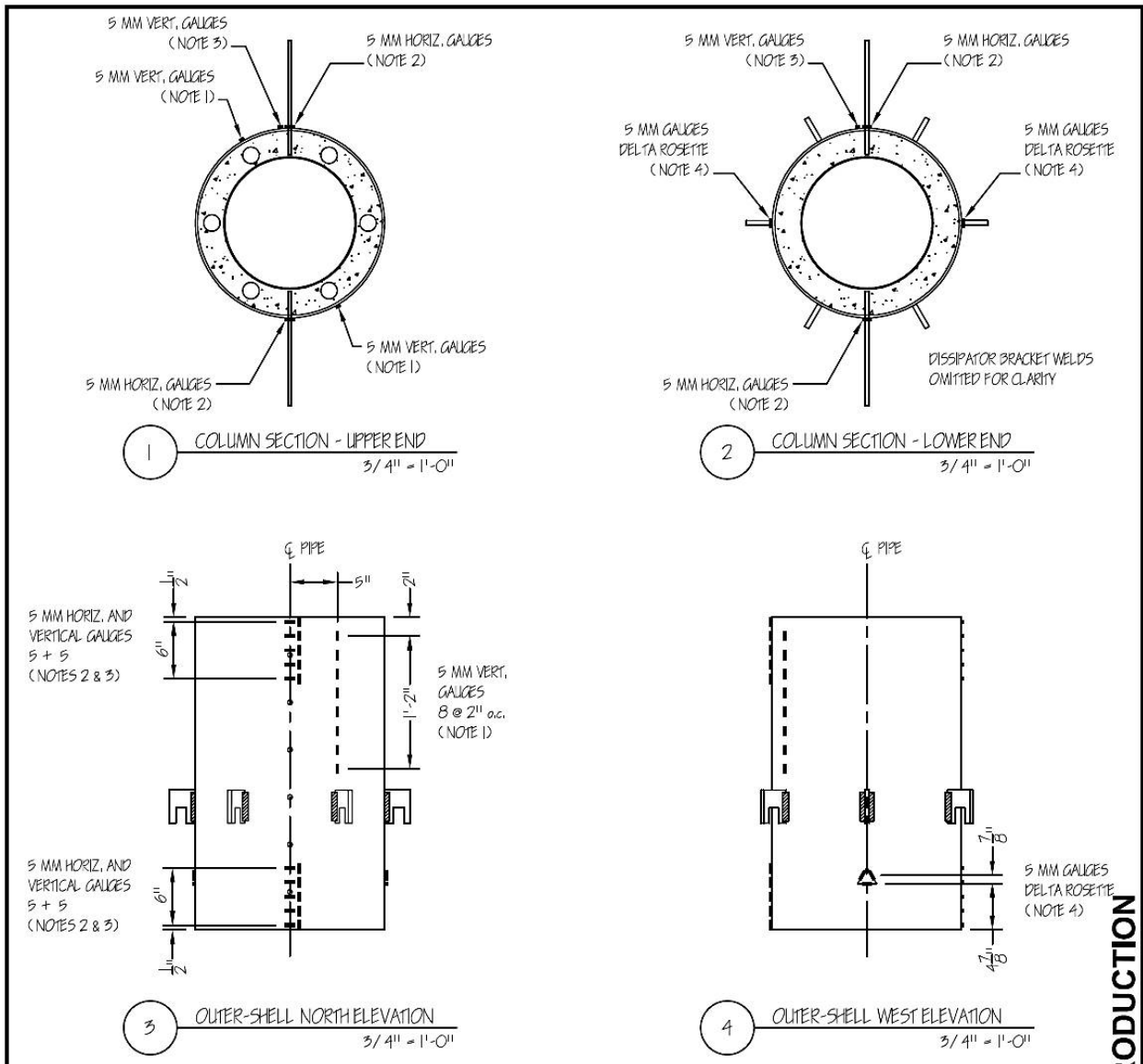
1. SIX INTERNAL DISSIPATORS NEED TO BE PROVIDED FOR THE COLUMN SPECIMEN PLUS THREE FOR MATERIAL TESTING
2. INTERNAL DISSIPATORS SHALL BE FIRST GROUTED INSIDE THE FOOTING DUCTS
3. AFTER THE UNIT HAS BEEN PLACED ON THE FOOTING, THE OTHER END OF THE DISSIPATORS SHALL BE GROUTED INSIDE THE COLUMN DUCTS

APPROVED FOR PRODUCTION



ADV. PRECAST CONCR. DUAL-SHELL STEEL COLUMNS
INTERNAL ENERGY DISSIPATOR DETAIL

| | | | | |
|------------------|------|---------------------------|---|-----------|
| SPECIMEN: UNIT I | | TEST: QUASI STATIC - UCSD | CONNECTION DETAIL: HYBRID DUAL-SHELL COLUMN | |
| BY: GG | CHK: | DATE: 12/12/11 | SCALE: 1/8" = 1" | SHEET: 11 |



NOTES:

1. VERTICAL STRAIN GAUGES SHALL BE LOCATED ON THE OUTER SHELL, IN FRONT OF TWO DIAMETRICALLY OPPOSITE INTERNAL DISSIPATOR BARS
2. HORIZONTAL STRAIN GAUGES SHALL BE PLACED AT BOTH ENDS, ON THE NORTH AND SOUTH FACES OF THE OUTER SHELL, AT 1/2", 1-3/4", 3", 5", 6-1/2" FROM EACH END
3. VERTICAL STRAIN GAUGES SHALL BE PLACED AT BOTH ENDS, ONLY ON THE NORTH FACE OF THE OUTER SHELL, AT 1/2", 1-3/4", 3", 5", 6-1/2" FROM EACH END
4. ONE DELTA ROSETTE SHALL BE PROVIDED ON THE WEST FACE AND ONE ON THE EAST FACE OF THE OUTER SHELL. STRAIN GAUGES SHALL BE PLACED ALONG THE SIDES OF A 2"-SIDE EQUILATERAL TRIANGLE.

NUMBER OF GAUGES REQUIRED FOR TEST #1:
5 MM 5 VERT. + 10 HORIZ. (15 TOTAL)

NUMBER OF GAUGES REQUIRED FOR TEST #2:
5 MM 21 VERT. + 10 HORIZ. (31 TOTAL)

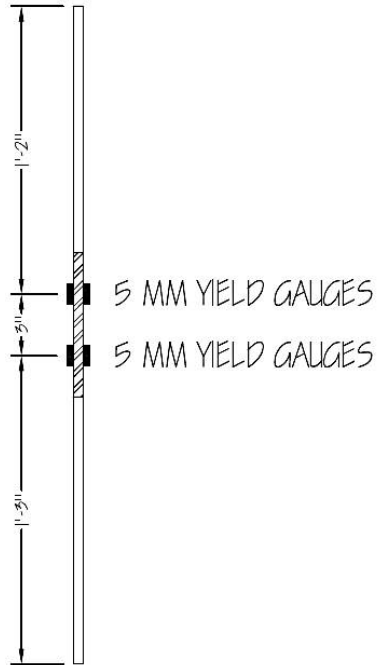
NUMBER OF GAUGES REQUIRED FOR BOTH TESTS:
5 MM 3 PER ROSETTE (6 TOTAL)

APPROVED FOR PRODUCTION



ADV. PRECAST CONCR. DUAL-SHELL STEEL COLUMNS
INSTRUMENTATION PLAN: OUTER SHELL

| | | | | | |
|------------------|------|---------------------------|---------------------|---|--|
| SPECIMEN: UNIT I | | TEST: QUASI STATIC - UCSD | | CONNECTION DETAIL: HYBRID DUAL-SHELL COLUMN | |
| BY: GG | CHK: | DATE: 11/08/11 | SCALE: 3/4" = 1'-0" | SHEET: 13 | |

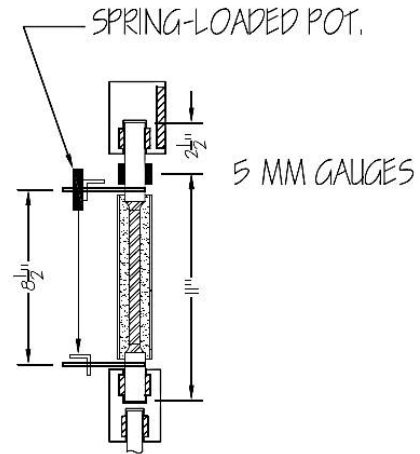


1 INTERNAL DISSIPATOR BAR
1/8" = 1"

NOTES:

1. TWO DIAMETRICALLY OPPOSITE DISSIPATOR BARS SHALL BE INSTRUMENTED
2. TWO STRAIN GAUGES SHALL BE PROVIDED AT EACH LOCATION, ON OPPOSITE SIDES OF THE BAR

NUMBER OF GAUGES REQUIRED:
5 MM YIELD 4 EA. BAR (8 TOTAL)



2 BUCKLING-RESTRAINED DISSIPATOR
1/8" = 1"

NOTES:

1. TWO DIAMETRICALLY OPPOSITE BUCKLING-RESTRAINED DISSIPATORS SHALL BE INSTRUMENTED
2. TWO STRAIN GAUGES SHALL BE PROVIDED AT EACH LOCATION, ON OPPOSITE SIDES OF THE BAR

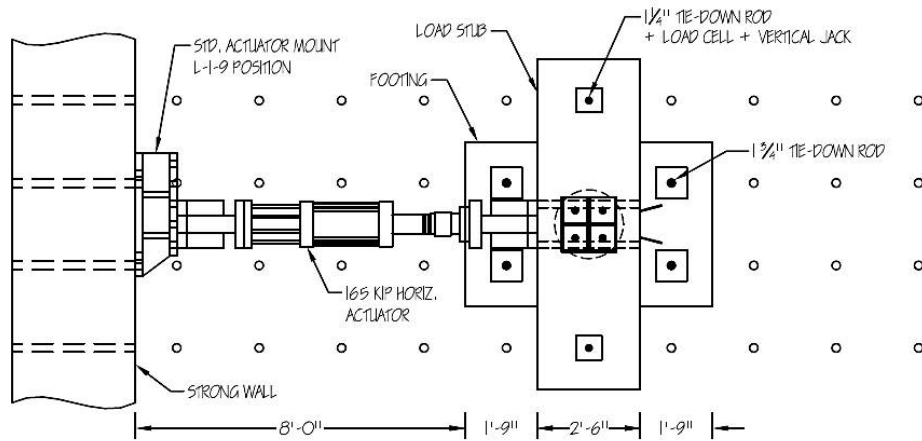
NUMBER OF GAUGES REQUIRED:
5 MM 2 EA. BAR (4 TOTAL)

APPROVED FOR PRODUCTION

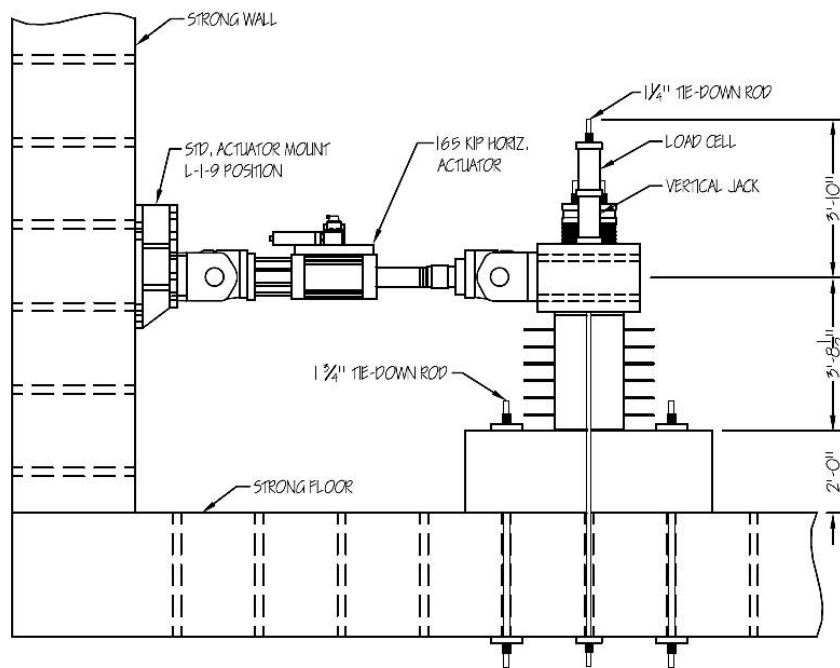


**ADV. PRECAST CONCR. DUAL-SHELL STEEL COLUMNS
INSTRUMENTATION PLAN: ENERGY DISSIPATORS**

| | | | | | | | | |
|-----------|--------|-------|---------------------|--------------------|--------------------------|-----------|--------|----|
| SPECIMEN: | UNIT 1 | TEST: | QUASI STATIC - UCSD | CONNECTION DETAIL: | HYBRID DUAL-SHELL COLUMN | | | |
| BY: | GG | CHK: | DATE: | 10/26/11 | SCALE: | 1/8" = 1" | SHEET: | 14 |



TEST SETUP PLAN VIEW
1/4" = 1'-0"



TEST SETUP ELEVATION
1/4" = 1'-0"

APPROVED FOR PRODUCTION



ADV. PRECAST CONCR. DUAL-SHELL STEEL COLUMNS

TEST SETUP OVERVIEW

| | | | | | | | | |
|-----------|--------|-------|---------------------|--------------------|--------------------------|--------------|--------|----|
| SPECIMEN: | UNIT 1 | TEST: | QUASI STATIC - UCSD | CONNECTION DETAIL: | HYBRID DUAL-SHELL COLUMN | | | |
| BY: | GG | CHK: | DATE: | 11/08/11 | SCALE: | 1/4" = 1'-0" | SHEET: | 15 |

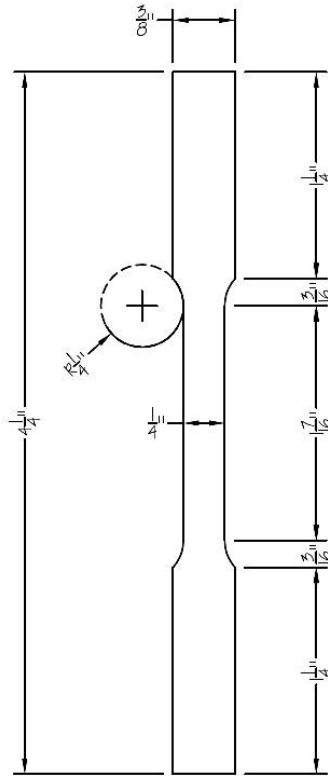


PLATE THICKNESS = $\frac{1}{4}$ "



NOTES:

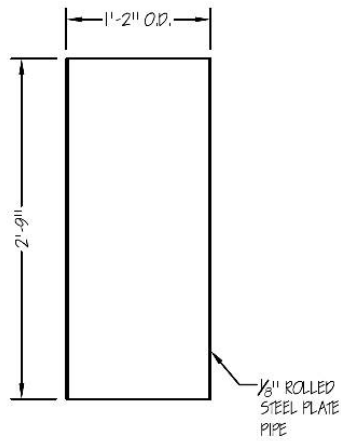
1. THREE COUPONS ARE NEEDED FOR MATERIAL TESTING
2. COUPONS SHALL BE TAKEN FROM THE SAME PLATE USED TO FABRICATE THE COLUMN OUTER SHELL

APPROVED FOR PRODUCTION

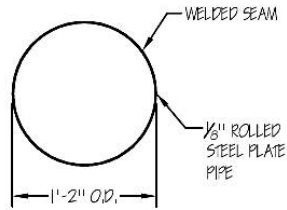


ADV. PRECAST CONCR. DUAL-SHELL STEEL COLUMNS
OUTER SHELL COUPON DETAIL

| | | | | | | | | |
|-----------|--------|-------|---------------------|--------------------|--------------------------|---------|--------|----|
| SPECIMEN: | UNIT I | TEST: | QUASI STATIC - UCSD | CONNECTION DETAIL: | HYBRID DUAL-SHELL COLUMN | | | |
| BY: | GG | CHK: | DATE: | 07/21/11 | SCALE: | 1" = 1" | SHEET: | 16 |



1 STEEL PIPE LONG SECTION
3/4" = 1'-0"



2 STEEL PIPE SECTION
3/4" = 1'-0"

NOTES:

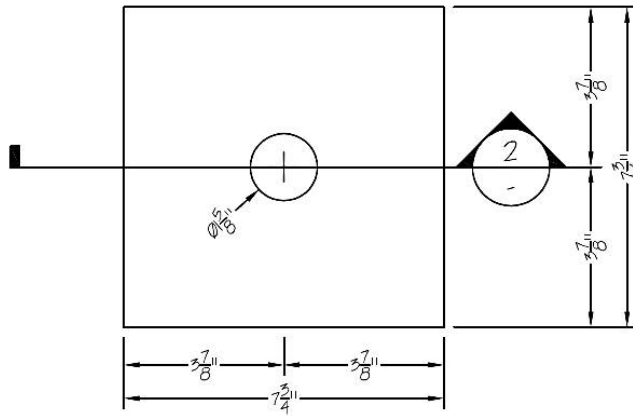
1. ROLLED STEEL PLATE PIPE SHALL BE A572 GRADE 50 AND WELDING SHALL BE COMPLETE JOINT PENETRATION.
2. ALL WELDING SHALL BE USING E70 ELECTRODE.

APPROVED FOR PRODUCTION

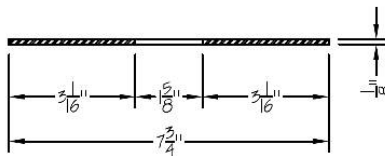


ADV. PRECAST CONCR. DUAL-SHELL STEEL COLUMNS
COLUMN INNER SHELL DETAIL

| | | | | | | |
|------------------|------|---------------------------|---|-----------|--|--|
| SPECIMEN: UNIT 1 | | TEST: QUASI STATIC - UCSD | CONNECTION DETAIL: HYBRID DUAL-SHELL COLUMN | | | |
| BY: GG | CHK: | DATE: 08/25/11 | SCALE: 3/4" = 1'-0" | SHEET: 17 | | |



1 SQUARE STEEL PLATE PLAN VIEW
1/4" = 1"



2 SQUARE STEEL PLATE SECTION
1/4" = 1"

NOTES:

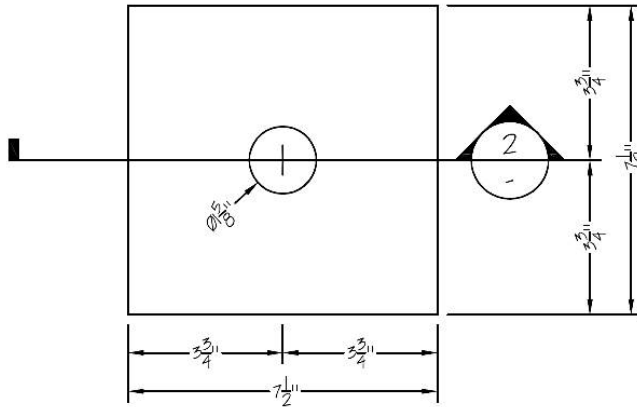
1. PLATES ARE 1/8" THICK
2. PLATES HAVE CENTRAL HOLE WITH 1-5/16" DIAMETER
3. TOLERANCE SMALLER THAN 1/32"
4. 30 PLATES NEED TO BE FABRICATED

APPROVED FOR PRODUCTION

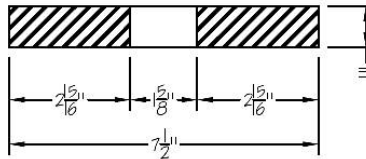


ADV. PRECAST CONCR. DUAL-SHELL STEEL COLUMNS
SQUARE STEEL PLATE FOR BEARING STACK

| | | | |
|-----------|-------|---------------------|--------------------------|
| SPECIMEN: | UNIT: | TEST: | CONNECTION DETAIL: |
| | GG | QUASI STATIC - UCSD | HYBRID DUAL-SHELL COLUMN |
| BY: | GG | CHK: | DATE: 10/25/11 |
| | | | SCALE: 1/4" = 1" |
| | | | SHEET: 18 |



1 SQUARE RUBBER PAD PLAN VIEW
1/4" = 1"



2 SQUARE RUBBER PAD SECTION
1/4" = 1"

NOTES:

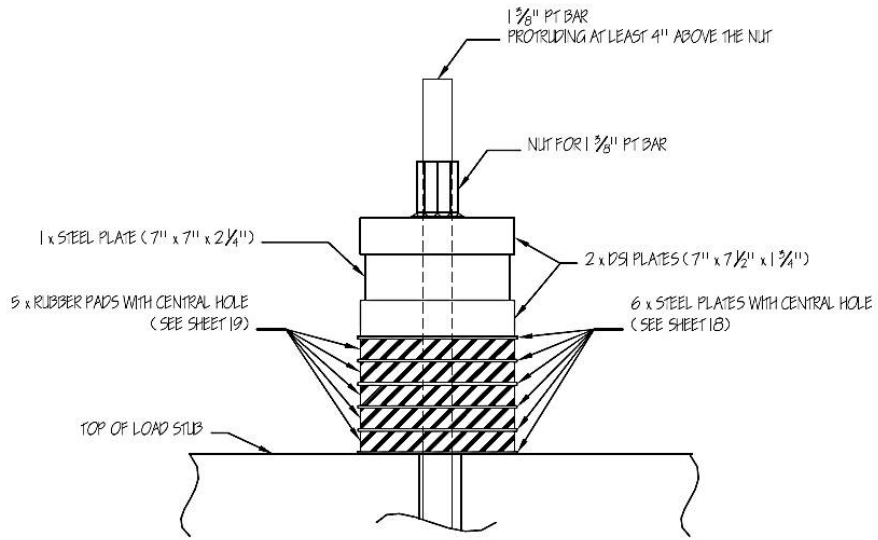
1. PADS ARE 1" THICK
2. PADS HAVE CENTRAL HOLE WITH 1-5/8" DIAMETER
3. SA-47 RUBBER MATERIAL SHALL BE USED
4. TOLERANCE SMALLER THAN 1/32"
5. 23 PADS NEED TO BE FABRICATED, MATERIAL TESTING INCLUDED

APPROVED FOR PRODUCTION



ADV. PRECAST CONCR. DUAL-SHELL STEEL COLUMNS
SQUARE RUBBER PAD FOR BEARING STACK

| | | | | | | | | |
|-----------|---------|-------|---------------------|--------------------|--------------------------|-----------|--------|----|
| SPECIMEN: | UNIT: I | TEST: | QUASI STATIC - UCSD | CONNECTION DETAIL: | HYBRID DUAL-SHELL COLUMN | | | |
| BY: | GG | CHK: | DATE: | 10/25/11 | SCALE: | 1/4" = 1" | SHEET: | 19 |



LOAD-STUB PT ANCHOR ASSEMBLY
1/8" = 1"

NOTES:

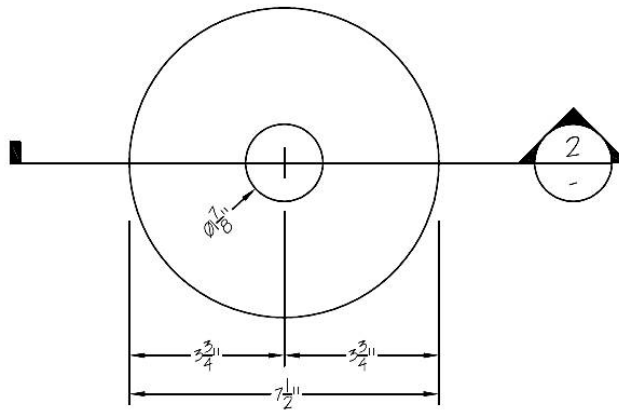
1. THIS SOLUTION IS FOR THE TEST SETUP WITH EXTERNAL DISSIPATORS
2. FOUR LOAD-STUB ANCHOR ASSEMBLIES NEED TO BE PROVIDED (ONE PER PT BAR)

APPROVED FOR PRODUCTION

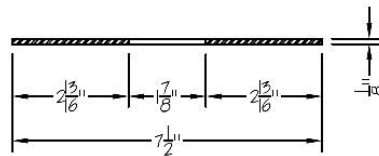


**ADV. PRECAST CONCR. DUAL-SHELL STEEL COLUMNS
PT-LOAD-STUB ANCHOR SYSTEM DETAIL (W/ EXTERNAL DISSIP.)**

| | | | | | |
|-----------|--------|-------|---------------------|--------------------|--------------------------|
| SPECIMEN: | UNIT I | TEST: | QUASI STATIC - UCSD | CONNECTION DETAIL: | HYBRID DUAL-SHELL COLUMN |
| BY: | GG | CHK: | | DATE: | 11/08/11 |
| | | | | SCALE: | 1/8" = 1" |
| | | | | SHEET: | 20 |



1 CIRCULAR STEEL PLATE PLAN VIEW
1/4" = 1"



2 CIRCULAR STEEL PLATE SECTION
1/4" = 1"

NOTES:

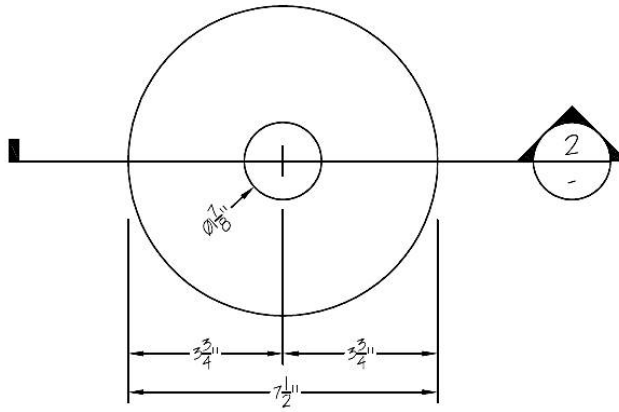
1. PLATES ARE 1/8" THICK
2. PLATES HAVE CENTRAL HOLE WITH 1-3/8" DIAMETER
3. TOLERANCE SMALLER THAN 1/32"
4. 28 PLATES NEED TO BE FABRICATED

APPROVED FOR PRODUCTION

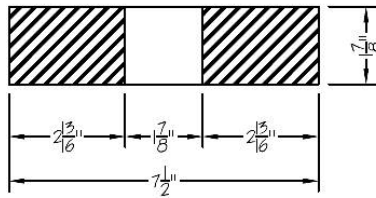


ADV. PRECAST CONCR. DUAL-SHELL STEEL COLUMNS
CIRCULAR STEEL PLATE FOR BEARING STACK

| | | | |
|-----------|--------|---------------------|--------------------------|
| SPECIMEN: | UNIT: | TEST: | CONNECTION DETAIL: |
| | UNIT 1 | QUASI STATIC - UCSD | HYBRID DUAL-SHELL COLUMN |
| BY: | GG | CHK: | DATE: 10/25/11 |
| | | | SCALE: 1/4" = 1" |
| | | | SHEET: 21 |



1 CIRCULAR FYFE DISC PLAN VIEW
1/4" = 1"



2 CIRCULAR FYFE DISC SECTION
1/4" = 1"

NOTES:

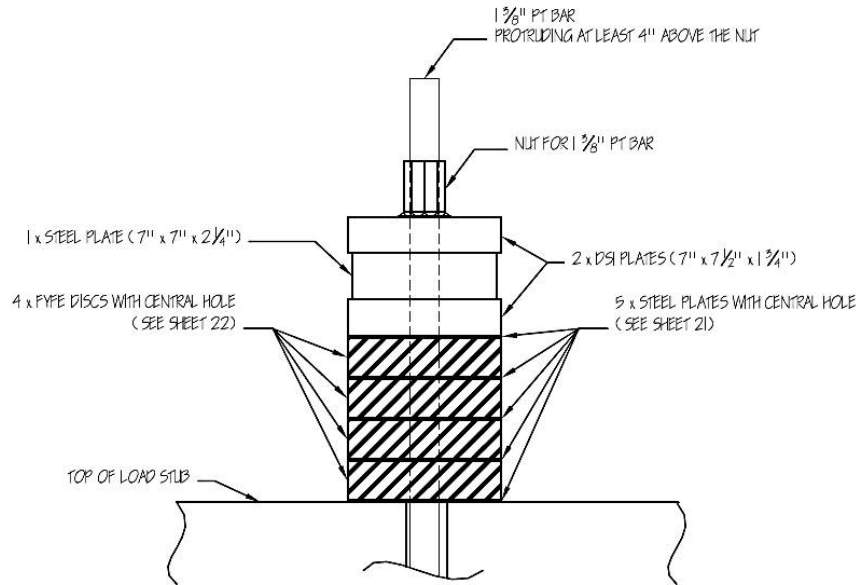
1. DISCS ARE 1-7/8" THICK
2. DISCS HAVE CENTRAL HOLE WITH 1-7/8" DIAMETER
3. 90-DUROMETER-A ADIPRENE MATERIAL SHALL BE USED
4. TOLERANCE SMALLER THAN 1/32"
5. 20 DISCS NEED TO BE FABRICATED, MATERIAL TESTING INCLUDED

APPROVED FOR PRODUCTION



ADV. PRECAST CONCR. DUAL-SHELL STEEL COLUMNS
CIRCULAR FYFE DISC FOR BEARING STACK

| | | | | | | | | |
|-----------|---------|-------|---------------------|--------------------|--------------------------|-----------|--------|----|
| SPECIMEN: | UNIT: I | TEST: | QUASI STATIC - UCSO | CONNECTION DETAIL: | HYBRID DUAL-SHELL COLUMN | | | |
| BY: | GG | CHK: | DATE: | 10/25/11 | SCALE: | 1/4" = 1" | SHEET: | 22 |



○ LOAD-STUB PT ANCHOR ASSEMBLY
1/8" = 1"

NOTES:

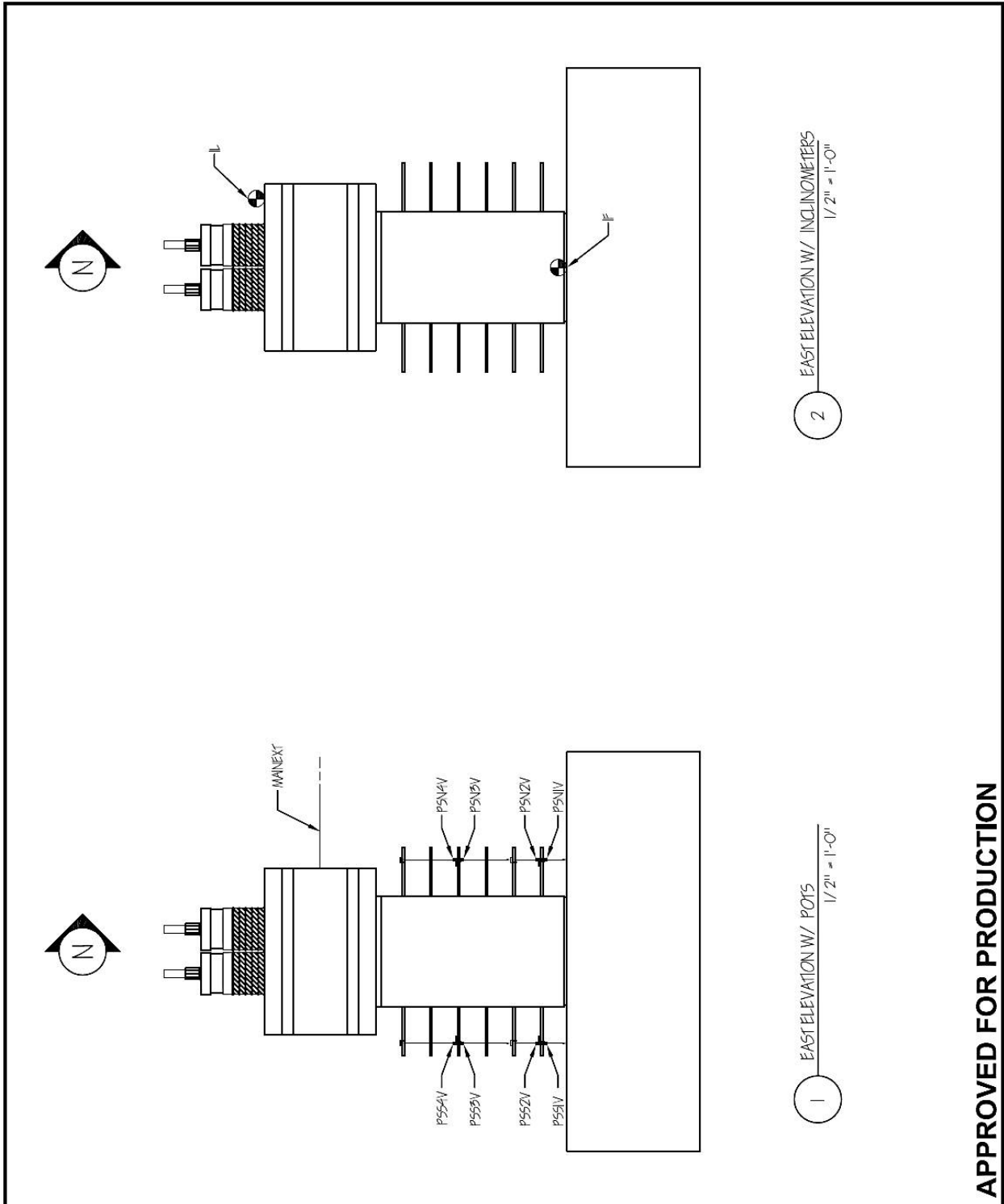
1. THIS SOLUTION IS FOR THE SETUP WITH INTERNAL ENERGY DISSIPATORS
2. FOUR LOAD-STUB ANCHOR ASSEMBLIES NEED TO BE PROVIDED (ONE PER PT BAR)

APPROVED FOR PRODUCTION



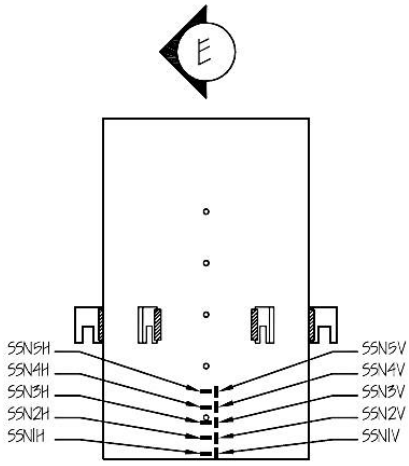
**ADV. PRECAST CONCR. DUAL-SHELL STEEL COLUMNS
PT-LOAD-STUB ANCHOR SYSTEM DETAIL (W/ INTERNAL DISSIP.)**

| | | | | | | | | |
|-----------|--------|-------|---------------------|--------------------|--------------------------|-----------|--------|----|
| SPECIMEN: | UNIT I | TEST: | QUASI STATIC - UCSD | CONNECTION DETAIL: | HYBRID DUAL-SHELL COLUMN | | | |
| BY: | GG | CHK: | DATE: | 12/12/11 | SCALE: | 1/8" = 1" | SHEET: | 23 |

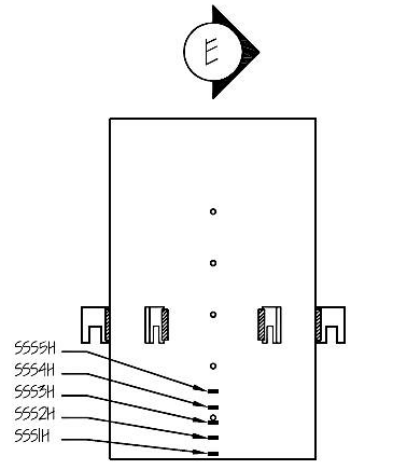


ADV. PRECAST CONCR. DUAL-SHELL STEEL COLUMNS
UNIT 1-A INSTRUM. LOG: POTENTIOMETERS AND INCLINOMETERS

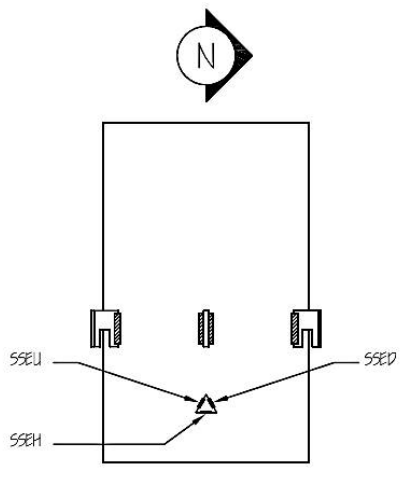
| | | | | | | | | |
|-----------|--------|-------|---------------------|--------------------|--------------------------|--------------|--------|----|
| SPECIMEN: | UNIT 1 | TEST: | QUASI STATIC - UCSD | CONNECTION DETAIL: | HYBRID DUAL-SHELL COLUMN | | | |
| BY: | GG | CHK: | DATE: | 12/12/11 | SCALE: | 1/2" = 1'-0" | SHEET: | 24 |



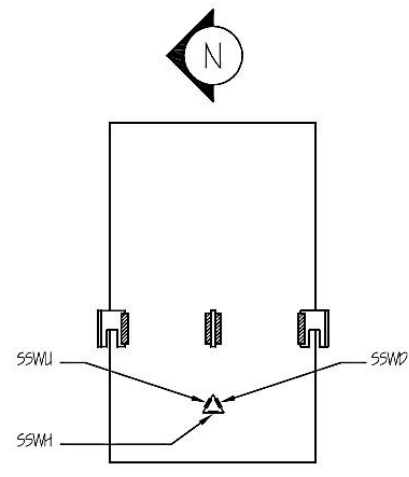
1 OUTER-SHELL NORTH ELEVATION
3/4" = 1'-0"



2 OUTER-SHELL SOUTH ELEVATION
3/4" = 1'-0"



3 OUTER-SHELL EAST ELEVATION
3/4" = 1'-0"



4 OUTER-SHELL WEST ELEVATION
3/4" = 1'-0"

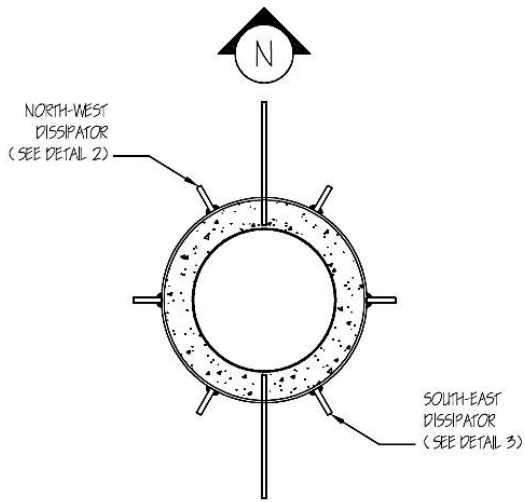
APPROVED FOR PRODUCTION



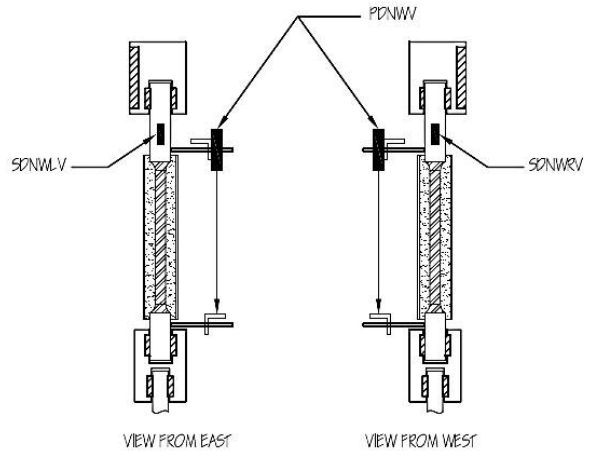
ADV. PRECAST CONCR. DUAL-SHELL STEEL COLUMNS

UNIT 1-A INSTRUMENTATION LOG: OUTER SHELL

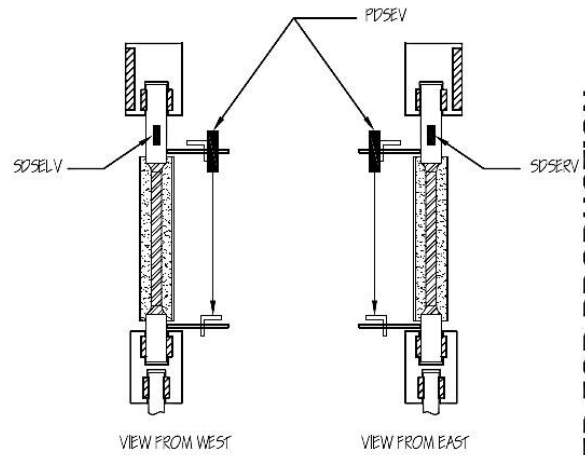
| | | | | | |
|-----------|--------|-------|---------------------|--------------------|--------------------------|
| SPECIMEN: | UNIT 1 | TEST: | QUASI STATIC - UCSD | CONNECTION DETAIL: | HYBRID DUAL-SHELL COLUMN |
| BY: | GG | CHK: | | DATE: | 12/12/11 |
| | | | | SCALE: | 3/4" = 1'-0" |
| | | | | SHEET: | 25 |



1 DISSIPATORS LOCATIONS
NTS



2 NORTH-WEST DISSIPATOR
1/8" = 1"



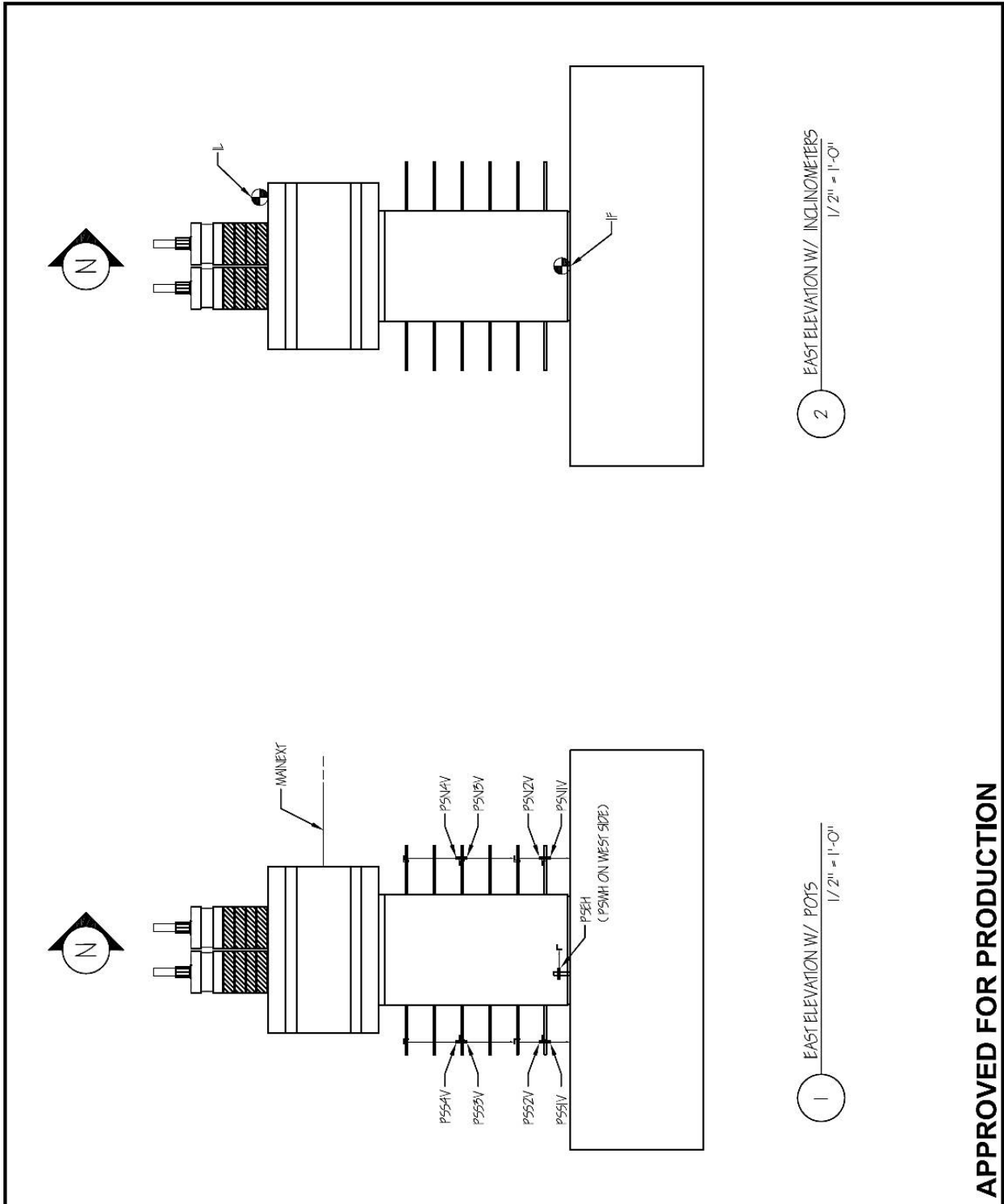
3 SOUTH-EAST DISSIPATOR
1/8" = 1"

APPROVED FOR PRODUCTION



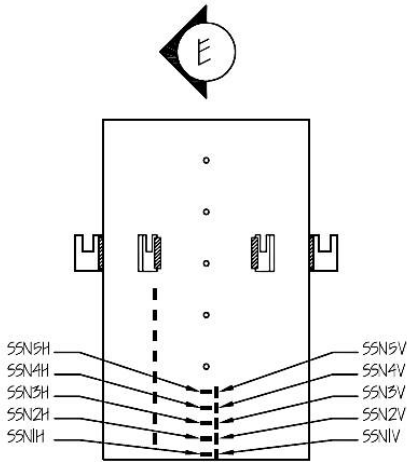
ADV. PRECAST CONCR. DUAL-SHELL STEEL COLUMNS
UNIT 1-A INSTRUMENTATION LOG: ENERGY DISSIPATORS

| | | | | | |
|-----------|--------|-------|---------------------|--------------------|--------------------------|
| SPECIMEN: | UNIT 1 | TEST: | QUASI STATIC - UCSD | CONNECTION DETAIL: | HYBRID DUAL-SHELL COLUMN |
| BY: | GG | CHK: | | DATE: | 11/08/11 |
| | | | | SCALE: | 1/8" = 1" |
| | | | | SHEET: | 26 |

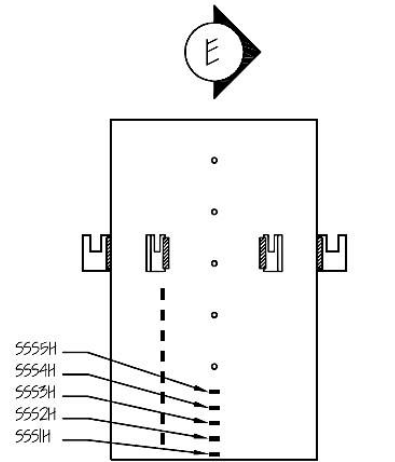


ADV. PRECAST CONCR. DUAL-SHELL STEEL COLUMNS
UNIT 1-B INSTRUM. LOG: POTENTIOMETERS AND INCLINOMETERS

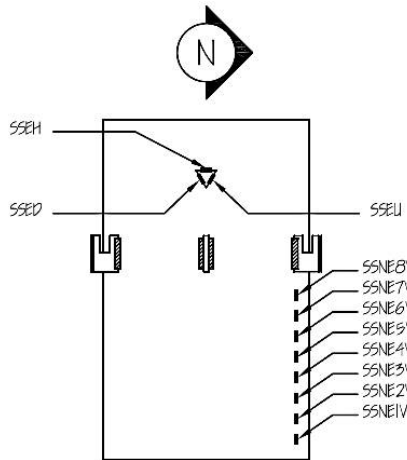
| | | | | | | | | |
|-----------|--------|-------|---------------------|--------------------|--------------------------|--------------|--------|----|
| SPECIMEN: | UNIT 1 | TEST: | QUASI STATIC - UCSD | CONNECTION DETAIL: | HYBRID DUAL-SHELL COLUMN | | | |
| BY: | GG | CHK: | DATE: | 12/12/11 | SCALE: | 1/2" = 1'-0" | SHEET: | 27 |



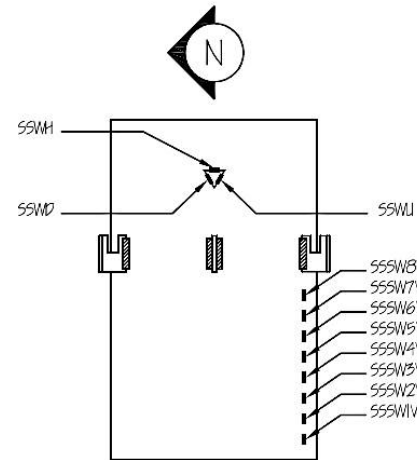
1 OUTER-SHELL NORTH ELEVATION
3/4" = 1'-0"



2 OUTER-SHELL SOUTH ELEVATION
3/4" = 1'-0"



3 OUTER-SHELL EAST ELEVATION
3/4" = 1'-0"



4 OUTER-SHELL WEST ELEVATION
3/4" = 1'-0"

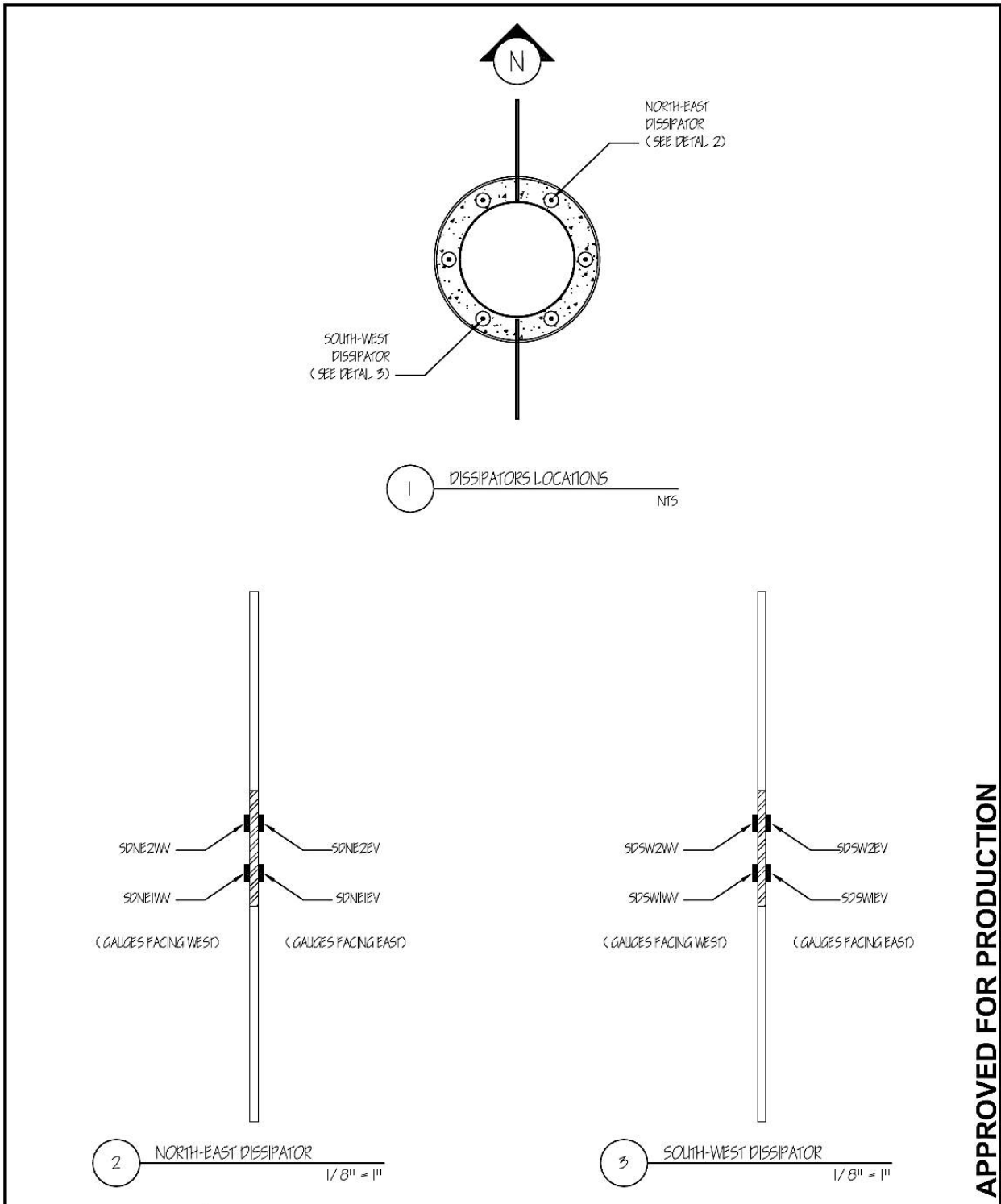
APPROVED FOR PRODUCTION



ADV. PRECAST CONCR. DUAL-SHELL STEEL COLUMNS

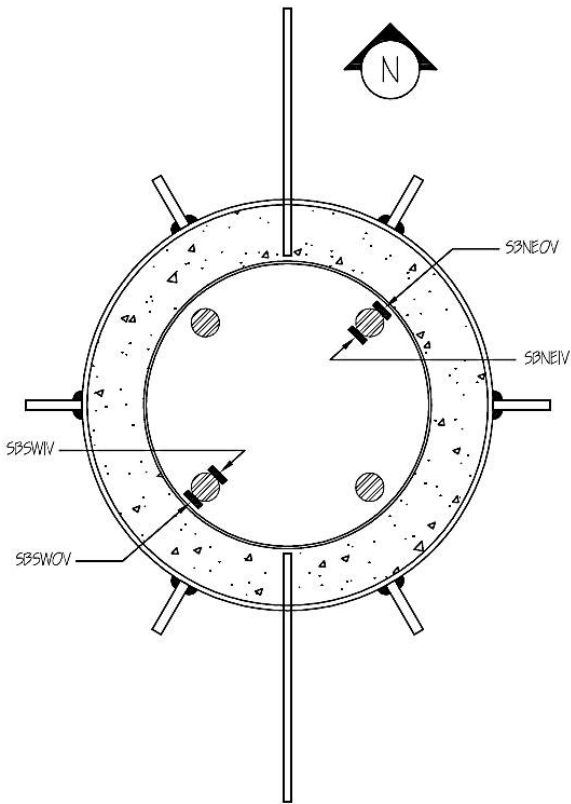
UNIT 1-B INSTRUMENTATION LOG: OUTER SHELL

| | | | | | | | | |
|-----------|--------|-------|---------------------|--------------------|--------------------------|--------------|--------|----|
| SPECIMEN: | UNIT 1 | TEST: | QUASI STATIC - UCSD | CONNECTION DETAIL: | HYBRID DUAL-SHELL COLUMN | | | |
| BY: | GG | CHK: | DATE: | 12/12/11 | SCALE: | 3/4" = 1'-0" | SHEET: | 28 |

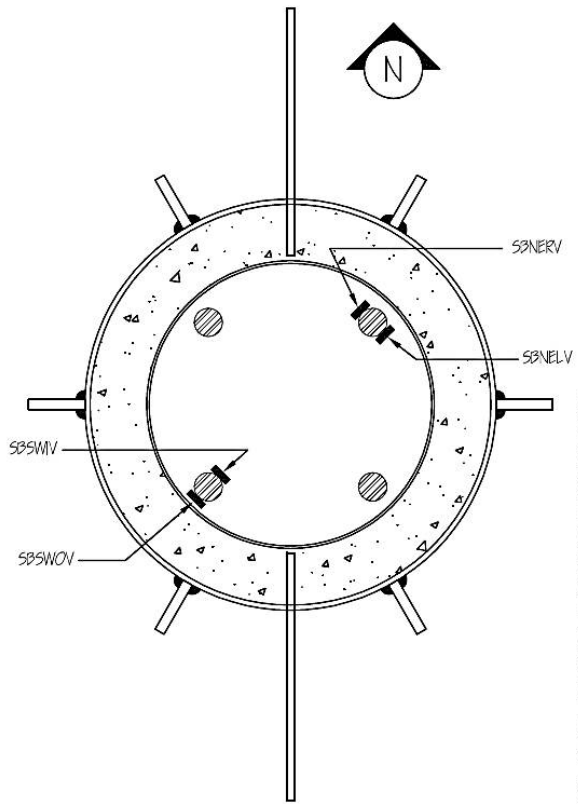


APPROVED FOR PRODUCTION

| | | | | | | | | |
|--------|---|--------------------------|--------------------|----------|--------|-----------|--------|----|
| | ADV. PRECAST CONCR. DUAL-SHELL STEEL COLUMNS | | | | | | | |
| | UNIT 1-B INSTRUMENTATION LOG: ENERGY DISSIPATORS | | | | | | | |
| | SPECIMEN: | TEST: | CONNECTION DETAIL: | | | | | |
| UNIT 1 | QUASI STATIC - UCSD | HYBRID DUAL-SHELL COLUMN | | | | | | |
| BY: | GG | CHK: | DATE: | 12/12/11 | SCALE: | 1/8" = 1" | SHEET: | 29 |



1 UNIT 1-A (EXTERNAL DISSIPATORS)
1/8" = 1"



2 UNIT 1-B (INTERNAL DISSIPATORS)
1/8" = 1"

APPROVED FOR PRODUCTION



ADV. PRECAST CONCR. DUAL-SHELL STEEL COLUMNS
UNITS 1-A & 1-B INSTRUMENTATION LOG: PT BAR STRAIN GAUGES

| | | | | | | | | |
|-----------|--------|-------|---------------------|--------------------|--------------------------|-----------|--------|----|
| SPECIMEN: | UNIT 1 | TEST: | QUASI STATIC - UCSD | CONNECTION DETAIL: | HYBRID DUAL-SHELL COLUMN | | | |
| BY: | GG | CHK: | DATE: | 12/12/11 | SCALE: | 1/8" = 1" | SHEET: | 30 |

Appendix B: OpenSees Scripts

For both units 1A and 1B, the OpenSees scripts are organized as follows:

- GO.tcl: main script, once launched drives the modeling and analysis process;
- UNITS.tcl: defines the units, their relationships and conversions;
- INPUT_geom.tcl: contains the input geometric dimensions of the system;
- INPUT_mat.tcl: contains the input material properties, and builds material models and section properties;
- TRANSF.tcl: defines the geometric transformations to be adopted;
- GENERATE_column.tcl: generates the column elements, assigning connectivity and section properties;
- GENERATE_dissipators_ext.tcl or GENERATE_dissipators_int.tcl: generate the external or internal energy dissipator elements, assigning connectivity and section properties;
- GENERATE_mortar.tcl: discretizes the mortar bed in the desired number of wedges and rings, then generates the corresponding truss elements, assigning connectivity and section properties;
- GENERATE_pt.tcl: generates the post-tensioning bar elements, assigning connectivity and section properties;
- GENERATE_rigid.tcl: generates all rigid links required to connect the other elements, assigning connectivity and section properties;
- RECORDERS.tcl: defines which response parameters are recorded in the output files;
- GRAVITY.tcl: defines and applies gravity-equivalent forces;
- ANALYSIS_cyclic.tcl: runs the cyclic pushover analysis in displacement control;
- LibAnalysisStaticParameters.tcl (by Silvia Mazzoni & Frank McKenna): sets analysis parameters, such as integrator, solution algorithm, tolerance, convergence, etc.;
- LibGeneratePeaks.tcl (by Silvia Mazzoni): builds the loading and unloading branches to and from the peak displacement for each cycle.

The OpenSees scripts are shown on the next pages. To avoid confusion, the full suite of scripts is reported separately for the two test specimen simulations. Due to formatting constraints, some command and comment lines have been broken in two or more. Given these alternations, the authors recommend keeping this in mind when using these scripts.

Unit 1A – GO.tcl

```
#####
# DUAL SHELL COLUMN UNIT1A      #
#-----#
# Athanassios Vervelidis      #
# Gabriele Guerrini           #
# UC San Diego                #
# 2011                        #
#####

# INITIALIZATION -----
wipe; # clear memory of all past model definitions
model BasicBuilder -ndm 3 -ndf 6; # define the model builder, ndm=#dimension, ndf=#dofs
set dataDir ResultsUnit1A; # set up name of data directory
file mkdir $dataDir; # create data directory
source UNITS.tcl; # define units
puts "MODEL SET-UP OK"

# INPUT -----
source INPUT_geom.tcl
puts "INPUT GEOMETRY OK"
source INPUT_mat.tcl
puts "INPUT MATERIALS OK"

# TRANSFORMATIONS -----
source TRANSF.tcl
puts "TRANSFORMATIONS OK"

# GENERATE ELEMENTS -----

# RC COLUMN
source GENERATE_column.tcl
puts "COLUMN OK"

# DISSIPATORS
source GENERATE_dissipators_ext.tcl
puts "DISSIPATORS OK"

# MORTAR BED
source GENERATE_mortar.tcl
puts "MORTAR SPRINGS OK"

# PT BARS
source GENERATE_pt.tcl
puts "PT BARS OK"

# RIGID LINKS
source GENERATE_rigid.tcl
puts "RIGID LINKS OK"

# RECORDERS -----
source RECORDERS.tcl
puts "RECORDERS OK"

# GRAVITY -----
source GRAVITY.tcl
puts "GRAVITY OK, MODEL BUILT"

# ANALYSIS -----
source ANALYSIS_cyclic.tcl
puts "ANALYSIS DONE"
```

Unit 1A – UNITS.tcl

```
#####
# DUAL SHELL COLUMN UNIT1A      #
#-----#
# Athanassios Vervelidis      #
# Gabriele Guerrini           #
# UC San Diego                #
# 2011                        #
#####

# UNITS -----
set in 1.; # define basic units -- output units
set kip 1.; # define basic units -- output units
set sec 1.; # define basic units -- output units
set LunitTXT "inch"; # define basic-unit text for output
set FunitTXT "kip"; # define basic-unit text for output
set TunitTXT "sec"; # define basic-unit text for output
set ft [expr 12.*$in]; # define engineering units
set ksi [expr $kip/pow($in,2)];
set psi [expr $ksi/1000.];
set lbf [expr $psi*$in*$in]; # pounds force
set pcf [expr $lbf/pow($ft,3)]; # pounds per cubic foot
set psf [expr $lbf/pow($ft,2)]; # pounds per square foot
set in2 [expr $in*$in]; # inch^2
set in4 [expr $in*$in*$in*$in]; # inch^4
set cm [expr $in/2.54]; # centimeter, needed for displacement input in MultipleSupport excitation
set cmsec2 [expr $cm/pow($sec,2)]; # cm/sec^2, needed for some ground accelerations
set m [expr $cm*100]; # meter
set mm [expr $cm/10]; # millimeter
set mm2 [expr $mm*$mm]; # millimeter^2
set kN [expr 0.2247*$kip]; # kilo newton
set MPa [expr 0.1450*$ksi]; # mega pascal
set GPa [expr 1000*$MPa]; # giga pascal
set pi [expr 2*asin(1.0)]; # define constants
set g [expr 32.2*$ft/pow($sec,2)]; # gravitational acceleration
set Ubig 1.e10; # a really large number
set Usmall [expr 1/$Ubig]; # a really small number
```

Unit 1A – INPUT_geom.tcl

```
#####
# DUAL SHELL COLUMN UNIT1A      #
#-----#
# Athanassios Vervelidis      #
# Gabriele Guerrini           #
# UC San Diego                #
# 2011                        #
#####

# COLUMN -----#
set lCol [expr 2.*$ft + 10.*$in]; # column length (including 1 in of upper joint)
set Dint [expr 14.*$in]; # internal diameter
set Dext [expr 20.*$in]; # external diameter
set Rint [expr $Dint/2.]; # internal radius
set Rext [expr $Dext/2.]; # external radius
set tint [expr (1./8.)*$in]; # internal shell thickness
set text [expr (1./4.)*$in]; # external shell thickness

# DISSIPATORS -----#
set nDiss 6; # number of dissipators
set dDiss [expr ($Rext + 15./16. + ((2. + 3./4.) - (11./16. + 15./16.))/2.)*$in]; # external
dissipators distance from column axis
set l1Diss [expr (2. + (5. + 7.)/16.)*$in]; # dissipators length (low part)
set l2Diss [expr (6. + 1./2.)*$in]; # dissipators length (milled part)
set l3Diss [expr (3. + (7. + 13.)/16.)*$in]; # dissipators length (upper part)
set lDiss [expr $l1Diss + $l2Diss + $l3Diss]; # dissipators length (total)
set diamDiss [expr 1.*$in]; # dissipator diameter
set diamDissDb [expr (9./16.)*$in]; # dissipator diameter (milled part)

# MORTAR -----#
set lMort [expr 0.5*$in]; # mortar thickness

# RIGID LINK FOR LOAD APPLICATION -----#
set lLoadStub [expr 1.*$ft + 8.*$in]; # load stub height
set lss [expr $lMort + $lCol + ($lLoadStub/2.)]; #shear span

# PT BARS -----#
set nPt 4; # number of pt bars
set rPt [expr 5.66*$in]; # bars distance from column axis
set lPt [expr 20.*$in + $lMort + $lCol + $lLoadStub + ((5.*1. + 6.*(1./8.)) + 0.5 + 4)*$in]; #
bar length
set lPtFound [expr 20.*$in]; # bar anchorage length inside foundation
set lPtEq [expr $lPtFound + $lss]; # equivalent bar length (shear span + anchorage inside
foundation)
```

Unit 1A – INPUT_mat.tcl

```
#####
# DUAL SHELL COLUMN UNIT1A #
#-----#
# Athanassios Vervelidis #
# Gabriele Guerrini #
# UC San Diego #
# 2011 #
#####

# COLUMN -----
set fc [expr 10.2*$ksil]; # concrete strength
set Ec [expr 57.*pow(1000.*$fc,0.5)]; # Young's modulus for concrete
set Es [expr 29000.*$ksil]; # Young's modulus for steel (cylinder)
set n [expr $Es/$Ec]; # Es/Ec ratio
set ni 0.2; # Poisson's coefficient for concrete
set Gc [expr ((1+$ni)/2.)*$Ec]; # shear modulus for concrete
set AColDw [expr ($pi)*(pow($Rext-$text,2) - pow($Rint,2))]; #cross-sectional area of element
(concrete)
set AColUp [expr ($pi)*(pow($Rext-$text,2) - pow($Rint,2)) + $n*($pi)*(pow($Rext,2) - pow($Rext-
$text,2))]; #cross-sectional area of element (concrete + external steel)
set IColDw [expr ($pi/4.)*(pow($Rext-$text,4) - pow($Rint,4))]; # second moment of area about the
local y and z-axes
set IShInt [expr ($pi/4.)*(pow($Rint+$tint,4) - pow($Rint,4))];
set IShExt [expr ($pi/4.)*(pow($Rext,4) - pow($text,4))];
set IColUp [expr ($pi/4.)*(pow($Rext-$text,4) - pow($Rint,4)) + ($IShInt + $IShExt)*($n-1.)];
set JColDw [expr 2*$IColDw]; # torsional moment of inertia of cross section
set JColUp [expr 2*$IColUp];

# DISSIPATORS -----
set matTagDissAxial 2001; # tag stee02 material for axial behavior of the dissipator's section
(external part)
set matTagDissMoment 2002; # tag for the Mz to add at the same section above
set matTagDissTorsion 2003; # tag for the torsional effects
set matTagDissDbAxial 2004; # tag stee02 material for axial behavior (milled part)
set matTagDissDbMoment 2005; # tag for the Mz to add at the same section above
set matTagDissDbTorsion 2006; # tag for the torsional effects
set FyDiss [expr 68.*$ksil]; # yielding strength
set E0Diss [expr 32000.*$ksil]; # initial elastic tangent
set eyDiss [expr $FyDiss/$E0Diss]; # yielding strain
set FuDiss [expr 71.*$ksil]; # ultimate strenght
set euDiss 0.06; # ultimate strain
set EuDiss [expr (($FuDiss-$FyDiss)/($euDiss-$eyDiss))]; # post-yield tangent
set bDiss [expr $EuDiss/$E0Diss]; # strain-hardening ratio (ratio between post-yield tangent and
initial elastic tangent)
set R0 18.; # parameters to control the transition from elastic to plastic branches
set cR1 0.925;
set cR2 0.15;
set a1Diss 0.07;
set a2Diss 3;
set a3Diss 0;
set a4Diss 1;
set sigInitDiss 0;
set rDiss [expr $diamDiss/2.]; # dissipator radius
set rDissDb [expr $diamDissDb/2.]; # dissipator radius (milled part)
set ADiss [expr $pi*pow($rDiss,2)]; # dissipator area
set ADissDb [expr $pi*pow($rDissDb,2)];
set IDiss [expr ($pi/4.)*pow($rDiss,4)]; # second moment of inertia
set IDissDb [expr ($pi/4.)*pow($rDissDb,4)];
set JDiss [expr ($pi/2.)*pow($rDiss,4)]; # torsional moment of inertia of cross section
set JDissDb [expr ($pi/2.)*pow($rDissDb,4)];
set nis 0.3; # Poisson's coefficient for steel
set GDiss [expr ((1+$nis)/2.)*$E0Diss]; # shear modulus

uniaxialMaterial Steel02 $matTagDissAxial [expr $FyDiss*$ADiss] [expr $ADiss*$E0Diss] $bDiss $R0
$cR1 $cR2 $a1Diss $a2Diss $a3Diss $a4Diss $sigInitDiss;
uniaxialMaterial Steel02 $matTagDissMoment [expr $FyDiss*($IDiss/$rDiss)] [expr $E0Diss*$IDiss]
$bDiss $R0 $cR1 $cR2 $a1Diss $a2Diss $a3Diss $a4Diss $sigInitDiss;
uniaxialMaterial Elastic $matTagDissTorsion [expr $GDiss*$JDiss];
uniaxialMaterial Steel02 $matTagDissDbAxial [expr $FyDiss*$ADissDb] [expr $ADissDb*$E0Diss]
$bDiss $R0 $cR1 $cR2 $a1Diss $a2Diss $a3Diss $a4Diss $sigInitDiss;
uniaxialMaterial Steel02 $matTagDissDbMoment [expr $FyDiss*($IDissDb/$rDissDb)] [expr
$E0Diss*$IDissDb] $bDiss $R0 $cR1 $cR2 $a1Diss $a2Diss $a3Diss $a4Diss $sigInitDiss;
uniaxialMaterial Elastic $matTagDissDbTorsion [expr $GDiss*$JDissDb];

# MORTAR -----
set matTagMort 3001; # integer tag identifying material
set fpc [expr -8.1*$ksil]; # mortar compressive strength
```

```

set ecc0 -0.004; # strain at maximum strength
set Lreal [expr 5*$in]; # length of extension of deformation
set ecc0eq [expr ($Lreal/$lMort)*$ecc0]; # fictitious strain at maximum strength
set fpc [expr -1*$ksi]; # crushing strength
set eccu -0.1511; # strain at crushing strength
set eccueq [expr ($Lreal/$lMort)*$eccu]; # fictitious strain at crushing strength

uniaxialMaterial Concrete01 $matTagMort $fpc $ecc0eq $fpc $eccueq;

# PT BARS -----
set matTagPt 4001; # integer tag identifying material
set FyPt [expr 120.*$ksi]; # yielding strength
set EPt [expr 29700.*$ksi]; # initial elastic tangent
set eyPt [expr $FyPt/$EPt]; # yielding strain
set FuPt [expr 156.51*$ksi]; # ultimate strength
set euPt 0.08; # ultimate strain
set EuPt [expr ($FuPt-$FyPt)/($euPt-$eyPt)]; # plastic tangent
set bPt [expr $EuPt/$EPt]; # strain-hardening ratio
set APt [expr 1.58*$in2]; # cross-sectional area of element
set Krb [expr 823.5*$kip/$in]; # bearing stiffness
set KPtEq [expr 1/((1/$Krb) + ($lPt/($EPt*$APt)))]]; # values for the equivalent pt system
set EPtEq [expr ($KPtEq*$lPtEq)/$APt];
set KuPtEq [expr 1/((1/$Krb) + ($lPt/($EuPt*$APt)))]];
set bPtEq [expr (($KuPtEq*$lPtEq)/$APt)/$EPtEq]; # equivalent strain-hardening ratio

uniaxialMaterial Steel02 $matTagPt $FyPt $EPtEq $bPtEq 18. 0.925 0.15 0 1 0 1 30;

# RIGID LINK FOR LOAD APPLICATION -----
set ARigCol [expr 1000.*$AColUp*($lLoadStub/2.)/$lss)]; # cross-sectional area of rigid element
set ERigCol [expr 29000.*$ksi]; # Young's modulus for rigid element
set GRigCol [expr ((1+$nis)/2.)*$ERigCol]; # shear modulus for rigid element
set JRigCol [expr 1000.*$JColUp]; # torsional moment of inertia of cross section
set IRigCol [expr 1000.*$IColUp]; # second moment of area

# RIGID LINK FOR DISSIPATORS -----
set ARigDiss [expr 1000.*$AColUp*($rDiss/$lss)]; # cross-sectional area of rigid element
set ESpring [expr 29000.*$ksi]; # Young's modulus for rigid element
set GRigDiss [expr ((1+$nis)/2.)*$ESpring]; # shear modulus for rigid element
set JRigDiss [expr 1000.*$JColUp]; # torsional moment of inertia of cross section
set IRigDiss [expr 1000.*$IColUp]; # second moment of area

# RIGID LINK FOR MORTAR SPRINGS -----
set ERigMort [expr 29000.*$ksi]; # Young's modulus for rigid element
set GRigMort [expr ((1+$nis)/2.)*$ERigMort]; # shear modulus for rigid element
set JRigMort [expr 1000.*$JColUp]; # torsional moment of inertia of cross section

# RIGID LINK FOR PT BARS -----
set ARigPt [expr 1000.*$AColUp*($rPt/$lss)]; # cross-sectional area of rigid element
set ERigPt [expr 29000.*$ksi]; # Young's modulus for rigid element
set GRigPt [expr ((1+$nis)/2.)*$ERigPt]; # shear modulus for rigid element
set JRigPt [expr 1000.*$JColUp]; # torsional moment of inertia of cross section
set IRigPt [expr 1000.*$IColUp]; # second moment of area

```

Unit 1A – TRANSF.tcl

```
#####  
# DUAL SHELL COLUMN UNIT1A      #  
#-----#  
# Athanassios Vervelidis      #  
# Gabriele Guerrini           #  
# UC San Diego                #  
# 2011                        #  
#####
```

```
# TRANSFORMATION -----  
set transfTagVert 1001; # associate a tag to the transformation  
geomTransf Linear $transfTagVert 0 0 -1; # linear geometric transformation  
  
set transfTagHoriz 1002; # associate a tag to the transformation  
geomTransf Linear $transfTagHoriz 0 1 0; # linear geometric transformation
```

Unit 1A – GENERATE_column.tcl

```
#####
# DUAL SHELL COLUMN UNIT1A      #
#-----#
# Athanassios Vervelidis      #
# Gabriele Guerrini           #
# UC San Diego                 #
# 2011                         #
#####

# GEOMETRY -----#
# nodal coordinates:
node 1001 0. $lMort 0.; # mortar
node 1002 0. $lDiss 0.; # master node for dissipator
node 1003 0. [expr $lMort + $lCol] 0.; # last node column
# boundary conditions:
fix 1001 1 0 1 0 0 0; # boundary condition (roller)

# ELEMENTS -----#
# element connectivity:
set eleTagColDw 1001; # unique element object tag (lower column)
set eleTagColUp 1002; # unique element object tag (upper column)

element elasticBeamColumn $eleTagColDw 1001 1002 $AColDw $Ec $Gc $JColDw $IColDw $IColDw
$transfTagVert;
element elasticBeamColumn $eleTagColUp 1002 1003 $AColUp $Ec $Gc $JColUp $IColUp $IColUp
$transfTagVert;
```

Unit 1A – GENERATE_dissipators_ext.tcl

```
#####
# DUAL SHELL COLUMN UNIT1A          #
#-----#
# Athanassios Vervelidis           #
# Gabriele Guerrini                 #
# UC San Diego                      #
# 2011                              #
#####

# GEOMETRY -----
set thetaDiss 2.*pi/$nDiss; # angle between dissipators
for {set iDiss 1} {$iDiss<=$nDiss} {incr iDiss} {
  set thetaiDiss [expr $thetaDiss/2. + ($iDiss - 1.)*$thetaDiss]; # bar angle
  set x [expr {$dDiss*cos($thetaiDiss)}]; # spring x coord
  set z [expr {$dDiss*sin($thetaiDiss)}]; # spring z coord
  node [expr {2000 + $iDiss}] $x 0. $z; # base nodes
  node [expr {2000 + $nDiss + $iDiss}] $x $l1Diss $z; # middle nodes
  node [expr {2000 + 2*$nDiss + $iDiss}] $x [expr $l1Diss + $l2Diss] $z; # middle nodes
  node [expr {2000 + 3*$nDiss + $iDiss}] $x $l1Diss $z; # top nodes
  fix [expr {2000 + $iDiss}] 1 1 1 1 1; # boundary condition base(fixed)
}

# SECTIONS -----
set secTagDiss1 2001; # unique section tag
set secTagDiss2 2002; # unique section tag
set secTagDiss3 2003; # unique section tag
set secTagDiss4 2004; # unique section tag

section Uniaxial $secTagDiss1 $matTagDissAxial P; # construct a UniaxialSection object
section Aggregator $secTagDiss2 $matTagDissMoment My $matTagDissMoment Mz $matTagDissTorsion T -
section $secTagDiss1; # aggregates previously-defined UniaxialMaterial objects into a single
section
section Uniaxial $secTagDiss3 $matTagDissDbAxial P; # construct a UniaxialSection object (milled
part)
section Aggregator $secTagDiss4 $matTagDissDbMoment My $matTagDissDbMoment Mz
$matTagDissDbTorsion T -section $secTagDiss3; # aggregates previously-defined UniaxialMaterial
objects into a single section

# ELEMENTS -----
# element connectivity:
set numIntgrPts 3; # number of integration points along the element.
for {set ieDiss 1} {$ieDiss<=$nDiss} {incr ieDiss} {
  element dispBeamColumn [expr {2000 + $ieDiss}] [expr {2000 + $ieDiss}] [expr {2000 + $nDiss +
$ieDiss}] $numIntgrPts $secTagDiss2 $transfTagVert;
  element dispBeamColumn [expr {2000 + $nDiss + $ieDiss}] [expr {2000 + $nDiss + $ieDiss}]
[expr {2000 + 2*$nDiss + $ieDiss}] $numIntgrPts $secTagDiss4 $transfTagVert;
  element dispBeamColumn [expr {2000 + 2*$nDiss + $ieDiss}] [expr {2000 + 2*$nDiss + $ieDiss}]
[expr {2000 + 3*$nDiss + $ieDiss}] $numIntgrPts $secTagDiss2 $transfTagVert;
}

```

Unit 1A – GENERATE_mortar.tcl

```
#####
# DUAL SHELL COLUMN UNIT1A          #
#-----#
# Athanassios Vervelidis            #
# Gabriele Guerrini                  #
# UC San Diego                       #
# 2011                                #
#####

# GEOMETRY -----#
set nMort 36; # number of wedges
set mMort 3; # number of rings
set tMort [expr {($Rext-$Rint)/$mMort}]; # ring thickness
set thetaMort [expr {2.*$pi/$nMort}]; # angle between wedges
for {set i 1} {$i<=$mMort} {incr i} {
  set riMort [expr {$Rint + ($tMort/2.) + ($i - 1.)*$tMort}]; # spring radius
  set AiMort [expr {($pi*(pow(($riMort + $tMort/2.),2) - pow(($riMort - $tMort/2.),2))
/$nMort)}]; # spring influence area
  for {set j 1} {$j<=$nMort} {incr j} {
    set thetajMort [expr {$thetaMort/2. + ($j - 1.)*$thetaMort}]; # spring angle
    set x [expr {$riMort*cos($thetajMort)}]; # spring x coord
    set z [expr {$riMort*sin($thetajMort)}]; # spring z coord
    node [expr {3000 + ($i - 1)*$nMort + $j}] $x 0. $z; # mortar bed (base)
    node [expr {3000 + $mMort*$nMort + ($i - 1)*$nMort + $j}] $x $lMort $z; # mortar bed
    (top)
    fix [expr {3000 + ($i - 1)*$nMort + $j}] 1 1 1 1 1; # boundary condition base(fixed)
  }
}

# ELEMENTS -----#
# element connectivity:
for {set i 1} {$i<=$mMort} {incr i} {
  for {set j 1} {$j<=$nMort} {incr j} {
    element truss [expr {3000 + ($i - 1)*$nMort + $j}] [expr {3000 + ($i - 1)*$nMort + $j}]
    [expr {3000 + $mMort*$nMort + ($i - 1)*$nMort + $j}] $AiMort $matTagMort;
  }
}
}
```

Unit 1A – GENERATE_pt.tcl

```
#####
# DUAL SHELL COLUMN UNIT1A          #
#-----#
# Athanassios Vervelidis           #
# Gabriele Guerrini                 #
# UC San Diego                      #
# 2011                              #
#####

# GEOMETRY -----#
set thetaPt 2.*pi/$nPt; # angle between bars
for {set ipt 1} {$iPt<=$nPt} {incr ipt} {
  set thetaiPt [expr $thetaPt/2. + ($iPt - 1.)*$thetaPt]; # bar angle
  set x [expr {$rPt*cos($thetaiPt)}]; # bar x coord
  set z [expr {$rPt*sin($thetaiPt)}]; # bar z coord
  node [expr {4000 + $iPt}] $x -$lPtFound $z; # base nodes
  node [expr {4000 + $nPt + $iPt}] $x 0 $z; # middle nodes
  node [expr {4000 + 2*$nPt + $iPt}] $x $lss $z; # top nodes
  fix [expr {4000 + $iPt}] 1 1 1 1 1 1; # boundary condition base(fixed)
  fix [expr {4000 + $nPt + $iPt}] 1 0 1 1 1 1; # boundary condition middle(slider)
}

# ELEMENTS -----#
# element connectivity:
for {set iePt 1} {$iePt<=$nPt} {incr iePt} {
  element truss [expr {4000 + $iePt}] [expr {4000 + $iePt}] [expr {4000 + $nPt + $iePt}] $APt
  $matTagPt;
  element truss [expr {4000 + $nPt + $iePt}] [expr {4000 + $nPt + $iePt}] [expr {4000 + 2*$nPt
  + $iePt}] $APt $matTagPt;
}
```

Unit 1A – GENERATE_rigid.tcl

```
#####
# DUAL SHELL COLUMN UNIT1A          #
#-----#
# Athanassios Vervelidis           #
# Gabriele Guerrini                 #
# UC San Diego                      #
# 2011                              #
#####

# LOADING POINT -----
node 5001 0. $lss 0.; # load application node
set eleTagRigCol 5001;
element elasticBeamColumn $eleTagRigCol 1003 5001 $ARigCol $ERigCol $GRigCol $JRigCol $IRigCol
$IRigCol $transfTagVert;

# RIGID CONNECTION FOR DISSIPATORS -----
for {set iRigDiss 1} {$iRigDiss<=$nDiss} {incr iRigDiss} {
  element elasticBeamColumn [expr {6000 + $iRigDiss}] 1002 [expr {2000 + 3*$nDiss + $iRigDiss}]
  $ARigDiss $ESpring $GRigDiss $JRigDiss $IRigDiss $IRigDiss $transfTagHoriz;
}

# RIGID CONNECTION FOR MORTAR -----
for {set iRigMort 1} {$iRigMort<=$mMort} {incr iRigMort} {
  set ARigMort [expr 1000.*$AColUp*($riMort/$lss)];
  set IRigMort [expr 1000.*$IColUp*($Ec/$ERigMort)*($riMort/$lss)];
  for {set jRigMort 1} {$jRigMort<=$nMort} {incr jRigMort} {
    element elasticBeamColumn [expr {7000 + ($iRigMort - 1)*$nMort + $jRigMort}] 1001 [expr
    {3000 + $mMort*$nMort + ($iRigMort - 1)*$nMort + $jRigMort}] $ARigMort $ERigMort
    $GRigMort $JRigMort $IRigMort $IRigMort $transfTagHoriz;
  }
}

# RIGID CONNECTION FOR PT BARS -----
for {set iRigPt 1} {$iRigPt<=$nPt} {incr iRigPt} {
  element elasticBeamColumn [expr {8000 + $iRigPt}] 5001 [expr {4000 + 2*$nPt + $iRigPt}]
  $ARigPt $ERigPt $GRigPt $JRigPt $IRigPt $IRigPt $transfTagHoriz;
}
```

Unit 1A – RECORDERS.tcl

```
#####
# DUAL SHELL COLUMN UNIT1A          #
#-----#
# Athanassios Vervelidis           #
# Gabriele Guerrini                 #
# UC San Diego                     #
# 2011                              #
#####

# COLUMN -----#
recorder Node -file $dataDir/ColDisp.out -time -node 5001 -dof 1 2 3 4 5 6 disp;
recorder Node -file $dataDir/ColBaseShear.out -time -node 1001 -dof 1 2 3 4 5 6 reaction;
recorder Node -file $dataDir/ColBaseDisp.out -time -node 1001 -dof 1 2 3 4 5 6 disp;
recorder Node -file $dataDir/ColReactDissLevel.out -time -node 1002 -dof 1 2 3 4 5 6 reaction;
recorder Node -file $dataDir/ColDispDissLevel.out -time -node 1002 -dof 1 2 3 4 5 6 disp;
recorder Element -file $dataDir/ColTopShear.out -time -ele $eleTagColUp globalForce;
recorder Element -file $dataDir/ColTopDef.out -time -ele $eleTagColUp deformation;
recorder Element -file $dataDir/ColShearDissLevel.out -time -ele $eleTagColDw force;
recorder Element -file $dataDir/ColDefDissLevel.out -time -ele $eleTagColDw deformation;

# DISSIPATORS -----#
for {set ieDiss 1} {$ieDiss<=$nDiss} {incr ieDiss} {
  recorder Element -file $dataDir/DissElem[expr {2000 + $ieDiss}]Force.out -time -ele [expr
  {2000 + $ieDiss}] section 2 force;
  recorder Element -file $dataDir/DissElem[expr {2000 + $ieDiss}]Def.out -time -ele [expr {2000
  + $ieDiss}] section 2 deformation;
  recorder Element -file $dataDir/DissDbElem[expr {2000 + $nDiss + $ieDiss}]Force.out -time -
  ele [expr {2000 + $nDiss + $ieDiss}] section 2 force;
  recorder Element -file $dataDir/DissDbElem[expr {2000 + $nDiss + $ieDiss}]Def.out -time -ele
  [expr {2000 + $nDiss + $ieDiss}] section 2 deformation;
  recorder Element -file $dataDir/DissElem[expr {2000 + 2*$nDiss + $ieDiss}]Force.out -time -
  ele [expr {2000 + 2*$nDiss + $ieDiss}] section 2 force;
  recorder Element -file $dataDir/DissElem[expr {2000 + 2*$nDiss + $ieDiss}]Def.out -time -ele
  [expr {2000 + 2*$nDiss + $ieDiss}] section 2 deformation;
}

# MORTAR -----#
for {set i 1} {$i<=$mMort} {incr i} {
  for {set j 1} {$j<=$nMort} {incr j} {
    recorder Node -file $dataDir/MortNode[expr {3000 + ($i - 1)*$nMort + $j}]React.out -time
    -node [expr {3000 + ($i - 1)*$nMort + $j}] -dof 1 2 3 reaction;
    recorder Element -file $dataDir/MortElem[expr {3000 + ($i - 1)*$nMort + $j}]Def.out -time
    -ele [expr {3000 + ($i - 1)*$nMort + $j}] deformation;
    recorder Element -file $dataDir/MortElem[expr {3000 + ($i - 1)*$nMort + $j}]Force.out -
    time -ele [expr {3000 + ($i - 1)*$nMort + $j}] force;
  }
}

# PT BARS -----#
for {set iePt 1} {$iePt<=$nPt} {incr iePt} {
  recorder Element -file $dataDir/PtElem[expr {4000 + $nPt + $iePt}]Def.out -time -ele [expr
  {4000 + $nPt + $iePt}] deformation;
  recorder Element -file $dataDir/PtElem[expr {4000 + $nPt + $iePt}]Force.out -time -ele [expr
  {4000 + $nPt + $iePt}] force;
}

# RIGID ELEMENTS -----#
# dissipators
for {set iRigDiss 1} {$iRigDiss<=$nDiss} {incr iRigDiss} {
  recorder Element -file $dataDir/RigDissElem[expr {6000 + $iRigDiss}]Force.out -time -ele
  [expr {6000 + $iRigDiss}] force;
}
# mortar
for {set iRigMort 1} {$iRigMort<=$mMort} {incr iRigMort} {
  for {set jRigMort 1} {$jRigMort<=$nMort} {incr jRigMort} {
    recorder Element -file $dataDir/RigMortElem[expr {7000 + ($iRigMort - 1)*$nMort +
    $jRigMort}]Force.out -time -ele [expr {7000 + ($iRigMort - 1)*$nMort + $jRigMort}] force;
  }
}
}
```

Unit 1A – GRAVITY.tcl

```
#####
# DUAL SHELL COLUMN UNIT1A      #
#-----#
# Athanassios Vervelidis      #
# Gabriele Guerrini           #
# UC San Diego                #
# 2011                        #
#####

# DEFINE GRAVITY LOAD PATTERN -----
set Pvert 65.89;
pattern Plain 1001 Linear {
    load 5001 0. -$Pvert 0. 0. 0. 0.
}

# APPLY GRAVITY -----
constraints Plain; # how it handles boundary conditions
numberer Plain; # mapping between equations and dofs
system ProfileSPD; # how to store and solve the system of equations in the analysis
set tol 1.0e-8; # convergence tolerance for test
test NormDispIncr $tol 100 0; # determine if convergence has been achieved at the end of an
iteration step, max_iterations=100
algorithm Newton; # use Newton's solution algorithm: updates tangent stiffness at every iteration
set NstepGravity 10; # apply gravity in 10 steps
set DGravity [expr 1./$NstepGravity]; # load increment
integrator LoadControl $DGravity; # determine the next time step for an analysis
analysis Static;
analyze $NstepGravity; # apply gravity
loadConst -time 0.0; # maintain constant gravity loads and reset time to zero
```

Unit 1A – ANALYSIS_cyclic.tcl

```
#####
# DUAL SHELL COLUMN UNIT1A          #
#-----#
# Athanassios Vervelidis           #
# Gabriele Guerrini                 #
# UC San Diego                      #
# 2011                              #
#####
# based on the script by Silvia Mazzoni

# CYCLIC LATERAL LOAD -----#
set DispF1 0.031685; # force controlled - first 3 cycles (25 kips)
set DispF2 0.109587; # force controlled - last 3 cycles (52 kips)
set DispD1 0.2225; # displacement controlled - 1st 3 cycles (0.5% drift)
set DispD2 0.33375; # displacement controlled - 2nd 3 cycles (0.75% drift)
set DispD3 0.445; # displacement controlled - 3rd 2 cycles (1% drift)
set DispD3b $DispD2; # 1 cycle at lower displacement
set DispD4 0.6675; # displacement controlled - 4th 2 cycles (1.5% drift)
set DispD4b $DispD3; # 1 cycle at lower displacement
set DispD5 0.89; # displacement controlled - 5th 2 cycles (2% drift)
set DispD5b $DispD4; # 1 cycle at lower displacement
set DispD6 1.335; # displacement controlled - 6th 2 cycles (3% drift)
set DispD6b $DispD5; # 1 cycle at lower displacement
set DispD7 2.225; # displacement controlled - 7th 2 cycles (5% drift)
set DispD7b $DispD6; # 1 cycle at lower displacement
set DispD8 3.3375; # displacement controlled - 8th 2 cycles (7.5% drift)
set DispD8b $DispD7; # 1 cycle at lower displacement
set DispD9 4.45; # displacement controlled - 9th 2 cycles (10% drift)
set DispD9b $DispD8; # 1 cycle at lower displacement

# control node and dof
set IDctrlNode 5001; # node where displacement is read for displacement control
set IDctrlDOF 1; # dof read for displacement control

# characteristics of cyclic analysis
set i1Dmax "$DispF1 $DispF2 $DispD1 $DispD2"; # vector of displacement-cycle peaks
set i2Dmax "$DispD3 $DispD3b $DispD4 $DispD4b $DispD5 $DispD5b $DispD6 $DispD6b $DispD7 $DispD7b $DispD8 $DispD8b $DispD9";
set Dincr 0.01; # displacement increment for pushover
set Fact 1; # scale drift ratio by storey height for displacement cycles
set CycleType Full; # Full cycle: 0->+peak->0->-peak->0
set N1cycles 3; # specify the number of cycles at each peak
set N2cycles 1;
set Tol 1.0e-4; # tolerance for convergence

# create load pattern for lateral pushover load
pattern Plain 1000 Linear {
    load 5001 1. 0. 0. 0. 0. 0.
}

# set up analysis parameters and generate peaks
source LibAnalysisStaticParameters.tcl; # constraintsHandler, DOFnumberer, system-ofequations,
convergenceTest, solutionAlgorithm, integrator
source LibGeneratePeaks.tcl

# RUN CYCLIC ANALYSIS -----#
# first series of cycles, 3 equal and then increase
set fmt1 "%s Cyclic analysis: CtrlNode %.3i, dof %.1i, Disp=%.4f %s"; # format for screen/file
output of DONE/PROBLEM analysis
foreach Dmax $i1Dmax {
    set iDstep [GeneratePeaks $Dmax $Dincr $CycleType $Fact]; # this proc is defined above
    for {set i 1} {$i <= $N1cycles} {incr i 1} {
        set zeroD 0
        set D0 0.0
        foreach Dstep $iDstep {
            set D1 $Dstep
            set Dincr [expr $D1 - $D0]
            integrator DisplacementControl $IDctrlNode $IDctrlDOF $Dincr
            analysis Static
            # -----first analyze command-----#
            set ok [analyze 1]
            # -----if convergence failure-----#
            if {$ok != 0} {
                # if analysis fails, we try some other stuff
                # performance is slower inside this loop
                if {$ok != 0} {
                    puts "Trying Newton with Initial Tangent .."
                    test NormDispIncr $Tol 2000 0
                }
            }
        }
    }
}

```

```

        algorithm Newton -initial
        set ok [analyze 1]
        test $testTypeStatic $TolStatic $maxNumIterStatic 0
        algorithm $algorithmTypeStatic
    }
    if {$ok != 0} {
        puts "Trying Broyden .."
        algorithm Broyden 8
        set ok [analyze 1]
        algorithm $algorithmTypeStatic
    }
    if {$ok != 0} {
        puts "Trying NewtonWithLineSearch .."
        algorithm NewtonLineSearch 0.8
        set ok [analyze 1]
        algorithm $algorithmTypeStatic
    }
    if {$ok != 0} {
        set putout [format $fmt1 "PROBLEM" $IDctrlNode $IDctrlDOF [nodeDisp
        $IDctrlNode $IDctrlDOF] $LunitTXT]
        puts $putout
        return -1
    }
}; # end if
}; # end if
# -----
set D0 $D1; # move to next step
}; # end Dstep
}; # end i
}; # end of iDmaxCycl

# second series of cycles, 2 equal, 1 smaller, and then increase
set fmt1 "%s Cyclic analysis: CtrlNode %.3i, dof %.1i, Disp=%.4f %s"; # format for screen/file
output of DONE/PROBLEM analysis
foreach Dmax $i2Dmax {
    set iDstep [GeneratePeaks $Dmax $Dincr $CycleType $Fact]; # this proc is defined above
    for {set i 1} {$i <= $N2cycles} {incr i 1} {
        set zeroD 0
        set D0 0.0
        foreach Dstep $iDstep {
            set D1 $Dstep
            set Dincr [expr $D1 - $D0]
            integrator DisplacementControl $IDctrlNode $IDctrlDOF $Dincr
            analysis Static
            # -----first analyze command-----
            set ok [analyze 1]
            # -----if convergence failure-----
            if {$ok != 0} {
                # if analysis fails, we try some other stuff
                # performance is slower inside this loop
                if {$ok != 0} {
                    puts "Trying Newton with Initial Tangent .."
                    test NormDispIncr $Tol 2000 0
                    algorithm Newton -initial
                    set ok [analyze 1]
                    test $testTypeStatic $TolStatic $maxNumIterStatic 0
                    algorithm $algorithmTypeStatic
                }
                if {$ok != 0} {
                    puts "Trying Broyden .."
                    algorithm Broyden 8
                    set ok [analyze 1]
                    algorithm $algorithmTypeStatic
                }
                if {$ok != 0} {
                    puts "Trying NewtonWithLineSearch .."
                    algorithm NewtonLineSearch 0.8
                    set ok [analyze 1]
                    algorithm $algorithmTypeStatic
                }
                if {$ok != 0} {
                    set putout [format $fmt1 "PROBLEM" $IDctrlNode $IDctrlDOF [nodeDisp
                    $IDctrlNode $IDctrlDOF] $LunitTXT]
                    puts $putout
                    return -1
                }
            }; # end if
        }; # end if
        # -----
        set D0 $D1; # move to next step
    }; # end Dstep
}; # end i
}; # end of iDmaxCycl

# analysis conclusion

```

```
if { $ok != 0 } {  
  puts [format $fmt1 "PROBLEM" $IDctrlNode $IDctrlDOF [nodeDisp $IDctrlNode $IDctrlDOF]  
        $LunitTXT]  
} else {  
  puts [format $fmt1 "DONE" $IDctrlNode $IDctrlDOF [nodeDisp $IDctrlNode $IDctrlDOF] $LunitTXT]  
}
```

Unit 1A – LibAnalysisStaticParameters.tcl

```
# Static Analysis Parameters
# I am setting all these variables as global variables (using variable rather than set command)
# so that these variables can be uploaded by a procedure
# By Silvia Mazzoni & Frank McKenna, 2006

# CONSTRAINTS handler -----
# (http://opensees.berkeley.edu/OpenSees/manuals/usermanual/617.htm)
# Determines how the constraint equations are enforced in the analysis
# Plain Constraints -- Removes constrained degrees of freedom from the system of equations
# (only for homogeneous equations)
# Lagrange Multipliers -- Uses the method of Lagrange multipliers to enforce constraints
# Penalty Method -- Uses penalty numbers to enforce constraints, good for static analysis
# with non-homogeneous eqns (rigidDiaphragm)
# Transformation Method -- Performs a condensation of constrained degrees of freedom
variable constraintsTypeStatic Plain; # default;
if { [info exists RigidDiaphragm] == 1 } {
    if { $RigidDiaphragm=="ON" } {
        variable constraintsTypeStatic Lagrange; # for large model, try Transformation
    }; # if rigid diaphragm is on
}; # if rigid diaphragm exists
constraints $constraintsTypeStatic

# DOF NUMBERER -----
# (http://opensees.berkeley.edu/OpenSees/manuals/usermanual/366.htm)
# Numbers the degrees of freedom in the domain
# Determines the mapping between equation numbers and degrees-of-freedom
# Plain -- Uses the numbering provided by the user
# RCM -- Renumbers the DOF to minimize the matrix band-width using the Reverse Cuthill-McKee
# algorithm
set numbererTypeStatic RCM
numberer $numbererTypeStatic

# SYSTEM -----
# (http://opensees.berkeley.edu/OpenSees/manuals/usermanual/371.htm)
# Linear Equation Solvers
# How to store and solve the system of equations in the analysis
# Provides the solution of the linear system of equations Ku = P
# Each solver is tailored to a specific matrix topology
# ProfileSPD -- Direct profile solver for symmetric positive definite matrices
# BandGeneral -- Direct solver for banded unsymmetric matrices
# BandSPD -- Direct solver for banded symmetric positive definite matrices
# SparseGeneral -- Direct solver for unsymmetric sparse matrices
# SparseSPD -- Direct solver for symmetric sparse matrices
# UmfPack -- Direct UmfPack solver for unsymmetric matrices
set systemTypeStatic BandGeneral; # try UmfPack for large model
system $systemTypeStatic

# TEST -----
# (http://opensees.berkeley.edu/OpenSees/manuals/usermanual/360.htm)
# Convergence test
# Accepts the current state of the domain as being on the converged solution path
# Determines if convergence has been achieved at the end of an iteration step
# NormUnbalance -- Specifies a tolerance on the norm of the unbalanced load at the current
# iteration
# NormDispIncr -- Specifies a tolerance on the norm of the displacement increments at the
# current iteration
# EnergyIncr -- Specifies a tolerance on the inner product of the unbalanced load and
# displacement increments at the current iteration
# RelativeNormUnbalance --
# RelativeNormDispIncr --
# RelativeEnergyIncr --
variable TolStatic 1.e-8; # Convergence Test: tolerance
variable maxNumIterStatic 6; # Convergence Test: maximum number of iterations that will be
# performed before "failure to converge" is returned
variable printFlagStatic 0; # Convergence Test: flag used to print information on convergence
# (optional) # 1: print information on each step;
variable testTypeStatic EnergyIncr ; # Convergence-test type
test $testTypeStatic $TolStatic $maxNumIterStatic $printFlagStatic;
# for improved-convergence procedure:
variable maxNumIterConvergeStatic 2000;
variable printFlagConvergeStatic 0;

# Solution ALGORITHM -----
# (http://opensees.berkeley.edu/OpenSees/manuals/usermanual/682.htm)
# Iterates from the last time step to the current
```

```

# Linear -- Uses the solution at the first iteration and continues
# Newton -- Uses the tangent at the current iteration to iterate to convergence
# ModifiedNewton -- Uses the tangent at the first iteration to iterate to convergence
# NewtonLineSearch --
# KrylovNewton --
# BFGS --
# Broyden --
variable algorithmTypeStatic Newton
algorithm $algorithmTypeStatic;

# INTEGRATOR -----
# (http://opensees.berkeley.edu/OpenSees/manuals/usermanual/689.htm)
# Static integrator -- Determines the next time step for an analysis without considering inertial
effects:
# LoadControl -- Specifies the incremental load factor to be applied to the loads in the
domain
# DisplacementControl -- Specifies the incremental displacement at a specified DOF in the
domain
# Minimum Unbalanced Displacement Norm -- Specifies the incremental load factor such that the
residual displacement norm is minimized
# Arc Length -- Specifies the incremental arc-length of the load-displacement path
# Transient integrator -- Determines the next time step for an analysis including inertial
effects:
# Newmark -- The two parameter time-stepping method developed by Newmark
# HHT -- The three parameter Hilbert-Hughes-Taylor time-stepping method
# Central Difference -- Approximates velocity and acceleration by centered finite differences
of displacement
integrator DisplacementControl $IDctrlNode $IDctrlDOF $Dincr

# ANALYSIS -----
# (http://opensees.berkeley.edu/OpenSees/manuals/usermanual/324.htm)
# Defines what type of analysis is to be performed
# Static Analysis -- solves the KU=R problem, without the mass or damping matrices.
# Transient Analysis -- solves the time-dependent analysis. The time step in this type
of analysis is constant. The time step in the output is also constant.
# variableTransient Analysis -- performs the same analysis type as the Transient Analysis
object. The time step, however, is variable. This method is used when there are convergence
problems with the Transient Analysis object at a peak or when the time step is too small. The
time step in the output is also variable.
set analysisTypeStatic Static
analysis $analysisTypeStatic

```

Unit 1A – LibGeneratePeaks.tcl

```
# GeneratePeaks $Dmax $DincrStatic $CycleType $Fact
proc GeneratePeaks {Dmax {DincrStatic 0.01} {CycleType "Full"} {Fact 1} } {;

# Generate incremental displacements for Dmax
# This procedure creates a file which defines a vector then executes the file to return the
vector of displacement increments
# By Silvia Mazzoni, 2006

# input variables
# $Dmax : peak displacement (can be + or negative)
# $DincrStatic : displacement increment (optional, default=0.01, independently of units)
# $CycleType : Push (0->+peak), Half (0->+peak->0), Full (0->+peak->0->-peak->0) (optional,
def=Full)
# $Fact : scaling factor (optional, default=1)
# $iDstepFileName : file name where displacement history is stored temporarily, until next
disp. peak

# output variable
# $iDstep : vector of displacement increments

file mkdir data
set outFileID [open data/tmpDsteps.tcl w]
set Disp 0.
puts $outFileID "set iDstep { ";puts $outFileID $Disp;puts $outFileID $Disp; # open vector
definition and some 0
set Dmax [expr $Dmax*$Fact]; # scale value
if {$Dmax<0} {; # avoid the divide by zero
set dx [expr -$DincrStatic]
} else {
set dx $DincrStatic;
}

set NstepsPeak [expr int(abs($Dmax)/$DincrStatic)]
for {set i 1} {$i <= $NstepsPeak} {incr i 1} {; # zero to one
set Disp [expr $Disp + $dx]
puts $outFileID $Disp; # write to file
}
if {$CycleType != "Push"} {
for {set i 1} {$i <= $NstepsPeak} {incr i 1} {; # one to zero
set Disp [expr $Disp - $dx]
puts $outFileID $Disp; # write to file
}
if {$CycleType != "Half"} {
for {set i 1} {$i <= $NstepsPeak} {incr i 1} {; # zero to minus one
set Disp [expr $Disp - $dx]
puts $outFileID $Disp; # write to file
}
for {set i 1} {$i <= $NstepsPeak} {incr i 1} {; # minus one to zero
set Disp [expr $Disp + $dx]
puts $outFileID $Disp; # write to file
}
}
}
}
puts $outFileID " }"; # close vector definition
close $outFileID
source data/tmpDsteps.tcl; # source tcl file to define entire vector
return $iDstep
}
```

Unit 1B – GO.tcl

```
#####
# DUAL SHELL COLUMN UNIT1B      #
#-----#
# Athanassios Vervelidis      #
# Gabriele Guerrini           #
# UC San Diego                #
# 2011                         #
#####

# INITIALIZATION -----
wipe; # clear memory of all past model definitions
model BasicBuilder -ndm 3 -ndf 6; # define the model builder, ndm=#dimension, ndf=#dofs
set dataDir ResultsUnit1B; # set up name of data directory
file mkdir $dataDir; # create data directory
source UNITS.tcl; # define units
puts "MODEL SET-UP OK"

# INPUT -----
source INPUT_geom.tcl
puts "INPUT GEOMETRY OK"
source INPUT_mat.tcl
puts "INPUT MATERIALS OK"

# TRANSFORMATIONS -----
source TRANSF.tcl
puts "TRANSFORMATIONS OK"

# GENERATE ELEMENTS -----

# RC COLUMN
source GENERATE_column.tcl
puts "COLUMN OK"

# DISSIPATORS
source GENERATE_dissipators_int.tcl
puts "DISSIPATORS OK"

# MORTAR SPRING BED
source GENERATE_mortar.tcl
puts "MORTAR SPRINGS OK"

# PT BARS
source GENERATE_pt.tcl
puts "PT BARS OK"

# RIGID LINKS
source GENERATE_rigid.tcl
puts "RIGID LINKS OK"

# RECORDERS -----
source RECORDERS.tcl
puts "RECORDERS OK"

# GRAVITY -----
source GRAVITY.tcl
puts "GRAVITY OK, MODEL BUILT"

# ANALYSIS -----
source ANALYSIS_cyclic.tcl
puts "ANALYSIS DONE"
```

Unit 1B – UNITS.tcl

```
#####
# DUAL SHELL COLUMN UNIT1B          #
#-----#
# Athanassios Vervelidis           #
# Gabriele Guerrini                 #
# UC San Diego                      #
# 2011                               #
#####

# UNITS -----
set in 1.; # define basic units -- output units
set kip 1.; # define basic units -- output units
set sec 1.; # define basic units -- output units
set LunitTXT "inch"; # define basic-unit text for output
set FunitTXT "kip"; # define basic-unit text for output
set TunitTXT "sec"; # define basic-unit text for output
set ft [expr 12.*$in]; # define engineering units
set ksi [expr $kip/pow($in,2)];
set psi [expr $ksi/1000.];
set lbf [expr $psi*$in*$in]; # pounds force
set pcf [expr $lbf/pow($ft,3)]; # pounds per cubic foot
set psf [expr $lbf/pow($ft,2)]; # pounds per square foot
set in2 [expr $in*$in]; # inch^2
set in4 [expr $in*$in*$in*$in]; # inch^4
set cm [expr $in/2.54]; # centimeter, needed for displacement input in MultipleSupport excitation
set cmsec2 [expr $cm/pow($sec,2)]; # cm/sec^2, needed for some ground accelerations
set m [expr $cm*100]; # meter
set mm [expr $cm/10]; # millimeter
set mm2 [expr $mm*$mm]; # millimeter^2
set kN [expr 0.2247*$kip]; # kilo newton
set MPa [expr 0.1450*$ksi]; # mega pascal
set GPa [expr 1000*$MPa]; # giga pascal
set pi [expr 2*asin(1.0)]; # define constants
set g [expr 32.2*$ft/pow($sec,2)]; # gravitational acceleration
set Ubig 1.e10; # a really large number
set Usmall [expr 1/$Ubig]; # a really small number
```

Unit 1B – INPUT_geom.tcl

```
#####
# DUAL SHELL COLUMN UNIT1B      #
#-----#
# Athanassios Vervelidis      #
# Gabriele Guerrini           #
# UC San Diego                 #
# 2011                         #
#####

# COLUMN -----#
set lCol [expr 2.*$ft + 10.*$in]; # column length (including 1 in of upper joint)
set Dint [expr 14.*$in]; # internal diameter
set Dext [expr 20.*$in]; # external diameter
set Rint [expr $Dint/2.]; # internal radius
set Rext [expr $Dext/2.]; # external radius
set tint [expr (1./8.)*$in]; # internal shell thickness
set text [expr (1./4.)*$in]; # external shell thickness

# DISSIPATORS -----#
set nDiss 6; # number of dissipators
set dDiss [expr $Rext - (1 + 3./4.)*$in]; # internal dissipators distance from column axis
set lDissUp [expr 4.*$in]; # dissipators length (low part)
set lDissDw [expr 3.*$in]; # dissipators length (upper part)
set diamDiss [expr 0.5*$in]; # dissipator diameter

# MORTAR -----#
set lMort [expr 0.5*$in]; # mortar thickness

# RIGID LINK FOR LOAD APPLICATION -----#
set lLoadStub [expr 1.*$ft + 8.*$in]; # load stub length
set lss [expr $lMort + $lCol + ($lLoadStub/2.)]; #shear span

# PT BARS -----#
set nPt 4; # number of pt bars
set rPt [expr 5.66*$in]; # bars distance from column axis
set lPt [expr 20.*$in + $lMort + $lCol + $lLoadStub + ((4.*(1. + 7./8.) + 5.*(1./8.)) + 0.5 + 4)*$in]; # bar length
set lPtFound [expr 20.*$in]; # bar anchorage length inside foundation
set lPtEq [expr $lPtFound + $lss]; # equivalent bar length (shear span + anchorage inside foundation)
```

Unit 1B – INPUT_mat.tcl

```
#####
# DUAL SHELL COLUMN UNIT1B #
#-----#
# Athanassios Vervelidis #
# Gabriele Guerrini #
# UC San Diego #
# 2011 #
#####

# COLUMN -----
set fc [expr 10.4*$ksi]; # concrete strength
set Ec [expr 57.*pow(1000.*$fc,0.5)]; # Young's modulus for concrete
set Es [expr 29000.*$ksi]; # Young's modulus for steel (cylinder)
set n [expr $Es/$Ec]; # Es/Ec ratio
set ni 0.2; # Poisson's coefficient for concrete
set Gc [expr ((1+$ni)/2.)*$Ec]; # shear modulus for concrete
set AColDw [expr ($pi)*(pow($Rext-$ttext,2) - pow($Rint,2))]; #cross-sectional area of element
(concrete)
set AColUp [expr ($pi)*(pow($Rext-$ttext,2) - pow($Rint,2)) + $n*($pi)*(pow($Rext,2) - pow($Rext-
$ttext,2))]; #cross-sectional area of element (concrete + omogenized external steel)
set IColDw [expr ($pi/4.)*(pow($Rext-$ttext,4) - pow($Rint,4))]; # second moment of area about the
local y and z-axes
set IShInt [expr ($pi/4.)*(pow($Rint+$tint,4) - pow($Rint,4))];
set IShExt [expr ($pi/4.)*(pow($Rext,4) - pow($Rext-$ttext,4))];
set IColUp [expr ($pi/4.)*(pow($Rext-$ttext,4) - pow($Rint,4)) + ($IShInt + $IShExt)*($n-1.)];
set JColDw [expr 2*$IColDw]; # torsional moment of inertia of cross section
set JColUp [expr 2*$IColUp];

# DISSIPATORS -----
set matTagDissAxial 2001; # tag steel material for axial behavior of the dissipator's section
(external part)
set matTagDissMoment 2002; # tag for the Mz to add at the same section above
set matTagDissTorsion 2003; # tag for the torsional effects (not necessary in plane case)
set FyDiss [expr 120.*$ksi]; # yielding strength (48)
set E0Diss [expr 29000.*$ksi]; # initial elastic tangent
set eyDiss [expr $FyDiss/$E0Diss]; #yielding strain
set FuDiss [expr 129.*$ksi]; # ultimate strenght
set euDiss 0.15; #ultimate strain (0.12)
set EuDiss [expr (($FuDiss-$FyDiss)/($euDiss-$eyDiss))]; # post-yield tangent
set bDiss [expr $EuDiss/$E0Diss]; # strain-hardening ratio (ratio between post-yield tangent and
initial elastic tangent)
set R0 18.; # parameters to control the transition from elastic to plastic branches
set cR1 0.925;
set cR2 0.15;
set a1Diss 0;
set a2Diss 1;
set a3Diss 0;
set a4Diss 1;
set sigInitDiss 0;
set rDiss [expr $diamDiss/2.]; # dissipator radius (external part)
set ADiss [expr $pi*pow($rDiss,2)]; # dissipator area
set IDiss [expr ($pi/4.)*pow($rDiss,4)]; # second moment of inertia
set JDiss [expr ($pi/2.)*pow($rDiss,4)]; # torsional moment of inertia of cross section
set nis 0.3; # Poisson's coefficient for steel
set GDiss [expr ((1+$nis)/2.)*$E0Diss]; # shear modulus

uniaxialMaterial Steel02 $matTagDissAxial [expr $FyDiss*$ADiss] [expr $ADiss*$E0Diss] $bDiss $R0
$cR1 $cR2 $a1Diss $a2Diss $a3Diss $a4Diss $sigInitDiss;
uniaxialMaterial Steel02 $matTagDissMoment [expr $FyDiss*($IDiss/$rDiss)] [expr $E0Diss*$IDiss]
$bDiss $R0 $cR1 $cR2 $a1Diss $a2Diss $a3Diss $a4Diss $sigInitDiss;
uniaxialMaterial Elastic $matTagDissTorsion [expr $GDiss*$JDiss];

# MORTAR -----
set matTagMort 3001; # integer tag identifying material
set fpc [expr -8.5*$ksi]; # compressive strength (compression is negative)
set ecc0 -0.004; # strain at maximum strength
set Lreal [expr 5*$in]; # length of extension of deformation
set ecc0eq [expr ($Lreal/$lMort)*$ecc0]; # fictitious strain at maximum strength
set fpcu [expr -1*$ksi]; # crushing strength
set eccu -0.1511; # strain at crushing
set eccueq [expr ($Lreal/$lMort)*$eccu]; # fictitious strain at crushing

uniaxialMaterial Concrete01 $matTagMort $fpc $ecc0eq $fpcu $eccueq;

# PT BARS -----
```

```

set matTagPt 4001; # integer tag identifying material
set FyPt [expr 120.*$ksi]; # yielding strength
set EPt [expr 29700.*$ksi]; # initial elastic tangent
set eyPt [expr $FyPt/$EPt]; # yielding strain
set FuPt [expr 156.51*$ksi]; # ultimate strength
set euPt 0.08; # ultimate strain
set EuPt [expr ($FuPt-$FyPt)/($euPt-$eyPt)]; # plastic tangent
set bPt [expr $EuPt/$EPt]; # strain-hardening ratio
set APt [expr 1.58*$in2]; # cross-sectional area of element
set Krb [expr 263.2*$kip/$in]; # bearing stiffness
set KPtEq [expr 1/((1/$Krb) + ($lPt/($EPt*$APt)))]]; # values for the equivalent pt system
set EPtEq [expr ($KPtEq*$lPtEq)/$APt];
set KuPtEq [expr 1/((1/$Krb) + ($lPt/($EuPt*$APt)))]];
set bPtEq [expr (($KuPtEq*$lPtEq)/$APt)/$EPtEq]; # equivalent strain-hardening ratio

uniaxialMaterial Steel02 $matTagPt $FyPt $EPtEq $bPtEq 18. 0.925 0.15 0 1 0 1 31.27;

# RIGID LINK FOR LOAD APPLICATION -----
set ARigCol [expr 1000.*$AColUp*($lLoadStub/2.)/$lss)]; # cross-sectional area of rigid element
set ERigCol [expr 29000.*$ksi]; # Young's modulus for rigid element
set GRigCol [expr ((1+$nis)/2.)*$ERigCol]; # shear modulus for rigid element
set JRigCol [expr 1000.*$JColUp]; # rigid link infinitely stiffer (1000 times) than column
set IRigCol [expr 1000.*$IColUp]; # second moment of area

# RIGID LINK FOR DISSIPATORS -----
set ARigDiss [expr 1000.*$AColUp*($rDiss/$lss)]; # cross-sectional area of rigid element
set ESpring [expr 29000.*$ksi]; # Young's modulus for rigid element
set GRigDiss [expr ((1+$nis)/2.)*$ESpring]; # shear modulus for rigid element
set JRigDiss [expr 1000.*$JColUp]; # torsional moment of inertia
set IRigDiss [expr 1000.*$IColUp]; # second moment of area

# RIGID LINK FOR MORTAR SPRINGS -----
set ERigMort [expr 29000.*$ksi]; # Young's modulus for rigid element
set GRigMort [expr ((1+$nis)/2.)*$ERigMort]; # shear modulus for rigid element
set JRigMort [expr 1000.*$JColUp]; # torsional moment of inertia

# RIGID LINK FOR PT BARS -----
set ARigPt [expr 1000.*$AColUp*($rPt/$lss)]; # cross-sectional area of rigid element
set ERigPt [expr 29000.*$ksi]; # Young's modulus for rigid element
set GRigPt [expr ((1+$nis)/2.)*$ERigPt]; # shear modulus for rigid element
set JRigPt [expr 1000.*$JColUp]; # torsional moment of inertia
set IRigPt [expr 1000.*$IColUp]; # second moment of area

```

Unit 1B – TRANSF.tcl

```
#####  
# DUAL SHELL COLUMN UNIT1B      #  
#-----#  
# Athanassios Vervelidis        #  
# Gabriele Guerrini              #  
# UC San Diego                  #  
# 2011                           #  
#####
```

```
# TRANSFORMATION -----  
set transfTagVert 1001; # associate a tag to the transformation  
geomTransf Linear $transfTagVert 0 0 -1; # linear geometric transformation  
  
set transfTagHoriz 1002; # associate a tag to the transformation  
geomTransf Linear $transfTagHoriz 0 1 0; # linear geometric transformation
```

Unit 1B – GENERATE_column.tcl

```
#####
# DUAL SHELL COLUMN UNIT1B          #
#-----#
# Athanassios Vervelidis           #
# Gabriele Guerrini                 #
# UC San Diego                       #
# 2011                               #
#####

# GEOMETRY -----#
# nodal coordinates:
node 1001 0. $lMort 0.; # mortar
node 1002 0. $lDissUp 0.; # master node for dissipator
node 1003 0. [expr $lMort + $lCol] 0.; # last node column
# boundary conditions:
fix 1001 1 0 1 0 0 0; # boundary condition (roller)

# ELEMENTS -----#
# element connectivity:
set eleTagColDw 1001; # unique element object tag (lower column)
set eleTagColUp 1002; # unique element object tag (upper column)

element elasticBeamColumn $eleTagColDw 1001 1002 $AColDw $Ec $Gc $JColDw $IColDw $IColDw
$transfTagVert;
element elasticBeamColumn $eleTagColUp 1002 1003 $AColUp $Ec $Gc $JColUp $IColUp $IColUp
$transfTagVert;
```

Unit 1B – GENERATE_dissipators_int.tcl

```
#####
# DUAL SHELL COLUMN UNIT1B          #
#-----#
# Athanassios Vervelidis           #
# Gabriele Guerrini                 #
# UC San Diego                      #
# 2011                              #
#####

# GEOMETRY -----#
set thetaDiss 2.*pi/$nDiss; # angle between dissipators
for {set iDiss 1} {$iDiss<=$nDiss} {incr iDiss} {
  set thetaiDiss [expr $thetaDiss/2. + ($iDiss - 1.)*$thetaDiss]; # bar angle
  set x [expr {$dDiss*cos($thetaiDiss)}]; # spring x coord
  set z [expr {$dDiss*sin($thetaiDiss)}]; # spring z coord
  node [expr {2000 + $iDiss}] $x -$lDissDw $z; # base nodes
  node [expr {2000 + $nDiss + $iDiss}] $x $lDissUp $z; # top nodes
  fix [expr {2000 + $iDiss}] 1 1 1 1 1; # boundary condition base(fixed)
}

# SECTIONS -----#
set secTagDiss1 2001; # unique section tag
set secTagDiss2 2002; # unique section tag

section Uniaxial $secTagDiss1 $matTagDissAxial P; # construct a UniaxialSection object
section Aggregator $secTagDiss2 $matTagDissMoment My $matTagDissMoment Mz $matTagDissTorsion T -
section $secTagDiss1; # aggregates previously-defined UniaxialMaterial objects into a single
section

# ELEMENTS -----#
# element connectivity:
set numIntgrPts 3; # number of integration points along the element.
for {set ieDiss 1} {$ieDiss<=$nDiss} {incr ieDiss} {
  element dispBeamColumn [expr {2000 + $ieDiss}] [expr {2000 + $ieDiss}]
  [expr {2000 + $nDiss + $ieDiss}] $numIntgrPts $secTagDiss2 $transfTagVert;
}
}
```

Unit 1B – GENERATE_mortar.tcl

```
#####
# DUAL SHELL COLUMN UNIT1B          #
#-----#
# Athanassios Vervelidis           #
# Gabriele Guerrini                 #
# UC San Diego                      #
# 2011                               #
#####

# GEOMETRY -----#
set nMort 36; # number of wedges
set mMort 3; # number of rings
set tMort [expr {($Rext-$Rint)/$mMort}]; # ring thickness
set thetaMort [expr {2.*$pi/$nMort}]; # angle between wedges
for {set i 1} {$i<=$mMort} {incr i} {
  set riMort [expr {$Rint + ($tMort/2.) + ($i - 1.)*$tMort}]; # spring radius
  set AiMort [expr {(($pi*(pow(($riMort + $tMort/2.),2) - pow(($riMort - $tMort/2.),2)))/
  $nMort)}]; # spring influence area
  for {set j 1} {$j<=$nMort} {incr j} {
    set thetajMort [expr {$thetaMort/2. + ($j - 1.)*$thetaMort}]; # spring angle
    set x [expr {$riMort*cos($thetajMort)}]; # spring x coord
    set z [expr {$riMort*sin($thetajMort)}]; # spring z coord
    node [expr {3000 + ($i - 1)*$nMort + $j}] $x 0. $z; #mortar bed (base)
    node [expr {3000 + $mMort*$nMort + ($i - 1)*$nMort + $j}] $x $lMort $z; # mortar bed
    (top)
    fix [expr {3000 + ($i - 1)*$nMort + $j}] 1 1 1 1 1 1; # boundary condition base(fixed)
  }
}

# ELEMENTS -----#
# element connectivity:
for {set i 1} {$i<=$mMort} {incr i} {
  for {set j 1} {$j<=$nMort} {incr j} {
    element truss [expr {3000 + ($i - 1)*$nMort + $j}] [expr {3000 + ($i - 1)*$nMort + $j}]
    [expr {3000 + $mMort*$nMort + ($i - 1)*$nMort + $j}] $AiMort $matTagMort;
  }
}
}
```

Unit 1B – GENERATE_pt.tcl

```
#####
# DUAL SHELL COLUMN UNIT1B          #
#-----#
# Athanassios Vervelidis           #
# Gabriele Guerrini                 #
# UC San Diego                      #
# 2011                              #
#####

# GEOMETRY -----#
set thetaPt 2.*pi/$nPt; # angle between bars
for {set ipt 1} {$iPt<=$nPt} {incr ipt} {
  set thetaiPt [expr $thetaPt/2. + ($iPt - 1.)*$thetaPt]; # bar angle
  set x [expr {$rPt*cos($thetaiPt)}]; # bar x coord
  set z [expr {$rPt*sin($thetaiPt)}]; # bar z coord
  node [expr {4000 + $iPt}] $x -$lPtFound $z; # base nodes
  node [expr {4000 + $nPt + $iPt}] $x 0 $z; # middle nodes
  node [expr {4000 + 2*$nPt + $iPt}] $x $lss $z; # top nodes
  fix [expr {4000 + $iPt}] 1 1 1 1 1 1; # boundary condition base(fixed)
  fix [expr {4000 + $nPt + $iPt}] 1 0 1 1 1 1; # boundary condition middle(slider)
}

# ELEMENTS -----#
# element connectivity:
for {set iePt 1} {$iePt<=$nPt} {incr iePt} {
  element truss [expr {4000 + $iePt}] [expr {4000 + $iePt}] [expr {4000 + $nPt + $iePt}] $APt
  $matTagPt;
  element truss [expr {4000 + $nPt + $iePt}] [expr {4000 + $nPt + $iePt}] [expr {4000 + 2*$nPt
  + $iePt}] $APt $matTagPt;
}
```

Unit 1B – GENERATE_rigid.tcl

```
#####
# DUAL SHELL COLUMN UNIT1B          #
#-----#
# Athanassios Vervelidis           #
# Gabriele Guerrini                 #
# UC San Diego                      #
# 2011                              #
#####

# LOADING POINT -----
node 5001 0. $lss 0.; # force application node
set eleTagRigCol 5001; # unique element object tag
element elasticBeamColumn $eleTagRigCol 1003 5001 $ARigCol $ERigCol $GRigCol $JRigCol $IRigCol
$IRigCol $transfTagVert;

# RIGID CONNECTION FOR DISSIPATORS -----
for {set iRigDiss 1} {$iRigDiss<=$nDiss} {incr iRigDiss} {
  element elasticBeamColumn [expr {6000 + $iRigDiss}] 1002 [expr {2000 + $nDiss + $iRigDiss}]
  $ARigDiss $ESpring $GRigDiss $JRigDiss $IRigDiss $IRigDiss $transfTagHoriz;
}

# RIGID CONNECTION FOR MORTAR -----
for {set iRigMort 1} {$iRigMort<=$mMort} {incr iRigMort} {
  set ARigMort [expr 1000.*$AColUp*($riMort/$lss)];
  set IRigMort [expr 1000.*$IColUp*($Ec/$ERigMort)*($riMort/$lss)];
  for {set jRigMort 1} {$jRigMort<=$nMort} {incr jRigMort} {
    element elasticBeamColumn [expr {7000 + ($iRigMort - 1)*$nMort + $jRigMort}] 1001 [expr
    {3000 + $mMort*$nMort + ($iRigMort - 1)*$nMort + $jRigMort}] $ARigMort $ERigMort
    $GRigMort $JRigMort $IRigMort $IRigMort $transfTagHoriz;
  }
}

# RIGID CONNECTION FOR PT BARS -----
for {set iRigPt 1} {$iRigPt<=$nPt} {incr iRigPt} {
  element elasticBeamColumn [expr {8000 + $iRigPt}] 5001 [expr {4000 + 2*$nPt + $iRigPt}]
  $ARigPt $ERigPt $GRigPt $JRigPt $IRigPt $IRigPt $transfTagHoriz;
}
```

Unit 1B – RECORDERS.tcl

```
#####
# DUAL SHELL COLUMN UNIT1B          #
#-----#
# Athanassios Vervelidis           #
# Gabriele Guerrini                 #
# UC San Diego                      #
# 2011                              #
#####

# COLUMN -----#
recorder Node -file $dataDir/ColDisp.out -time -node 5001 -dof 1 2 3 4 5 6 disp;
recorder Node -file $dataDir/ColBaseShear.out -time -node 1001 -dof 1 2 3 4 5 6 reaction;
recorder Node -file $dataDir/ColBaseDisp.out -time -node 1001 -dof 1 2 3 4 5 6 disp;
recorder Node -file $dataDir/ColReactDissLevel.out -time -node 1002 -dof 1 2 3 4 5 6 reaction;
recorder Node -file $dataDir/ColDispDissLevel.out -time -node 1002 -dof 1 2 3 4 5 6 disp;
recorder Element -file $dataDir/ColTopShear.out -time -ele $eleTagColUp globalForce;
recorder Element -file $dataDir/ColTopDef.out -time -ele $eleTagColUp deformation;
recorder Element -file $dataDir/ColShearDissLevel.out -time -ele $eleTagColDw force;
recorder Element -file $dataDir/ColDefDissLevel.out -time -ele $eleTagColDw deformation;

# DISSIPATORS -----#
for {set ieDiss 1} {$ieDiss<=$nDiss} {incr ieDiss} {
  recorder Element -file $dataDir/DissElem[expr {2000 + $ieDiss}]Force.out -time -ele [expr
    {2000 + $ieDiss}] section 2 force;
  recorder Element -file $dataDir/DissElem[expr {2000 + $ieDiss}]Def.out -time -ele [expr {2000
    + $ieDiss}] section 2 deformation;
  recorder Node -file $dataDir/DissNode[expr {2000 + $ieDiss}]React.out -time -node [expr {2000
    + $ieDiss}] -dof 1 2 3 reaction;
}

# MORTAR -----#
for {set i 1} {$i<=$mMort} {incr i} {
  for {set j 1} {$j<=$nMort} {incr j} {
    recorder Node -file $dataDir/MortNode[expr {3000 + ($i - 1)*$nMort + $j}]React.out -time
      -node [expr {3000 + ($i - 1)*$nMort + $j}] -dof 1 2 3 reaction;
    recorder Element -file $dataDir/MortElem[expr {3000 + ($i - 1)*$nMort + $j}]Def.out -time
      -ele [expr {3000 + ($i - 1)*$nMort + $j}] deformation;
    recorder Element -file $dataDir/MortElem[expr {3000 + ($i - 1)*$nMort + $j}]Force.out -
      time -ele [expr {3000 + ($i - 1)*$nMort + $j}] force;
  }
}

# PT BARS -----#
for {set iePt 1} {$iePt<=$nPt} {incr iePt} {
  recorder Element -file $dataDir/PtElem[expr {4000 + $nPt + $iePt}]Def.out -time -ele [expr
    {4000 + $nPt + $iePt}] deformation;
  recorder Element -file $dataDir/PtElem[expr {4000 + $nPt + $iePt}]Force.out -time -ele [expr
    {4000 + $nPt + $iePt}] force;
}

# RIGID ELEMENTS -----#
# dissipators
for {set iRigDiss 1} {$iRigDiss<=$nDiss} {incr iRigDiss} {
  recorder Element -file $dataDir/RigDissElem[expr {6000 + $iRigDiss}]Force.out -time -ele
    [expr {6000 + $iRigDiss}] force;
}
# mortar
for {set iRigMort 1} {$iRigMort<=$mMort} {incr iRigMort} {
  for {set jRigMort 1} {$jRigMort<=$nMort} {incr jRigMort} {
    recorder Element -file $dataDir/RigMortElem[expr {7000 + ($iRigMort - 1)*$nMort +
      $jRigMort}]Force.out -time -ele [expr {7000 + ($iRigMort - 1)*$nMort + $jRigMort}] force;
  }
}
}
```

Unit 1B – GRAVITY.tcl

```
#####
# DUAL SHELL COLUMN UNIT1B      #
#-----#
# Athanassios Vervelidis      #
# Gabriele Guerrini           #
# UC San Diego                #
# 2011                        #
#####

# DEFINE GRAVITY LOAD PATTERN -----
set Pvert 60.27;
pattern Plain 1001 Linear {
    load 5001 0. -$Pvert 0. 0. 0. 0.
}

# APPLY GRAVITY -----
constraints Transformation; # how it handles boundary conditions
numberer Plain; # mapping between equations and dofs
system ProfileSPD; # how to store and solve the system of equations in the analysis
set tol 1.0e-8; # convergence tolerance for test
test NormDispIncr $tol 100 0; # determine if convergence has been achieved at the end of an
iteration step, max_iterations=100
algorithm Newton; # use Newton's solution algorithm: updates tangent stiffness at every iteration
set NstepGravity 10; # apply gravity in 10 steps
set DGravity [expr 1./$NstepGravity]; # load increment;
integrator LoadControl $DGravity; # determine the next time step for an analysis
analysis Static;
analyze $NstepGravity; # apply gravity
loadConst -time 0.0; # maintain constant gravity loads and reset time to zero
```

Unit 1B – ANALYSIS_cyclic.tcl

```
#####
# DUAL SHELL COLUMN UNIT1B          #
#-----#
# Athanassios Vervelidis            #
# Gabriele Guerrini                  #
# UC San Diego                       #
# 2011                                #
#####
# based on the script by Silvia Mazzoni

# CYCLIC LATERAL LOAD -----
set DispF1 0.031685; # force controlled - first 3 cycles (25 kips)
set DispF2 0.109587; # force controlled - last 3 cycles (52 kips)
set DispD1 0.2225; # displacement controlled - 1st 3 cycles (0.5% drift)
set DispD2 0.33375; # displacement controlled - 2nd 3 cycles (0.75% drift)
set DispD3 0.445; # displacement controlled - 3rd 2 cycles (1% drift)
set DispD3b $DispD2; # 1 cycle at lower displacement
set DispD4 0.6675; # displacement controlled - 4th 2 cycles (1.5% drift)
set DispD4b $DispD3; # 1 cycle at lower displacement
set DispD5 0.89; # displacement controlled - 5th 2 cycles (2% drift)
set DispD5b $DispD4; # 1 cycle at lower displacement
set DispD6 1.335; # displacement controlled - 6th 2 cycles (3% drift)
set DispD6b $DispD5; # 1 cycle at lower displacement
set DispD7 2.225; # displacement controlled - 7th 2 cycles (5% drift)
set DispD7b $DispD6; # 1 cycle at lower displacement
set DispD8 3.3375; # displacement controlled - 8th 2 cycles (7.5% drift)
set DispD8b $DispD7; # 1 cycle at lower displacement
set DispD9 4.45; # displacement controlled - 9th 2 cycles (10% drift)
set DispD9b $DispD8; # 1 cycle at lower displacement

# control node and dof
set IDctrlNode 5001; # node where displacement is read for displacement control
set IDctrlDOF 1; # dof read for displacement control

# characteristics of cyclic analysis
set i1Dmax "$DispF1 $DispF2 $DispD1 $DispD2"; # vector of displacement-cycle peaks
set i2Dmax "$DispD3 $DispD3b $DispD4 $DispD4b $DispD5 $DispD5b $DispD6 $DispD6b $DispD7 $DispD7b $DispD8 $DispD8b $DispD9 $DispD9b";
set Dincr 0.01; # displacement increment
set Fact 1; # scale drift ratio by storey height for displacement cycles
set CycleType Full; # Full cycle: 0->+peak->0->-peak->0
set N1cycles 3; # specify the number of cycles at each peak
set N2cycles 1;
set Tol 1.0e-4; # tolerance for convergence

# create load pattern for lateral pushover load
pattern Plain 1000 Linear {
    load 5001 1. 0. 0. 0. 0. 0.
}

# set up analysis parameters and generate peaks
source LibAnalysisStaticParameters.tcl; # constraintsHandler, DOFnumberer, system-ofequations,
convergenceTest, solutionAlgorithm, integrator
source LibGeneratePeaks.tcl

# RUN CYCLIC ANALYSIS -----
# first series of cycles, 3 equal and then increase
set fmt1 "%s Cyclic analysis: CtrlNode %.3i, dof %.1i, Disp=%.4f %s"; # format for screen/file
output of DONE/PROBLEM analysis
foreach Dmax $i1Dmax {
    set iDstep [GeneratePeaks $Dmax $Dincr $CycleType $Fact]; # this proc is defined above
    for {set i 1} {$i <= $N1cycles} {incr i 1} {
        set zeroD 0
        set D0 0.0
        foreach Dstep $iDstep {
            set D1 $Dstep
            set Dincr [expr $D1 - $D0]
            integrator DisplacementControl $IDctrlNode $IDctrlDOF $Dincr
            analysis Static
            # -----first analyze command-----
            set ok [analyze 1]
            # -----if convergence failure-----
            if {$ok != 0} {
                # if analysis fails, we try some other stuff
                # performance is slower inside this loop
                if {$ok != 0} {
                    puts "Trying Newton with Initial Tangent .."
                    test NormDispIncr $Tol 2000 0
                }
            }
        }
    }
}

```

```

        algorithm Newton -initial
        set ok [analyze 1]
        test $testTypeStatic $TolStatic $maxNumIterStatic 0
        algorithm $algorithmTypeStatic
    }
    if {$ok != 0} {
        puts "Trying Broyden .."
        algorithm Broyden 8
        set ok [analyze 1]
        algorithm $algorithmTypeStatic
    }
    if {$ok != 0} {
        puts "Trying NewtonWithLineSearch .."
        algorithm NewtonLineSearch 0.8
        set ok [analyze 1]
        algorithm $algorithmTypeStatic
    }
    if {$ok != 0} {
        set putout [format $fmt1 "PROBLEM" $IDctrlNode $IDctrlDOF [nodeDisp
        $IDctrlNode $IDctrlDOF] $LunitTXT]
        puts $putout
        return -1
    }
}; # end if
}; # end if
# -----
set D0 $D1; # move to next step
}; # end Dstep
}; # end i
}; # end of iDmaxCycl

# second series of cycles, 2 equal, 1 smaller, and then increase
set fmt1 "%s Cyclic analysis: CtrlNode %.3i, dof %.1i, Disp=%.4f %s"; # format for screen/file
output of DONE/PROBLEM analysis
foreach Dmax $i2Dmax {
    set iDstep [GeneratePeaks $Dmax $Dincr $CycleType $Fact]; # this proc is defined above
    for {set i 1} {$i <= $N2cycles} {incr i 1} {
        set zeroD 0
        set D0 0.0
        foreach Dstep $iDstep {
            set D1 $Dstep
            set Dincr [expr $D1 - $D0]
            integrator DisplacementControl $IDctrlNode $IDctrlDOF $Dincr
            analysis Static
            # -----first analyze command-----
            set ok [analyze 1]
            # -----if convergence failure-----
            if {$ok != 0} {
                # if analysis fails, we try some other stuff
                # performance is slower inside this loop
                if {$ok != 0} {
                    puts "Trying Newton with Initial Tangent .."
                    test NormDispIncr $Tol 2000 0
                    algorithm Newton -initial
                    set ok [analyze 1]
                    test $testTypeStatic $TolStatic $maxNumIterStatic 0
                    algorithm $algorithmTypeStatic
                }
                if {$ok != 0} {
                    puts "Trying Broyden .."
                    algorithm Broyden 8
                    set ok [analyze 1]
                    algorithm $algorithmTypeStatic
                }
                if {$ok != 0} {
                    puts "Trying NewtonWithLineSearch .."
                    algorithm NewtonLineSearch 0.8
                    set ok [analyze 1]
                    algorithm $algorithmTypeStatic
                }
                if {$ok != 0} {
                    set putout [format $fmt1 "PROBLEM" $IDctrlNode $IDctrlDOF [nodeDisp
                    $IDctrlNode $IDctrlDOF] $LunitTXT]
                    puts $putout
                    return -1
                }
            }; # end if
        }; # end if
        # -----
        set D0 $D1; # move to next step
    }; # end Dstep
}; # end i
}; # end of iDmaxCycl

# analysis conclusion

```

```
if { $ok != 0 } {  
  puts [format $fmt1 "PROBLEM" $IDctrlNode $IDctrlDOF [nodeDisp $IDctrlNode $IDctrlDOF]  
        $LunitTXT]  
} else {  
  puts [format $fmt1 "DONE" $IDctrlNode $IDctrlDOF [nodeDisp $IDctrlNode $IDctrlDOF] $LunitTXT]  
}
```

Unit 1B – LibAnalysisStaticParameters.tcl

```
# Static Analysis Parameters
# I am setting all these variables as global variables (using variable rather than set command)
# so that these variables can be uploaded by a procedure
# By Silvia Mazzoni & Frank McKenna, 2006

# CONSTRAINTS handler -----
# (http://opensees.berkeley.edu/OpenSees/manuals/usermanual/617.htm)
# Determines how the constraint equations are enforced in the analysis
# Plain Constraints -- Removes constrained degrees of freedom from the system of equations
# (only for homogeneous equations)
# Lagrange Multipliers -- Uses the method of Lagrange multipliers to enforce constraints
# Penalty Method -- Uses penalty numbers to enforce constraints, good for static analysis
# with non-homogeneous eqns (rigidDiaphragm)
# Transformation Method -- Performs a condensation of constrained degrees of freedom
variable constraintsTypeStatic Plain; # default;
if { [info exists RigidDiaphragm] == 1 } {
  if { $RigidDiaphragm == "ON" } {
    variable constraintsTypeStatic Lagrange; # for large model, try Transformation
  }; # if rigid diaphragm is on
}; # if rigid diaphragm exists
constraints $constraintsTypeStatic

# DOF NUMBERER -----
# (http://opensees.berkeley.edu/OpenSees/manuals/usermanual/366.htm)
# Numbers the degrees of freedom in the domain
# Determines the mapping between equation numbers and degrees-of-freedom
# Plain -- Uses the numbering provided by the user
# RCM -- Renumbers the DOF to minimize the matrix band-width using the Reverse Cuthill-McKee
algorithm
set numbererTypeStatic RCM
numberer $numbererTypeStatic

# SYSTEM -----
# (http://opensees.berkeley.edu/OpenSees/manuals/usermanual/371.htm)
# Linear Equation Solvers
# How to store and solve the system of equations in the analysis
# Provides the solution of the linear system of equations Ku = P
# Each solver is tailored to a specific matrix topology
# ProfileSPD -- Direct profile solver for symmetric positive definite matrices
# BandGeneral -- Direct solver for banded unsymmetric matrices
# BandSPD -- Direct solver for banded symmetric positive definite matrices
# SparseGeneral -- Direct solver for unsymmetric sparse matrices
# SparseSPD -- Direct solver for symmetric sparse matrices
# UmfPack -- Direct UmfPack solver for unsymmetric matrices
set systemTypeStatic BandGeneral; # try UmfPack for large model
system $systemTypeStatic

# TEST -----
# (http://opensees.berkeley.edu/OpenSees/manuals/usermanual/360.htm)
# Convergence test
# Accepts the current state of the domain as being on the converged solution path
# Determines if convergence has been achieved at the end of an iteration step
# NormUnbalance -- Specifies a tolerance on the norm of the unbalanced load at the current
iteration
# NormDispIncr -- Specifies a tolerance on the norm of the displacement increments at the
current iteration
# EnergyIncr -- Specifies a tolerance on the inner product of the unbalanced load and
displacement increments at the current iteration
# RelativeNormUnbalance --
# RelativeNormDispIncr --
# RelativeEnergyIncr --
variable TolStatic 1.e-8; # Convergence Test: tolerance
variable maxNumIterStatic 6; # Convergence Test: maximum number of iterations that will be
performed before "failure to converge" is returned
variable printFlagStatic 0; # Convergence Test: flag used to print information on convergence
(optional) # 1: print information on each step;
variable testTypeStatic EnergyIncr ; # Convergence-test type
test $testTypeStatic $TolStatic $maxNumIterStatic $printFlagStatic;
# for improved-convergence procedure:
variable maxNumIterConvergeStatic 2000;
variable printFlagConvergeStatic 0;

# Solution ALGORITHM -----
# (http://opensees.berkeley.edu/OpenSees/manuals/usermanual/682.htm)
# Iterates from the last time step to the current
```

```

# Linear -- Uses the solution at the first iteration and continues
# Newton -- Uses the tangent at the current iteration to iterate to convergence
# ModifiedNewton -- Uses the tangent at the first iteration to iterate to convergence
# NewtonLineSearch --
# KrylovNewton --
# BFGS --
# Broyden --
variable algorithmTypeStatic Newton
algorithm $algorithmTypeStatic;

# INTEGRATOR -----
# (http://opensees.berkeley.edu/OpenSees/manuals/usermanual/689.htm)
# Static integrator -- Determines the next time step for an analysis without considering inertial
effects:
# LoadControl -- Specifies the incremental load factor to be applied to the loads in the
domain
# DisplacementControl -- Specifies the incremental displacement at a specified DOF in the
domain
# Minimum Unbalanced Displacement Norm -- Specifies the incremental load factor such that the
residual displacement norm is minimized
# Arc Length -- Specifies the incremental arc-length of the load-displacement path
# Transient integrator -- Determines the next time step for an analysis including inertial
effects:
# Newmark -- The two parameter time-stepping method developed by Newmark
# HHT -- The three parameter Hilbert-Hughes-Taylor time-stepping method
# Central Difference -- Approximates velocity and acceleration by centered finite differences
of displacement
integrator DisplacementControl $IDctrlNode $IDctrlDOF $Dincr

# ANALYSIS -----
# (http://opensees.berkeley.edu/OpenSees/manuals/usermanual/324.htm)
# Defines what type of analysis is to be performed
# Static Analysis -- solves the KU=R problem, without the mass or damping matrices.
# Transient Analysis -- solves the time-dependent analysis. The time step in this type
of analysis is constant. The time step in the output is also constant.
# variableTransient Analysis -- performs the same analysis type as the Transient Analysis
object. The time step, however, is variable. This method is used when there are convergence
problems with the Transient Analysis object at a peak or when the time step is too small. The
time step in the output is also variable.
set analysisTypeStatic Static
analysis $analysisTypeStatic

```

Unit 1B – LibGeneratePeaks.tcl

```
# GeneratePeaks $Dmax $DincrStatic $CycleType $Fact
proc GeneratePeaks {Dmax {DincrStatic 0.01} {CycleType "Full"} {Fact 1} } {;

# Generate incremental displacements for Dmax
# This procedure creates a file which defines a vector then executes the file to return the
vector of displacement increments
# By Silvia Mazzoni, 2006

# input variables
# $Dmax : peak displacement (can be + or negative)
# $DincrStatic : displacement increment (optional, default=0.01, independently of units)
# $CycleType : Push (0->+peak), Half (0->+peak->0), Full (0->+peak->0->-peak->0) (optional,
def=Full)
# $Fact : scaling factor (optional, default=1)
# $iDstepFileName : file name where displacement history is stored temporarily, until next
disp. peak

# output variable
# $iDstep : vector of displacement increments

file mkdir data
set outFileID [open data/tmpDsteps.tcl w]
set Disp 0.
puts $outFileID "set iDstep { ";puts $outFileID $Disp;puts $outFileID $Disp; # open vector
definition and some 0
set Dmax [expr $Dmax*$Fact]; # scale value
if {$Dmax<0} {; # avoid the divide by zero
set dx [expr -$DincrStatic]
} else {
set dx $DincrStatic;
}

set NstepsPeak [expr int(abs($Dmax)/$DincrStatic)]
for {set i 1} {$i <= $NstepsPeak} {incr i 1} {; # zero to one
set Disp [expr $Disp + $dx]
puts $outFileID $Disp; # write to file
}
if {$CycleType !="Push"} {
for {set i 1} {$i <= $NstepsPeak} {incr i 1} {; # one to zero
set Disp [expr $Disp - $dx]
puts $outFileID $Disp; # write to file
}
if {$CycleType !="Half"} {
for {set i 1} {$i <= $NstepsPeak} {incr i 1} {; # zero to minus one
set Disp [expr $Disp - $dx]
puts $outFileID $Disp; # write to file
}
for {set i 1} {$i <= $NstepsPeak} {incr i 1} {; # minus one to zero
set Disp [expr $Disp + $dx]
puts $outFileID $Disp; # write to file
}
}
}
}
puts $outFileID " }"; # close vector definition
close $outFileID
source data/tmpDsteps.tcl; # source tcl file to define entire vector
return $iDstep
}
```


PEER REPORTS

PEER reports are available as a free PDF download from http://peer.berkeley.edu/publications/peer_reports_complete.html. Printed hard copies of PEER reports can be ordered directly from our printer by following the instructions at http://peer.berkeley.edu/publications/peer_reports.html. For other related questions about the PEER Report Series, contact the Pacific Earthquake Engineering Research Center, 325 Davis Hall, Mail Code 1792, Berkeley, CA 94720. Tel.: (510) 642-3437; Fax: (510) 642-1655; Email: clairejohnson@berkeley.edu

- PEER 2015/13** *Self-Centering Precast Concrete Dual-Steel-Shell Columns for Accelerated Bridge Construction: Seismic Performance, Analysis, and Design.* Gabriele Guerrini, José I. Restrepo, Athanassios Vervelidis, and Milena Massari. December 2015.
- PEER 2015/12** *Shear-Flexure Interaction Modeling for Reinforced Concrete Structural Walls and Columns under Reversed Cyclic Loading.* Kristijan Kolozvari, Kutay Orakcal, and John Wallace. December 2015.
- PEER 2015/11** *Selection and Scaling of Ground Motions for Nonlinear Response History Analysis of Buildings in Performance-Based Earthquake Engineering.* N. Simon Kwong and Anil K. Chopra. December 2015.
- PEER 2015/10** *Structural Behavior of Column-Bent Cap Beam-Box Girder Systems in Reinforced Concrete Bridges Subjected to Gravity and Seismic Loads. Part II: Hybrid Simulation and Post-Test Analysis.* Mohamed A. Moustafa and Khalid M. Mosalam. November 2015.
- PEER 2015/09** *Structural Behavior of Column-Bent Cap Beam-Box Girder Systems in Reinforced Concrete Bridges Subjected to Gravity and Seismic Loads. Part I: Pre-Test Analysis and Quasi-Static Experiments.* Mohamed A. Moustafa and Khalid M. Mosalam. September 2015.
- PEER 2015/08** *NGA-East: Adjustments to Median Ground-Motion Models for Center and Eastern North America.* August 2015.
- PEER 2015/07** *NGA-East: Ground-Motion Standard-Deviation Models for Central and Eastern North America.* Linda Al Atik. June 2015.
- PEER 2015/06** *Adjusting Ground-Motion Intensity Measures to a Reference Site for which $V_{S30} = 3000$ m/sec.* David M. Boore. May 2015.
- PEER 2015/05** *Hybrid Simulation of Seismic Isolation Systems Applied to an APR-1400 Nuclear Power Plant.* Andreas H. Schellenberg, Alireza Sarebanha, Matthew J. Schoettler, Gilberto Mosqueda, Gianmario Benzoni, and Stephen A. Mahin. April 2015.
- PEER 2015/04** *NGA-East: Median Ground-Motion Models for the Central and Eastern North America Region.* April 2015.
- PEER 2015/03** *Single Series Solution for the Rectangular Fiber-Reinforced Elastomeric Isolator Compression Modulus.* James M. Kelly and Niel C. Van Engelen. March 2015.
- PEER 2015/02** *A Full-Scale, Single-Column Bridge Bent Tested by Shake-Table Excitation.* Matthew J. Schoettler, José I. Restrepo, Gabriele Guerrini, David E. Duck, and Francesco Carrea. March 2015.
- PEER 2015/01** *Concrete Column Blind Prediction Contest 2010: Outcomes and Observations.* Vesna Terzic, Matthew J. Schoettler, José I. Restrepo, and Stephen A Mahin. March 2015.
- PEER 2014/20** *Stochastic Modeling and Simulation of Near-Fault Ground Motions for Performance-Based Earthquake Engineering.* Mayssa Dabaghi and Armen Der Kiureghian. December 2014.
- PEER 2014/19** *Seismic Response of a Hybrid Fiber-Reinforced Concrete Bridge Column Detailed for Accelerated Bridge Construction.* Wilson Nguyen, William Trono, Marios Panagiotou, and Claudia P. Ostertag. December 2014.
- PEER 2014/18** *Three-Dimensional Beam-Truss Model for Reinforced Concrete Walls and Slabs Subjected to Cyclic Static or Dynamic Loading.* Yuan Lu, Marios Panagiotou, and Ioannis Koutromanos. December 2014.
- PEER 2014/17** *PEER NGA-East Database.* Christine A. Goulet, Tadahiro Kishida, Timothy D. Ancheta, Chris H. Cramer, Robert B. Darragh, Walter J. Silva, Youssef M.A. Hashash, Joseph Harmon, Jonathan P. Stewart, Katie E. Wooddell, and Robert R. Youngs. October 2014.
- PEER 2014/16** *Guidelines for Performing Hazard-Consistent One-Dimensional Ground Response Analysis for Ground Motion Prediction.* Jonathan P. Stewart, Kioumars Afshari, and Youssef M.A. Hashash. October 2014.
- PEER 2014/15** *NGA-East Regionalization Report: Comparison of Four Crustal Regions within Central and Eastern North America using Waveform Modeling and 5%-Damped Pseudo-Spectral Acceleration Response.* Jennifer Dreiling, Marius P. Isken, Walter D. Mooney, Martin C. Chapman, and Richard W. Godbee. October 2014.
- PEER 2014/14** *Scaling Relations between Seismic Moment and Rupture Area of Earthquakes in Stable Continental Regions.* Paul Somerville. August 2014.

- PEER 2014/13** *PEER Preliminary Notes and Observations on the August 24, 2014, South Napa Earthquake.* Grace S. Kang and Stephen A. Mahin, Editors. September 2014.
- PEER 2014/12** *Reference-Rock Site Conditions for Central and Eastern North America: Part II – Attenuation (Kappa) Definition.* Kenneth W. Campbell, Youssef M.A. Hashash, Byungmin Kim, Albert R. Kottke, Ellen M. Rathje, Walter J. Silva, and Jonathan P. Stewart. August 2014.
- PEER 2014/11** *Reference-Rock Site Conditions for Central and Eastern North America: Part I - Velocity Definition.* Youssef M.A. Hashash, Albert R. Kottke, Jonathan P. Stewart, Kenneth W. Campbell, Byungmin Kim, Ellen M. Rathje, Walter J. Silva, Sissy Nikolaou, and Cheryl Moss. August 2014.
- PEER 2014/10** *Evaluation of Collapse and Non-Collapse of Parallel Bridges Affected by Liquefaction and Lateral Spreading.* Benjamin Turner, Scott J. Brandenberg, and Jonathan P. Stewart. August 2014.
- PEER 2014/09** *PEER Arizona Strong-Motion Database and GMPEs Evaluation.* Tadahiro Kishida, Robert E. Kayen, Olga-Joan Ktenidou, Walter J. Silva, Robert B. Darragh, and Jennie Watson-Lamprey. June 2014.
- PEER 2014/08** *Unbonded Pretensioned Bridge Columns with Rocking Detail.* Jeffrey A. Schaefer, Bryan Kennedy, Marc O. Eberhard, and John F. Stanton. June 2014.
- PEER 2014/07** *Northridge 20 Symposium Summary Report: Impacts, Outcomes, and Next Steps.* May 2014.
- PEER 2014/06** *Report of the Tenth Planning Meeting of NEES/E-Defense Collaborative Research on Earthquake Engineering.* December 2013.
- PEER 2014/05** *Seismic Velocity Site Characterization of Thirty-One Chilean Seismometer Stations by Spectral Analysis of Surface Wave Dispersion.* Robert Kayen, Brad D. Carkin, Skye Corbet, Camilo Pinilla, Allan Ng, Edward Gorbis, and Christine Truong. April 2014.
- PEER 2014/04** *Effect of Vertical Acceleration on Shear Strength of Reinforced Concrete Columns.* Hyerin Lee and Khalid M. Mosalam. April 2014.
- PEER 2014/03** *Retest of Thirty-Year-Old Neoprene Isolation Bearings.* James M. Kelly and Niel C. Van Engelen. March 2014.
- PEER 2014/02** *Theoretical Development of Hybrid Simulation Applied to Plate Structures.* Ahmed A. Bakhaty, Khalid M. Mosalam, and Sanjay Govindjee. January 2014.
- PEER 2014/01** *Performance-Based Seismic Assessment of Skewed Bridges.* Peyman Kaviani, Farzin Zareian, and Ertugrul Taciroglu. January 2014.
- PEER 2013/26** *Urban Earthquake Engineering.* Proceedings of the U.S.-Iran Seismic Workshop. December 2013.
- PEER 2013/25** *Earthquake Engineering for Resilient Communities: 2013 PEER Internship Program Research Report Collection.* Heidi Tremayne (Editor), Stephen A. Mahin (Editor), Jorge Archbold Monterossa, Matt Brosman, Shelly Dean, Katherine deLaveaga, Curtis Fong, Donovan Holder, Rakeeb Khan, Elizabeth Jachens, David Lam, Daniela Martinez Lopez, Mara Minner, Geffen Oren, Julia Pavicic, Melissa Quinonez, Lorena Rodriguez, Sean Salazar, Kelli Slaven, Vivian Steyert, Jenny Taing, and Salvador Tena. December 2013.
- PEER 2013/24** *NGA-West2 Ground Motion Prediction Equations for Vertical Ground Motions.* September 2013.
- PEER 2013/23** *Coordinated Planning and Preparedness for Fire Following Major Earthquakes.* Charles Scawthorn. November 2013.
- PEER 2013/22** *GEM-PEER Task 3 Project: Selection of a Global Set of Ground Motion Prediction Equations.* Jonathan P. Stewart, John Douglas, Mohammad B. Javanbarg, Carola Di Alessandro, Yousef Bozorgnia, Norman A. Abrahamson, David M. Boore, Kenneth W. Campbell, Elise Delavaud, Mustafa Erdik, and Peter J. Stafford. December 2013.
- PEER 2013/21** *Seismic Design and Performance of Bridges with Columns on Rocking Foundations.* Grigorios Antonellis and Marios Panagiotou. September 2013.
- PEER 2013/20** *Experimental and Analytical Studies on the Seismic Behavior of Conventional and Hybrid Braced Frames.* Jiun-Wei Lai and Stephen A. Mahin. September 2013.
- PEER 2013/19** *Toward Resilient Communities: A Performance-Based Engineering Framework for Design and Evaluation of the Built Environment.* Michael William Mieler, Bozidar Stojadinovic, Robert J. Budnitz, Stephen A. Mahin, and Mary C. Comerio. September 2013.
- PEER 2013/18** *Identification of Site Parameters that Improve Predictions of Site Amplification.* Ellen M. Rathje and Sara Navidi. July 2013.
- PEER 2013/17** *Response Spectrum Analysis of Concrete Gravity Dams Including Dam-Water-Foundation Interaction.* Arnkjell Løkke and Anil K. Chopra. July 2013.

- PEER 2013/16** *Effect of Hoop Reinforcement Spacing on the Cyclic Response of Large Reinforced Concrete Special Moment Frame Beams.* Marios Panagiotou, Tea Visnjic, Grigorios Antonellis, Panagiotis Galanis, and Jack P. Moehle. June 2013.
- PEER 2013/15** *A Probabilistic Framework to Include the Effects of Near-Fault Directivity in Seismic Hazard Assessment.* Shrey Kumar Shahi, Jack W. Baker. October 2013.
- PEER 2013/14** *Hanging-Wall Scaling using Finite-Fault Simulations.* Jennifer L. Donahue and Norman A. Abrahamson. September 2013.
- PEER 2013/13** *Semi-Empirical Nonlinear Site Amplification and its Application in NEHRP Site Factors.* Jonathan P. Stewart and Emel Seyhan. November 2013.
- PEER 2013/12** *Nonlinear Horizontal Site Response for the NGA-West2 Project.* Ronnie Kamai, Norman A. Abramson, Walter J. Silva. May 2013.
- PEER 2013/11** *Epistemic Uncertainty for NGA-West2 Models.* Linda Al Atik and Robert R. Youngs. May 2013.
- PEER 2013/10** *NGA-West 2 Models for Ground-Motion Directionality.* Shrey K. Shahi and Jack W. Baker. May 2013.
- PEER 2013/09** *Final Report of the NGA-West2 Directivity Working Group.* Paul Spudich, Jeffrey R. Bayless, Jack W. Baker, Brian S.J. Chiou, Badie Rowshandel, Shrey Shahi, and Paul Somerville. May 2013.
- PEER 2013/08** *NGA-West2 Model for Estimating Average Horizontal Values of Pseudo-Absolute Spectral Accelerations Generated by Crustal Earthquakes.* I. M. Idriss. May 2013.
- PEER 2013/07** *Update of the Chiou and Youngs NGA Ground Motion Model for Average Horizontal Component of Peak Ground Motion and Response Spectra.* Brian Chiou and Robert Youngs. May 2013.
- PEER 2013/06** *NGA-West2 Campbell-Bozorgnia Ground Motion Model for the Horizontal Components of PGA, PGV, and 5%-Damped Elastic Pseudo-Acceleration Response Spectra for Periods Ranging from 0.01 to 10 sec.* Kenneth W. Campbell and Yousef Bozorgnia. May 2013.
- PEER 2013/05** *NGA-West 2 Equations for Predicting Response Spectral Accelerations for Shallow Crustal Earthquakes.* David M. Boore, Jonathan P. Stewart, Emel Seyhan, and Gail M. Atkinson. May 2013.
- PEER 2013/04** *Update of the AS08 Ground-Motion Prediction Equations Based on the NGA-West2 Data Set.* Norman Abrahamson, Walter Silva, and Ronnie Kamai. May 2013.
- PEER 2013/03** *PEER NGA-West2 Database.* Timothy D. Ancheta, Robert B. Darragh, Jonathan P. Stewart, Emel Seyhan, Walter J. Silva, Brian S.J. Chiou, Katie E. Wooddell, Robert W. Graves, Albert R. Kottke, David M. Boore, Tadahiro Kishida, and Jennifer L. Donahue. May 2013.
- PEER 2013/02** *Hybrid Simulation of the Seismic Response of Squat Reinforced Concrete Shear Walls.* Catherine A. Whyte and Bozidar Stojadinovic. May 2013.
- PEER 2013/01** *Housing Recovery in Chile: A Qualitative Mid-program Review.* Mary C. Comerio. February 2013.
- PEER 2012/08** *Guidelines for Estimation of Shear Wave Velocity.* Bernard R. Wair, Jason T. DeJong, and Thomas Shantz. December 2012.
- PEER 2012/07** *Earthquake Engineering for Resilient Communities: 2012 PEER Internship Program Research Report Collection.* Heidi Tremayne (Editor), Stephen A. Mahin (Editor), Collin Anderson, Dustin Cook, Michael Erceg, Carlos Esparza, Jose Jimenez, Dorian Krausz, Andrew Lo, Stephanie Lopez, Nicole McCurdy, Paul Shipman, Alexander Strum, Eduardo Vega. December 2012.
- PEER 2012/06** *Fragilities for Precarious Rocks at Yucca Mountain.* Matthew D. Purvance, Rasool Anooshehpour, and James N. Brune. December 2012.
- PEER 2012/05** *Development of Simplified Analysis Procedure for Piles in Laterally Spreading Layered Soils.* Christopher R. McGann, Pedro Arduino, and Peter Mackenzie-Helnwein. December 2012.
- PEER 2012/04** *Unbonded Pre-Tensioned Columns for Bridges in Seismic Regions.* Phillip M. Davis, Todd M. Janes, Marc O. Eberhard, and John F. Stanton. December 2012.
- PEER 2012/03** *Experimental and Analytical Studies on Reinforced Concrete Buildings with Seismically Vulnerable Beam-Column Joints.* Sangjoon Park and Khalid M. Mosalam. October 2012.
- PEER 2012/02** *Seismic Performance of Reinforced Concrete Bridges Allowed to Uplift during Multi-Directional Excitation.* Andres Oscar Espinoza and Stephen A. Mahin. July 2012.
- PEER 2012/01** *Spectral Damping Scaling Factors for Shallow Crustal Earthquakes in Active Tectonic Regions.* Sanaz Rezaeian, Yousef Bozorgnia, I. M. Idriss, Kenneth Campbell, Norman Abrahamson, and Walter Silva. July 2012.
- PEER 2011/10** *Earthquake Engineering for Resilient Communities: 2011 PEER Internship Program Research Report Collection.* Heidi Faison and Stephen A. Mahin, Editors. December 2011.

- PEER 2011/09** *Calibration of Semi-Stochastic Procedure for Simulating High-Frequency Ground Motions.* Jonathan P. Stewart, Emel Seyhan, and Robert W. Graves. December 2011.
- PEER 2011/08** *Water Supply in regard to Fire Following Earthquake.* Charles Scawthorn. November 2011.
- PEER 2011/07** *Seismic Risk Management in Urban Areas.* Proceedings of a U.S.-Iran-Turkey Seismic Workshop. September 2011.
- PEER 2011/06** *The Use of Base Isolation Systems to Achieve Complex Seismic Performance Objectives.* Troy A. Morgan and Stephen A. Mahin. July 2011.
- PEER 2011/05** *Case Studies of the Seismic Performance of Tall Buildings Designed by Alternative Means.* Task 12 Report for the Tall Buildings Initiative. Jack Moehle, Yousef Bozorgnia, Nirmal Jayaram, Pierson Jones, Mohsen Rahnama, Nilesh Shome, Zeynep Tuna, John Wallace, Tony Yang, and Farzin Zareian. July 2011.
- PEER 2011/04** *Recommended Design Practice for Pile Foundations in Laterally Spreading Ground.* Scott A. Ashford, Ross W. Boulanger, and Scott J. Brandenburg. June 2011.
- PEER 2011/03** *New Ground Motion Selection Procedures and Selected Motions for the PEER Transportation Research Program.* Jack W. Baker, Ting Lin, Shrey K. Shahi, and Nirmal Jayaram. March 2011.
- PEER 2011/02** *A Bayesian Network Methodology for Infrastructure Seismic Risk Assessment and Decision Support.* Michelle T. Bensi, Armen Der Kiureghian, and Daniel Straub. March 2011.
- PEER 2011/01** *Demand Fragility Surfaces for Bridges in Liquefied and Laterally Spreading Ground.* Scott J. Brandenburg, Jian Zhang, Pirooz Kashighandi, Yili Huo, and Minxing Zhao. March 2011.
- PEER 2010/05** *Guidelines for Performance-Based Seismic Design of Tall Buildings.* Developed by the Tall Buildings Initiative. November 2010.
- PEER 2010/04** *Application Guide for the Design of Flexible and Rigid Bus Connections between Substation Equipment Subjected to Earthquakes.* Jean-Bernard Dastous and Armen Der Kiureghian. September 2010.
- PEER 2010/03** *Shear Wave Velocity as a Statistical Function of Standard Penetration Test Resistance and Vertical Effective Stress at Caltrans Bridge Sites.* Scott J. Brandenburg, Naresh Bellana, and Thomas Shantz. June 2010.
- PEER 2010/02** *Stochastic Modeling and Simulation of Ground Motions for Performance-Based Earthquake Engineering.* Sanaz Rezaeian and Armen Der Kiureghian. June 2010.
- PEER 2010/01** *Structural Response and Cost Characterization of Bridge Construction Using Seismic Performance Enhancement Strategies.* Ady Aviram, Božidar Stojadinović, Gustavo J. Parra-Montesinos, and Kevin R. Mackie. March 2010.
- PEER 2009/03** *The Integration of Experimental and Simulation Data in the Study of Reinforced Concrete Bridge Systems Including Soil-Foundation-Structure Interaction.* Matthew Dryden and Gregory L. Fenves. November 2009.
- PEER 2009/02** *Improving Earthquake Mitigation through Innovations and Applications in Seismic Science, Engineering, Communication, and Response.* Proceedings of a U.S.-Iran Seismic Workshop. October 2009.
- PEER 2009/01** *Evaluation of Ground Motion Selection and Modification Methods: Predicting Median Interstory Drift Response of Buildings.* Curt B. Haselton, Editor. June 2009.
- PEER 2008/10** *Technical Manual for Strata.* Albert R. Kottke and Ellen M. Rathje. February 2009.
- PEER 2008/09** *NGA Model for Average Horizontal Component of Peak Ground Motion and Response Spectra.* Brian S.-J. Chiou and Robert R. Youngs. November 2008.
- PEER 2008/08** *Toward Earthquake-Resistant Design of Concentrically Braced Steel Structures.* Patxi Uriz and Stephen A. Mahin. November 2008.
- PEER 2008/07** *Using OpenSees for Performance-Based Evaluation of Bridges on Liquefiable Soils.* Stephen L. Kramer, Pedro Arduino, and HyungSuk Shin. November 2008.
- PEER 2008/06** *Shaking Table Tests and Numerical Investigation of Self-Centering Reinforced Concrete Bridge Columns.* Hyung IL Jeong, Junichi Sakai, and Stephen A. Mahin. September 2008.
- PEER 2008/05** *Performance-Based Earthquake Engineering Design Evaluation Procedure for Bridge Foundations Undergoing Liquefaction-Induced Lateral Ground Displacement.* Christian A. Ledezma and Jonathan D. Bray. August 2008.
- PEER 2008/04** *Benchmarking of Nonlinear Geotechnical Ground Response Analysis Procedures.* Jonathan P. Stewart, Annie On-Lei Kwok, Youssef M. A. Hashash, Neven Matasovic, Robert Pyke, Zhiliang Wang, and Zhaohui Yang. August 2008.
- PEER 2008/03** *Guidelines for Nonlinear Analysis of Bridge Structures in California.* Ady Aviram, Kevin R. Mackie, and Božidar Stojadinović. August 2008.

- PEER 2008/02** *Treatment of Uncertainties in Seismic-Risk Analysis of Transportation Systems.* Evangelos Stergiou and Anne S. Kiremidjian. July 2008.
- PEER 2008/01** *Seismic Performance Objectives for Tall Buildings.* William T. Holmes, Charles Kircher, William Petak, and Nabih Youssef. August 2008.
- PEER 2007/12** *An Assessment to Benchmark the Seismic Performance of a Code-Conforming Reinforced Concrete Moment-Frame Building.* Curt Haselton, Christine A. Goulet, Judith Mitrani-Reiser, James L. Beck, Gregory G. Deierlein, Keith A. Porter, Jonathan P. Stewart, and Ertugrul Taciroglu. August 2008.
- PEER 2007/11** *Bar Buckling in Reinforced Concrete Bridge Columns.* Wayne A. Brown, Dawn E. Lehman, and John F. Stanton. February 2008.
- PEER 2007/10** *Computational Modeling of Progressive Collapse in Reinforced Concrete Frame Structures.* Mohamed M. Talaat and Khalid M. Mosalam. May 2008.
- PEER 2007/09** *Integrated Probabilistic Performance-Based Evaluation of Benchmark Reinforced Concrete Bridges.* Kevin R. Mackie, John-Michael Wong, and Božidar Stojadinović. January 2008.
- PEER 2007/08** *Assessing Seismic Collapse Safety of Modern Reinforced Concrete Moment-Frame Buildings.* Curt B. Haselton and Gregory G. Deierlein. February 2008.
- PEER 2007/07** *Performance Modeling Strategies for Modern Reinforced Concrete Bridge Columns.* Michael P. Berry and Marc O. Eberhard. April 2008.
- PEER 2007/06** *Development of Improved Procedures for Seismic Design of Buried and Partially Buried Structures.* Linda Al Atik and Nicholas Sitar. June 2007.
- PEER 2007/05** *Uncertainty and Correlation in Seismic Risk Assessment of Transportation Systems.* Renee G. Lee and Anne S. Kiremidjian. July 2007.
- PEER 2007/04** *Numerical Models for Analysis and Performance-Based Design of Shallow Foundations Subjected to Seismic Loading.* Sivapalan Gajan, Tara C. Hutchinson, Bruce L. Kutter, Prishati Raychowdhury, José A. Ugalde, and Jonathan P. Stewart. May 2008.
- PEER 2007/03** *Beam-Column Element Model Calibrated for Predicting Flexural Response Leading to Global Collapse of RC Frame Buildings.* Curt B. Haselton, Abbie B. Liel, Sarah Taylor Lange, and Gregory G. Deierlein. May 2008.
- PEER 2007/02** *Campbell-Bozorgnia NGA Ground Motion Relations for the Geometric Mean Horizontal Component of Peak and Spectral Ground Motion Parameters.* Kenneth W. Campbell and Yousef Bozorgnia. May 2007.
- PEER 2007/01** *Boore-Atkinson NGA Ground Motion Relations for the Geometric Mean Horizontal Component of Peak and Spectral Ground Motion Parameters.* David M. Boore and Gail M. Atkinson. May 2007.
- PEER 2006/12** *Societal Implications of Performance-Based Earthquake Engineering.* Peter J. May. May 2007.
- PEER 2006/11** *Probabilistic Seismic Demand Analysis Using Advanced Ground Motion Intensity Measures, Attenuation Relationships, and Near-Fault Effects.* Polsak Tothong and C. Allin Cornell. March 2007.
- PEER 2006/10** *Application of the PEER PBEE Methodology to the I-880 Viaduct.* Sashi Kunnath. February 2007.
- PEER 2006/09** *Quantifying Economic Losses from Travel Forgone Following a Large Metropolitan Earthquake.* James Moore, Sungbin Cho, Yue Yue Fan, and Stuart Werner. November 2006.
- PEER 2006/08** *Vector-Valued Ground Motion Intensity Measures for Probabilistic Seismic Demand Analysis.* Jack W. Baker and C. Allin Cornell. October 2006.
- PEER 2006/07** *Analytical Modeling of Reinforced Concrete Walls for Predicting Flexural and Coupled-Shear-Flexural Responses.* Kutay Orakcal, Leonardo M. Massone, and John W. Wallace. October 2006.
- PEER 2006/06** *Nonlinear Analysis of a Soil-Drilled Pier System under Static and Dynamic Axial Loading.* Gang Wang and Nicholas Sitar. November 2006.
- PEER 2006/05** *Advanced Seismic Assessment Guidelines.* Paolo Bazzurro, C. Allin Cornell, Charles Menun, Maziar Motahari, and Nicolas Luco. September 2006.
- PEER 2006/04** *Probabilistic Seismic Evaluation of Reinforced Concrete Structural Components and Systems.* Tae Hyung Lee and Khalid M. Mosalam. August 2006.
- PEER 2006/03** *Performance of Lifelines Subjected to Lateral Spreading.* Scott A. Ashford and Teerawat Juirnarongrit. July 2006.
- PEER 2006/02** *Pacific Earthquake Engineering Research Center Highway Demonstration Project.* Anne Kiremidjian, James Moore, Yue Yue Fan, Nesrin Basoz, Ozgur Yazali, and Meredith Williams. April 2006.
- PEER 2006/01** *Bracing Berkeley. A Guide to Seismic Safety on the UC Berkeley Campus.* Mary C. Comerio, Stephen Tobriner, and Ariane Fehrenkamp. January 2006.

- PEER 2005/16** *Seismic Response and Reliability of Electrical Substation Equipment and Systems.* Junho Song, Armen Der Kiureghian, and Jerome L. Sackman. April 2006.
- PEER 2005/15** *CPT-Based Probabilistic Assessment of Seismic Soil Liquefaction Initiation.* R. E. S. Moss, R. B. Seed, R. E. Kayen, J. P. Stewart, and A. Der Kiureghian. April 2006.
- PEER 2005/14** *Workshop on Modeling of Nonlinear Cyclic Load-Deformation Behavior of Shallow Foundations.* Bruce L. Kutter, Geoffrey Martin, Tara Hutchinson, Chad Harden, Sivapalan Gajan, and Justin Phalen. March 2006.
- PEER 2005/13** *Stochastic Characterization and Decision Bases under Time-Dependent Aftershock Risk in Performance-Based Earthquake Engineering.* Gee Liek Yeo and C. Allin Cornell. July 2005.
- PEER 2005/12** *PEER Testbed Study on a Laboratory Building: Exercising Seismic Performance Assessment.* Mary C. Comerio, Editor. November 2005.
- PEER 2005/11** *Van Nuys Hotel Building Testbed Report: Exercising Seismic Performance Assessment.* Helmut Krawinkler, Editor. October 2005.
- PEER 2005/10** *First NEES/E-Defense Workshop on Collapse Simulation of Reinforced Concrete Building Structures.* September 2005.
- PEER 2005/09** *Test Applications of Advanced Seismic Assessment Guidelines.* Joe Maffei, Karl Telleen, Danya Mohr, William Holmes, and Yuki Nakayama. August 2006.
- PEER 2005/08** *Damage Accumulation in Lightly Confined Reinforced Concrete Bridge Columns.* R. Tyler Ranf, Jared M. Nelson, Zach Price, Marc O. Eberhard, and John F. Stanton. April 2006.
- PEER 2005/07** *Experimental and Analytical Studies on the Seismic Response of Freestanding and Anchored Laboratory Equipment.* Dimitrios Konstantinidis and Nicos Makris. January 2005.
- PEER 2005/06** *Global Collapse of Frame Structures under Seismic Excitations.* Luis F. Ibarra and Helmut Krawinkler. September 2005.
- PEER 2005/05** *Performance Characterization of Bench- and Shelf-Mounted Equipment.* Samit Ray Chaudhuri and Tara C. Hutchinson. May 2006.
- PEER 2005/04** *Numerical Modeling of the Nonlinear Cyclic Response of Shallow Foundations.* Chad Harden, Tara Hutchinson, Geoffrey R. Martin, and Bruce L. Kutter. August 2005.
- PEER 2005/03** *A Taxonomy of Building Components for Performance-Based Earthquake Engineering.* Keith A. Porter. September 2005.
- PEER 2005/02** *Fragility Basis for California Highway Overpass Bridge Seismic Decision Making.* Kevin R. Mackie and Božidar Stojadinović. June 2005.
- PEER 2005/01** *Empirical Characterization of Site Conditions on Strong Ground Motion.* Jonathan P. Stewart, Yoojoong Choi, and Robert W. Graves. June 2005.
- PEER 2004/09** *Electrical Substation Equipment Interaction: Experimental Rigid Conductor Studies.* Christopher Stearns and André Filiatrault. February 2005.
- PEER 2004/08** *Seismic Qualification and Fragility Testing of Line Break 550-kV Disconnect Switches.* Shakhzod M. Takhirov, Gregory L. Fenves, and Eric Fujisaki. January 2005.
- PEER 2004/07** *Ground Motions for Earthquake Simulator Qualification of Electrical Substation Equipment.* Shakhzod M. Takhirov, Gregory L. Fenves, Eric Fujisaki, and Don Clyde. January 2005.
- PEER 2004/06** *Performance-Based Regulation and Regulatory Regimes.* Peter J. May and Chris Koski. September 2004.
- PEER 2004/05** *Performance-Based Seismic Design Concepts and Implementation: Proceedings of an International Workshop.* Peter Fajfar and Helmut Krawinkler, Editors. September 2004.
- PEER 2004/04** *Seismic Performance of an Instrumented Tilt-up Wall Building.* James C. Anderson and Vitelmo V. Bertero. July 2004.
- PEER 2004/03** *Evaluation and Application of Concrete Tilt-up Assessment Methodologies.* Timothy Graf and James O. Malley. October 2004.
- PEER 2004/02** *Analytical Investigations of New Methods for Reducing Residual Displacements of Reinforced Concrete Bridge Columns.* Junichi Sakai and Stephen A. Mahin. August 2004.
- PEER 2004/01** *Seismic Performance of Masonry Buildings and Design Implications.* Kerri Anne Taeko Tokoro, James C. Anderson, and Vitelmo V. Bertero. February 2004.
- PEER 2003/18** *Performance Models for Flexural Damage in Reinforced Concrete Columns.* Michael Berry and Marc Eberhard. August 2003.

- PEER 2003/17** *Predicting Earthquake Damage in Older Reinforced Concrete Beam-Column Joints.* Catherine Pagni and Laura Lowes. October 2004.
- PEER 2003/16** *Seismic Demands for Performance-Based Design of Bridges.* Kevin Mackie and Božidar Stojadinović. August 2003.
- PEER 2003/15** *Seismic Demands for Nondeteriorating Frame Structures and Their Dependence on Ground Motions.* Ricardo Antonio Medina and Helmut Krawinkler. May 2004.
- PEER 2003/14** *Finite Element Reliability and Sensitivity Methods for Performance-Based Earthquake Engineering.* Terje Haukaas and Armen Der Kiureghian. April 2004.
- PEER 2003/13** *Effects of Connection Hysteretic Degradation on the Seismic Behavior of Steel Moment-Resisting Frames.* Janise E. Rodgers and Stephen A. Mahin. March 2004.
- PEER 2003/12** *Implementation Manual for the Seismic Protection of Laboratory Contents: Format and Case Studies.* William T. Holmes and Mary C. Comerio. October 2003.
- PEER 2003/11** *Fifth U.S.-Japan Workshop on Performance-Based Earthquake Engineering Methodology for Reinforced Concrete Building Structures.* February 2004.
- PEER 2003/10** *A Beam-Column Joint Model for Simulating the Earthquake Response of Reinforced Concrete Frames.* Laura N. Lowes, Nilanjan Mitra, and Arash Altoontash. February 2004.
- PEER 2003/09** *Sequencing Repairs after an Earthquake: An Economic Approach.* Marco Casari and Simon J. Wilkie. April 2004.
- PEER 2003/08** *A Technical Framework for Probability-Based Demand and Capacity Factor Design (DCFD) Seismic Formats.* Fatemeh Jalayer and C. Allin Cornell. November 2003.
- PEER 2003/07** *Uncertainty Specification and Propagation for Loss Estimation Using FOSM Methods.* Jack W. Baker and C. Allin Cornell. September 2003.
- PEER 2003/06** *Performance of Circular Reinforced Concrete Bridge Columns under Bidirectional Earthquake Loading.* Mahmoud M. Hachem, Stephen A. Mahin, and Jack P. Moehle. February 2003.
- PEER 2003/05** *Response Assessment for Building-Specific Loss Estimation.* Eduardo Miranda and Shahram Taghavi. September 2003.
- PEER 2003/04** *Experimental Assessment of Columns with Short Lap Splices Subjected to Cyclic Loads.* Murat Melek, John W. Wallace, and Joel Conte. April 2003.
- PEER 2003/03** *Probabilistic Response Assessment for Building-Specific Loss Estimation.* Eduardo Miranda and Hesameddin Aslani. September 2003.
- PEER 2003/02** *Software Framework for Collaborative Development of Nonlinear Dynamic Analysis Program.* Jun Peng and Kincho H. Law. September 2003.
- PEER 2003/01** *Shake Table Tests and Analytical Studies on the Gravity Load Collapse of Reinforced Concrete Frames.* Kenneth John Elwood and Jack P. Moehle. November 2003.
- PEER 2002/24** *Performance of Beam to Column Bridge Joints Subjected to a Large Velocity Pulse.* Natalie Gibson, André Filiatrault, and Scott A. Ashford. April 2002.
- PEER 2002/23** *Effects of Large Velocity Pulses on Reinforced Concrete Bridge Columns.* Greg L. Orozco and Scott A. Ashford. April 2002.
- PEER 2002/22** *Characterization of Large Velocity Pulses for Laboratory Testing.* Kenneth E. Cox and Scott A. Ashford. April 2002.
- PEER 2002/21** *Fourth U.S.-Japan Workshop on Performance-Based Earthquake Engineering Methodology for Reinforced Concrete Building Structures.* December 2002.
- PEER 2002/20** *Barriers to Adoption and Implementation of PBEE Innovations.* Peter J. May. August 2002.
- PEER 2002/19** *Economic-Engineered Integrated Models for Earthquakes: Socioeconomic Impacts.* Peter Gordon, James E. Moore II, and Harry W. Richardson. July 2002.
- PEER 2002/18** *Assessment of Reinforced Concrete Building Exterior Joints with Substandard Details.* Chris P. Pantelides, Jon Hansen, Justin Nadauld, and Lawrence D. Reaveley. May 2002.
- PEER 2002/17** *Structural Characterization and Seismic Response Analysis of a Highway Overcrossing Equipped with Elastomeric Bearings and Fluid Dampers: A Case Study.* Nicos Makris and Jian Zhang. November 2002.
- PEER 2002/16** *Estimation of Uncertainty in Geotechnical Properties for Performance-Based Earthquake Engineering.* Allen L. Jones, Steven L. Kramer, and Pedro Arduino. December 2002.

- PEER 2002/15** *Seismic Behavior of Bridge Columns Subjected to Various Loading Patterns.* Asadollah Esmaeily-Gh. and Yan Xiao. December 2002.
- PEER 2002/14** *Inelastic Seismic Response of Extended Pile Shaft Supported Bridge Structures.* T.C. Hutchinson, R.W. Boulanger, Y.H. Chai, and I.M. Idriss. December 2002.
- PEER 2002/13** *Probabilistic Models and Fragility Estimates for Bridge Components and Systems.* Paolo Gardoni, Armen Der Kiureghian, and Khalid M. Mosalam. June 2002.
- PEER 2002/12** *Effects of Fault Dip and Slip Rake on Near-Source Ground Motions: Why Chi-Chi Was a Relatively Mild M7.6 Earthquake.* Brad T. Aagaard, John F. Hall, and Thomas H. Heaton. December 2002.
- PEER 2002/11** *Analytical and Experimental Study of Fiber-Reinforced Strip Isolators.* James M. Kelly and Shakhzod M. Takhirov. September 2002.
- PEER 2002/10** *Centrifuge Modeling of Settlement and Lateral Spreading with Comparisons to Numerical Analyses.* Sivapalan Gajan and Bruce L. Kutter. January 2003.
- PEER 2002/09** *Documentation and Analysis of Field Case Histories of Seismic Compression during the 1994 Northridge, California, Earthquake.* Jonathan P. Stewart, Patrick M. Smith, Daniel H. Whang, and Jonathan D. Bray. October 2002.
- PEER 2002/08** *Component Testing, Stability Analysis and Characterization of Buckling-Restrained Unbonded Braces™.* Cameron Black, Nicos Makris, and Ian Aiken. September 2002.
- PEER 2002/07** *Seismic Performance of Pile-Wharf Connections.* Charles W. Roeder, Robert Graff, Jennifer Soderstrom, and Jun Han Yoo. December 2001.
- PEER 2002/06** *The Use of Benefit-Cost Analysis for Evaluation of Performance-Based Earthquake Engineering Decisions.* Richard O. Zerbe and Anthony Falit-Baiamonte. September 2001.
- PEER 2002/05** *Guidelines, Specifications, and Seismic Performance Characterization of Nonstructural Building Components and Equipment.* André Filiatrault, Constantin Christopoulos, and Christopher Stearns. September 2001.
- PEER 2002/04** *Consortium of Organizations for Strong-Motion Observation Systems and the Pacific Earthquake Engineering Research Center Lifelines Program: Invited Workshop on Archiving and Web Dissemination of Geotechnical Data, 4–5 October 2001.* September 2002.
- PEER 2002/03** *Investigation of Sensitivity of Building Loss Estimates to Major Uncertain Variables for the Van Nuys Testbed.* Keith A. Porter, James L. Beck, and Rustem V. Shaikhutdinov. August 2002.
- PEER 2002/02** *The Third U.S.-Japan Workshop on Performance-Based Earthquake Engineering Methodology for Reinforced Concrete Building Structures.* July 2002.
- PEER 2002/01** *Nonstructural Loss Estimation: The UC Berkeley Case Study.* Mary C. Comerio and John C. Stallmeyer. December 2001.
- PEER 2001/16** *Statistics of SDF-System Estimate of Roof Displacement for Pushover Analysis of Buildings.* Anil K. Chopra, Rakesh K. Goel, and Chatpan Chintanapakdee. December 2001.
- PEER 2001/15** *Damage to Bridges during the 2001 Nisqually Earthquake.* R. Tyler Ranf, Marc O. Eberhard, and Michael P. Berry. November 2001.
- PEER 2001/14** *Rocking Response of Equipment Anchored to a Base Foundation.* Nicos Makris and Cameron J. Black. September 2001.
- PEER 2001/13** *Modeling Soil Liquefaction Hazards for Performance-Based Earthquake Engineering.* Steven L. Kramer and Ahmed-W. Elgamal. February 2001.
- PEER 2001/12** *Development of Geotechnical Capabilities in OpenSees.* Boris Jeremić. September 2001.
- PEER 2001/11** *Analytical and Experimental Study of Fiber-Reinforced Elastomeric Isolators.* James M. Kelly and Shakhzod M. Takhirov. September 2001.
- PEER 2001/10** *Amplification Factors for Spectral Acceleration in Active Regions.* Jonathan P. Stewart, Andrew H. Liu, Yoojoong Choi, and Mehmet B. Baturay. December 2001.
- PEER 2001/09** *Ground Motion Evaluation Procedures for Performance-Based Design.* Jonathan P. Stewart, Shyh-Jeng Chiou, Jonathan D. Bray, Robert W. Graves, Paul G. Somerville, and Norman A. Abrahamson. September 2001.
- PEER 2001/08** *Experimental and Computational Evaluation of Reinforced Concrete Bridge Beam-Column Connections for Seismic Performance.* Clay J. Naito, Jack P. Moehle, and Khalid M. Mosalam. November 2001.
- PEER 2001/07** *The Rocking Spectrum and the Shortcomings of Design Guidelines.* Nicos Makris and Dimitrios Konstantinidis. August 2001.

- PEER 2001/06** *Development of an Electrical Substation Equipment Performance Database for Evaluation of Equipment Fragilities.* Thalia Agnanos. April 1999.
- PEER 2001/05** *Stiffness Analysis of Fiber-Reinforced Elastomeric Isolators.* Hsiang-Chuan Tsai and James M. Kelly. May 2001.
- PEER 2001/04** *Organizational and Societal Considerations for Performance-Based Earthquake Engineering.* Peter J. May. April 2001.
- PEER 2001/03** *A Modal Pushover Analysis Procedure to Estimate Seismic Demands for Buildings: Theory and Preliminary Evaluation.* Anil K. Chopra and Rakesh K. Goel. January 2001.
- PEER 2001/02** *Seismic Response Analysis of Highway Overcrossings Including Soil-Structure Interaction.* Jian Zhang and Nicos Makris. March 2001.
- PEER 2001/01** *Experimental Study of Large Seismic Steel Beam-to-Column Connections.* Egor P. Popov and Shakhzod M. Takhirov. November 2000.
- PEER 2000/10** *The Second U.S.-Japan Workshop on Performance-Based Earthquake Engineering Methodology for Reinforced Concrete Building Structures.* March 2000.
- PEER 2000/09** *Structural Engineering Reconnaissance of the August 17, 1999 Earthquake: Kocaeli (Izmit), Turkey.* Halil Sezen, Kenneth J. Elwood, Andrew S. Whittaker, Khalid Mosalam, John J. Wallace, and John F. Stanton. December 2000.
- PEER 2000/08** *Behavior of Reinforced Concrete Bridge Columns Having Varying Aspect Ratios and Varying Lengths of Confinement.* Anthony J. Calderone, Dawn E. Lehman, and Jack P. Moehle. January 2001.
- PEER 2000/07** *Cover-Plate and Flange-Plate Reinforced Steel Moment-Resisting Connections.* Taejin Kim, Andrew S. Whittaker, Amir S. Gilani, Vitelmo V. Bertero, and Shakhzod M. Takhirov. September 2000.
- PEER 2000/06** *Seismic Evaluation and Analysis of 230-kV Disconnect Switches.* Amir S. J. Gilani, Andrew S. Whittaker, Gregory L. Fenves, Chun-Hao Chen, Henry Ho, and Eric Fujisaki. July 2000.
- PEER 2000/05** *Performance-Based Evaluation of Exterior Reinforced Concrete Building Joints for Seismic Excitation.* Chandra Clyde, Chris P. Pantelides, and Lawrence D. Reaveley. July 2000.
- PEER 2000/04** *An Evaluation of Seismic Energy Demand: An Attenuation Approach.* Chung-Che Chou and Chia-Ming Uang. July 1999.
- PEER 2000/03** *Framing Earthquake Retrofitting Decisions: The Case of Hillside Homes in Los Angeles.* Detlof von Winterfeldt, Nels Roselund, and Alicia Kitsuse. March 2000.
- PEER 2000/02** *U.S.-Japan Workshop on the Effects of Near-Field Earthquake Shaking.* Andrew Whittaker, Editor. July 2000.
- PEER 2000/01** *Further Studies on Seismic Interaction in Interconnected Electrical Substation Equipment.* Armen Der Kiureghian, Kee-Jeung Hong, and Jerome L. Sackman. November 1999.
- PEER 1999/14** *Seismic Evaluation and Retrofit of 230-kV Porcelain Transformer Bushings.* Amir S. Gilani, Andrew S. Whittaker, Gregory L. Fenves, and Eric Fujisaki. December 1999.
- PEER 1999/13** *Building Vulnerability Studies: Modeling and Evaluation of Tilt-up and Steel Reinforced Concrete Buildings.* John W. Wallace, Jonathan P. Stewart, and Andrew S. Whittaker, Editors. December 1999.
- PEER 1999/12** *Rehabilitation of Nonductile RC Frame Building Using Encasement Plates and Energy-Dissipating Devices.* Mehrdad Sasani, Vitelmo V. Bertero, James C. Anderson. December 1999.
- PEER 1999/11** *Performance Evaluation Database for Concrete Bridge Components and Systems under Simulated Seismic Loads.* Yael D. Hose and Frieder Seible. November 1999.
- PEER 1999/10** *U.S.-Japan Workshop on Performance-Based Earthquake Engineering Methodology for Reinforced Concrete Building Structures.* December 1999.
- PEER 1999/09** *Performance Improvement of Long Period Building Structures Subjected to Severe Pulse-Type Ground Motions.* James C. Anderson, Vitelmo V. Bertero, and Raul Bertero. October 1999.
- PEER 1999/08** *Envelopes for Seismic Response Vectors.* Charles Menun and Armen Der Kiureghian. July 1999.
- PEER 1999/07** *Documentation of Strengths and Weaknesses of Current Computer Analysis Methods for Seismic Performance of Reinforced Concrete Members.* William F. Cofer. November 1999.
- PEER 1999/06** *Rocking Response and Overturning of Anchored Equipment under Seismic Excitations.* Nicos Makris and Jian Zhang. November 1999.
- PEER 1999/05** *Seismic Evaluation of 550 kV Porcelain Transformer Bushings.* Amir S. Gilani, Andrew S. Whittaker, Gregory L. Fenves, and Eric Fujisaki. October 1999.

- PEER 1999/04** *Adoption and Enforcement of Earthquake Risk-Reduction Measures.* Peter J. May, Raymond J. Burby, T. Jens Feeley, and Robert Wood. August 1999.
- PEER 1999/03** *Task 3 Characterization of Site Response General Site Categories.* Adrian Rodriguez-Marek, Jonathan D. Bray and Norman Abrahamson. February 1999.
- PEER 1999/02** *Capacity-Demand-Diagram Methods for Estimating Seismic Deformation of Inelastic Structures: SDF Systems.* Anil K. Chopra and Rakesh Goel. April 1999.
- PEER 1999/01** *Interaction in Interconnected Electrical Substation Equipment Subjected to Earthquake Ground Motions.* Armen Der Kiureghian, Jerome L. Sackman, and Kee-Jeung Hong. February 1999.
- PEER 1998/08** *Behavior and Failure Analysis of a Multiple-Frame Highway Bridge in the 1994 Northridge Earthquake.* Gregory L. Fenves and Michael Ellery. December 1998.
- PEER 1998/07** *Empirical Evaluation of Inertial Soil-Structure Interaction Effects.* Jonathan P. Stewart, Raymond B. Seed, and Gregory L. Fenves. November 1998.
- PEER 1998/06** *Effect of Damping Mechanisms on the Response of Seismic Isolated Structures.* Nicos Makris and Shih-Po Chang. November 1998.
- PEER 1998/05** *Rocking Response and Overturning of Equipment under Horizontal Pulse-Type Motions.* Nicos Makris and Yiannis Roussos. October 1998.
- PEER 1998/04** *Pacific Earthquake Engineering Research Invitational Workshop Proceedings, May 14–15, 1998: Defining the Links between Planning, Policy Analysis, Economics and Earthquake Engineering.* Mary Comerio and Peter Gordon. September 1998.
- PEER 1998/03** *Repair/Upgrade Procedures for Welded Beam to Column Connections.* James C. Anderson and Xiaojing Duan. May 1998.
- PEER 1998/02** *Seismic Evaluation of 196 kV Porcelain Transformer Bushings.* Amir S. Gilani, Juan W. Chavez, Gregory L. Fenves, and Andrew S. Whittaker. May 1998.
- PEER 1998/01** *Seismic Performance of Well-Confined Concrete Bridge Columns.* Dawn E. Lehman and Jack P. Moehle. December 2000.

ONLINE PEER REPORTS

The following PEER reports are available by Internet only at http://peer.berkeley.edu/publications/peer_reports_complete.html.

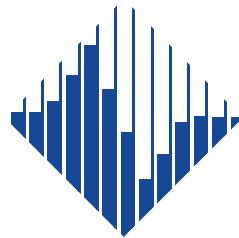
- PEER 2012/103** *Performance-Based Seismic Demand Assessment of Concentrically Braced Steel Frame Buildings*. Chui-Hsin Chen and Stephen A. Mahin. December 2012.
- PEER 2012/102** *Procedure to Restart an Interrupted Hybrid Simulation: Addendum to PEER Report 2010/103*. Vesna Terzic and Božidar Stojadinovic. October 2012.
- PEER 2012/101** *Mechanics of Fiber Reinforced Bearings*. James M. Kelly and Andrea Calabrese. February 2012.
- PEER 2011/107** *Nonlinear Site Response and Seismic Compression at Vertical Array Strongly Shaken by 2007 Niigata-ken Chuetsu-oki Earthquake*. Eric Yee, Jonathan P. Stewart, and Kohji Tokimatsu. December 2011.
- PEER 2011/106** *Self Compacting Hybrid Fiber Reinforced Concrete Composites for Bridge Columns*. Pardeep Kumar, Gabriel Jen, William Trono, Marios Panagiotou, and Claudia Ostertag. September 2011.
- PEER 2011/105** *Stochastic Dynamic Analysis of Bridges Subjected to Spatially Varying Ground Motions*. Katerina Konakli and Armen Der Kiureghian. August 2011.
- PEER 2011/104** *Design and Instrumentation of the 2010 E-Defense Four-Story Reinforced Concrete and Post-Tensioned Concrete Buildings*. Takuya Nagae, Kenichi Tahara, Taizo Matsumori, Hitoshi Shiohara, Toshimi Kabeyasawa, Susumu Kono, Minehiro Nishiyama (Japanese Research Team) and John Wallace, Wassim Ghannoum, Jack Moehle, Richard Sause, Wesley Keller, Zeynep Tuna (U.S. Research Team). June 2011.
- PEER 2011/103** *In-Situ Monitoring of the Force Output of Fluid Dampers: Experimental Investigation*. Dimitrios Konstantinidis, James M. Kelly, and Nicos Makris. April 2011.
- PEER 2011/102** *Ground-Motion Prediction Equations 1964–2010*. John Douglas. April 2011.
- PEER 2011/101** *Report of the Eighth Planning Meeting of NEES/E-Defense Collaborative Research on Earthquake Engineering*. Convened by the Hyogo Earthquake Engineering Research Center (NIED), NEES Consortium, Inc. February 2011.
- PEER 2010/111** *Modeling and Acceptance Criteria for Seismic Design and Analysis of Tall Buildings*. Task 7 Report for the Tall Buildings Initiative - Published jointly by the Applied Technology Council. October 2010.
- PEER 2010/110** *Seismic Performance Assessment and Probabilistic Repair Cost Analysis of Precast Concrete Cladding Systems for Multistory Buildings*. Jeffrey P. Hunt and Božidar Stojadinovic. November 2010.
- PEER 2010/109** *Report of the Seventh Joint Planning Meeting of NEES/E-Defense Collaboration on Earthquake Engineering. Held at the E-Defense, Miki, and Shin-Kobe, Japan, September 18–19, 2009*. August 2010.
- PEER 2010/108** *Probabilistic Tsunami Hazard in California*. Hong Kie Thio, Paul Somerville, and Jascha Polet, preparers. October 2010.
- PEER 2010/107** *Performance and Reliability of Exposed Column Base Plate Connections for Steel Moment-Resisting Frames*. Ady Aviram, Božidar Stojadinovic, and Armen Der Kiureghian. August 2010.
- PEER 2010/106** *Verification of Probabilistic Seismic Hazard Analysis Computer Programs*. Patricia Thomas, Ivan Wong, and Norman Abrahamson. May 2010.
- PEER 2010/105** *Structural Engineering Reconnaissance of the April 6, 2009, Abruzzo, Italy, Earthquake, and Lessons Learned*. M. Selim Günay and Khalid M. Mosalam. April 2010.
- PEER 2010/104** *Simulating the Inelastic Seismic Behavior of Steel Braced Frames, Including the Effects of Low-Cycle Fatigue*. Yuli Huang and Stephen A. Mahin. April 2010.
- PEER 2010/103** *Post-Earthquake Traffic Capacity of Modern Bridges in California*. Vesna Terzic and Božidar Stojadinović. March 2010.
- PEER 2010/102** *Analysis of Cumulative Absolute Velocity (CAV) and JMA Instrumental Seismic Intensity (I_{JMA}) Using the PEER–NGA Strong Motion Database*. Kenneth W. Campbell and Yousef Bozorgnia. February 2010.
- PEER 2010/101** *Rocking Response of Bridges on Shallow Foundations*. Jose A. Ugalde, Bruce L. Kutter, and Boris Jeremic. April 2010.
- PEER 2009/109** *Simulation and Performance-Based Earthquake Engineering Assessment of Self-Centering Post-Tensioned Concrete Bridge Systems*. Won K. Lee and Sarah L. Billington. December 2009.
- PEER 2009/108** *PEER Lifelines Geotechnical Virtual Data Center*. J. Carl Stepp, Daniel J. Ponti, Loren L. Turner, Jennifer N. Swift, Sean Devlin, Yang Zhu, Jean Benoit, and John Bobbitt. September 2009.

- PEER 2009/107** *Experimental and Computational Evaluation of Current and Innovative In-Span Hinge Details in Reinforced Concrete Box-Girder Bridges: Part 2: Post-Test Analysis and Design Recommendations.* Matias A. Hube and Khalid M. Mosalam. December 2009.
- PEER 2009/106** *Shear Strength Models of Exterior Beam-Column Joints without Transverse Reinforcement.* Sangjoon Park and Khalid M. Mosalam. November 2009.
- PEER 2009/105** *Reduced Uncertainty of Ground Motion Prediction Equations through Bayesian Variance Analysis.* Robb Eric S. Moss. November 2009.
- PEER 2009/104** *Advanced Implementation of Hybrid Simulation.* Andreas H. Schellenberg, Stephen A. Mahin, Gregory L. Fenves. November 2009.
- PEER 2009/103** *Performance Evaluation of Innovative Steel Braced Frames.* T. Y. Yang, Jack P. Moehle, and Božidar Stojadinovic. August 2009.
- PEER 2009/102** *Reinvestigation of Liquefaction and Nonliquefaction Case Histories from the 1976 Tangshan Earthquake.* Robb Eric Moss, Robert E. Kayen, Liyuan Tong, Songyu Liu, Guojun Cai, and Jiaer Wu. August 2009.
- PEER 2009/101** *Report of the First Joint Planning Meeting for the Second Phase of NEES/E-Defense Collaborative Research on Earthquake Engineering.* Stephen A. Mahin et al. July 2009.
- PEER 2008/104** *Experimental and Analytical Study of the Seismic Performance of Retaining Structures.* Linda Al Atik and Nicholas Sitar. January 2009.
- PEER 2008/103** *Experimental and Computational Evaluation of Current and Innovative In-Span Hinge Details in Reinforced Concrete Box-Girder Bridges. Part 1: Experimental Findings and Pre-Test Analysis.* Matias A. Hube and Khalid M. Mosalam. January 2009.
- PEER 2008/102** *Modeling of Unreinforced Masonry Infill Walls Considering In-Plane and Out-of-Plane Interaction.* Stephen Kadsiewicz and Khalid M. Mosalam. January 2009.
- PEER 2008/101** *Seismic Performance Objectives for Tall Buildings.* William T. Holmes, Charles Kircher, William Petak, and Nabih Youssef. August 2008.
- PEER 2007/101** *Generalized Hybrid Simulation Framework for Structural Systems Subjected to Seismic Loading.* Tarek Elkhoraibi and Khalid M. Mosalam. July 2007.
- PEER 2007/100** *Seismic Evaluation of Reinforced Concrete Buildings Including Effects of Masonry Infill Walls.* Alidad Hashemi and Khalid M. Mosalam. July 2007.

The Pacific Earthquake Engineering Research Center (PEER) is a multi-institutional research and education center with headquarters at the University of California, Berkeley. Investigators from over 20 universities, several consulting companies, and researchers at various state and federal government agencies contribute to research programs focused on performance-based earthquake engineering.

These research programs aim to identify and reduce the risks from major earthquakes to life safety and to the economy by including research in a wide variety of disciplines including structural and geotechnical engineering, geology/seismology, lifelines, transportation, architecture, economics, risk management, and public policy.

PEER is supported by federal, state, local, and regional agencies, together with industry partners.



PEER Core Institutions:
University of California, Berkeley (Lead Institution)
California Institute of Technology
Oregon State University
Stanford University
University of California, Davis
University of California, Irvine
University of California, Los Angeles
University of California, San Diego
University of Southern California
University of Washington

PEER reports can be ordered at http://peer.berkeley.edu/publications/peer_reports.html or by contacting

Pacific Earthquake Engineering Research Center
University of California, Berkeley
325 Davis Hall, mail code 1792
Berkeley, CA 94720-1792
Tel: 510-642-3437
Fax: 510-642-1655
Email: peer_editor@berkeley.edu

ISSN 1547-0587X